Durham E-Theses

The pulsations and energy transfers in a double-orifice combustor

Beale, C. K.

How to cite:

Beale, C. K. (1945) *The pulsations and energy transfers in a double-orifice combustor*, Durham theses, Durham University. Available at Durham E-Theses Online: http://etheses.dur.ac.uk/8202/

Use policy

The Pulsations and Energy Transfers

in a Double-Orifice Combustor

by

C. K. Beale, B.Sc.

Thesis submitted for the degree of

Doctor of Philosophy in the

University of Durham.

Department of Engineering Science   March 1975

ABSTRACT

This work examines the effect of longitudinal oscillations on
the heat transfer in a naturally-aspirating, propane-fuelled combustor.
Previous investigations in the field have been predominantly
experimental in nature, although theoretical studies of the effect of
oscillations on local heat transfer coefficients have been made.   In
this work, a linearised wave equation, which governs the propagation
of sound waves in a gas confined by a straight tube and exhibiting an
axial temperature variation, is used to correlate local heat transfer
coefficients by a quasi-steady-state method.   An apparatus was
constructed, and measurements of the gas, wall and water temperatures
and of the gas pressure amplitudes were taken in a concentric tube heat
exchanger, which formed part of the resonating section.

CONTENTS

SYMBOLS AND CONSTANTS

Section 1

A_1, A_2, A_3, B constants

$\bar{c}$	time-averaged velocity of sound	m/s
c_p	specific heat at constant pressure	kJ/kg K
c_v	specific heat at constant volume	kJ/kg K
$\hat{E}$	amplitude of kinetic energy in oscillation	kJ
$\bar{E}$	time-averaged kinetic energy of flow	kJ
f	frequency	Hz
Gz	Graetz number	
L	length	m
n	integer	
N	rotational speed	rev/minute
$\overline{Nu}_p$	time-averaged Nusselt number in pulsating flow	
Nu	Nusselt number in steady flow	
$\hat{P}$	pressure amplitude	N/m^2
$\bar{P}$	time-averaged pressure	N/m^2
ΔP	pressure amplitude of Koshkin (37)	N/m^2
$\bar{\bar{P}}$	working pressure of Koshkin (37)	N/m^2
Pr	Prandtl number	
Re	Reynolds number	
SPL	sound pressure level	dB
$\hat{u}$	velocity amplitude	m/s
$\bar{u}$	time-averaged velocity	m/s
x	axial distance	m
λ	wavelength	m
$\mathcal{U}$	ratio of cp/cv	
ρ	density	kg/m^3
ϕ_{AT}	pulsation energy attenuation factor of Galitseysky et al. (38)	

ω	angular frequency	radian/s

Section 2

A	constant	
B_A	bulk modulus of air	N/m^2
c_o	velocity of sound at $x = 0$	m/s
e	specific internal energy	kJ/kg
E_c	Eckert number	
h	local heat transfer coefficient	$W/m^2 K$
J_n	Bessel function of first kind - order n	
k	thermal conductivity	W/m K
L	length	m
M_1	constant defined by equation 2.2.28	
$\dot{m}$	mass flowrate	kg/h
N_1	constant defined by equation 2.2.29	
P	pressure	N/m^2
$\hat{P}_o$	pressure amplitude at $x = 0$	N/m^2
q	heat transfer	kJ
R	specific gas constant for air 0.2871	kJ/kg
S	Strouhal number $= \dfrac{\omega d}{\bar{u}}$	
t	time	s
T	temperature	$^\circ C$
T_o	temperature at $x = 0$	$^\circ C$
u	velocity	m/s
x	axial distance	m
X	function of x	
Y_n	Bessel function of second kind - order n	
y	coordinate	m
z	change of variable	
z	coordinate	m

ζ	axial displacement of pressure wave	m
$\propto$	constant	
θ	function of time	
λ	wavelength	m
ϕ	function	
μ	dynamic viscosity	kg/m s
ρ	density	kg/m^3

Section 3

D_I	diameter of aerodynamic valve	m
h	damping ratio	
L_n	connecting length for pressure transducer	m
$\dot{m}_{GC}$	mass flowrate of chamber coolant	kg/h
$\dot{m}_P$	mass flowrate of propane	kg/h
$\dot{m}_W$	mass flowrate of water	kg/h
P_{An}	pressure amplitude at site n	N/m^2
P_P	regulated pressure of propane	Bar
r	radius of connecting tube	m
T_{An}	temperature of air at site n	°C
T_P	temperature of propane in flowmeter	°C
T_{Sn}	surface temperature at site n	°C
T_{WIN}	outlet temperature of water from injector	°C
T_{Wn}	temperature of water at site n	°C
x_{AUG}	axial position of augmenter	m
ω_n	natural frequency	radian/s

Section 4

c	velocity of sound	m/s
D_{EQ}	equivalent diameter of annulus	m
D_I	diameter of aerodynamic valve	m

D_o	diameter of inner tube of heat exchanger A	m
f	frequency	Hz
h_{AS}	heat transfer coefficient between air and tube surface	W/m^2 K
h_{SW}	heat transfer coefficient between tube surface and water	W/m^2 K
k_A	thermal conductivity of air	W/m K
k_W	thermal conductivity of water	W/m K
L	length	m
L_A	length of heat exchanger A	m
$\dot{m}_{AA}$	mass flowrate of air through resonating section	kg/h
$\dot{m}_P$	mass flowrate of propane	kg/h
n	wave number	
n	integer	
$P_{A(x)}$	pressure amplitude at point x	N/m^2
$\hat{P}_{A(x)}$	maximum pressure amplitude	N/m^2
P_{Ac}	combustion chamber pressure amplitude	N/m^2
$\overline{Re}_A$	time-averaged Reynolds number of air flow	
Re_W	Reynolds number of water flow	
S	Strouhal number	
S_S	surface area of section of heat exchanger A	m^2
$T_{A(x)}$	temperature of air at point x	$°C$
$\overline{T}_{An}$	temperature of air at site n	$°C$
$\overline{T}_A$	mean air temperature in section	$°C$
$\overline{T}_S$	mean surface temperature in section	$°C$
$\overline{T}_W$	mean water temperature in section	$°C$
$\overline{u}_A$	time-averaged velocity of air flow	m/s
$\hat{u}$	velocity amplitude of air	m/s
x	axial distance	m
ρ_A	density of air	kg/m^3
μ_A	dynamic viscosity of air	kg/m s
η_{th}	thermal efficiency	

Section 6

a_g	gravitational acceleration	m/s^2
c	velocity of sound	m/s
C_c	capitance of connecting leads	pF
C_i	capitance of amplifier input	pF
C_m	capitance of microphone	nF
c_{pA}	specific heat at constant pressure of air	kJ/kg K
c_{pw}	specific heat at constant pressure of water	kJ/kg K
D_{L1}	internal diameter of chamber lagging	m
D_{L2}	external diameter of chamber lagging	m
d_o	diameter of inner tube of heat exchanger	m
d_{SH}	diameter of sheath	m
$f(x)$	function of x	
f	frequency	Hz
g_o	constant in Newton's Second Law	$kg\ m/N\ s^2$
h	mean heat transfer coefficient	$W/m^2\ K$
h	specific enthalpy of pure substance	kJ/kg
h_c	convection heat transfer coefficient	$W/m^2\ K$
h_r	radiation heat transfer coefficient	$W/m^2\ K$
k_{LAG}	thermal conductivity of chamber lagging	$W/m\ K$
k_{SH}	thermal conductivity of sheath	$W/m\ K$
L	immersion of thermocouple	m
L	length of tube	m
L_A	length of Heat exchanger A	m
L_{CL}	length of chamber lagging	m
$\dot{m}_A$	mass flowrate of fluid	kg/h
$\dot{m}_{AA}$	mass flowrate of air through resonating section	kg/h
$\dot{m}_{ABC}$	mass flowrate of air through Heat exchangers B & C	kg/h
$\dot{m}_{GC}$	mass flowrate of chamber coolant	kg/h
$\dot{m}_p$	mass flowrate of propane	kg/h

$\dot{m}_W$	mass flowrate of water	kg/h
$\dot{m}_1$	defined by equation 6 - C.7	
Nu_d	Nusselt number based on tube diameter	
p	pressure	N/m^2
P_{AO}	ambient pressure	N/m^2
P_o	reference pressure $\quad$ 1.01325×10^5	n/m^2
$\dot{Q}$	rate of heat transfer	W
$\dot{Q}_{LCL}$	rate of heat transfer through chamber lagging	W
r	radial ordinate	m
R	radius of tube	m
R_d	Reynolds number of flow in tube	
S_B'	surface area of thermocouple bead	m
S_{CHARGE}	charge sensitivity of microphone	$pC/N/m^2$
S_V	voltage sensitivity of microphone	mV/μBar
$S_{V(c)}$	connected sensitivity of microphone	mV/μBar
T_{Am}	mean air temperature over length Δx	$^\circ C$
T_{An}	connected air temperature	$^\circ C$
T_{An}'	temperature recorded by thermocouple	$^\circ C$
T_{Ao}	ambient temperature	$^\circ C$
T_{EXIT}	exhaust gas temperature	$^\circ C$
T_{LAG}	outer surface temperature of chamber lagging	$^\circ C$
T_o	reference temperature $\quad$ 273.16	K
T_{Sc}	chamber surface temperature	$^\circ C$
t_{SH}	thickness of sheath wall	m
T_{Wn}	mean water temperature over length Δx	$^\circ C$
u	specific internal energy of substance	kJ/kg
$\dot{W}_x$	rate of external work	W
x	axial distance along tube	m
x_c	cold end of Heat exchanger A	m
x_H	hot end of Heat exchanger A	m

y	change of variable	
z	elevation of system above arbitrary datum	m
$\Delta \dot{H}$	rate of change of enthalpy	W
$[\Delta \dot{H}']_{t_0}$	rate of increase of enthalpy of propane fuel in isothermal reaction	W
ΔT_W	change in water temperature over Δx	K
ε_B	normal total emissivity of bead	
ε_{SH}	normal total emissivity of sheath	
σ	Stefan-Boltzmann constant 5.67×10^{-8}	$W/m^2 \ K^4$
ρ	density	kg/m^3
$\bar{\rho}$	time-averaged density	kg/m^3
ω	angular frequency	radian/s
η_{th}	thermal efficiency	
E_c	ECKERT N$^{\underline{o}}$ $= \dfrac{\bar{u}^2}{c_p \Delta T}$	

1. Introduction

This work studies the effect of combustion-driven oscillations
on the process of heat transfer in a double-orifice pulsating combustor.
Such a combustor consists of a combustion chamber, into which fuel and
air are admitted, and a resonating exhaust tube in which convective
heat transfer occurs. When in operation, the predominant oscillations
occur in a standing, longitudinal mode and are sustained by a
correctly-phased variation in the rate of energy release in the
combustion chamber. The oscillations are regarded as stable when the
pressure amplitude neither increases nor decreases, which indicates
that the energy added to the wave motion is exactly damped out by
viscous dissipation. The advantages of constant volume over constant
pressure combustion are generally held to be increased volumetric
combustion rate, increased combustion efficiency and increased rate of
convective heat transfer, the chief disadvantage being noise. Although
considerable interest has been shown in the pulsating combustor, there
have been few commercial applications.

One of the earliest observations of combustion-driven oscillations
was recorded by Higgins (1) in 1777 when he found that a hydrogen
diffusion flame, enclosed by a large tube (open at both ends), oscillated
audibly for certain lengths of the fuel supply line. In 1859 Reijke (2)
reported an acoustically-driven oscillation in an air column when a
hot metal gauze was positioned one quarter of the way up a vertical
open-ended tube. In 1883 Mallard and Le Chatelier (3) noticed that a
flame, propagating from the open to the closed end of a tube, began to
oscillate with increasing violence until detonation occurred.

In 1904 Lemale and Armengaud (4) built one of the first constant
pressure gas turbines but obtained no external shaft power as the

output of the turbine was absorbed by the compressor.   Holzwarth (5) recognised that the negative compression work had to be reduced and suggested that a constant volume combustion process should be employed. A number of patents were taken out - by Esnault-Pelterie in 1905 (6), Karawodine, 1906 (7) Armengaud, 1907 (8) and Marconnet, 1910 (9). Each of these designs consisted principally of a rigid volume with two openings, one for the injection of the combustible mixture and the other for the expulsion of the combustion products.   In these valve-actuated chambers, the constant-volume combustion produced a considerable pressure gain although this pressure could only be expanded in the turbine with a poor efficiency, due to the variation in the exhaust gas velocity.   In the course of these early experiments, it was observed that the transmission of energy from the intermittent flow of exhaust gases to the cooled walls of the outlet tubes was very apparent, and this led to the development of a steam boiler, the Velox, by the Brown Boveri Company.

In 1930 Schmidt (10) patented a pulsating combustion tube which was designed to thrust a column of air out of the open end by means of the "rapidly repeated combustion of fuel and air in small quantities" at the accoustically closed end.   It was this tube, 'Das Schmidt-Rohr', that was later developed by the Argus Engine Company to propel the 'Vergeltungswaffe - 1' flying bomb, shown in Figure 1.1.   Manganiello (10) has reported that a replica of the propulsion unit developed up to 520 kW at the operating frequency of 40 Hz.

In 1933 Reynst (11) patented a combustion chamber which consisted of a rigid volume with only one opening for the alternate passage of fresh mixture and exhaust products.   Reynst took out a further patent (12) in 1938, concerning an invention, based on his earlier patent, to
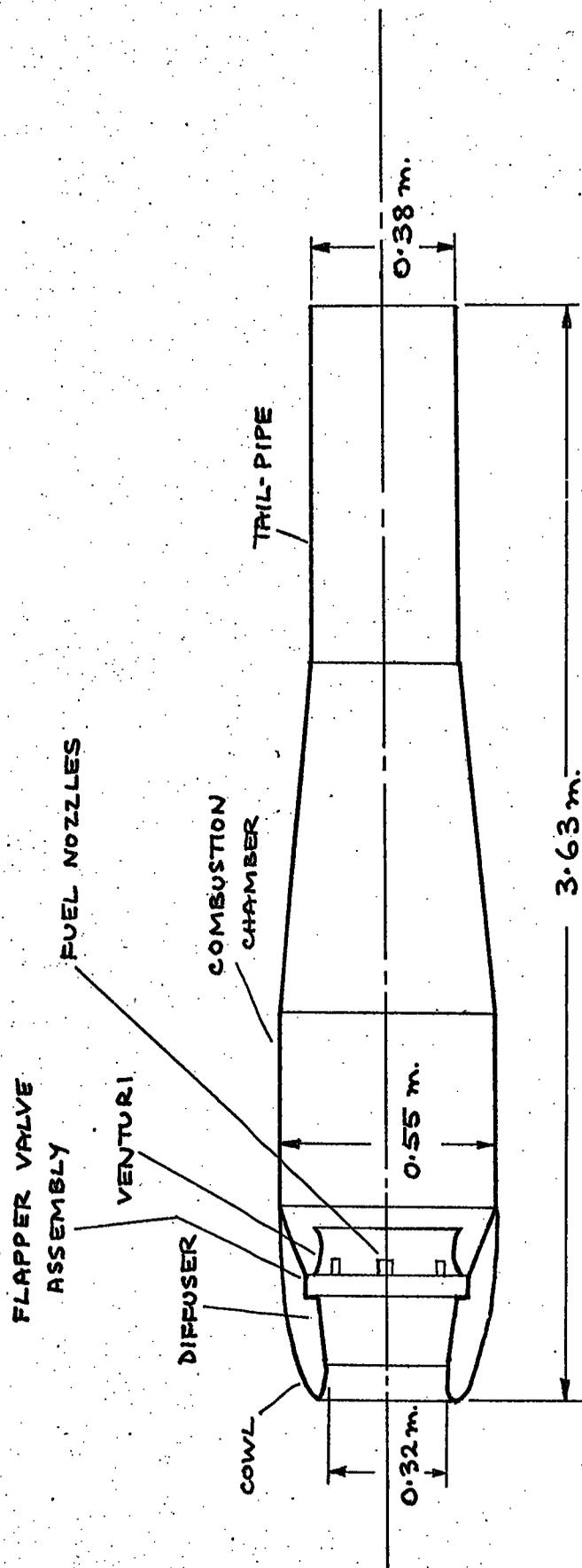
FIGURE 1.1 : THE SCHMIDT TUBE

Labels in figure: 0.38 m., TAIL-PIPE, 3.63 m., FUEL NOZZLES, COMBUSTION CHAMBER, FLAPPER VALVE ASSEMBLY, VENTURI, 0.55 m., DIFFUSER, COWL, 0.32 m.

4
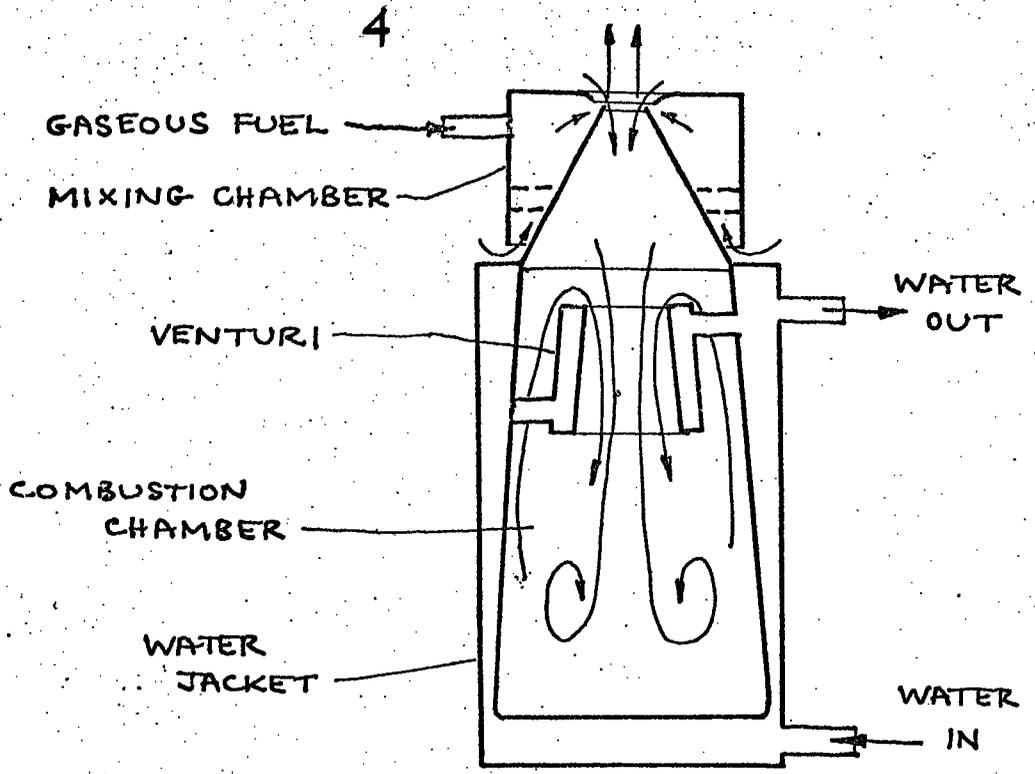
FIGURE 1.2 : THE REYNST POT
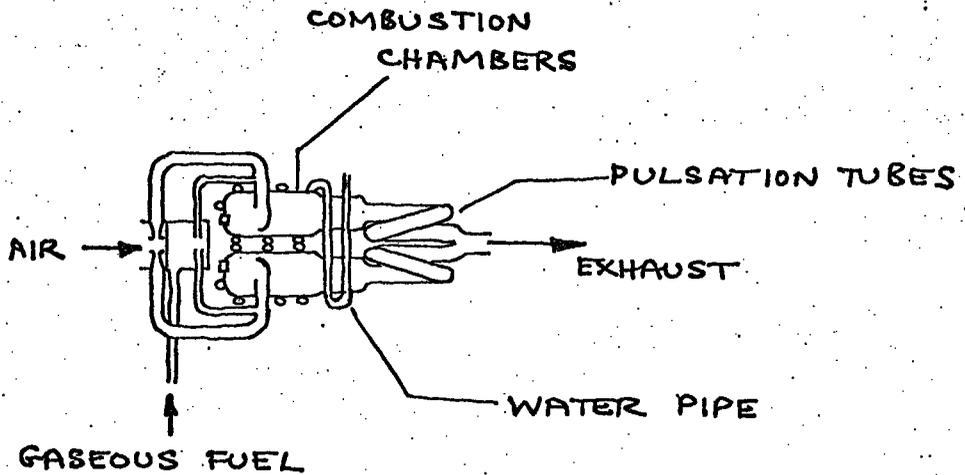
FIGURE 1.3 : HUBER WATER HEATER

produce and transfer heat efficiently by means of a detonative combustion process (see Figure 1.2).

1.1 Water/air heating pulsating combustors

In 1943 Reynst (13) reported work on a single-orifice combustor; volumetric combustion rate was 17.5 MW/m^3 at an operating frequency of 128 Hz, and the maximum rate of heat transfer was 0.28 W/m^2 K for an outlet water temperature of 50°C. An analysis of the exhaust gases gave 13% CO_2, 1.5% O_2 and 0% CO, and the unit was said to be unpleasantly noisy. In 1948 Huber (14) began to market the 'Schwingfeuergerat'; this unit incorporated a two-orifice combustor, fuelled by petrol at first, but by natural gas after 1950. The device was intended to preheat the cooling water of internal combustion engines prior to starting in cold weather, and was rated at 5.8 kW. Huber later developed the 'Schwing Calor' air-heater for the heating of temporary shelters and, more recently, a continuous-flow water heater (Figure 1.3) in conjunction with the Junkers Company. This unit comprised a pair of two-orifice pulsating combustors coupled at their inlet ends. Each chamber (Figure 1.4) worked alternately; the fuel was drawn from a common chamber into a mixing tube, and the resultant mixture passed into the combustion chamber via a funnel and burned explosively. The combustion-driven oscillations occurred first in one chamber and then the other, and most of the hot gases were expelled through the heat exchangers at the end of the combustion chambers into the pulsation tubes. A small proportion of the hot gases were forced back through the mixing tube, due to the relatively low resistance to flow in the inlet tubes; these were connected to restrict this back-flow. The operating frequency of the heater was 130 Hz on town gas, and 122 Hz

SPARKING PLUG

AIR INLET

SWIRLING GAS

COMBUSTION CHAMBER

GAS INLET

MIXING TUBE

WATER TUBE

FINNED HEAT EXCHANGER

CONNECTION TO RESONATING TUBE
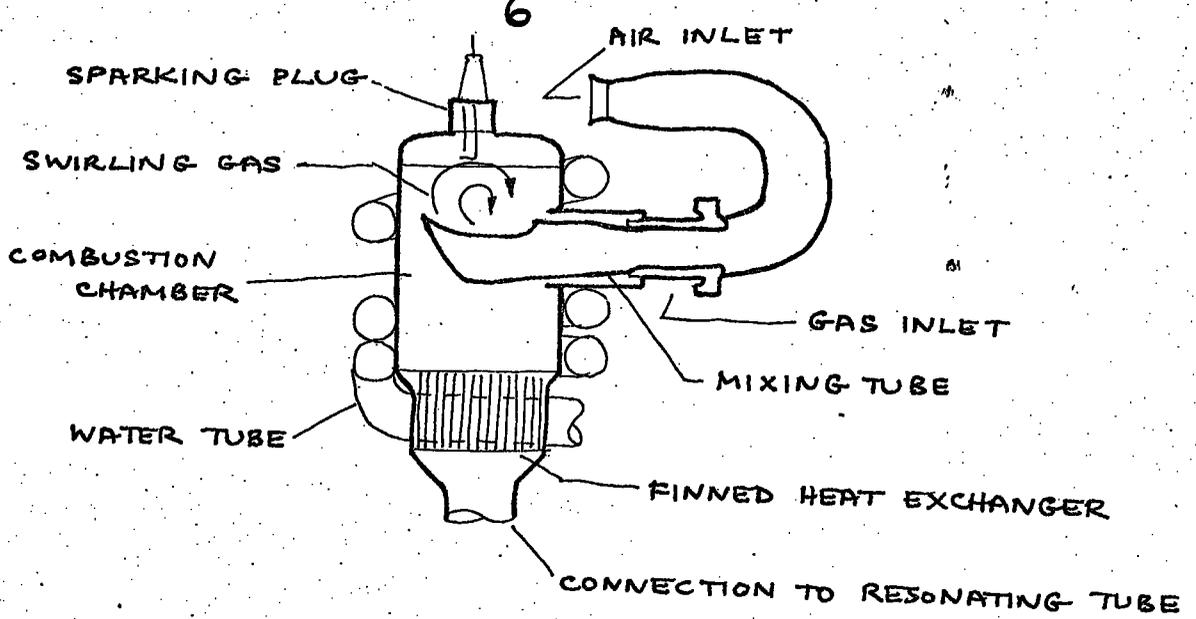
FIGURE 1.4 :   HUBER COMBUSTION CHAMBER

CONTROL SYSTEM

FUEL GAS IN

GAS CUSHION CHAMBER

HOT WATER OUT

SPARK PLUG

COMBUSTION CHAMBER

AIR IN

EXHAUST CUSHION CHAMBERS

EXHAUST

COLD WATER IN

OUTER CASING
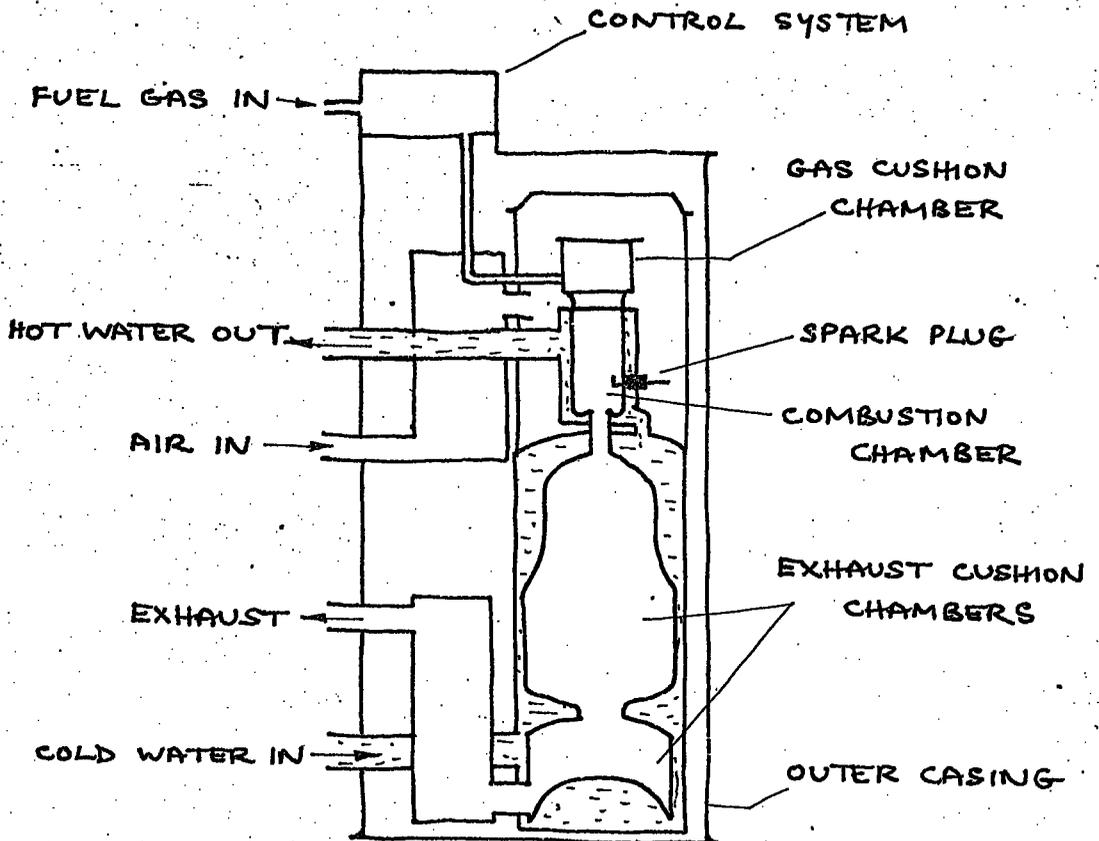
FIGURE 1.5 :   PULSAMATIC WATER HEATER

with propane, due to the different temperature profile, and it was rated at 23.2 kW.

Another commercial application of pulsating combustion has been to central heating. The 'Pulsamatic' (see Figure 1.5) was developed in Canada and was rated at 30 kW. This boiler was investigated by Alebon et al (15) with a view to improving the method of silencing. They found that the volumetric combustion rate was 44.5 MW/m^3 at an operating frequency of 70 Hz, the overall rate of heat transfer was 58.6 kW/m^2, and an exhaust gas analysis gave 8.56% CO_2, 3.06% O_2 and 0.0% CO. The overall thermal efficiency of the unit varied between 87% and 93% and the water outlet temperature varied between 32°C and 95°C. The authors managed to reduce the noise output from the device from 107 dB to 68 dB. A notable feature was that physically it was smaller than designs for steady combustion of a similar rating. However, it was noted by Bottoms (16) that the CO content in the exhaust gases increased when the unit was operated at less than its maximum rating.

In 1963 Francis et al (17) reported a preliminary study by the Gas Council on pulsating combustors to assess their use in industry, particularly for heating water and air. Two types of combustor were examined - 'Schmidt' and 'Helmholtz' (see Figure 1.6) - were examined for quality of combustion, thermal efficiency and stability of operation. The dimensions of these units were typically of 50-75 mm. internal diameter and between 2.1 m and 3.3 m long, and were fired by natural gas; both aerodynamic and mechanical values were studied for their effect on performance. The authors concluded that the combustion in their devices was efficient, provided that ;

GAS

SPARK PLUG

RESONANCE TUBE

AIR →

FLAP VALVES

SCHMIDT-TYPE BURNER

GAS

SPARK PLUG

EXHAUST TUBE

AIR →

HELMHOLTZ-TYPE BURNER
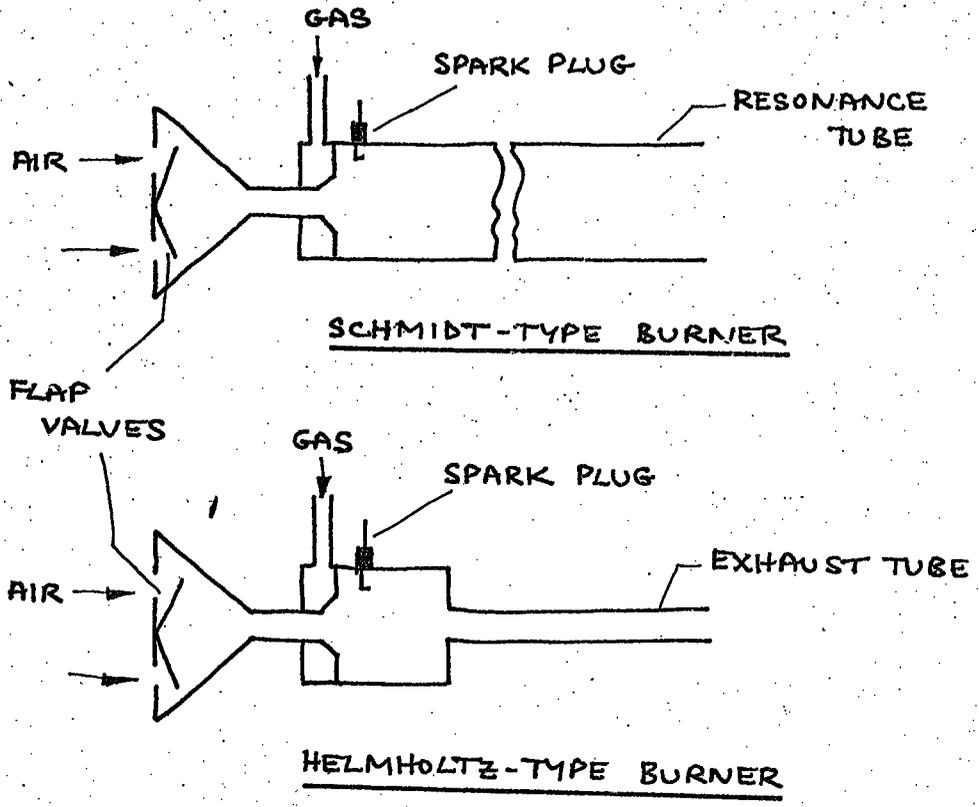
FIGURE 1.6 : FRANCIS BURNER CLASSIFICATION

RESONATING TUBE

AUGMENTER

APPROX. 2°
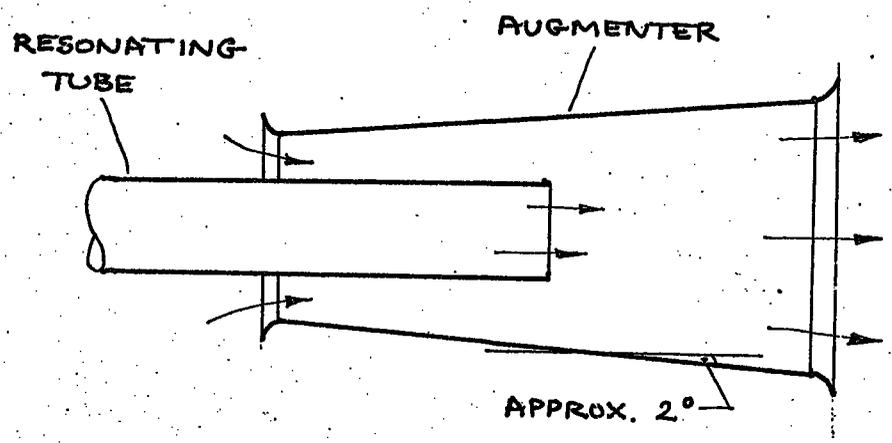
FIGURE 1.7 : MULLER AUGMENTER

a) multiple gas jets were used to achieve a uniform air/fuel
   mixture;

b) the fuel flowrate was not excessive;

c) the combustors were 'well-tuned'.

The authors found that extending the exhaust tube of the combustor
moved the pressure anti-node of the acoustic oscillation away from the
flame, thus adversely affecting the stability of the oscillation.
This observation was explained by the criterion of Rayleigh (18).
Their correlation between this expression and experiment was not
conclusive, and it was recommended that more attention should be paid
to the effect of the inlet valve section on combustor frequency and to
the effect of axial temperature gradients on exhaust pipe frequency.

Further work by the Gas Council has been reported by Reay (20).
It was found that the thermal efficiencies of the combustors ranged
between 70% and 80%, and the noise levels of 125 dB from the unsilenced
state could be reduced to approximately 80 dB using Burgess 'straight-
through' absorption silencers. It was also found that the thermal
efficiencies under pulsating flow conditions were from 30% to 50% higher
than those predicted theoretically for steady flow. The equation used
by Reay for this comparison assumed that the heat transfer in the
combustors was predominantly convective, and it is possible that
neglecting radiation led to slightly low values of the steady combustion
efficiency. It was observed that no fully satisfactory design
procedure for these units had yet been evolved and that the effect of
the many parameters on combustion stability was not clear.

In 1967 Muller (19) reported the development of a resonant
combustion heater for drying applications. Simple acoustic theory was
used to design two combustors, one of the Helmholtz type and the other
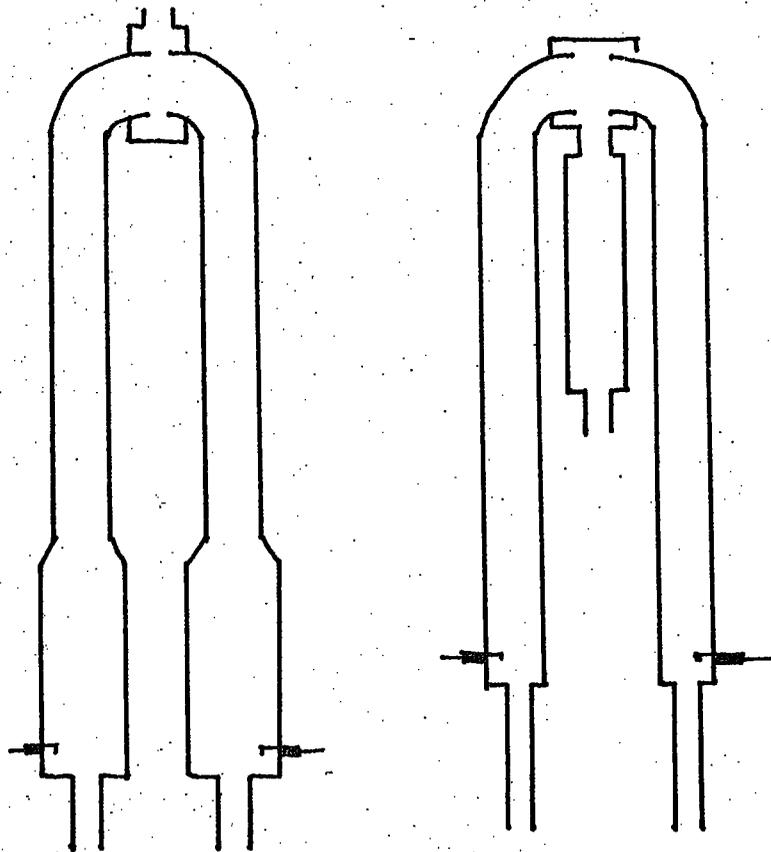
HELMHOLTZ UNITS

SCHMIDT TUBES
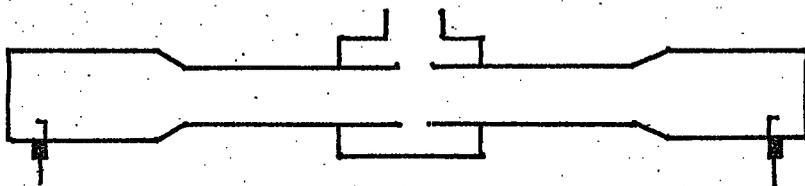
HELMHOLTZ UNITS WITH TANGENTIAL INJECTION

FIGURE 1.8 : BRIFFA BURNER CONFIGURATIONS

of a mixture of Helmholtz and Schmidt types. Both units developed approximately 90 kW of LPG; the volumetric combustion rate of the first was 71 MW/m^3 at a frequency of 153 Hz (estimated), and that of the second was 150 MW/m^3 at a frequency of 210 Hz. Muller made use of augmenters (see Figure 1.7) to increase the quantity of air pumped by his combustors, and noted that the length of the augmenter had an important influence on performance and had to be such that its natural frequency was some multiple of the combustor frequency.

In 1971 Briffa et al. (21) reported work on both Schmidt and Helmholtz type combustors (Figure 1.8) which were fuelled by a mixture of methane and air injected into short inlet tubes. The aims of the study were to examine methods of noise suppression. It was concluded that some reduction in noise was obtained by coupling the exhausts of two identical pulsating combustors and that reductions of up to 30 dB were attained when the coupled units operated in opposed phase and produced identical pressure waveforms. It was also noted that the Schmidt combustors gave a smoother and more sinusoidal pressure wave than the Helmholtx combustors and were thus more suitable for the method of anti-phase silencing.

1.2 Pulsating combustors in steam generating plant

In 1948 Reynst (22) advocated the use of pulsating combustion in boiler furnaces fired by pulverized solid fuels to increase the volumetric combustion rate. This idea was pursued by Sommers 1954 (23) who reported the conversion of a tube boiler to pulsating combustion. Preliminary experiments were undertaken on a double-orifice combustor fitted with a mechanical valve. It was found that, when the combustor was water-cooled, it would operate only with an
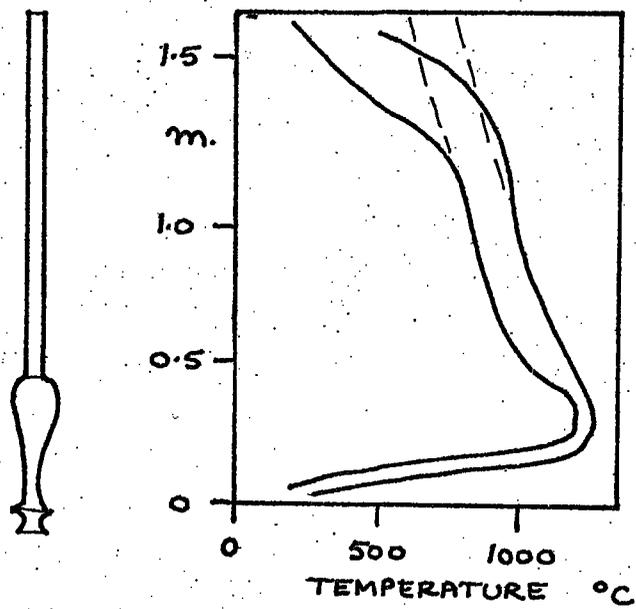
FIGURE 1.9 : GAS TEMPERATURE DISTRIBUTION
   IN   PULSATING   COMBUSTOR
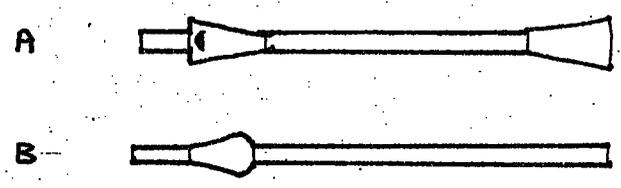
FIGURE 1.10 : TYPICAL PULSATING COMBUSTOR
              FORMS :
                  A :   GOOD ASPIRATION
                  B :   GOOD COMBUSTION

approximately stoichiometric mixture, whereas, when the combustor was either uncooled or lagged and supplied with pre-heated air, the mixture ratio could be varied widely. It was noted that the combustion-driven oscillations ceased when the maximum temperature in the combustion chamber fell below $1200^\circ C$. Sommers estimated that the amplitude of the oscillations was approximately 0.65m by extrapolating the slope of the temperature distributions (Figure 1.9) in the combustor towards the open end.

Sommers carried out a study of the effect of tube shape and type of inlet valve on the intensity of pulsation, and a wide range of configurations were tested. The results for the work on aerodynamic valves, are summarized in Figure 1.10. Configuration A was found to present the most resistance to back-flow through the inlet valve and to inflow at the exhaust end; whereas configuration B proved to be the best shape for complete combustion, particularly if the combustion chamber was maintained at a high temperature.

Sommers finally installed a double-orifice combustor, developed from the earlier work, in a tube boiler (see Figure 1.11). The maximum volumetric combustion rate attained was $21MW/m^3$ at a coal consumption rate of 1900kg/h and an operating frequency of 35Hz. The volumetric combustion rate was estimated to be several times that of a contemporary cyclone burner. Sommers concluded that attention to the design of both the aerodynamic valve and the pulsating tube would improve performance.

In 1965 Babkin (24) reported a project similar to that of Sommers. The investigation into pulsating combustion had been undertaken in 1958 with the purpose of intensifying combustion and heat transfer in the furnaces of steam boilers. A preliminary study was made of the
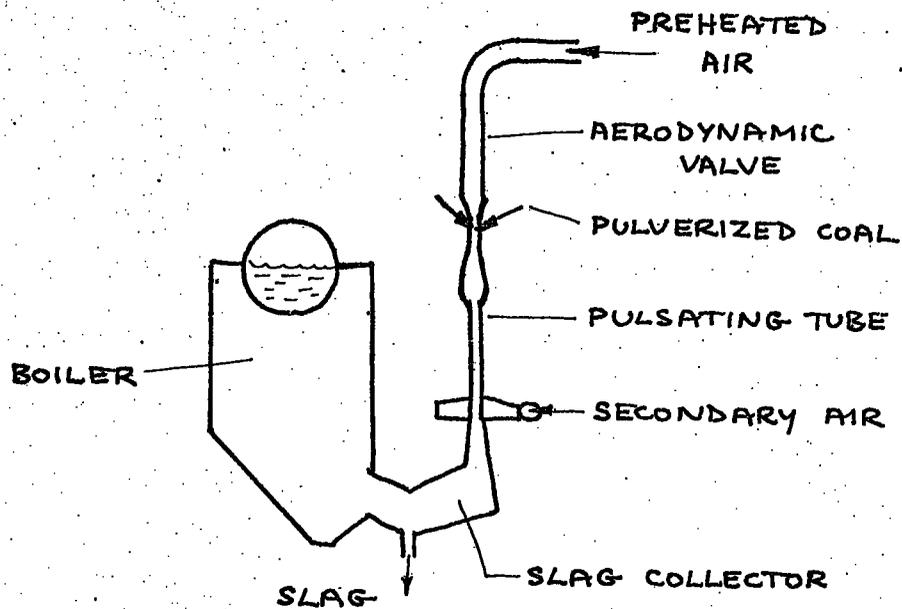
FIGURE 1.11 : SHAMROCK TEST PLANT
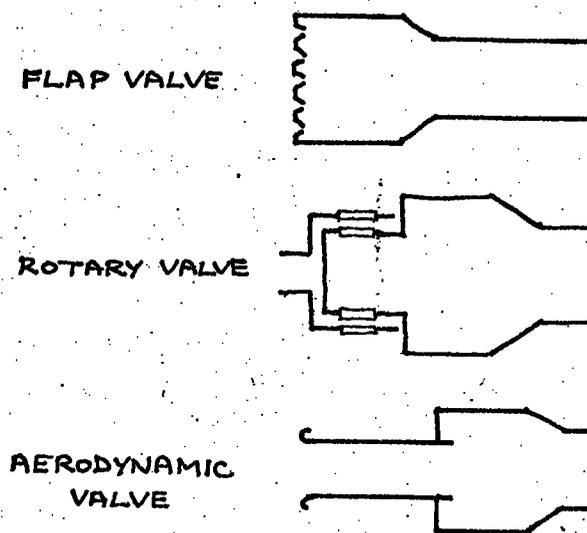
FIGURE 1.12 : MECHANICAL AND AERODYNAMIC VALVES

two types of valve - mechanical (flap and rotary) and aerodynamic (see Figure 1.12). Tests showed that intense pulsating combustion and self-aspiration were easily obtained in chambers fitted with flap valves but these suffered from fatigue failure. Rotary valves were tested but they were found to be impractical for chambers of more than 15 MW. rating. Aerodynamic valves were then studied, and it was found that:

a) the ability of the pulsating combustion chamber to self-aspirate was sharply diminished when air preheat was introduced;

b) the pressure amplitude of the oscillations increased when the inlet pipe length was increased, but, beyond a critical length, the oscillations would break down;

c) the oscillations ceased if the aerodynamic valve was connected to any inlet duct, even of much greater cross-section.

The design of the aerodynamic valve used in the investigation is shown in Figure 1.13; it consisted of a hemi-spherical stabilizer, telescopic connecting piece through which the fuel oil was fed, and turoidal shield. It was found that combustion of heavy fuel oils was particularly efficient in chambers fitted with such a valve which did not completely prevent back-flow and thus permitted a certain amplitude of flame movement in the region of the fuel injector. In 1960 a double-tube counter-phase pulsating combustion unit was installed in a steam boiler (see Figure 1.14 and A in Table 1.A). On the basis of measurements taken from this apparatus, a further unit was designed and installed in another boiler (see Figure 1.15 and B in Table 1.A) in 1963. Both furnaces were fired by fuel oil. It is apparent from Table 1.A that the volumetric combustion rate of B was less than half that of A.
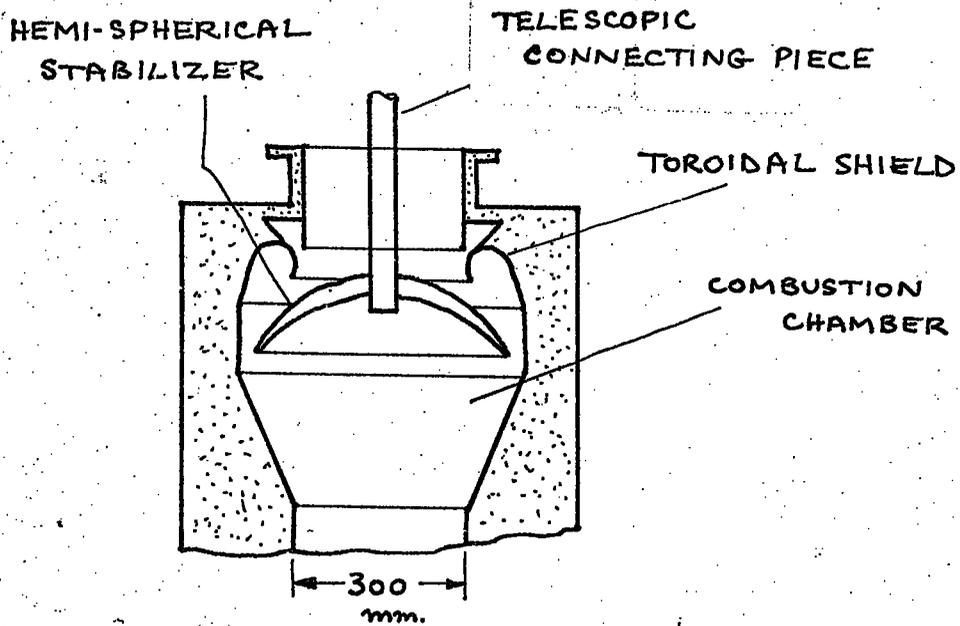
FIGURE 1.13 : AERODYNAMIC VALVE OF BABKIN
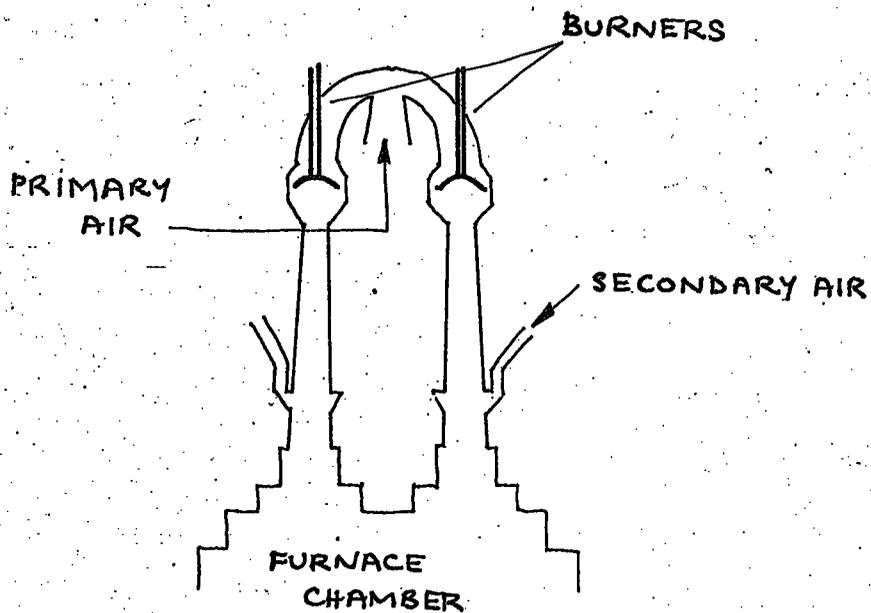

FIGURE 1.14 : COUNTER-PHASE PULSATING COMBUSTER
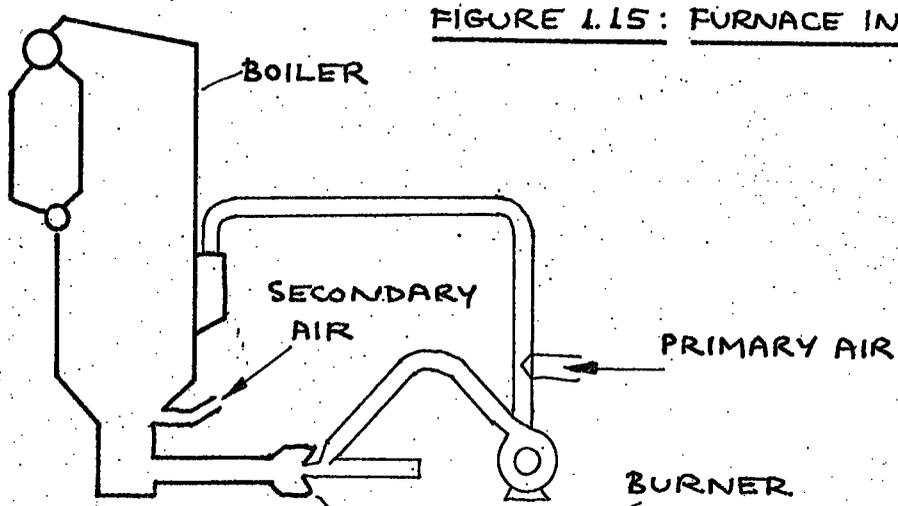
FIGURE 1.15 : FURNACE INSTALLATION

Table 1.A   Furnaces of Babkin

PULSATING COMBUSTION FURNACE	A	B	
Total rate of oil consumption	1500	4200	kg/h
Frequency of oscillations	68	31	Hz
Pressure amplitude of oscillations	30	15	kN/m^2
Volumetric combustion rate	18.6	7.2	MW/m^3

In 1968 Hanby and Brown (25) reported an investigation into a pulsating combustor fired by pulverized coal.   A full-scale perspex model of the combustor design was used to study the effect of various designs of fuel injectors on the mixing process.   The flows of air through the inlet pipe and of fuel through the injectors were modelled by water and by chemical tracer respectively.   The quality of the injection process was then assessed by sampling the mixture at a number of points in the combustor model.   The final design (Figure 1.16), which was similar to that of Sommers, was constructed in steel, the combustion chamber and first part of the exhaust tube being lined with refractory material.   It was found that the volumetric combustion rate was 8.3 MW/m^3 on a coal consumption of 23 kg/h. at an operation frequency of 75 Hz., and the gas temperature distribution in the combustor is shown in Figure 1.17.   It is interesting to note that the sharp change in gas temperature gradient observed by Sommers near the open end of his early combustor (see Figure 1.9) is not evident here. The combustor of Sommers operated at pressure amplitudes up to 100 kN/m^2 while that of Hanby and Brown attained a maximum of 12.5 kN/m^2.
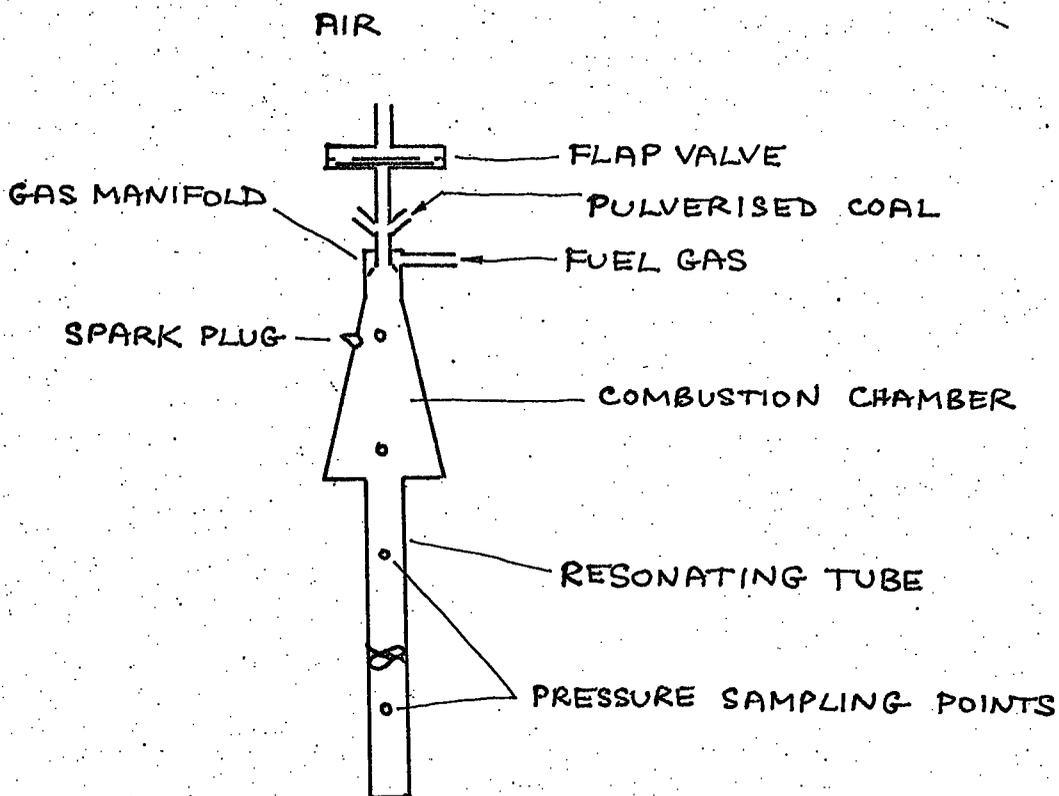
FIGURE 1.16:   PULSATING COMBUSTOR OF
   HANBY & BROWN
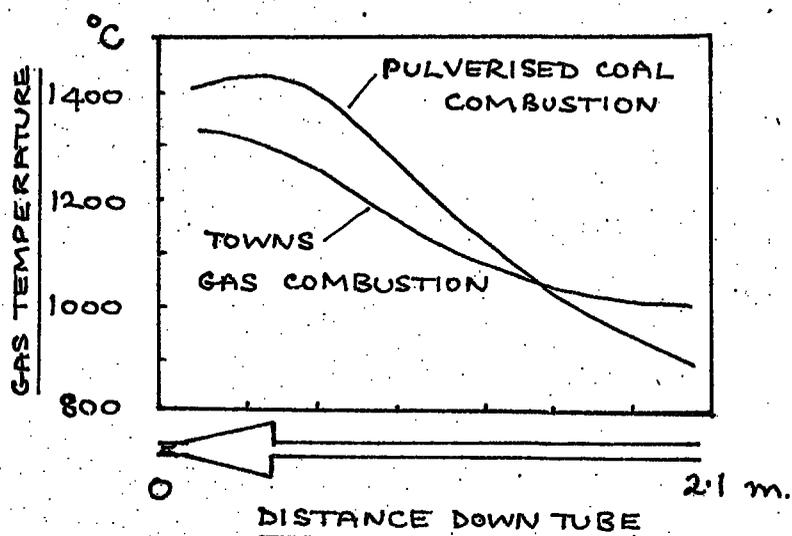
FIGURE 1.17 : GAS TEMPERATURE DISTRIBUTION

Therefore the reverse flow of cool air up the exhaust tube occurred
to a far greater extent in the combustor of Sommers than in that of
Hanby and Brown, and this perhaps explains the difference in shape
of the gas temperature distributions in the two combustors.   Hanby
and Brown finally measured a noise level of 80 dB. near their furnace
and concluded that considerable work on this aspect of pulsating
combustion was necessary before an industrial use of the process could
be envisaged.

1.3   Heat transfer in unsteady flow

The subject of heat transfer in unsteady flow has received
considerable attention since the work of Martinelli and Boelter (26)
in 1938.   They found that the rate of heat transfer increased with
increasing amplitude of vibration beyond a critical value of Reynolds
number of approximately 1000.

In 1943 Martinelli et al. (27) measured heat transfer between
condensing steam and water flowing in a vertical concentric-tube heat
exchanger.   The data for the heat transfer coefficients in steady flow
were obtained using a centrifugal pump, and those for periodic flow,
using a reciprocating pump.

The oscillating flow was not strictly sinusoinal.   Keeping the
stroke of the reciprocating pump constant and varying the rotational
speed, N, in the range 13 N 265 r.p.m., enabled the periodic heat
transfer to be examined over the range of frequency, f, $0.22 < f < 44.2$ Hz.
and over 'the periodic Reynolds number', Re, range of $2660 < Re < 77300$.
The experiments showed that frequency per se had little effect on
Nuselt number and that the velocity emplitude was the main parameter.
The results were correlated by the quasi-steady-state method (see

Section 2.4.2), previously used by Schultz-Grunow (28) and Estel (29).

In 1959 Jackson et al. (30) reported an experimental study of the effect of acoustic vibrations on the heat transfer of air flowing through a vertical brass tube, 95 mm. internal diameter by 1.5 m. long. The wall temperature of the tube was maintained at a constant temperature by the condensation of saturated steam at atmospheric pressure onto its outer surface. Heat transfer coefficients were deduced from the quantity of condensate collected by ten collecting cups, equally spaced down the tube. The working fluid, air, was passed through the test section from a plenum chamber by a centrifugal fan and was excited by a horn at the lower end of the tube, the sound pressure level being measured at the mouth of the tube in the plenum chamber. Results were presented for Reynolds number of 2300 over a range of sound pressure level, 108 $<$ SPL $<$ 138 dB., at a frequency of 520 Hz., the third harmonic of the tube under the experimental conditions. It was found that the sound pressure level had little effect upon the heat transfer up to 118 dB., above which the effect was quite marked. This is evident from Figure 1.18, where the distribution of the ratio:

$$\frac{\overline{Nu_p}}{Nu} = \frac{\text{time-averaged Nusselt number in pulsating flow}}{\text{steady state Nusselt number}}$$

against axial displacement has been replotted for two sound pressure levels, 118 dB. and 129 dB., from the data of Jackson. The ratio $\frac{\overline{Nu_p}}{Nu}$ rises to a maximum of 1.8 at $x/L = 0.3$, corresponding to the position of a velocity antinode, and thereafter diminishes approximately linearly, the overall effect being one of an improvement in the heat
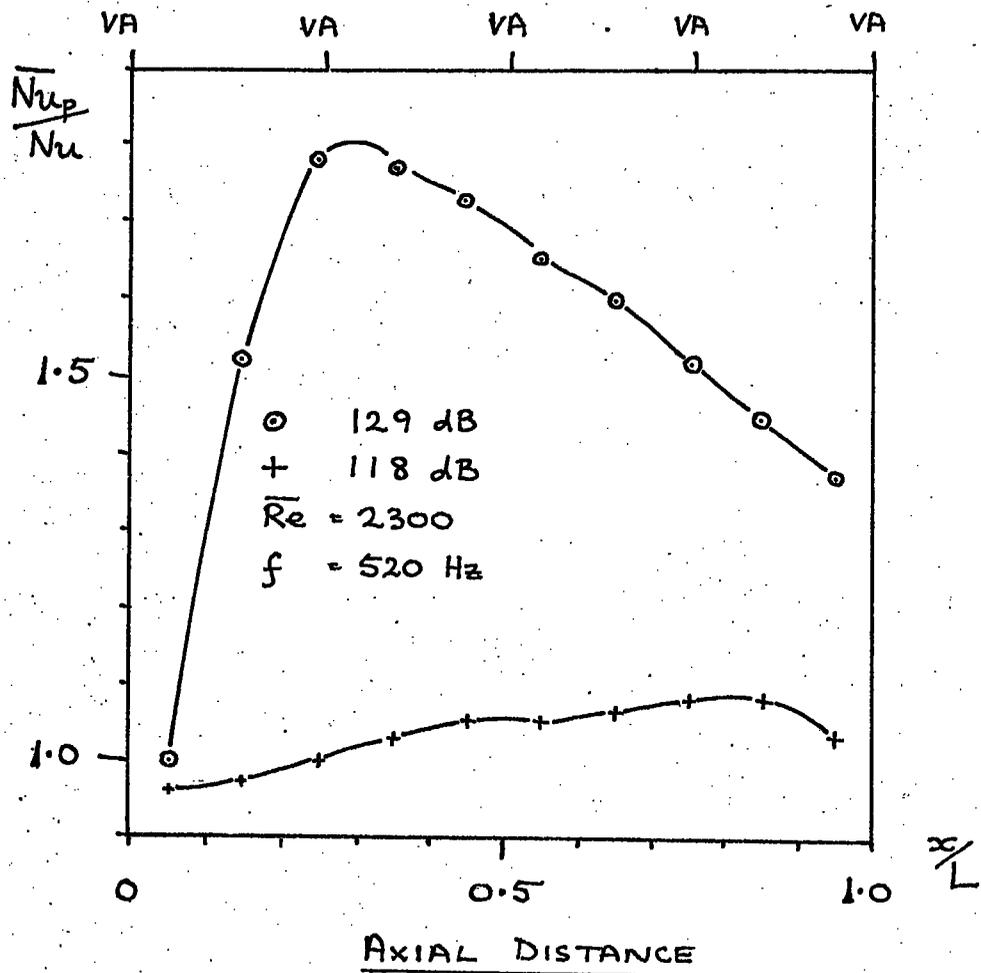
FIGURE 1.18 : GRAPH OF NUSSELT NUMBER RATIO AGAINST DISTANCE FROM DATA OF JACKSON ET AL

transfer.   The authors sought a relationship between the Nusselt
number at any cross-section of the tube and the sound pressure level,
as measured by the microphone, and gave:

$$\overline{Nu}_{P_x} = 2 \cdot 52 \left\{ \frac{\exp(SPL/69 \cdot 5)}{(\overline{Re})^{0 \cdot 25}} \right\} \sqrt{Gz}_x \qquad \qquad 1.3.1$$

which was claimed to be valid within $\pm$ 25% for SPL $\rangle$ 118 dB.   Using
further data for resonant frequencies of 125, 250 and 2000 Hz. obtained
under otherwise similar conditions, a further empirical relationship,
incorporating a frequency term, was given:

$$\overline{Nu}_{P_x} = 5 \cdot 7 \left\{ \frac{\exp(SPL/69 \cdot 5)}{(\overline{Re})^{0 \cdot 25} f} \right\} \sqrt{Gz}_x \qquad \qquad 1.3.2$$

which was valid within $\pm$ 16% if the data for 125 Hz. were ignored.
The authors concluded that it was difficult to separate the effect of
frequency upon heat transfer from that of sound pressure level, an
observation also made by Martinelli.

In 1961 Zartmann and Churchill (31) reported an investigation into
the effect of combustion-driven oscillations on the local heat transfer
coefficients in a water-cooled cylindrical burner, 125 mm. internal
diameter and 0.68 m. long.   Preliminary studies (32) had shown that
intense longitudinal and transverse oscillations could be attained in
such a tube over the range of flow, Re = 5000 to 20000.   The frequency
of the longitudinal oscillations in the water-cooled burner was found
to be 350 Hz, and that of the transverse oscillations to be 4000 Hz.
The combustion was stabilized by a bluff-body flame-holder, upstream
of which was sited a microphone to measure the sound pressure level.

POSITION OF VELOCITY
ANTINODES
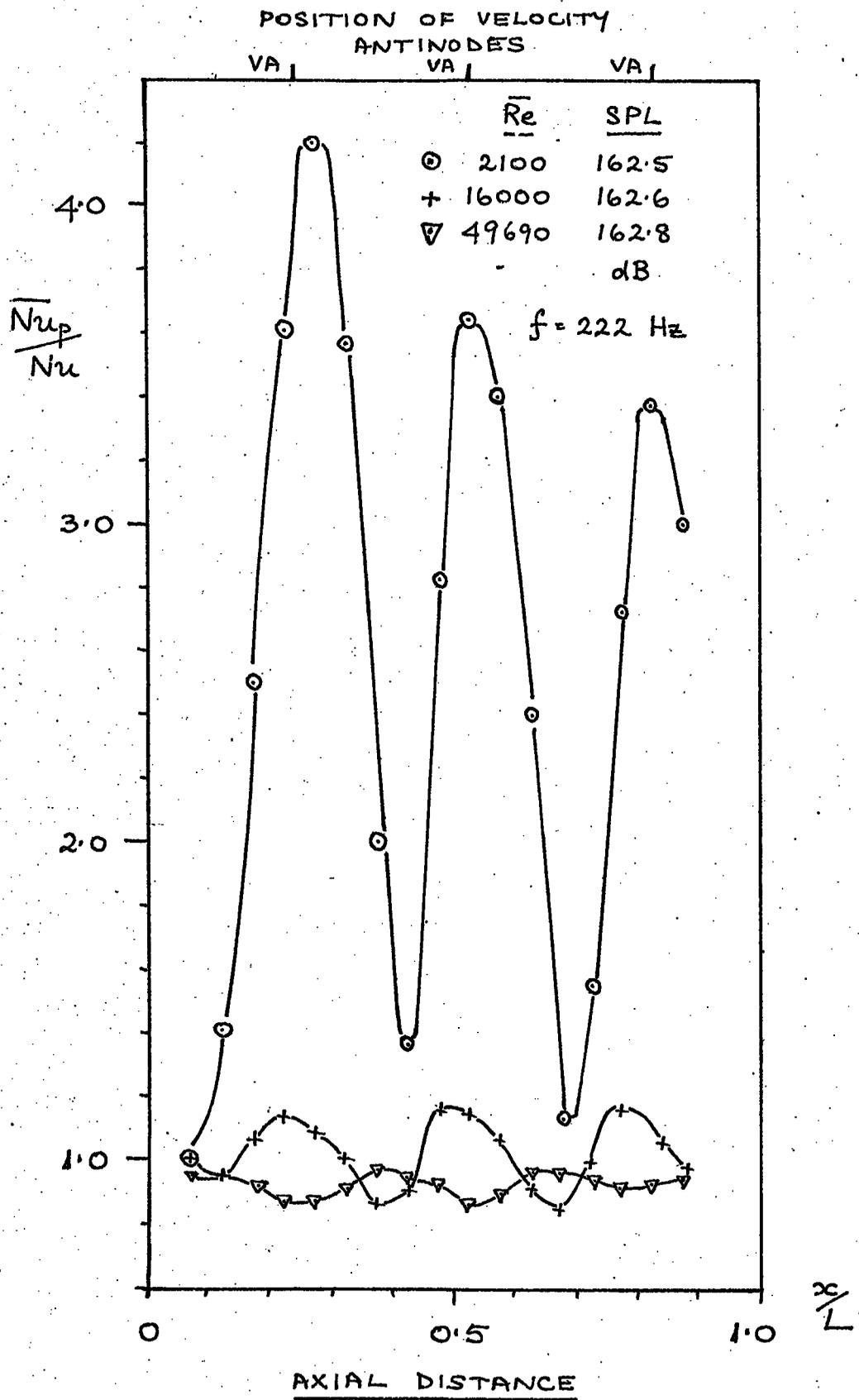
FIGURE 1.19 : GRAPH OF NUSSELT NUMBER
RATIO AGAINST DISTANCE
FROM JACKSON & PURDY

This was found to be 130 dB. in the absence of oscillations, and to vary from 148 to 155 dB with oscillations. From measurements of the local heat transfer coefficient with and without oscillations, the authors obtained a linear correlation between $\overline{Nu}_p$ and $\hat{p}$ of the form:

$$\frac{\overline{Nu}_p}{\overline{Nu}} = A\frac{\hat{p}}{\overline{P}} + B$$

where A and B are constants. This result was consistent with that of Harrje (33) who also observed a linear increase in forced convection heat transfer with pressure amplitude.

In 1965 Jackson and Purdy (34) reported a study of the performance of a simple convective heat exchanger under the influence of acoustic oscillations. The apparatus was similarly constructed to that of (30), except that it was sited horizontally. Air was passed through a copper tube, 98 mm. internal diameter by 3.0 m. long, the walls of which were maintained at a constant temperature. The sound field was introduced by a horn placed at the exit of the tube, and the sound pressure level could be measured at any cross-section by a microphone mounted on a rod inserted into the tube from the upstream end. Heat transfer coefficients were deduced from the quantity of condensate cooled over lengths of 153 mm., and the range of experimental conditions was $2000 < Re < 200,000$ and $0 < SPL < 163$ dB. Results were presented for Re = 2100, 16,000 and 49,690 for the sound pressure level range of 152 to 163 dB., and three of the tests have been replotted in Figure 1.19, which again shows the variation of the ratio $\frac{\overline{Nu}_p}{\overline{Nu}}$ with axial displacement, x/L. It is evident from the graph that, except for Re = 49,690, the maximum values of $\frac{\overline{Nu}_p}{\overline{Nu}}$ occur at the velocity antinodes,

that the maxima of $\dfrac{\overline{Nu_p}}{Nu}$ for Re = 2100 decrease along the tube, and that the effect of the oscillations at Re = 16000 and 49,690 is considerably less than at Re = 2100. The authors correlated the ratio $\dfrac{\overline{Nu_p}}{Nu}$ with axial position in the tube using the relationships given in Table 1.B.

Table 1.B   Correlations of Jackson and Purdy

$\overline{Re}$	$\dfrac{\overline{Nu_p}}{Nu}$
2100	$\left[1 + \dfrac{A_3}{P_r^{0.167}} \left(\dfrac{\lambda}{\nu} \right) \dfrac{\hat{u}^2}{\bar{u}} \cos^2 \left(\dfrac{2\pi x}{\lambda} \right) \cos^2 (\omega t) \right]^{0.4}$
16000	$A_2 \left(\dfrac{\hat{u}}{\bar{u}} \right)^{0.8} \left[1 + \cos \left(\dfrac{4\pi x}{\lambda} \right) \right]^{0.4}$
49690	$1 - A_1 \left(\dfrac{\hat{u}}{\bar{u}} \right)^2 \left\{ 1 + \cos \left(\dfrac{4\pi x}{\lambda} \right) \right\}$
	where A_1 A_2 A_3 are constants.

It is interesting to note that, apart from the transcendental terms, the ratio $\dfrac{\hat{u}}{\bar{u}}$ occurs in each equation. This ratio signifies

$$\dfrac{\text{velocity amplitude of the oscillation}}{\text{mean flow velocity}}$$

at any cross-section of the tube, and, for an acoustic oscillation in an isothermal gas, varies sinusiodally in amplitude along the tube. From the information provided in the paper, the values of $\dfrac{\hat{u}}{\bar{u}}$ at the velocity antinodes have been calculated and are given in Table 1.C., together with the corresponding mean values of $\dfrac{\overline{Nu_p}}{Nu}$.

Table 1.C Calculated $\hat{u}/\bar{u}$ from Jackson and Purdy

$\overline{Re}$	$\dfrac{\overline{Nu_p}}{Nu}$	$\hat{u}/\bar{u}$
2100	3.74	26.3
16000	1.16	3.5
49690	0.87	1.1

Table 1.C has been plotted in Figure 1.20 and may be seen to be approximately linear, although it is unfortunate that there is a lack of data in the range $6 < \dfrac{\hat{u}}{\bar{u}} < 22$. The equation of the line is:

$$\frac{\overline{Nu_p}}{Nu} = 0.72 + 0.114\,\frac{\hat{u}}{\bar{u}} \qquad\qquad 1.3.3$$

It may be concluded tentatively from these estimates that, at any cross-section of the tube, the heat transfer coefficient is linearly dependent on the dimensionless velocity amplitude. In this paper, Jackson and Purdy regarded the flow of air through the tube at Re = 2100 as laminar, which is a questionable assumption. The transition from the laminar to the turbulent regime has been studied by Miller and Fejer (35) who examined the flow of air over a flat plate under the influence of oscillations produced by a set of rotating butterfly valves. The frequency of the oscillations could be varied from 4 to 125 Hz., and the range of dimensionless velocity amplitude was $0.585 < \dfrac{\hat{u}}{\bar{u}} < 0.667$. The value of the transitional Reynolds number was found to be 954,000 under steady flow conditions but, under the influence of the oscillations, it varied from only 350,000 to 200,000 and was independent of frequency.

FIGURE 1.20: GRAPH OF NUSSELT NUMBER RATIO AGAINST VELOCITY AMPLITUDE RATIO FROM DATA OF JACKSON & PURDY
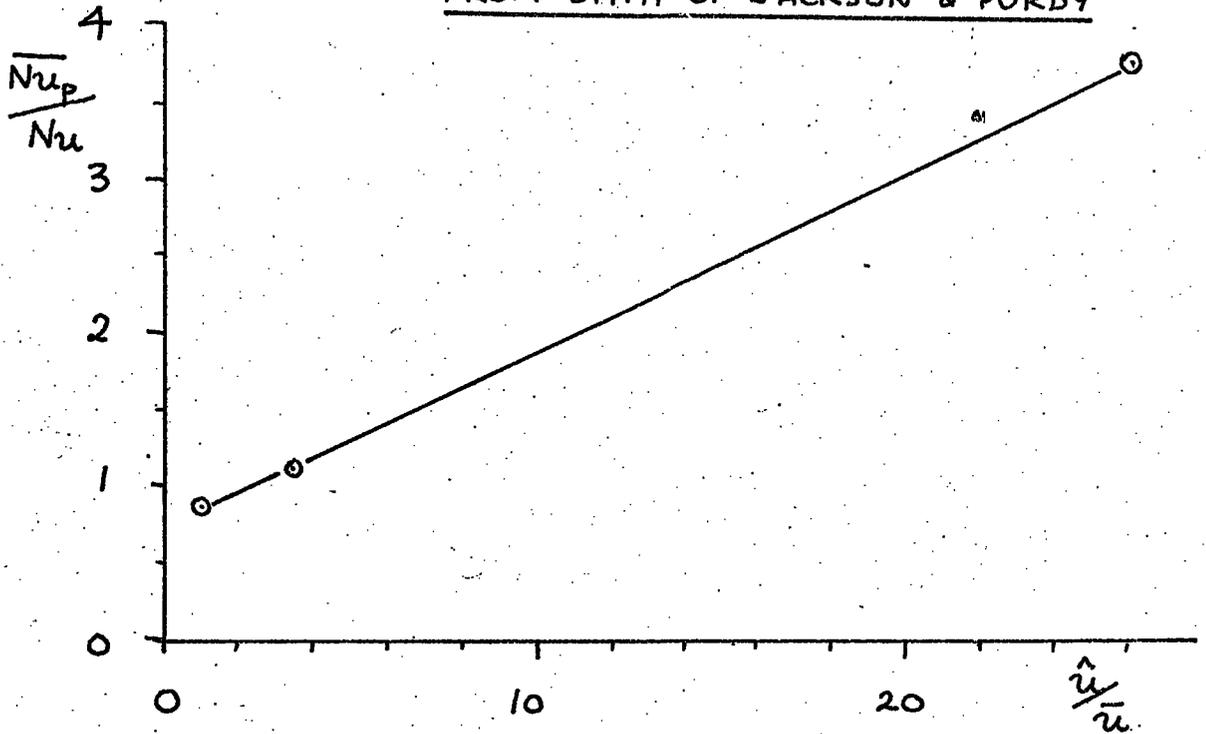

FIGURE 1.21: GRAPH OF NUSSELT NUMBER RATIO AGAINST DISTANCE FROM KOSHKIN
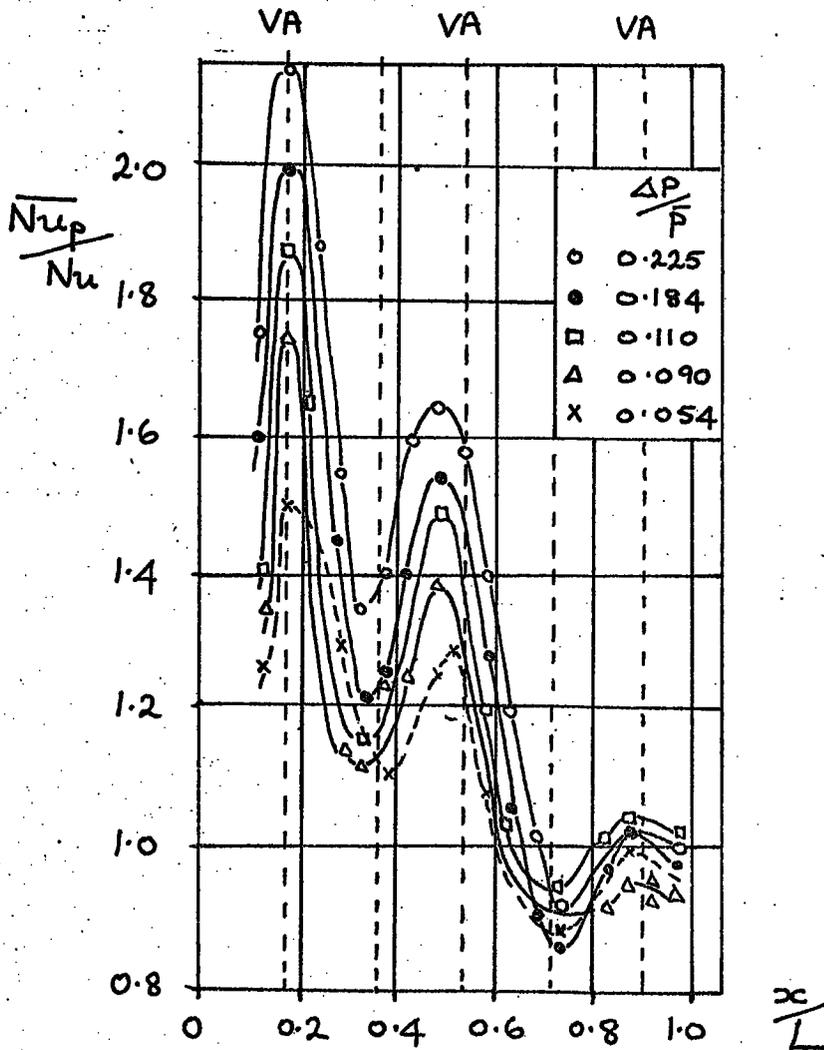
These results are not directly applicable to flow through tubes, as
the Reynolds numbers are based on length, but the work indicates that
the onset of transition is advanced by macroscopic oscillations in a
flow and that the transitional Reynolds number decreased with increasing
dimensionless velocity amplitude.   In 1964 Purdy et al. (36) reported
a theoretical examination of the effect of oscillations on laminar
flow and supported their hypothesis of 'standing vortices' with a
visualization study, using a smoke-filled transparent tube.   It is
notable that, in these experiments, the flow did not exceed a Reynolds
number of 478.   Furthermore, Martinelli and Boelter (26) observed
that the rate of heat transfer increased with increasing velocity
amplitude only when a Reynolds number of 1000 was exceeded.   This
worker feels that, for moderate values of Reynolds number and of
dimensionless velocity amplitude, an approximate estimate of the
transition from the laminar to the turbulent regime in oscillating
flow through a tube may be gained by consideration of the instantaneous
Reynolds number;   if, at any instant during the cycle of oscillation,
the instantaneous Reynolds number approaches 2000, then the flow may
be regarded as on the point of transition.

In 1966 Koshkin et al. (37) reported a study of time-averaged
heat transfer rates in an acoustically-closed tube for a wide range
of experimental conditions.   The apparatus consisted of a stainless
steel tube, 5.4 mm. internal diameter by 1.2 mm. long, which was heated
by passing low voltage alternating current through its length.
Ambient air was passed through the tube at pressures between 5 to 20
bar for Reynolds numbers of 10,000 and 100,000 and was excited by a
rotating valve at the resonant frequencies of the tube, 90, 180, 270

360 and 450 Hz. The pressure amplitude was expressed as a fraction of the working pressure, and the range studied was $0.01 < \dfrac{\Delta P}{\bar{P}} < 0.25$. The flow was claimed to be hydrodynamically developed at the entrance to the test section. The results of the work showed that the maxima of $\dfrac{\overline{Nu_p}}{Nu}$ occurred at the velocity antinodes, as is evident in Figure 1.21. For this range of Reynolds numbers, the evidence conflicts with that of Jackson and Purdy (Figure 1.19), although the frequencies of the two sets of data, 270 and 222 Hz. respectively, are not dissimilar. It is possible that the ratio $\dfrac{\hat{u}}{\bar{u}}$ in the work of Koshkin et al was far greater than in the case of Jackson (see Table 1.C) but, due to the method of presentation of the experimental conditions, the values of $\dfrac{\hat{u}}{\bar{u}}$ in the Russian work remain obscure and further comparison is of dubious value. Koshkin et al. made an analysis of the effects of the oscillations on heat transfer in their apparatus and proposed that the ratio $\dfrac{\overline{Nu_p}}{Nu}$ was proportional to $\dfrac{\hat{E}}{\bar{E}}$, given by:

$$\frac{\hat{E}}{\bar{E}} = \frac{\text{amplitude of kinetic energy in oscillation}}{\text{mean kinetic energy of flow}}$$

The analysis took into account energy dissipation down the tube and also considered the non-isothermal effects in the flow. Due to the temperature gradient in the tube, the velocity of sound was regarded as a function of axial distance, and thus mean velocity of sound was given by:

$$\bar{c}_x = \frac{1}{x} \int_0^x c(x)\, dx \qquad\qquad 1.3.4$$

It was concluded that for any value of $\frac{\Delta P}{\bar{P}}$ the distribution of $\frac{\overline{Nu_p}}{Nu}$ along the tube followed that of $\frac{\hat{E}}{\bar{E}}$ closely, but, due to the method used to normalize coefficients, again it is difficult to pursue the analyses further.

In 1967 Galitseysky et al. (38) reported a study of the effect of longitudinal oscillations on heat transfer in a tube when the driving frequency was displaced from resonance. The apparatus and experimental conditions were very similar to those of Koshkin (37) except that the tube diameter was 9.7 mm. and the frequency range 45 to 135 Hz. The experiments showed that the maximum value of $\frac{\overline{Nu_p}}{Nu}$ occurred at 90 Hz., the fundamental of the tube, and that at the extreme anti-resonant frequencies of 45 and 135 Hz., the heat transfer data compared closely with the steady state values. The authors made an analyses in this paper of the non-isothermal and dissipation effects in the tube. The velocity of sound, c, was, as before, regarded as a function of the axial co-ordinate, x, and, by introducing a change of variable, q_x, the acoustic wave equation was re-expressed:

$$\frac{\partial^2 \Delta(\rho u)}{\partial t^2} = \frac{\partial^2 \Delta(\rho u)}{\partial q_x^2} \qquad 1.3.5$$

where

$$q_x = \int_o^x \frac{dx}{c(x)}$$

Then, by assuming a perfect gas, the distribution of $\frac{\hat{E}}{\bar{E}}$ in the tube was obtained:

$$\frac{\hat{E}}{\bar{E}} = \frac{1}{2\nu}\left(\frac{\Delta P}{\bar{P}}\right)_{max}^2 \left\{ \sin\left(n\pi \frac{q_x^*}{q_L^*}\right)\right\}^2 \qquad 1.3.6$$

where $\frac{q_x^*}{q_L^*}$ represented a further change of variable to permit the

analysis of resonant frequencies. This expression, 1.3.6, was
expanded to the case of non-isothermal flow of a viscous gas by
assuming that the kinetic energy of the oscillations attenuated
exponentially along the tube:

$$\frac{\hat{E}}{\bar{E}} = \frac{1}{2\mu}\left(\frac{\Delta P}{\bar{P}}\right)^2_{max} exp\left(-\phi_{AT}\frac{q^*_x}{q^*_L}\right)\left\{sin\left(n\pi\frac{q^*_x}{q^*_L}\right)\right\}^2 \quad 1.3.7$$

where ϕ_{AT} was the pulsation energy attenuation factor.

In 1968 Hanby (39) reported an experimental investigation of
the effect of combustion-driven oscillations on convective heat
transfer. The apparatus consisted of a stainless steel tube, 51 mm.
internal diameter by 1.9 m. long, which was water cooled for most of
its length. Propane and air were injected under pressure at one end
of the tube, which, being thus constricted, behaved as an acoustically-
closed end. Two water-cooled cylinders with adjustable pistons were
attached to the main tube at the closed end, so that the amplitude of
the oscillations could be controlled. The local heat transfer
coefficients were measured directly at five points along the tube by
means of a heat flux transducer. Results were obtained for Reynolds
numbers of 6000 to 16,000, and, from the data provided, $\frac{\overline{Nu_p}}{Nu}$ has
been plotted against $\frac{x}{L}$ in Figure 1.22. It is evident that these
results are in accord with those of Jackson and Purdy in Figure 1.19
over this range of Reynolds numbers. The maximum of $\frac{\overline{Nu_p}}{Nu}$ occurs in
the region of the velocity antinode at the open end of the tube, and
the minimum near the combustion zone, a velocity node. In these
experiments, the pressure amplitude was found to vary approximately
sinusoidally along the tube, from a maximum of 38 kN/m^2 (186 dB.) to
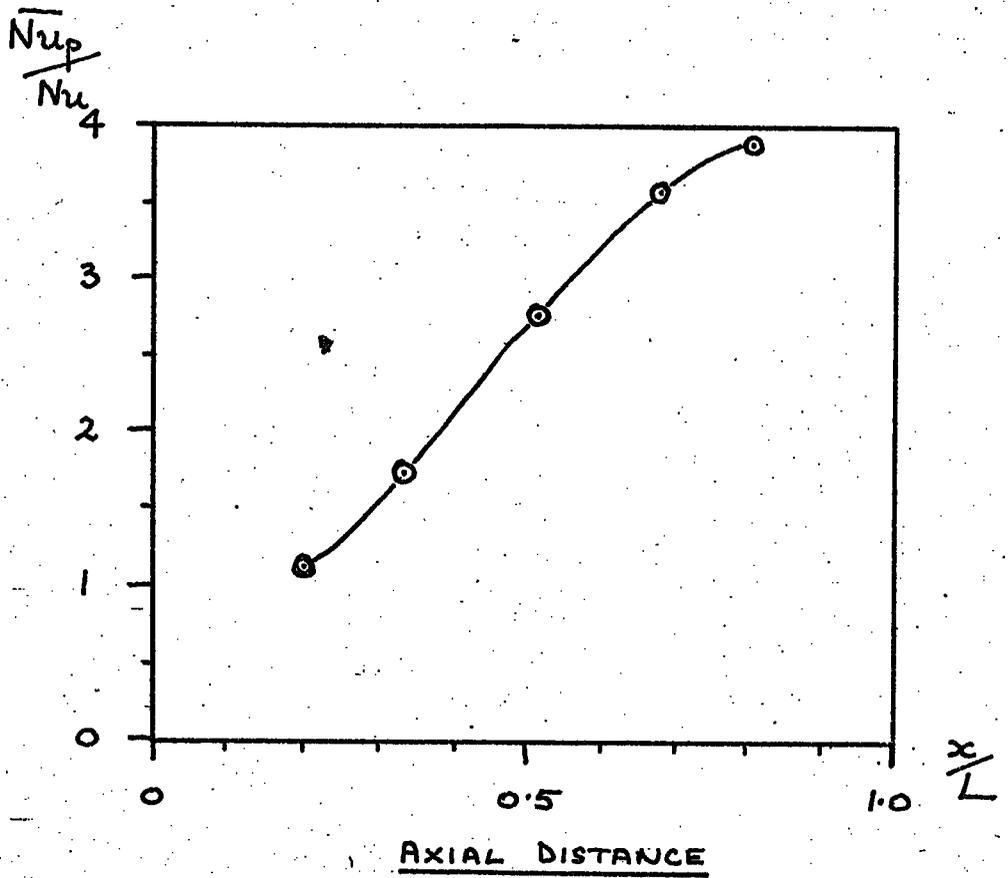
FIGURE 1.22 : GRAPH OF NUSSELT NUMBER
RATIO AGAINST DISTANCE
FROM HANBY

zero at the open end. This level is greatly in excess of those found in the apparatus of Jackson et al. (30) or Jackson and Purdy (34). Hanby used acoustic relationships, based on the one-dimensional wave equation, to derive an expression for the dimensionless velocity amplitude:

$$\frac{\hat{u}}{\bar{u}} = \frac{\hat{p}}{\bar{p}} \frac{c}{\mu} \tan\left(\frac{2\pi x}{\lambda}\right) \qquad 1.3.8$$

An analysis of the effect of the oscillations on heat transfer was made, using the quasi-steady state approach (see Section 2.4.2); then, by assuming that the gas particle velocity in an acoustic wave superimposed on a mean flow could be represented by:

$$u = \bar{u}\left(1 + \frac{\hat{u}}{\bar{u}} \cos \omega t\right) \qquad 1.3.9$$

it was shown that:

$$\frac{\overline{Nu_p}}{Nu} = \frac{1}{2\pi} \int_0^{2\pi} \left(\left|1 + \frac{\hat{u}}{\bar{u}} \cos \omega t\right|\right)^{0.8} d\omega t \qquad 1.3.10$$

The result of a numerical integration of 1.3.10 is shown in Figure 2.6, and Hanby found that his experimental data fitted this curve to a standard deviation of ±5% over the range of possible values, $0.5 < \frac{\hat{u}}{\bar{u}} < 4.8$. This graph, 2.6, is very similar to that of Figure 1.20, as both show an approximately linear increase in $\frac{\overline{Nu_p}}{Nu}$ with $\frac{\hat{u}}{\bar{u}}$ greater that 1.0, but the slopes are not the same, being 0.377 and 0.114 respectively.

1.4 Aims of the Investigation

The review of previous work revealed that studies of the
effect of longitudinal oscillations on local heat transfer
coefficients using sirens and microphones were reasonably numerous.
Also there existed a number of investigations into pulsating combustors
of various designs. The only studies of local heat transfer
coefficients in pulsating combustors were those of Hanby and Reay,
who used a closed-open organ pipe and flap-valves respectively. It
was decided to study a pulsating combustor with an aerodynamic valve,
and to measure local heat transfer coefficients between the hot
combusted gases and the heat exchanger wall. The results of this
could be correlated in a similar manner to that used by Hanby, whose
work indicated a dependence of $\dfrac{\overline{Nu}_p}{\overline{Nu}}$ on the local dimensionless
velocity amplitude, $\dfrac{\hat{u}}{\bar{u}}$. As Hanby had ignored non-isothermal
effects, it was decided to make an analysis the propagation of sound
waves through a gas exhibiting a severe temperature gradient in one
direction. Due to the complexity of operation of combustors with
aerodynamic valves, it was hoped to make a contribution to the under-
standing of the subject. Finally, it was decided to attempt a
simplified analysis of the flow capacity of the aerodynamic valve.

2.1 Acoustic Wave Equation - Isothermal Fluid

The acoustic wave equation for plane waves of small waves of small amplitude propagating through an isothermal compressible fluid is:

$$\frac{\partial^2 \zeta}{\partial t^2} = c^2 \frac{\partial^2 \zeta}{\partial x^2} \qquad 2.1.1$$

The solutions to this equation for the case of standing waves in a straight, rigid duct of large L/d , closed at $x = 0$ and open at $x = L$, are:

$$\zeta(x,t) = \frac{\hat{p}_o c}{\omega B_A} \sin(\omega t) \sin\left(\frac{\omega x}{c}\right) \qquad 2.1.2$$

$$u(x,t) = \frac{\hat{p}_o c}{B_A} \sin\left(\omega t + \frac{\pi}{2}\right) \sin\left(\frac{\omega x}{c}\right) \qquad 2.1.3$$

$$p(x,t) = \hat{p}_o \sin(\omega t) \cos\left(\frac{\omega x}{c}\right) \qquad 2.1.4$$

$$\omega = \frac{\pi c (2n-1)}{2L} \qquad n = 1, 2, 3 \ldots \qquad 2.1.5$$

The boundary conditions and co-ordinates for this system are shown in Figure 2.1.

2.2 Acoustic Wave Equation - Exponential variation of Fluid Temperature

Now consider the propagation of plane waves of small amplitude through a compressible fluid which, as before, is confined in a straight, rigid duct of large L/d but whose temperature varies exponentially along it, as shown in Figure 2.2. For a perfect gas, the velocity of sound is a function of the absolute temperature only. Therefore, if the variation in the fluid temperature is written:

$$T = T_o e^{-2\alpha x} \qquad 2.2.1$$

$\xi(0,t) = 0$

$u(0,t) = 0$

$p\left(0, \dfrac{(2n-1)\pi}{\omega}\right) = \hat{p}_0$
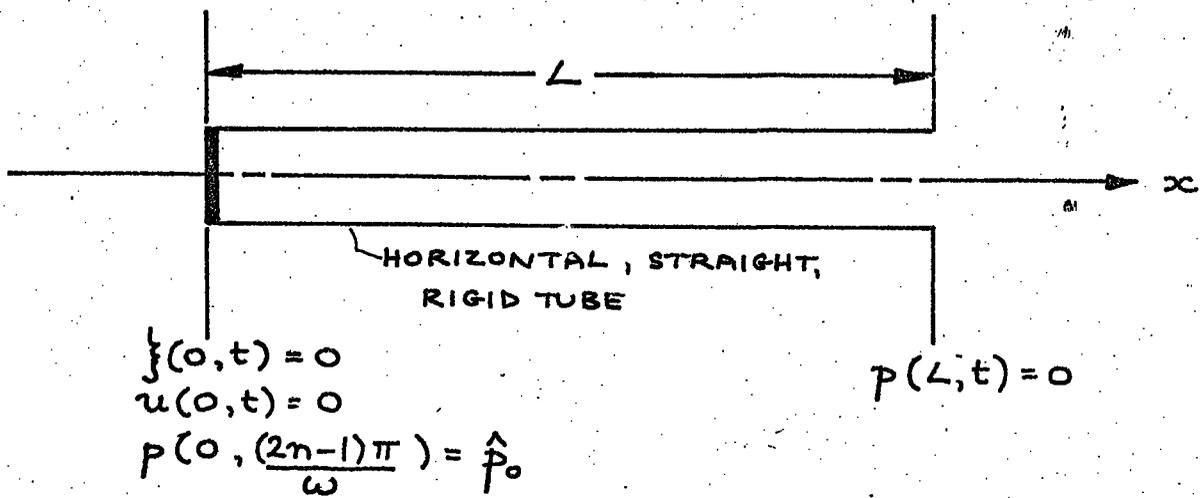
FIGURE 2.1 : BOUNDARY CONDITIONS & CO-ORDINATE
SYSTEM FOR ISOTHERMAL FLUID

$\bar{\bar{T}} = T_0 e^{-2\alpha x}$

$\bar{\bar{T}} = \bar{\bar{T}}(x)$
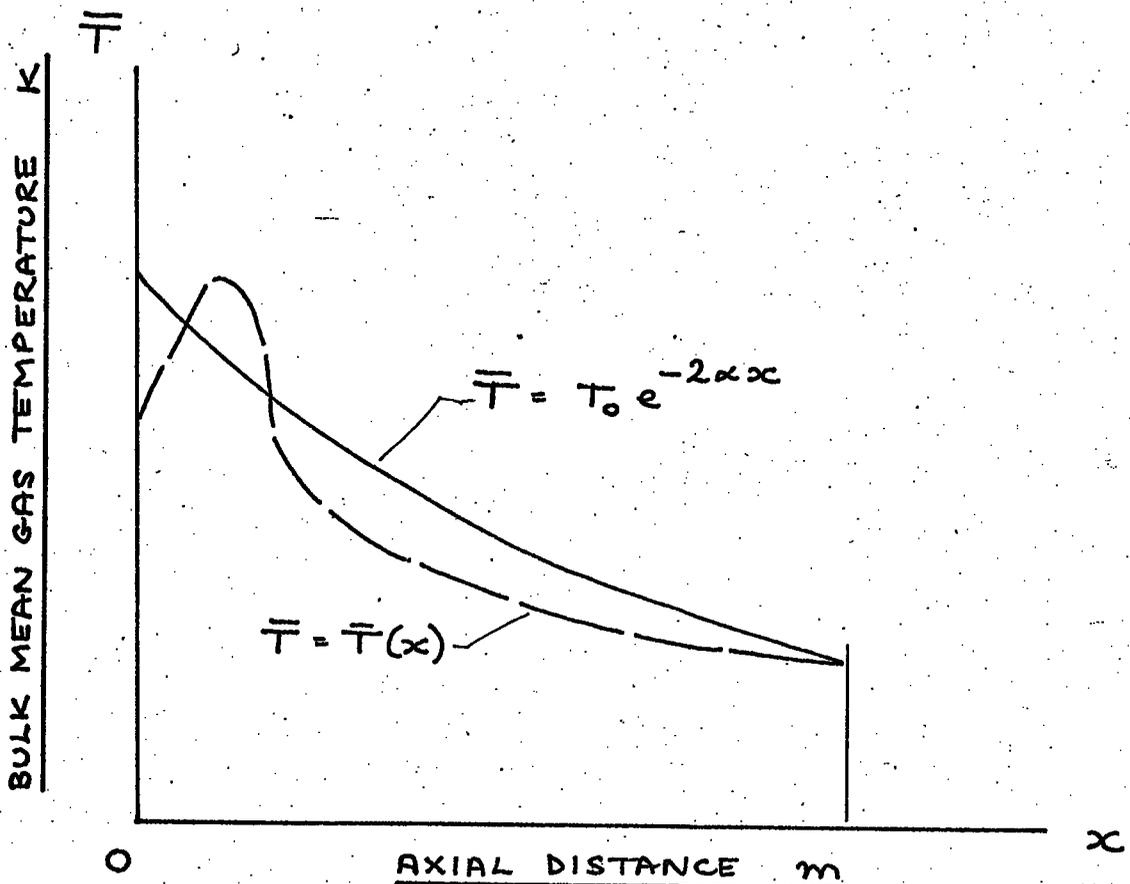
FIGURE 2.2 : EXPONENTIAL AND GENERAL VARIATIONS
OF GAS TEMPERATURE ALONG TUBE

the variation in the velocity of sound becomes:

$$c = c_0 e^{-\alpha x}$$

2.2.2

The wave equation 2.1.1 may be solved with c now being a function of x.
Putting:

$$\zeta(x,t) = X(x)\,\theta(t)$$

2.2.3

and separating variables, 2.1.1 becomes:

$$c^2 \frac{X''}{X} = \frac{\ddot{\theta}}{\theta} = -\omega^2$$

2.2.4

where ω is the separation constant. Thus

$$\ddot{\theta} + \omega^2 \theta = 0$$

2.2.5

and $$X'' + \frac{\omega^2}{c^2} X = 0$$

2.2.6

The solution to equation 2.2.5 is:

$$\theta(t) = A \sin(\omega t + \varepsilon)$$

2.2.7

where A and ε are constants. Substitution of 2.2.2 into equation
2.2.6 yields:

$$X'' + \lambda^2 e^{2\alpha x} X = 0$$

2.2.8

where $$\lambda = \frac{\omega}{c_0}$$

2.2.9

Now putting $$z = \frac{\lambda}{\alpha} e^{\alpha x}$$

2.2.10

and substituting into equation 2.2.8 gives:

$$\frac{d^2 X}{dz^2} + \frac{1}{z}\frac{dX}{dz} + X = 0 \qquad 2.2.11$$

provided that $\alpha \neq 0$. Equation 2.2.11 is Bessel's Function of the Second Kind, and the general solution is:

$$X(z) = M_1 J_0(z) + N_1 Y_0(z) \qquad 2.2.12$$

where M and N are constants. Thus the general solution to 2.1.1 for an exponential variation in the velocity of sound is, from 2.2.3:

$$\zeta(x,t) = \left\{ M_1 J_0(z) + N_1 Y_0(z) \right\} A \sin(\omega t + \varepsilon) \qquad 2.2.13$$

Noting that the displacement and pressure in an acoustic wave are related by:

$$p = - B_A \frac{\partial \zeta}{\partial x} \qquad 2.2.14$$

where B_A is the adiabatic bulk modulus of elasticity of the fluid and is independent of temperature, the variation in pressure may be obtained:

$$p(x,t) = - \left\{ M_1 J_1(z) + N_1 Y_1(z) \right\} A \lambda e^{\alpha x} B_A \sin(\omega t + \varepsilon) \qquad 2.2.15$$

Application of the boundary conditions:

$$u(0,t) = 0$$

and

$$p(L,t) = 0$$

from Figure 2.1 yields respectively:

$$M_1 J_1(z_0) + N_1 Y_1(z_0) = 0 \qquad 2.2.16$$

and

$$M_1 J_1(z_L) + N_1 Y_1(z_L) = 0 \qquad 2.2.17$$

where
$$z_0 = \frac{1}{\alpha} \qquad\qquad 2.2.18$$

$$z_L = \frac{1}{\alpha} e^{\alpha L} \qquad\qquad 2.2.19$$

The equations 2.2.16 and 2.2.17 must be solved simultaneously for λ :

$$f(\lambda) \equiv J_0(b\lambda) Y_1(a\lambda) - J_1(a\lambda) Y_0(b\lambda) = 0 \qquad 2.2.20$$

where
$$a = \frac{1}{\alpha} e^{\alpha L} \qquad\qquad 2.2.21$$

$$b = \frac{1}{\alpha} \qquad\qquad 2.2.22$$

The Newton-Raphson method may be used to find the zeroes of $f(\lambda)$ and is of the form:

$$\lambda_{m+1} = \lambda_m - \frac{f(\lambda_m)}{f'(\lambda_m)} \qquad\qquad 2.2.23$$

where $f'(\lambda)$ is given by:

$$f'(\lambda) = -\frac{1}{2} \Big\{ a Y_0(b\lambda)\big[J_0(a\lambda) - J_2(a\lambda)\big]$$
$$+ b J_1(a\lambda)\big[-2Y_1(b\lambda)\big] - b Y_1(a\lambda)\big[-2J_1(b\lambda)\big] \qquad 2.2.24$$
$$- a J_0(b\lambda)\big[Y_0(a\lambda) - Y_2(a\lambda)\big] \Big\}$$

The particular solutions to the wave equation 2.1.1 for an exponential variation in the velocity of sound are, therefore:

$$\xi(x,t) = \frac{\hat{p}_0 c_0}{\omega B_A} \sin(\omega t) \big\{ M_1 J_0(z) + N_1 Y_0(z)\big\} \qquad 2.2.25$$

$$u(x,t) = \frac{\hat{p}_0 c_0}{B_A} \sin(\omega t + \tfrac{\pi}{2})\big\{ M_1 J_0(z) + N_1 Y_0(z)\big\} \qquad 2.2.26$$

$$p(x,t) = \hat{p}_0 \sin(\omega t) e^{\alpha x}\big\{ M_1 J_1(z) + N_1 Y_1(z)\big\} \qquad 2.2.27$$

where
$$M_1 = \frac{-Y_0(z_0)}{\big[J_0(z_0) Y_1(z_0) - J_1(z_0) Y_0(z_0)\big]} \qquad 2.2.28$$

$$N_1 = \frac{J_0(z_0)}{\big[J_0(z_0) Y_1(z_0) - J_1(z_0) Y_0(z_0)\big]} \qquad 2.2.29$$

2.3 General Wave Equation - Arbitrary Variation in Fluid Temperature

Consider now a flow of hot gas through a smooth, horizontal tube, the hot end of which behaves as though acoustically closed, and the cold end of which as though acoustically open (see Figure 2.3). As convective heat transfer occurs between the hot gas and the externally-cooled wall of the tube, the temperature of the gas falls in the direction of flow as shown in Figure 2.2. Therefore, the time-averaged temperature, $\overline{T}$, may be regarded as a function of x:

$$\overline{T} = \overline{T}(x) \qquad\qquad 2.3.1$$

and, as the problem is effectively one-dimensional, changes in the y and z directions may be ignored. Consider the elemental control volume in Figure 2.4; equating the rate of increase of mass within the control volume with the rate of efflux minus the rate of influx yields:

$$\frac{\partial \rho}{\partial t}\,\delta x\,\delta y\,\delta z = \left(\rho + \frac{\partial \rho}{\partial x}\,\delta x\right)\left(u + \frac{\partial u}{\partial x}\,\delta x\right)\delta y\,\delta z - \rho u\,\delta y\,\delta z$$

Ignoring quadratic terms, the conservation of mass equation becomes:

$$\frac{\partial \rho}{\partial t} + u\frac{\partial \rho}{\partial x} + \rho\frac{\partial u}{\partial x} = 0 \qquad\qquad 2.3.2$$

Equating the forces acting on the element with the rate of change of momentum yields:

$$p\,\delta y\,\delta z - \left(p + \frac{\partial p}{\partial x}\,\delta x\right)\delta y\,\delta z = -\rho\,\delta x\,\delta y\,\delta z\,\frac{Du}{Dt}$$

and the equation of motion becomes, for an inviscid fluid:

$$\frac{\partial p}{\partial x} + \rho\frac{\partial u}{\partial t} + \rho u\frac{\partial u}{\partial x} = 0 \qquad\qquad 2.3.3$$

$$u'(o,t) = o$$
$$p'(0, \frac{(2n-1)\pi}{\omega}) = \hat{p}_o$$
$$\bar{u} = \bar{u}_o$$

$$p'(o,t) = o$$
$$\bar{u} = \bar{u}_L$$
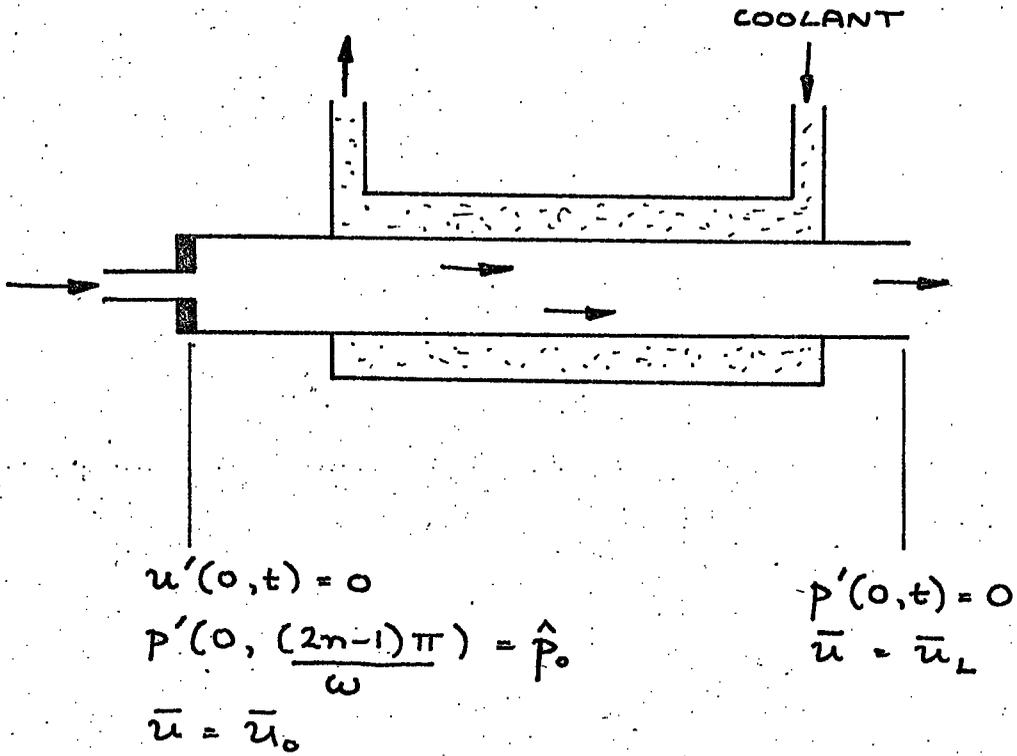
FIGURE 2.3 : OSCILLATING FLOW OF COMPRESSIBLE FLUID THROUGH SIMPLE HEAT EXCHANGER
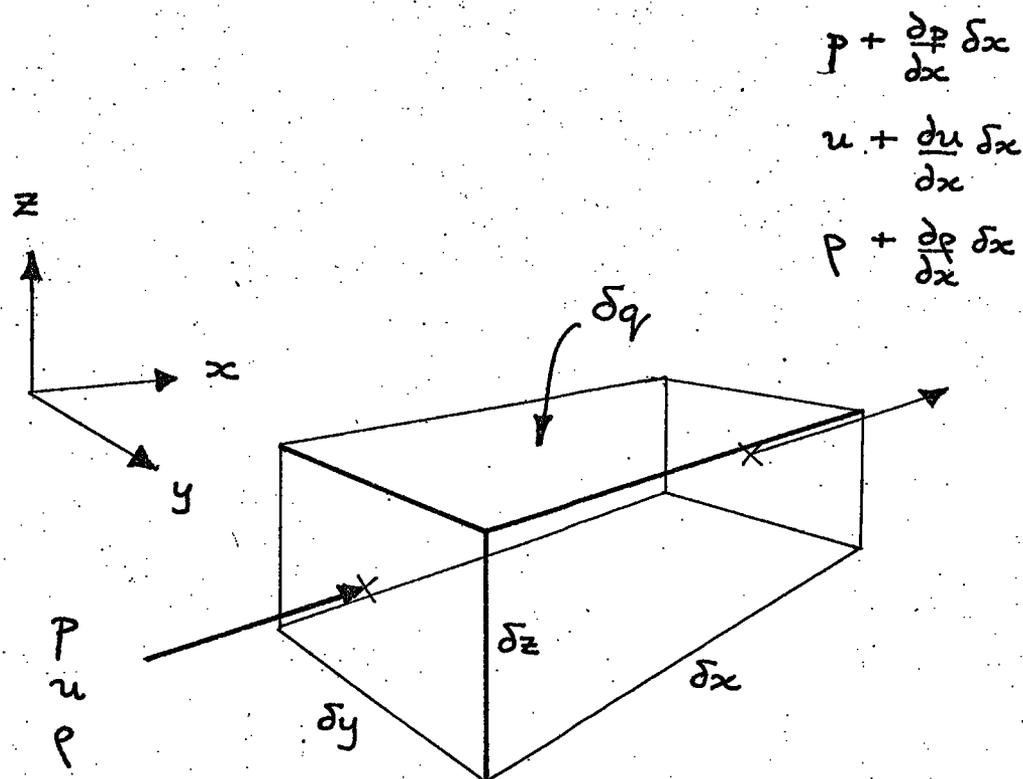
FIGURE 2.4: ELEMENTAL CONTROL VOLUME OF THE SYSTEM SHOWN IN FIGURE 2.3

Equating the rate of change of internal energy of the element with the heat and work transfers from the surroundings yields:

$$\rho\, \partial x\, \partial y\, \partial z\, \frac{De}{Dt} = p\, u\, \partial y\, \partial z - \left\{ \left(p + \frac{\partial p}{\partial x}\delta x \right) \times \right.$$

$$\left. \left(u + \frac{\partial u}{\partial x}\delta x \right)\delta y\, \delta z \right\} + \delta q\, 2(\delta x\, \delta y + \delta x\, \delta z)$$

and the conservation of energy equation, in the absence of capillary, magnetic and electric effects, becomes:

$$\rho\,\frac{De}{Dt} + u\,\frac{\partial p}{\partial x} + p\,\frac{\partial u}{\partial x} = \frac{\partial q}{\partial x} \qquad\qquad 2.3.4$$

Consider now the effect of small perturbations on the flow, such that:

$$p = \bar{p} + p' \qquad\qquad 2.3.5.$$

$$u = \bar{u} + u' \qquad\qquad 2.3.6$$

$$\rho = \bar{\rho} + \rho' \qquad\qquad 2.3.7$$

the equations 2.2.3, 2.3.3 and 2.3.4 may now be examined again. From the equation of state of a perfect gas, it is evident that:

$$\frac{p'}{\bar{p}} = \frac{\rho'}{\bar{\rho}} \qquad\qquad 2.3.8$$

The analysis will now be limited to pressure amplitudes, $\hat{p}'$, such that:

$$\frac{\hat{p}'}{\bar{p}} < 0.15 \qquad\qquad 2.3.9$$

as recommended by Bogdanoff (40). The approximations may then be made:

$$\frac{\partial p}{\partial x} \doteqdot \frac{\partial \bar{p}}{\partial x} \qquad\qquad \frac{\partial \rho}{\partial x} \doteqdot \frac{\partial \bar{\rho}}{\partial x} \qquad\qquad 2.3.10$$

Consider:

$$\left| u\,\frac{\partial u}{\partial x} \Big/ \frac{\partial u}{\partial t} \right| = O\left(\frac{u^2}{L} \Big/ \omega c \right) \qquad\qquad 2.3.11$$

$$= O\left(\frac{u}{c} \right)^2$$

from equation 2.1.5. Thus, for flows of low Mach number, the term $u \frac{\partial u}{\partial x}$ is negligible compared with $\frac{\partial u}{\partial t}$. Assuming that the time-averaged pressure drop along the tube is negligible:

$$\frac{\partial \bar{p}}{\partial x} \doteq 0 \qquad\qquad 2.3.12$$

and using the definitions:

$$\frac{\partial p}{\partial t} \doteq \frac{\partial p'}{\partial t} \qquad\qquad \frac{\partial \rho}{\partial t} \doteq \frac{\partial \rho'}{\partial t} \qquad\qquad 2.3.13$$

the equations 2.3.2 and 2.3.3 become, respectively:

$$\frac{\partial \rho'}{\partial t} + u \frac{\partial \bar{\rho}}{\partial x} + \bar{\rho} \frac{\partial u}{\partial x} = 0 \qquad\qquad 2.3.14$$

$$\frac{\partial u}{\partial t} + \frac{1}{\bar{\rho}} \frac{\partial p'}{\partial x} = 0 \qquad\qquad 2.3.15$$

and using equation 2.3.14, the energy equation 2.3.4 becomes:

$$\rho \frac{De}{Dt} = \frac{p}{\bar{\rho}} \left\{ \frac{\partial \rho'}{\partial t} + u \frac{\partial \bar{\rho}}{\partial x} \right\} + \frac{\partial q}{\partial x} \qquad\qquad 2.3.16$$

For the flow of a perfect gas with negligible kinetic energy, the specific internal energy, e, may be expressed:

$$e = c_v T = \frac{1}{\mu - 1} \frac{p}{\rho}$$

Therefore:

$$\frac{De}{Dt} = \frac{1}{\mu - 1} \left\{ \frac{1}{\rho} \left(\frac{\partial p}{\partial t} + u \frac{\partial p}{\partial x} \right) - \frac{p}{\rho^2} \left(\frac{\partial \rho}{\partial t} + u \frac{\partial \rho}{\partial x} \right) \right\}$$

Using 2.3.10, 2.3.12 and 2.3.13 and noting that:

$$c^2 = \mu R T$$

equation 2.3.16 becomes:

$$\frac{\partial p'}{\partial t} = c^2 \left(\frac{\partial \rho'}{\partial t} + u \frac{\partial \bar{\rho}}{\partial x} \right) + (\mu - 1) \frac{\partial q}{\partial x}$$

Thus equations 2.3.2, 2.3.3 and 2.3.4 have been reduced to 2.3.14, 2.3.15 and 2.3.18 respectively. Differentiation of equation 2.3.14 with respect to t yields:

$$\frac{\partial^2 u}{\partial x \partial t} = \left\{ \frac{1}{\bar{e}^2} \frac{\partial p'}{\partial x} \frac{\partial \bar{e}}{\partial x} - \frac{1}{\bar{e}} \frac{\partial^2 p'}{\partial x^2} \right\} \qquad 2.3.19$$

and differentiation of equation 2.3.15 with respect to x yields:

$$\frac{\partial^2 u}{\partial t \partial x} = \frac{\partial}{\partial t} \left\{ -\frac{1}{\bar{e}} \left[\frac{1}{c^2} \frac{\partial p'}{\partial t} + (1-\nu) \frac{\partial q}{\partial x} \right] \right\} \qquad 2.3.20$$

using equation 2.3.18. Equating 2.3.19 and 2.3.20 yields:

$$\frac{\partial^2 p'}{\partial x^2} - \frac{1}{\bar{e}} \frac{\partial \bar{e}}{\partial x} \frac{\partial p'}{\partial x} - \frac{1}{c^2} \frac{\partial^2 p'}{\partial t^2} = \frac{1-\nu}{\bar{e}} \frac{\partial^2 q}{\partial t \partial x} \qquad 2.3.21$$

Now q, the heat flux, is dependent on the difference between the bulk mean gas temperature and the tube wall temperature, and thus is dependent on x. For high frequencies, this temperature difference may be regarded as independent of time, due to the thermal inertia of the wall and the small oscillations in the gas temperature. Therefore:

$$\frac{\partial}{\partial t} \left(\frac{\partial q}{\partial x} \right) \preceq 0 \qquad 2.3.22$$

If sinusoidal oscillations of p', u' and e' are now assumed, a solution of the type:

$$p' = p_x \sin(\omega t) \qquad 2.3.23$$

may be used. Equation 2.3.21 then becomes:

$$\frac{\partial^2 p_x}{\partial x^2} - \left(\frac{1}{\bar{e}} \frac{\partial \bar{e}}{\partial x} \right) \frac{\partial p_x}{\partial x} + \frac{\omega^2}{c^2} p_x = 0 \qquad 2.3.24$$

or $\quad \dfrac{d^2 p_x}{dx^2} + \left(\dfrac{1}{\overline{T}} \dfrac{\partial \overline{T}}{\partial x} \right) \dfrac{dp_x}{dx} + \dfrac{\omega^2}{\nu RT} p_x = 0 \qquad 2.3.25$

Equation 2.3.25 requires numerical solution, and the Runge-Kutta method was used, (see Appendix A). As in the case of the exponential

temperature variation, it is necessary to obtain ω by an iterative procedure from the boundary condition:

$$p_x (L) = 0$$

In this section, a general wave equation, similar to that of Kapur et al. (41), has been derived for the propagation of small amplitude waves at high frequency through a non-isothermal, perfect gas, flowing at small Mach number through a horizontal, straight tube. It may be noted that equation 2.3.21 reduces to the one-dimensional acoustic wave for a static, isothermal gas.

2.4 Forced convection heat transfer and longitudinal oscillations

2.4.1 Dimensional Analysis

Some insight into the important parameters of heat transfer in oscillating flow may be gained by the application of dimensional analysis. Consider first the steady flow of a gas in a straight, horizontal tube of circular cross-section, as shown in Figure 2.5; assuming that the flow of hot gas upstream of the heat exchanging section is hydro-dynamically developed and that the effects of natural convection are negligible, the local heat transfer coefficient becomes a function of nine parameters:

$$h = \phi (\rho , T , \mu , k , c_p , T_s , u , x , D) \qquad 2.4.1$$

By selecting ρ, c_p, u and T as the repeating variables and using Buckingham's Pi Theorem, the following relationship is established:

$$Nu = \phi (Re , Pr, \frac{x}{D} , \frac{T}{T_s} , E_c) \qquad 2.4.2$$

Now, by superimposing small oscillations on the flow, and assuming that they may be characterized by the angular frequency, ω, and the local velocity amplitude, $\hat{u}$, equation 2.4.1 becomes:

COOLANT

STRAIGHT, SMOOTH, HORIZONTAL TUBE

WALL SURFACE TEMPERATURE, T_S

D_o

x

FULLY DEVELOPED TURBULENT FLOW — u, T, ρ, μ, c_p, k WITH $\omega, \hat{u}$ SUPERIMPOSED FOR PULSATING FLOW
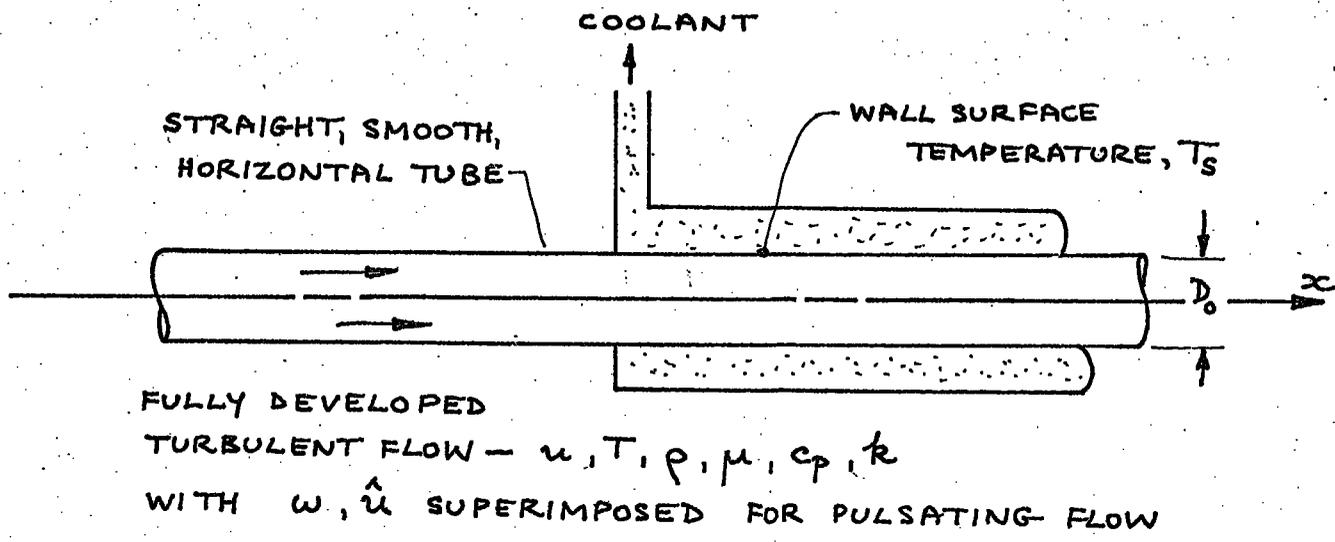
FIGURE 2.5 :   PARAMETERS OF THE FLOW

$\dfrac{\overline{Nu_p}}{Nu}$

4.0

3.0

2.0

1.0

0

0   2   4   6   8   10

$\hat{u}/\bar{u}$

$$\frac{\overline{Nu_p}}{Nu} = \frac{1}{2\pi} \int_0^{2\pi} \left(\left| 1 + \frac{\hat{u}}{\bar{u}} \cos(\omega t) \right| \right)^{0.8} d\omega t$$

DIMENSIONLESS VELOCITY AMPLITUDE
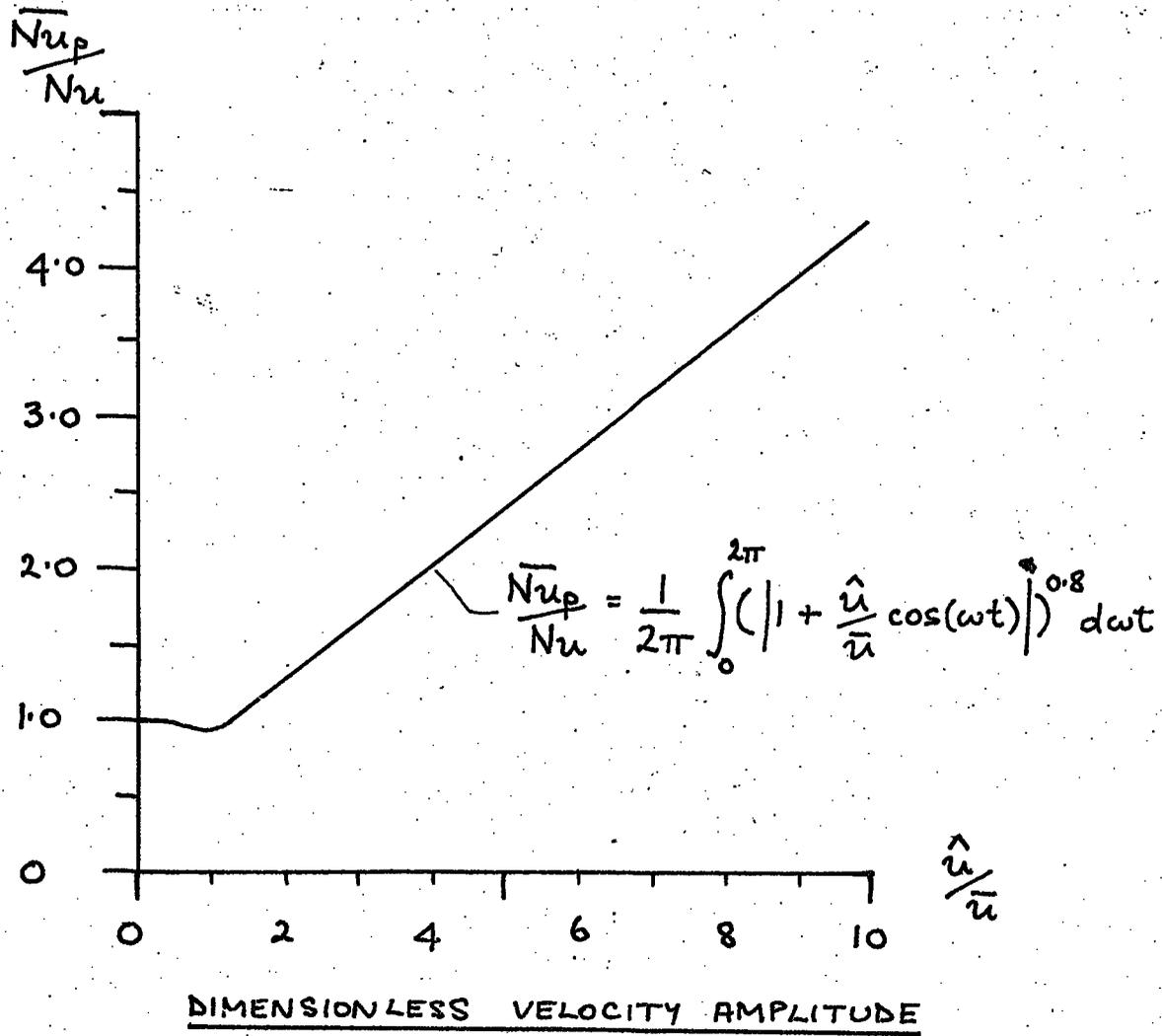
FIGURE 2.6 : QUASI-STEADY STATE THEORY

$$\bar{h}_p = \phi(\bar{\rho}, \bar{T}, \mu, \hat{k}, c_p, T_s, \bar{u}, x, D, \omega, \hat{u})$$

which leads to:

$$\overline{Nu}_p = \phi(\overline{Re}, P_r, \frac{x}{D}, \frac{\bar{T}}{T_s}, \bar{E}_c, \frac{\hat{u}}{\bar{u}}, S) \qquad 2.4.4$$

Thus the superimposition of small oscillations on the flow gives rise to two additional π factors, the dimensionless velocity amplitude X and the Strouhal number, S . As the analysis of the slow is confined to flows of small Mach number (see Section 2.3), the effect of the Eckert number, $\bar{E}_c$, upon the heat transfer may be ignored. Therefore, if the other parameters are kept constant, a relationship may be sought between $\overline{Nu}_p, \frac{\hat{u}}{\bar{u}}$ and S .

2.4.2. Quasi-steady-state Analysis

The principle of this method, which has been used by Schultz-Grunow (28), Martinelli (27), Morell (42) and Hanby (39), is that an empirical relationship for forced convection in steady flow may be applied during any instant of the cycle of oscillation superimposed on the flow. The chief objection to this approach is that the velocity and temperature profiles will change throughout the cycle, and this in turn affects the accuracy of the relationship. For turbulent flow, the equation of Sieder and Tate (43) was chosen:

$$Nu = 0.027 (Re)^{0.8} (P_r)^{0.33} \left(\frac{\mu}{\mu_s}\right)^{0.14} \qquad 2.4.5.$$

This expression is valid for $\frac{L}{d} > 60$, for $(\bar{T} - T_s) > 56°C$ and for $0.7 < P_r < 16700$. All properties are evaluated at the bulk mean gas temperature, except for μ_s , which is evaluated at the tube surface temperature. Now from equations 2.3.6 and 2.3.23, the velocity at any instant may be expressed:

$$u = \bar{u} + \hat{u} \cos(\omega t) \qquad 2.4.6$$

Equation 2.4.5 becomes, on substitution of equation 2.4.6:

$$Nu_p = 0.027(\overline{Re})^{0.8}(Pr)^{0.33}\left(\frac{\mu}{\mu_s}\right)^{0.14}\left[1 + \frac{\hat{u}}{\overline{u}}\cos(\omega t)\right]^{0.8} \qquad 2.4.7$$

Dividing 2.4.7 by 2.4.5 and integrating over the period of one oscillation yields:

$$\frac{\overline{Nu_p}}{Nu} = \frac{1}{2\pi}\int_0^{2\pi}\left(\left|1 + \frac{\hat{u}}{\overline{u}}\cos(\omega t)\right|\right)^{0.8}d\omega t \qquad 2.4.8$$

This curve is shown in Figure 2.6.

The effects predicted by these analyses were calculated for the arrangement as shown in Figure 2.4. A comparison between equations 2.1.4 and 2.2.27 is shown in Figure 2.7, where it is apparent that a temperature gradient causes a nodal shift towards the cooler end of the tube. The maximum pressure amplitude increases by approximately 30%. Figure 2.8 illustrates the increase in local heat transfer coefficient predicted by the quasi-steady approach. At velocity antinodes the increases range from 20 to 200%. Figure 2.9 demonstrates the increases to be expected in overall heat transfer rates. These are less dramatic, ranging from 0 to 17.5%. At higher frequencies, increases are approximately 2% more than at low.

2.4.3 Dimensionless velocity amplitude

From the acoustic wave equation, the dimensionless velocity amplitude for the isothermal state is given by:

$$\frac{\hat{u}}{\overline{u}} = \frac{\hat{p}_0}{\overline{u}}\frac{c}{B_A}\sin\left(\frac{\omega x}{c}\right) \qquad 2.4.9$$

and for the exponential temperature variation:

$$\frac{\hat{u}}{\overline{u}} = \frac{\hat{p}_0}{\overline{u}}\frac{c_0}{B_A}\left\{M_1 J_0(z) + N_1 Y_0(z)\right\} \qquad 2.4.10$$

FIGURE 2.7 : VARIATION OF PRESSURE AMPLITUDE ALONG COMBUSTOR FOR LINEAR TEMPERATURE GRADIENT. COMPARISON OF GENERAL SOLUTION WITH SIMPLE ACOUSTIC THEORY.
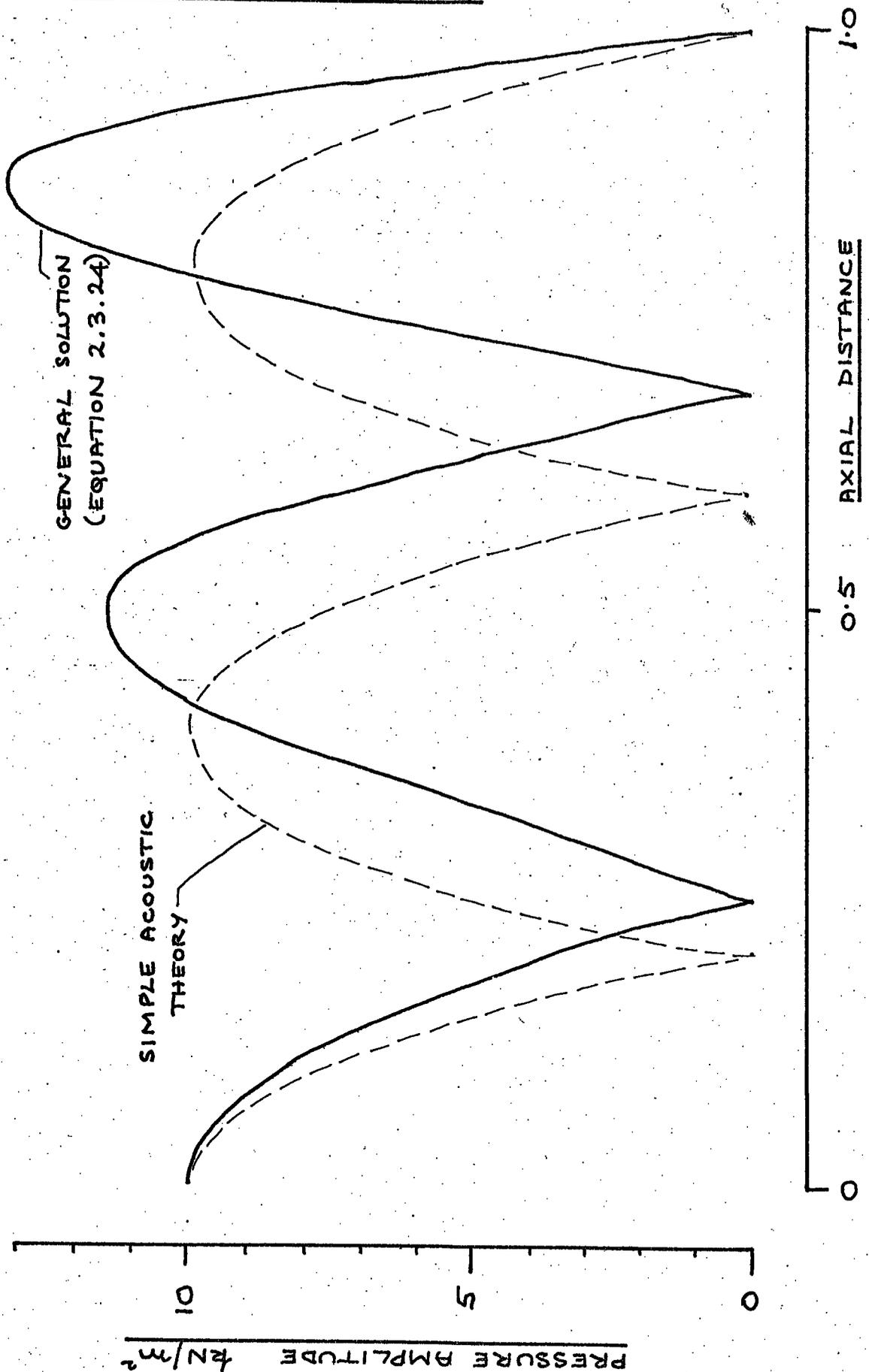
FIGURE 2.8: PREDICTED VARIATION OF LOCAL HEAT TRANSFER COEFFICIENT ALONG HEAT EXCHANGER
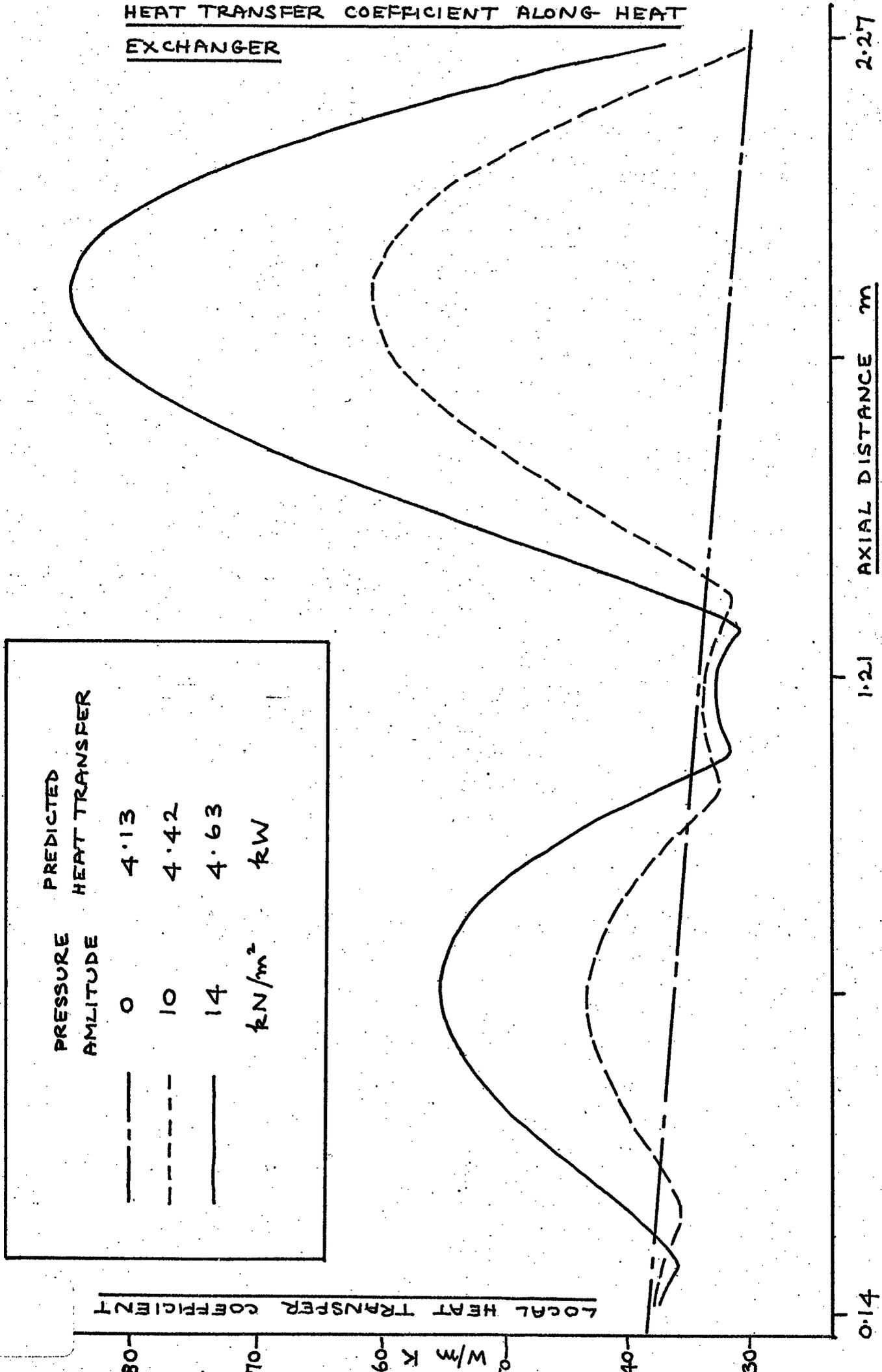
FIGURE 2.9 : PREDICTED VARIATION OF OVERALL HEAT TRANSFER IMPROVEMENT RATIO FOR FOUR HARMONICS

OVERALL HEAT TRANSFER IMPROVEMENT RATIO

FREQUENCY	
⊙	40
+	120
▣	200
△	280
	Hz

COMBUSTION CHAMBER PRESSURE
AMPLITUDE kN/m^2
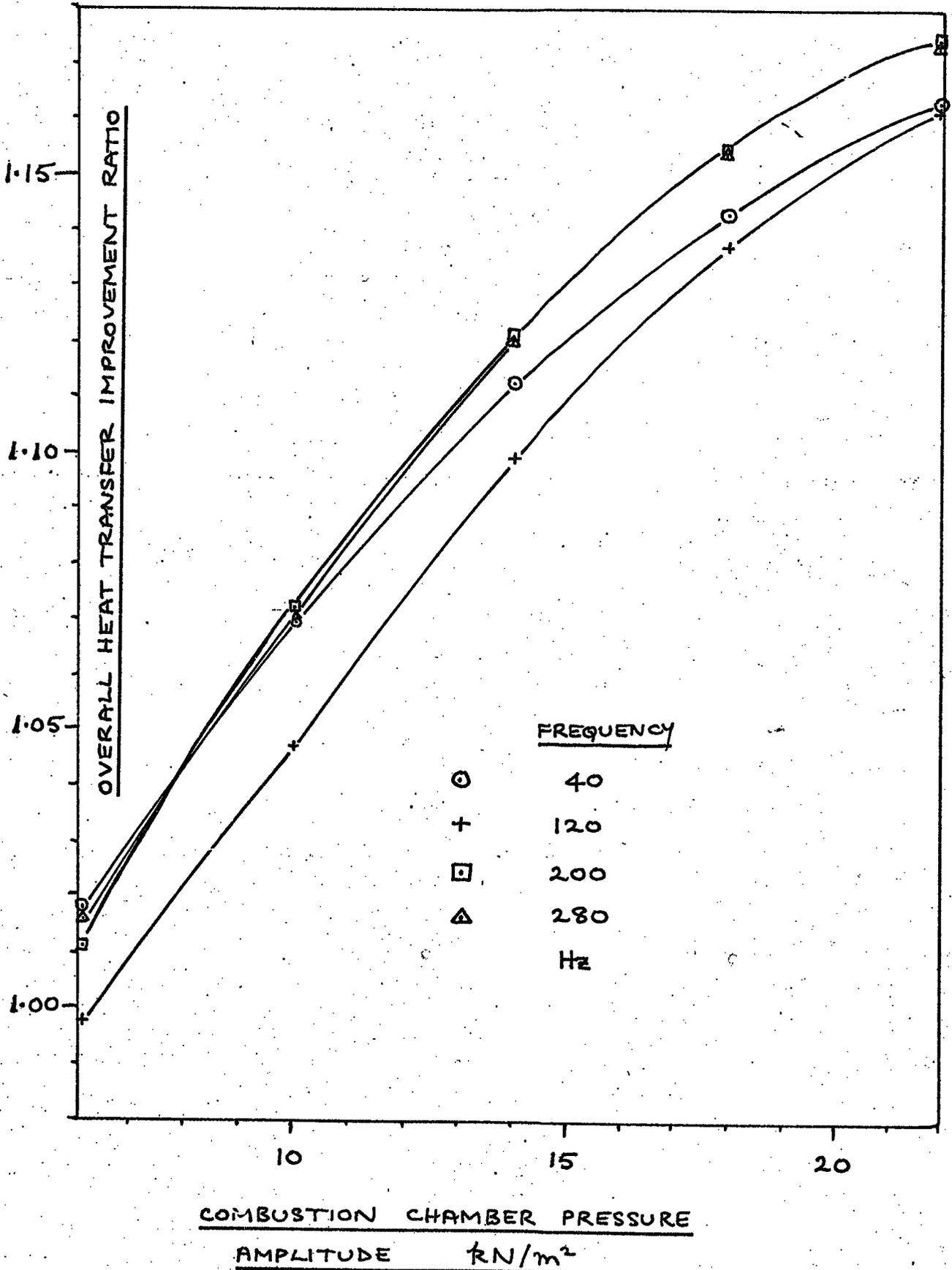
For the general case, $\bar{T} = \bar{T}(x)$, it is necessary to solve equation 2.3.25 and derive u from equations 2.3.25 and 2.3.23:

$$\frac{\partial u}{\partial t} = - \frac{1}{\bar{\varrho}} \frac{\partial p_x}{\partial x} \sin(\omega t) \qquad 2.4.11$$

Integration gives:

$$u = \bar{u} + \frac{1}{\omega \bar{\varrho}} \frac{\partial p_x}{\partial x} \cos(\omega t) \qquad 2.4.12$$

from which

$$\frac{\hat{u}}{\bar{u}} = \frac{1}{\bar{u} \omega \bar{\varrho}} \frac{\partial p_x}{\partial x} \qquad 2.4.13$$

2.5 Analysis of aerodynamic valve

It was decided to analyse the flow through the aerodynamic valve in order to predict the net mass flowrate of air through it for a given pressure variation in the combustion chamber.   During the induction part of the cycle, air, and possibly rejected gases of the previous cycle, are drawn into the combustion chamber.   After the expansion of the combustion process, hot products are rejected back through the valve.   It was decided to simplify the problem by assuming that the induced fluid was air at atmospheric temperature and that the exhausted fluid was air at a high temperature.   The analysis uses a quasi-steady state approach.   From Lewitt (44), the isentropic steady state relation for the frictionless flow of a gas through a nozzle is:

$$\dot{m} = A_e \left\{ 2 p_1 \varrho_1 \left(\frac{\mu}{\mu-1} \right) \left(\frac{p_2}{p_1} \right)^{2/\nu} \left[1 - \left(\frac{p_2}{p_1} \right)^{\frac{\mu-1}{\mu}} \right] \right\}^{1/2} \qquad 2.5.1$$

where μ is evaluated at T_2.   The velocity at 2 is given by:

$$u_2 = \left\{ 2 \frac{p_1}{\varrho_1} \left(\frac{\mu}{\mu-1} \right) \left[1 - \left(\frac{p_2}{p_1} \right)^{\frac{\mu-1}{\mu}} \right] \right\}^{1/2} \qquad 2.5.2$$

The situation is illustrated in Figure 2.10. The effective area of the valve is less than its actual cross-sectional area, and is given by Shapiro (45) to be:

$$A_e = A \times C_d \qquad 2.5.3$$

C_d, the coefficient of discharge is given by:

$$C_d = \frac{1}{\mu M^2} \left\{ \left[1 + \left(\frac{\mu - 1}{2} \right) M^2 \right]^{\frac{\mu}{\mu - 1}} - 1 \right\} \qquad 2.5.4$$

M, being the Mach number of the flow through the nozzle at 2. Using the binomial series to expand equation 2.5.4 and simplifying, the coefficient of discharge becomes, approximately:

$$C_d = \frac{1}{2} + \frac{M^2}{8} + \frac{M^4}{24} \qquad 2.5.5$$

provided $M < 1$.

The oscillation of pressure within the combustion chamber is assumed to be sinusoidal, and the steady state flow relation through the valve is assumed to hold over the whole cycle. The induction and exhaust sequence is shown in Figure 2.11.

Induction

At any instant then:

$$\dot{m}_{IN} = A_e \left\{ 2 p_1 \rho_1 \left(\frac{\mu_2}{\mu_2 - 1} \right) \left(\frac{p_2}{p_1} \right)^{2/\mu_2} \left[1 - \left(\frac{p_2}{p_1} \right)^{\frac{\mu_2 - 1}{\mu_2}} \right] \right\}^{1/2} \qquad 2.5.6$$

Equation 2.5.6 must be integrated over the time:

$$\frac{\pi}{\omega} \leqslant t \leqslant \frac{2\pi}{\omega} \qquad 2.5.7$$

when the pressure in the combustion chamber is less than atmospheric. Thus ;

ATMOSPHERE

COMBUSTION
CHAMBER

T_1
ρ_1
P_1

T_2
ρ_2
P_2

1

2
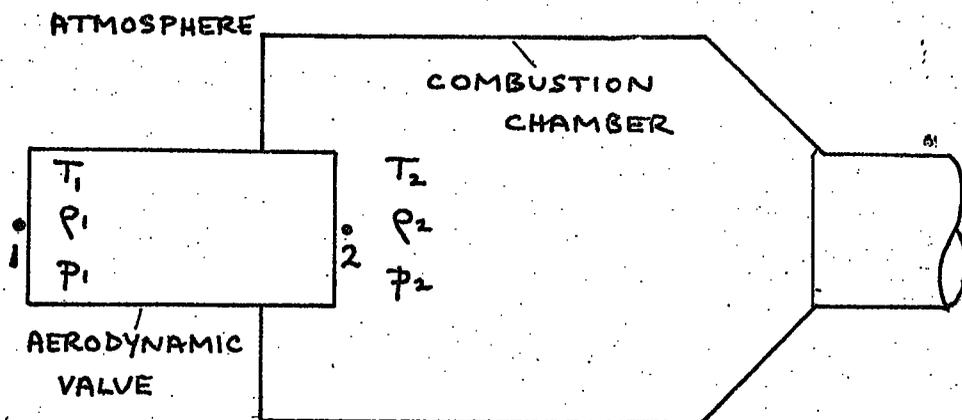
AERODYNAMIC
VALVE

FIGURE 2.10 : FRICTIONLESS FLOW OF GAS
THROUGH AERODYNAMIC VALVE

P

EXHAUST

$P_2 = P_0 \sin(\omega t)$

0

ATMOSPHERIC
PRESSURE

$\frac{\pi}{\omega}$

$\frac{2\pi}{\omega}$

t
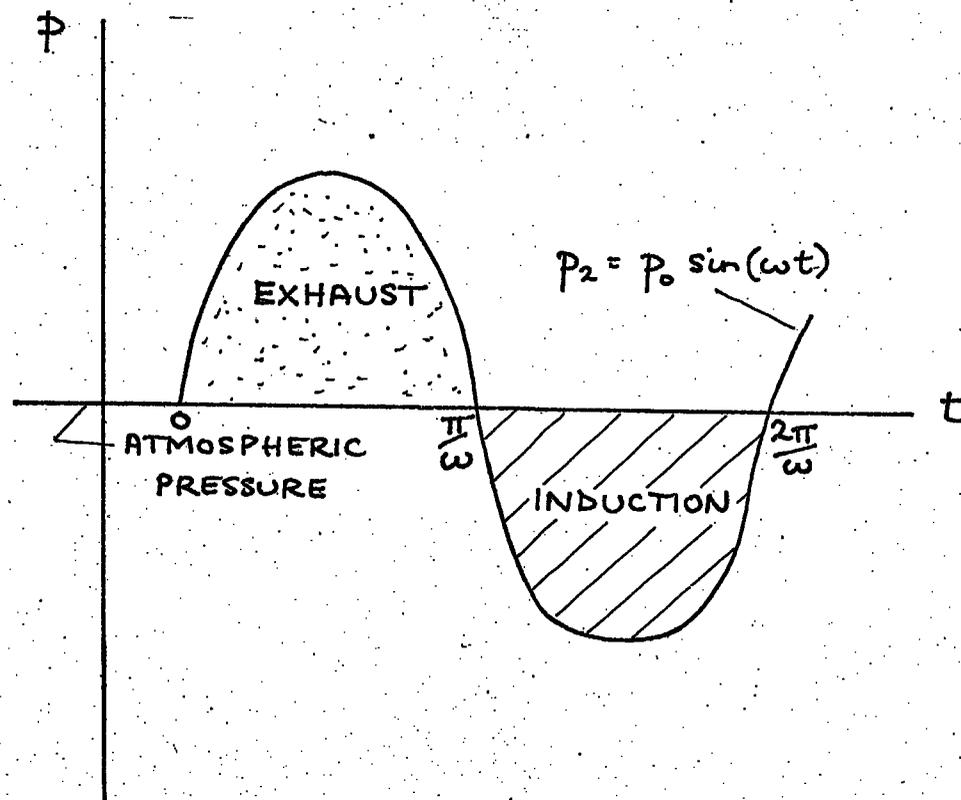
INDUCTION

FIGURE 2.11 : INDUCTION AND EXHAUST
SEQUENCE THROUGH VALVE

$$\sum \dot{m}_{IN} = \left\{ 2 \, p_1 \, \rho_1 \left(\frac{\mu_2}{\mu_2 - 1} \right) \right\}^{1/2} \int_{\frac{\pi}{\omega}}^{\frac{2\pi}{\omega}} A_e \left(\frac{p_2}{p_1} \right)^{1/\mu} \left\{ 1 - \left(\frac{p_2}{p_1} \right)^{\frac{\mu_2 - 1}{\mu_2}} \right\}^{1/2} dt \qquad 2.5.8$$

and

$$u_2 = \left\{ 2 \, \frac{p_1}{\rho_1} \left(\frac{\mu_2}{\mu_2 - 1} \right) \left[1 - \left(\frac{p_2}{p_1} \right)^{\frac{\mu_2 - 1}{\mu_2}} \right] \right\}^{1/2} \qquad 2.5.9$$

Exhaust

By similar considerations, for when the pressure in the combustion chamber exceeds atmospheric, the total mass of air exhausted is given by:

$$\sum \dot{m}_{OUT} = \left\{ 2 \, p_2 \, \rho_2 \left(\frac{\mu_1}{\mu_1 - 1} \right) \right\}^{1/2} \int_{0}^{\pi/\omega} A_e \left(\frac{p_1}{p_2} \right)^{1/\mu} \left\{ 1 - \left(\frac{p_1}{p_2} \right)^{\frac{\mu_1 - 1}{\mu_1}} \right\}^{1/2} dt \qquad 2.5.10$$

and

$$u_1 = \left\{ 2 \, \frac{p_2}{\rho_2} \left(\frac{\mu_1}{\mu_1 - 1} \right) \left[1 - \left(\frac{p_1}{p_2} \right)^{\frac{\mu_1 - 1}{\mu_1}} \right] \right\}^{1/2} \qquad 2.5.11$$

ρ_2 may be expressed in terms of ρ_1, by the isentropic relation:

$$\rho_2 = \rho_1 \left(\frac{p_2}{p_1} \right)^{1/\mu} \qquad 2.5.12$$

The necessary integrations may be carried out using Simpsons Rule. The net flow of air into the combustion is then given by:

$$\dot{m}_{AA} = \sum \dot{m}_{IN} + \sum \dot{m}_{OUT} \qquad 2.5.13$$

3. Experimental Work

As stated in Section 1.4, it was decided that a pulsating combustor, comprising an aerodynamic valve, combustion chamber and heat exchanger, should be constructed with an exhaust tube dimension of 26 mm. internal diameter. Due to the lack of experience in the field, a preliminary investigation into the general behaviour of a pulsating combustor was carried out. This work is reported in Appendix B, and the conclusions were:

a) a Helmholtz-type combustor was suitable for the purpose of the work;

b) the aerodynamic valve should be 50 mm. long and 12 - 26 mm. internal diameter;

c) the apparatus should include two heat exchangers, one through which the reverse flow back past the valve could be arranged to pass.

The general arrangement of the apparatus is shown in Figure 3.1. It was mounted on a rigid steel framework, which was tilted a few degrees from the horizontal to allow condensate to drain. The apparatus was separated from the frame by wooden vee-blocks to reduce conduction losses and permit expansion. The exhaust gases vented at atmospheric pressure into the laboratory beside an extractor fan that pumped them away. The inlets to the combustor were placed near an open window to ensure a continuous supply of fresh air. The apparatus was constructed in several sections which were flanged and bolted together, sealed by copper gaskets.

3.1 The Resonating Section

The resonating section of the apparatus is shown in Figure 3.2 and comprised a combustion chamber with aerodynamic valve, settling

58
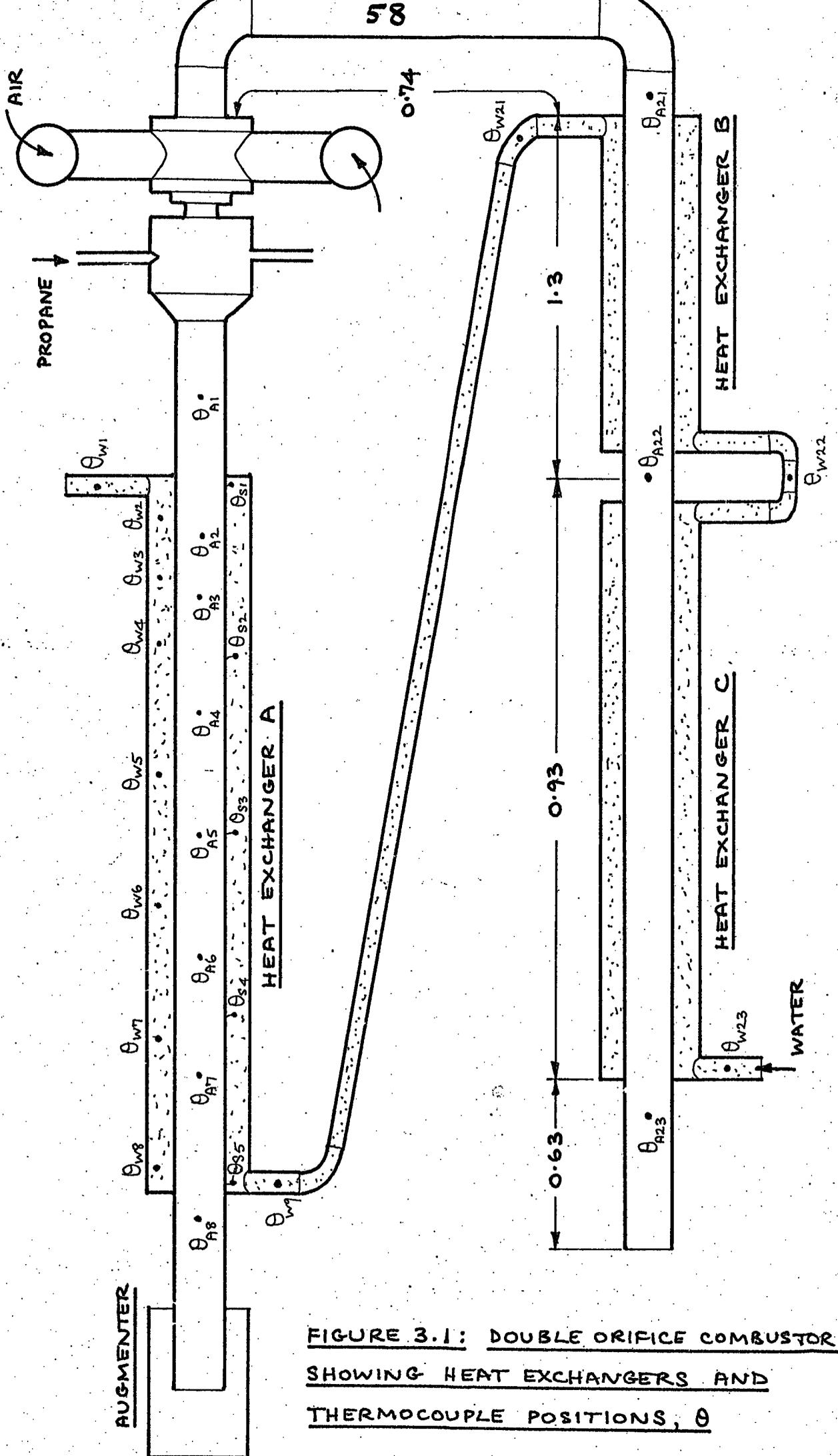
FIGURE 3.1: DOUBLE ORIFICE COMBUSTOR, SHOWING HEAT EXCHANGERS AND THERMOCOUPLE POSITIONS, θ
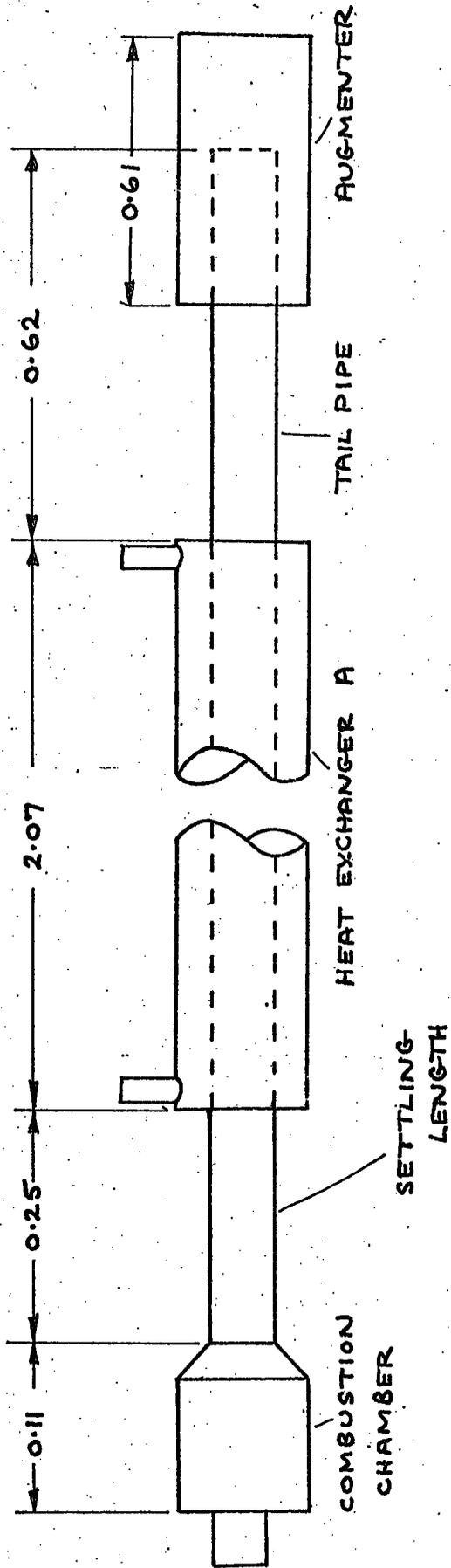
FIGURE 3.2 : MAIN RESONATING SECTION

length, heat exchanger A , tail-pipe and augmenter. The total
length of the section was 3.05 m. and therefore was 0.65 m. longer
than the development combustor. The purpose of this increase was to
permit the use of a longer heat exchanger (2.07 m. compared to 1.65 m.)
and a settling length of approximately 10 tube diameters between the
combustion chamber and the heat exchanger. It was found necessary
also to increase the length of the augmenter from 0.276 to 0.61 m.

3.1.1 The Combustion Chamber

The combustion chamber is shown in Figure 3.3. Internally it
was an exact reproduction of the chambers used in earlier experiments.
The chamber itself was constructed from a bar of stainless steel. It
had six radial holes into which components could be screwed, of which
the fuel injector and sparking plug are shown. Due to trouble
experienced with proprietory sparking plugs, a special one was built.
This consisted of a stainless steel body into which a long-reach KLG
electrode and insulator fitted, being retained by a threaded ring.
This design proved to be very convenient for cleaning the electrode of
deposits and for realignment, often necessary after a prolonged period
of combustor operation. The cooling annulus around the chamber was
intended to provide some control over the chamber wall temperature,
so that the gas temperature gradient, and hence the operating mode,
could be changed if required. The metal temperature was measured by
Chromel-Alumel thermocouple only one measurement being taken as it was
felt that this temperature was not critical. Also shown in Figure 3.3
is an aerodynamic valve screwed into the combustion chamber. The
valves, which were 51 mm. long and from 9.5 to 25 mm. internal diameter,
were constructed from stainless steel hexagon bar. Apart from removing
sharp corners, no attempt was made to streamline the bores. An air

THREADED TAPPING FOR KISTLER
PRESSURE TRANSDUCER AT POINT 'X'

FUEL INJECTOR

COOLING
WATER

COOLING
ANNULUS

AERODYNAMIC
VALVE

CHROMEL-ALUMEL
THERMOCOUPLE

SPARKING PLUG
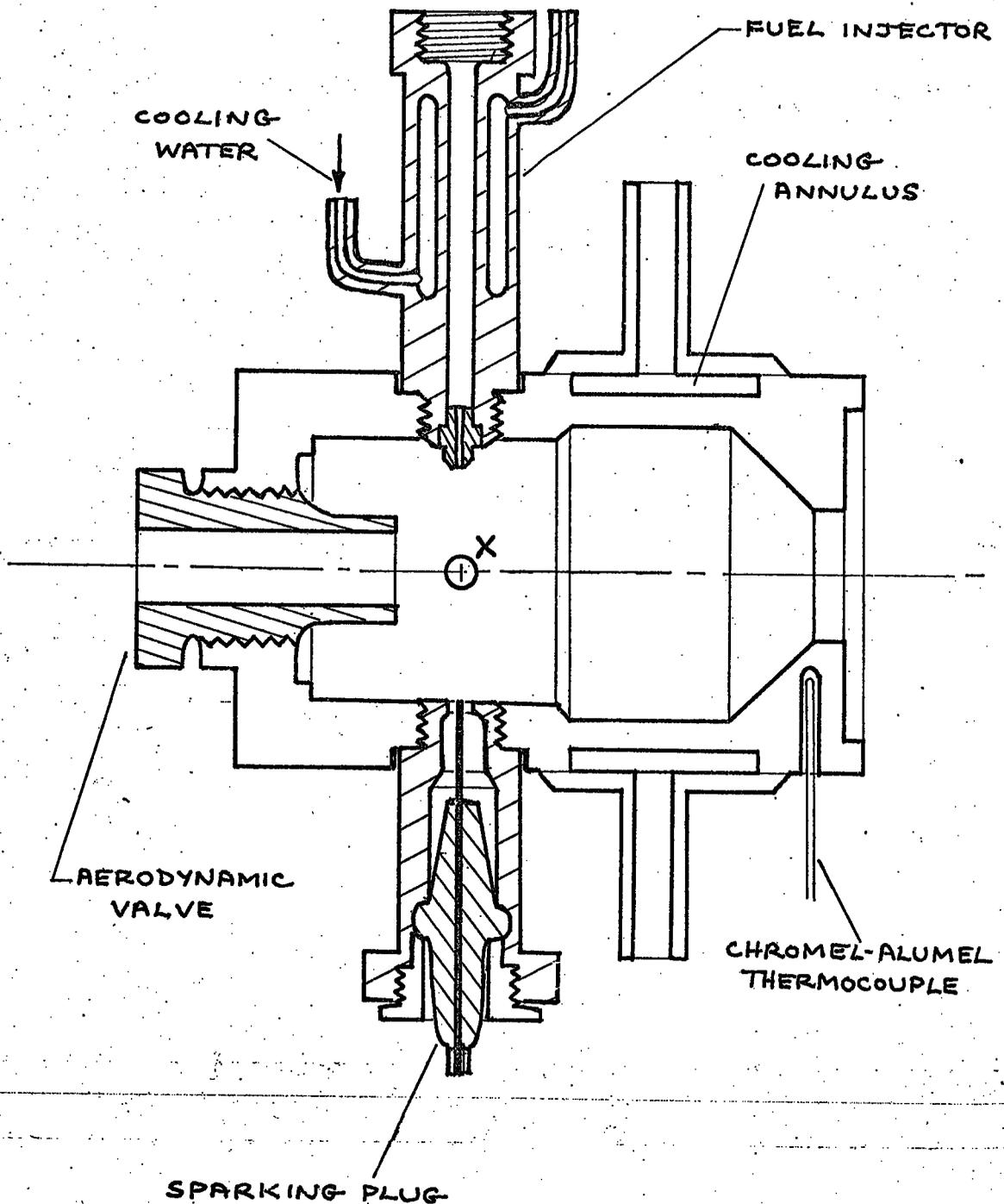
FIGURE 3.3 :   COMBUSTION CHAMBER

SCALE : 3/4 FULL SIZE

THIS FACE BOLTED ONTO
CONNECTION TO AUXILIARY
HEAT EXCHANGERS

THIS FACE BOLTED ONTO
COMBUSTION CHAMBER
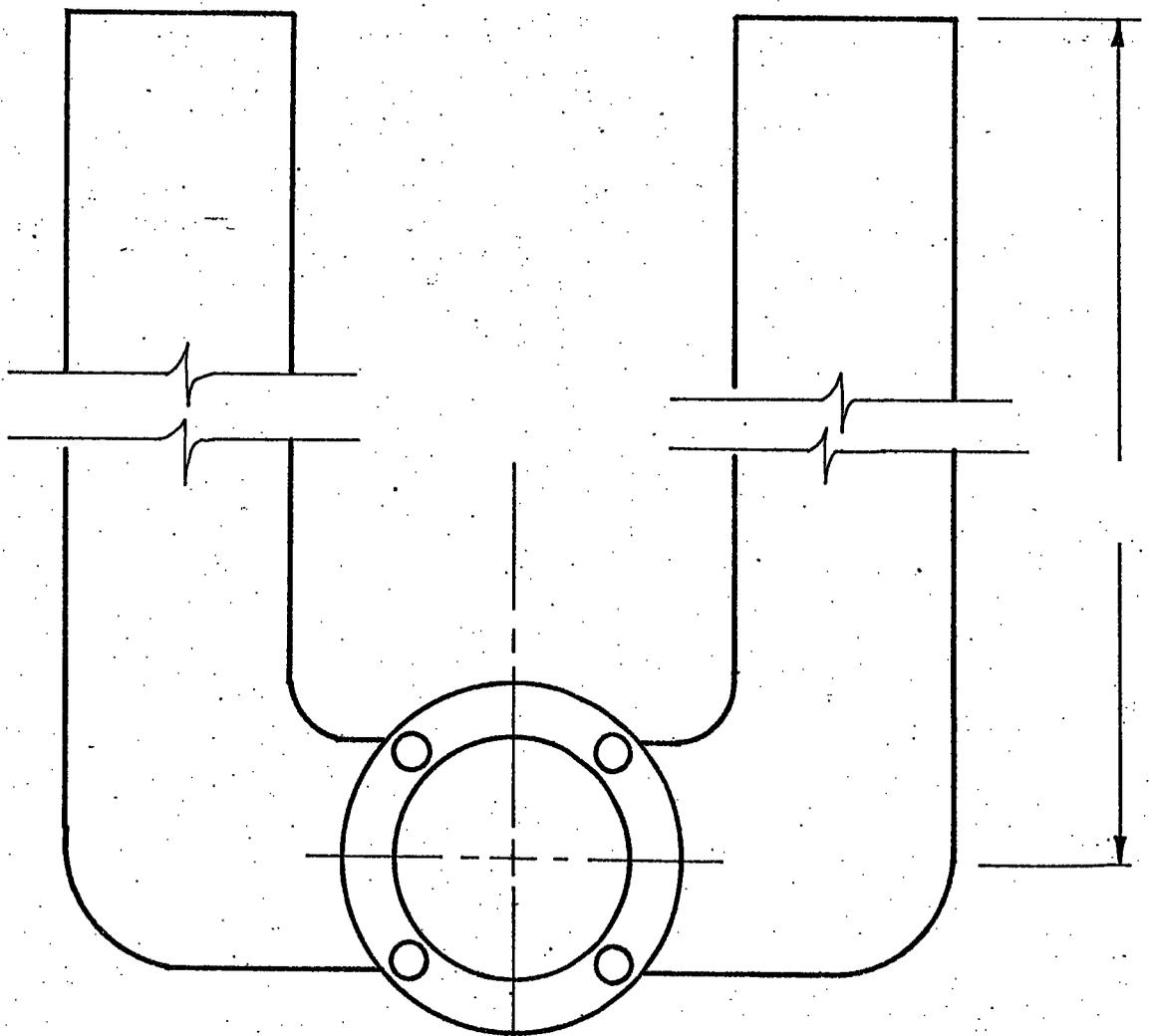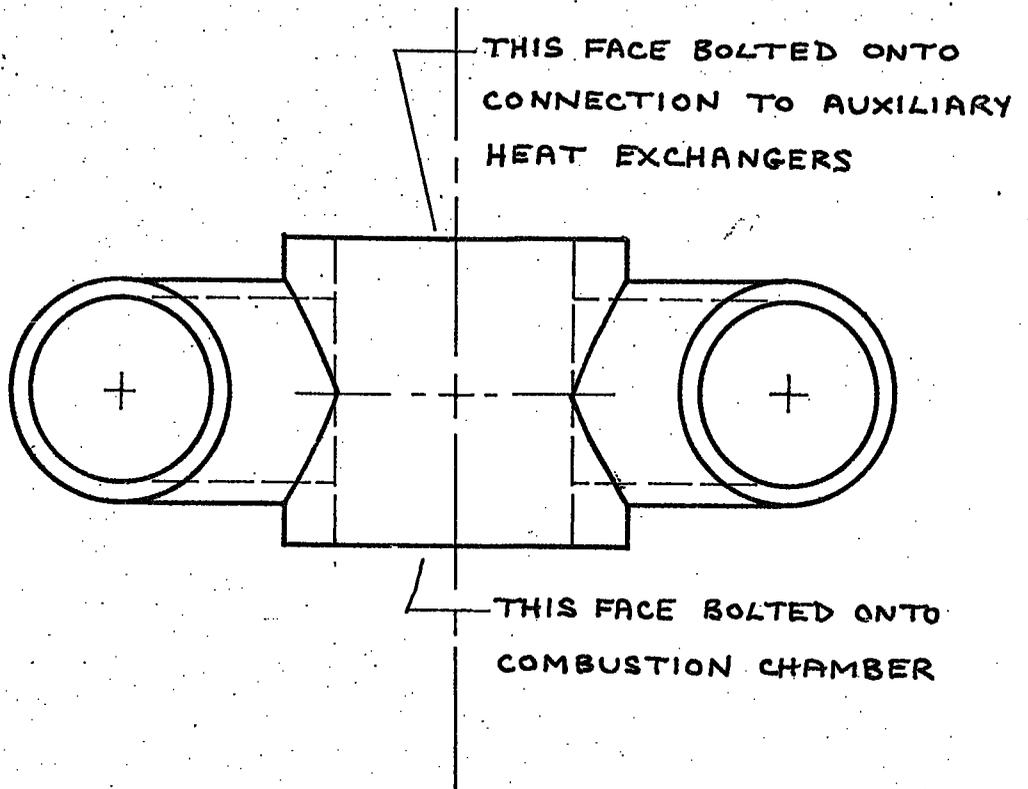
FIGURE 3.4: AIR INLET MANIFOLD

inlet manifold, which enclosed the valve, was bolted to the end of the combustion chamber and is shown in Figure 3.4. The purpose of the manifold was to guide the air inducted by the combustor into the valve and thus, by using a suitable flowmeter, to make a direct measurement of the flow.

The combustion chamber and ancillaries were lagged by winding asbestos rope around them, and enclosing that with preformed sections of calcium silicate, 0.23 m. outside diameter, obtained from Newalls Insulation Company.

3.1.2 Heat Exchanger A

As heat exchanger A formed part of the resonating section of the apparatus, it was constructed so that measurements of local heat transfer coefficients and of local pressure amplitudes could be made. It consisted principally of two concentric copper tubes, of 26 and 38 mm. nominal diameter, which were located at the ends by two brass adaptors. The arrangement is shown in Figure 3.5. The exchanger, which was 2.14 m. long overall, had a heat exchange surface of 2.07 m. length, giving a surface area (based on the outside diameter, 28.3 mm., of the inner tube) of 0.184 m^2. Along this length, were sited six instrument mountings, into which a temperature probe (see Section 3.4.1) or a pressure transducer (see Section 3.5.2) could be screwed. Seven thermocouples were mounted in the annular space to measure the water temperature (see Section 3.4.2), and five other thermocouples were soldered to the heat exchange surface to measure the wall temperature. The seven water thermocouples were threaded through mounting pads and bent to face upstream to oppose the water flow. This meant that the wires led axially away from the junction and thus not along an isotherm, but it was felt that, as the axial temperature gradient in the water flow did not exceed 0.05 $^{\circ}$C/mm., the error due to conduction along the
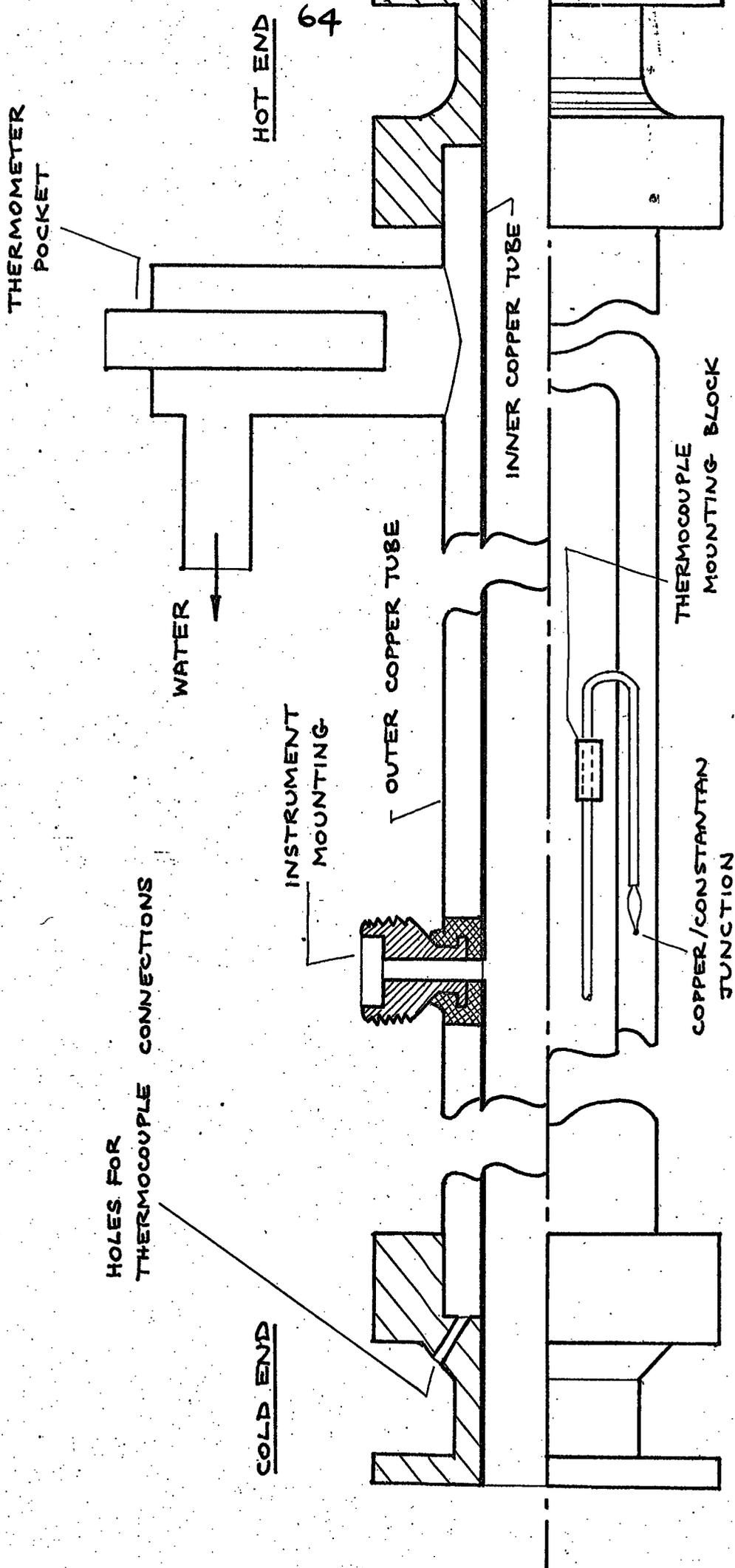
FIGURE 3.5: HEAT EXCHANGER A

wires was small. The thermocouples were laid adjacently where possible and clamped with wire to the inner tube. The free ends were passed through holes in the brass adaptor at the cold end and connected to copper wires in an isothermal wooden box, clamped to the tail-pipe.

The water connections to heat exchanger A consisted of vertical thermometer pockets at each end, to which 13 mm. diameter tubes were soldered for connection to the water system. The exchanger was lagged by preformed glass-fibre sections of 82 mm. outside diameter. During the construction of this piece of apparatus, a solid 25 mm. diameter mild steel bar was passed through the inner tube in order to minimise distortion during the welding operations. When complete, the annulus was tested up to 270 kN/m^2 water pressure; minor leaks were found and these were repaired with araldite.

3.1.3 The Tail-pipe and Augmenter

The tail-pipe was constructed from a piece of copper tube, 26 mm. nominal diameter and 0.62 m. long. Onto the outer end were glued three steel rods of small diameter and 38 mm. long, over which the augmenter could slide axially. The augmenter consisted of a piece of tube, 38 mm. nominal diameter and 0.61 m. long. The arrangement is shown in Figure 3.6.

3.2 The Fuel System

The fuel used in the investigation was commercial grade propane (B.S.4250:1968) obtained from the British Oxygen Company in quantities of 47 kg. in the liquid state. The arrangement of the fuel system is shown in Figure 3.7. The flowrate was measured by a viscous flowmeter,

66

THREE EQUI-SPACED
AXIAL SLIDES

AUGMENTER
(ADJUSTABLE)

0.61 m.

0.62 m.

TAIL-PIPE

STATIC PRESSURE
TAPPINGS
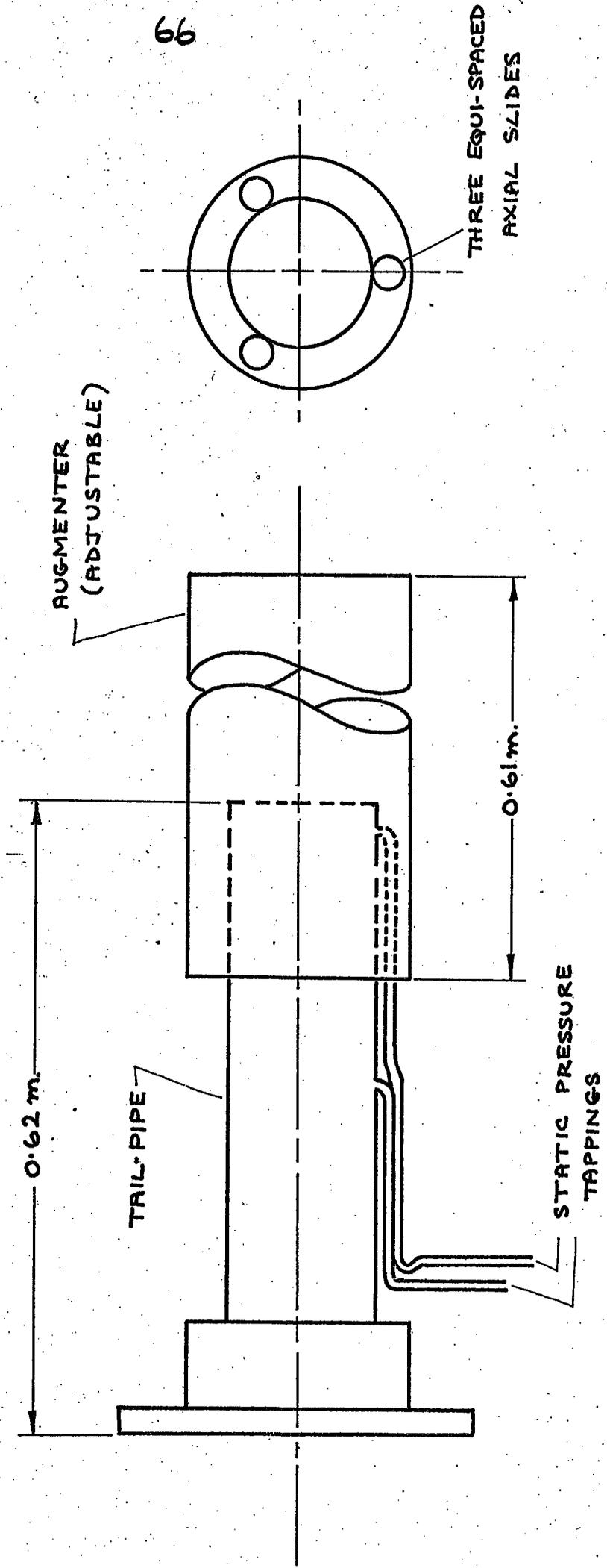
FIGURE 3.6 : TAIL-PIPE AND AUGMENTER

Type R837951/G, supplied by the Rotameter Manufacturing Company and calibrated over the range 0.13 to 1.3 kg/h. at standard atmospheric conditions to $\pm$ 2 per cent of indicated flow. The pressure in the flowmeter was displayed by a Bourdon gauge, supplied by the Budenburg Gauge Company and calibrated to $\pm$ 0.25 per cent of indicated pressure. The pressure drop at maximum flow through the meter was quoted (46) to be 0.1 kN/m^2. It was thus negligible compared with the working pressure. The temperature of the propane was measured to $\pm$ 2 per cent by a Type T thermocouple inserted into the top of the meter and was controlled at 20 $\pm$ 3 $^{\circ}$C by manual adjustment of the isothermal bath temperature. A straight, settling length of 0.6 m. was placed between the heat exchanger coil and the meter to damp out disturbances in the flow, and this was lagged to reduce heat losses. The rate of flow of the fuel was controlled by a precision pressure regulator and a needle valve, with a shut-off valve in case of emergency.

The fuel was forced radially into the combustion chamber through a water-cooled injector, (see Figure 3.3). Brass jets, which were obtained from Amal in sizes ranging from 0.2 to 2.5 mm. internal diameter, screwed into the injector. This was water-cooled to prevent premature decomposition of the fuel due to the high chamber temperature.

It was found that a jet of 0.86 mm. internal diameter performed best in the fuel injector. If a larger jet was fitted, the pressure drop across it was less, and the oscillations in the chamber affected the propane flowmeter. If a smaller one was fitted, the combustor did not always oscillate smoothly, and the flame occasionally failed. This was possibly due to the high injection velocity which could have prevented good mixing in the chamber and retarded the rate of reaction.

CONTROL VALVE

FUEL INJECTOR

SHUT-OFF VALVE

COOLING JACKET

VISCOUS FLOWMETER

THERMOCOUPLE

PRESSURE REGULATOR

LAGGED SETTLING LENGTH

WATER-FILLED ISOTHERMAL BATH

COIL OF COPPER TUBE

PROPANE RESERVOIR
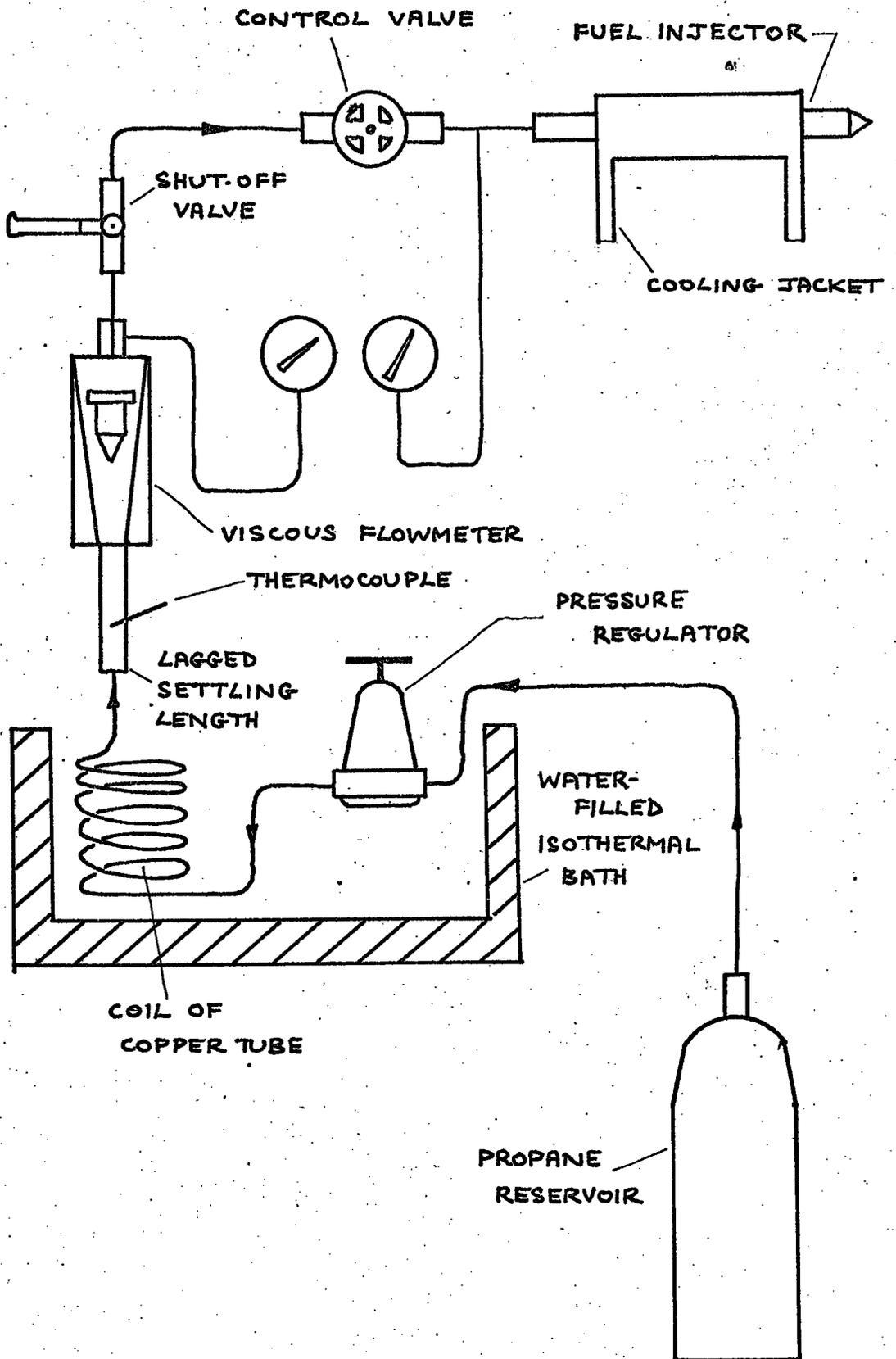
FIGURE 3.7: LAY-OUT OF FUEL SYSTEM
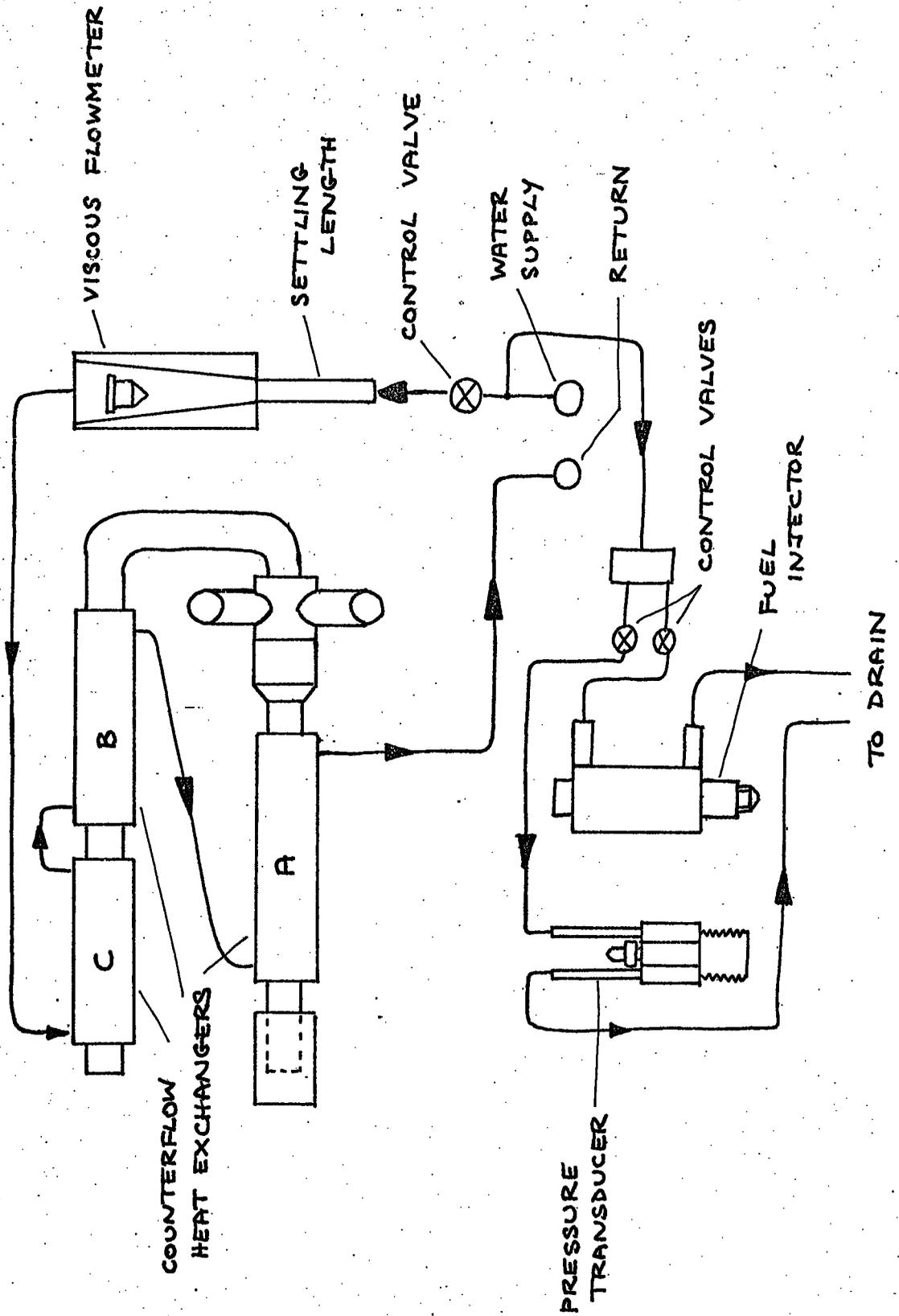
FIGURE 3.8: COOLING WATER SYSTEM

In addition a small jet set a limit on the maximum fuel flowrate, as the maximum propane regulator pressure was approximately 270 kN/m^2.

3.3 The Water System

The water, which was passed in a counterflow direction through heat exchangers A, B and C, was drawn from the Laboratory cooling system for heat engines. A diagram of the circuit is shown in Figure 3.8. The rate of flow was measured by a viscous flowmeter, Rotameter Type Metric 24E. A scale, graduated in litres/minute, was supplied with this instrument but, as only the lower part of it was used during the experiments, it was necessary to improve the accuracy of $\pm$ 5 per cent full scale reading. A calibration of the flowmeter was therefore made, using a vessel, a weighing machine and a stopwatch to measure the mass of water flowing per second for a given scale reading. The result is shown in Figure 3.9, the accuracy being improved to $\pm$ 0.5 per cent of indicated flow. As the laboratory cooling water contained small quantities of grit and rust, it was necessary to clean the tube and float occasionally.

The flowrates of cooling water through the fuel injector and through the transducer adaptor were each measured with a graduated flask and a stopwatch, the method being accurate to $\pm$ 0.3 per cent of the reading.

3.4 Measurement of Temperature

The measurement of gas and water temperatures within the apparatus was made with thermocouples and thermometers of the types shown in Table 3.1, and the circuit used for all the thermocouples is shown in Figure 3.10.

FIGURE 3.9 : CALIBRATION OF ROTAMETER TYPE METRIC 24E FOR WATER
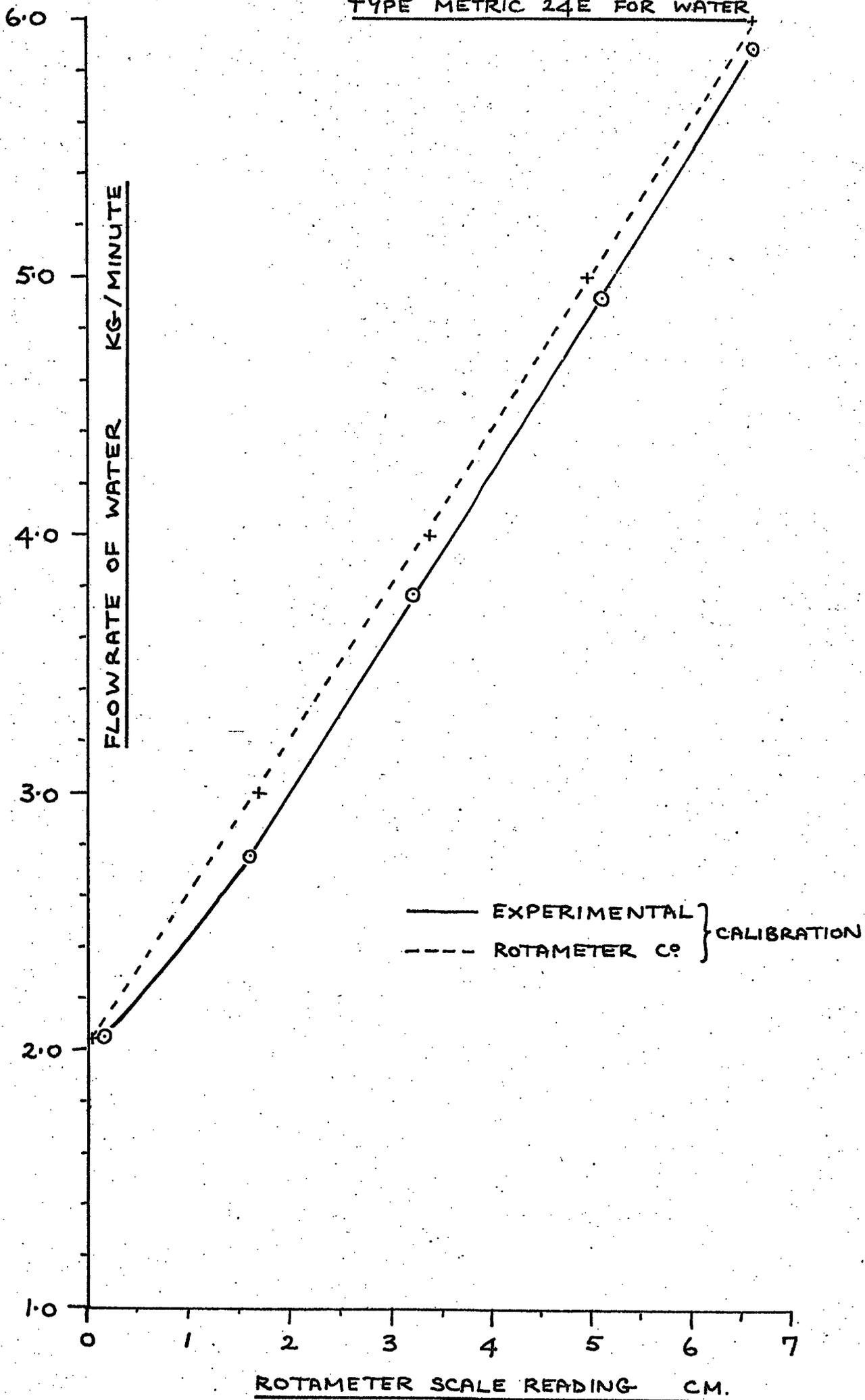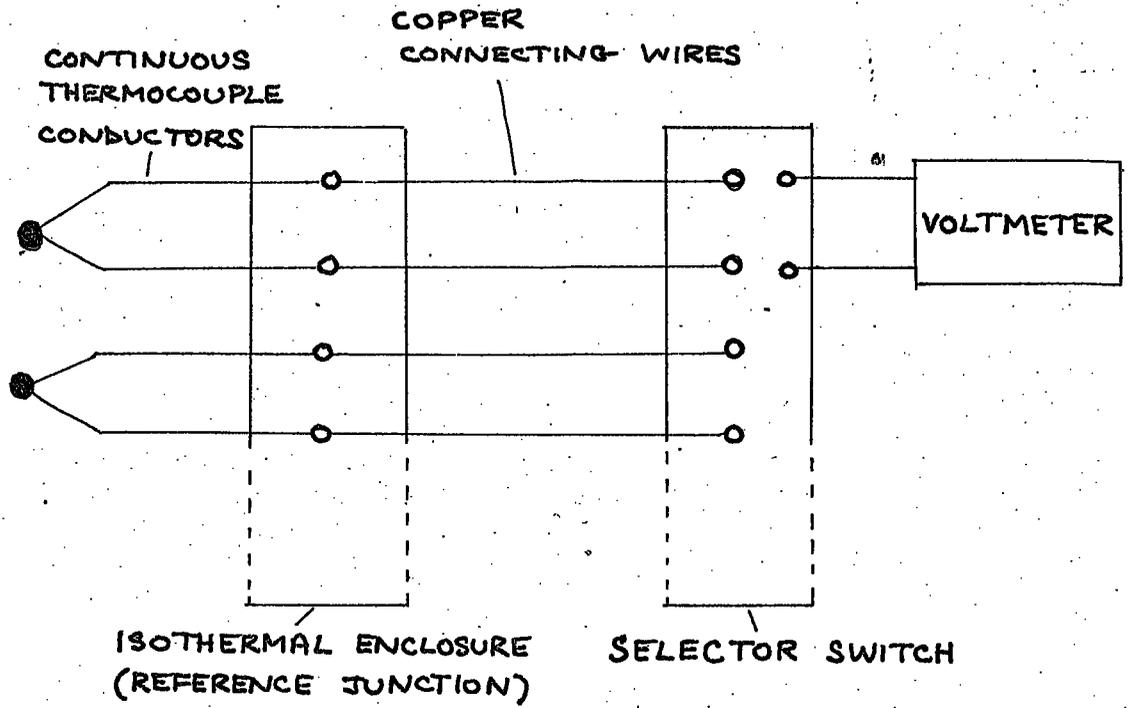
FIGURE 3.10 : THERMOCOUPLE CIRCUIT
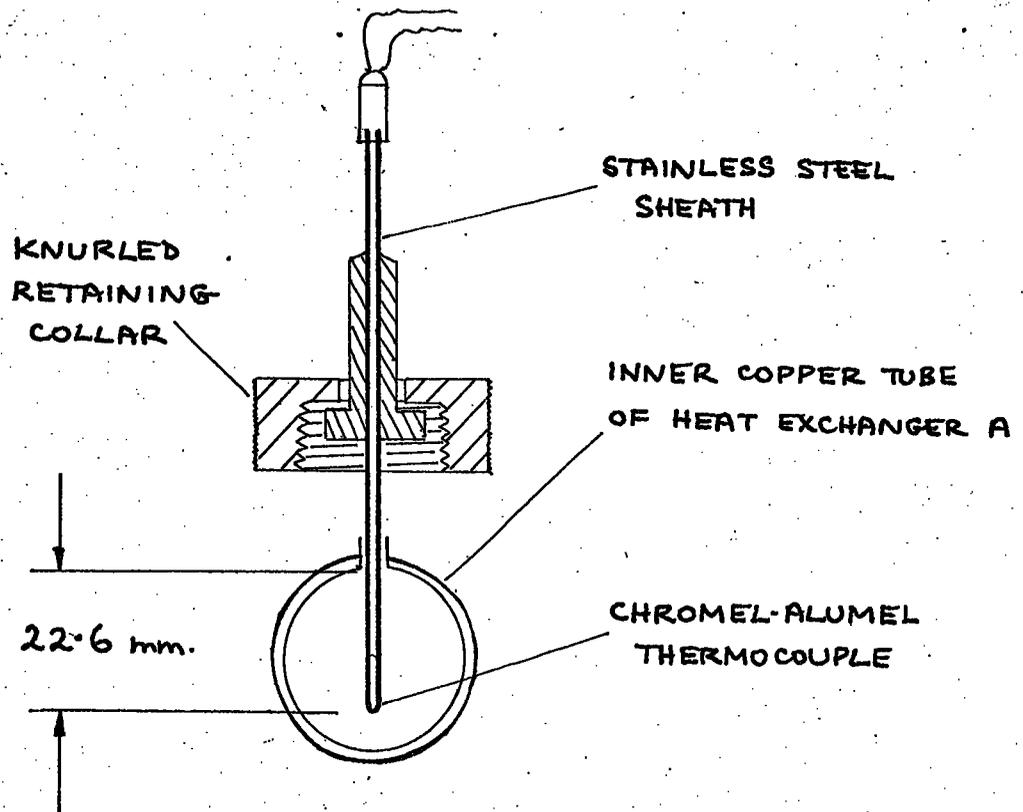
FIGURE 3.11 : GAS TEMPERATURE THERMOCOUPLE
— TYPE K

Table 3.1 Types of thermocouple and thermometer

Thermocouple	Type K	Ni-Ch/Ni-Al	$\pm 3°C$ $< 400°C$ $\pm 0.75\%$ $> 400°C$
Thermocouple	Type S	Pt-10%Rh/Pt	$\pm 1.5\%$
Thermocouple	Type T	Cu/Con	$\pm 1°C$
Thermometer		Hg-in-glass	$\pm 0.2°C$

The unbroken thermocouple wires were led to an isothermal enclosure, comprising a wooden box, where connections were made, using electrical 'tagstrip', to the copper connection wires. These wires were connected to a selecting switch, mounted on an isothermal enclosure, again using the 'tagstrip'. The selecting switches were supplied by the Croydon Precision Instrument Company and had silver-plated terminals. The output terminals were connected to a digital voltmeter, Solartron Type LM.1420.2.

3.4.1 Gas Temperature

The gas temperatures, $T_{A2} - T_{A8}$, were each measured by screwing into the instrument sites the probe shown in Figure 3.11. When in position, the thermocouple junction projected approximately 22 mm. into the tube. The temperature of the junction was not that of the flowing gas as it was influenced by the effects of radiation, conduction and convection. Corrections were complicated by the presence of the oscillations. An analysis of the errors of this measurement has been made in Appendix C. The highest gas temperature, T_{A1}, was measured by a thermocouple mounted in a silica tube, shown in Figure 3.12. The tube, which had a nominal outside diameter of 4.8 mm., possessed twin

SILICA TUBE

CROSS-SECTION
OF SILICA TUBE

SETTLING LENGTH
OF MAIN RESONATING
SECTION

9.0 mm.

PLATINUM – 10%
RHODIUM/PLATINUM
THERMOCOUPLE
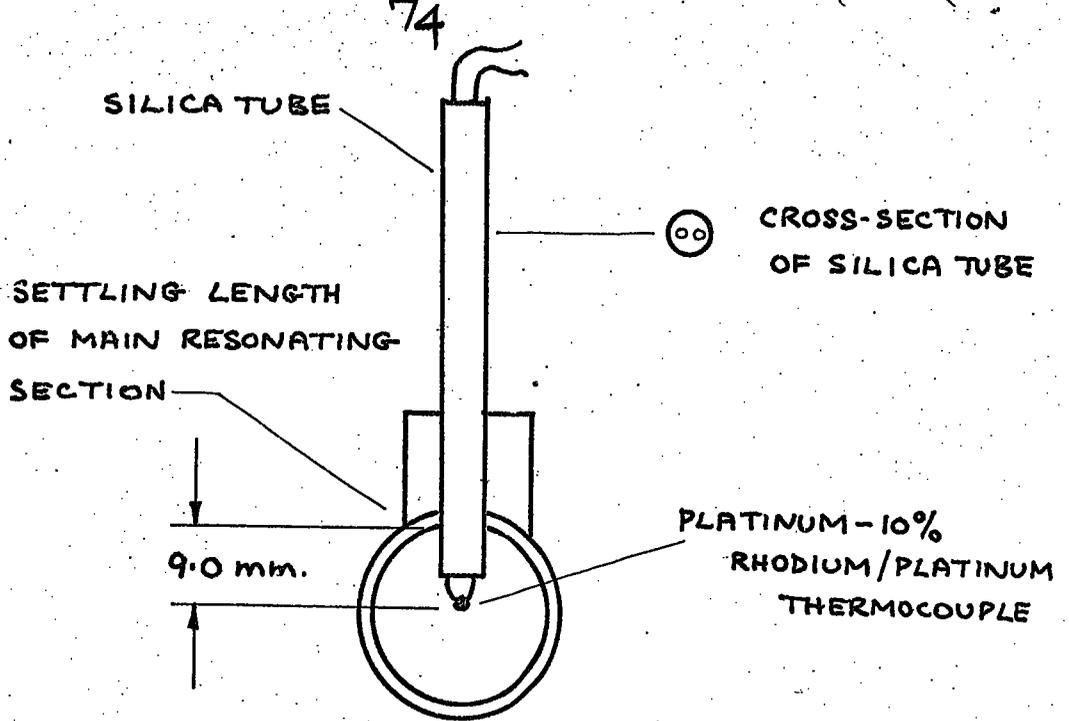
FIGURE 3.12 : GAS TEMPERATURE THERMOCOUPLE
— TYPE S

MAGNESIA
INSULATION

MILD STEEL
SHEATH

ARALDITE SEAL

CONDUCTORS

COPPER-CONSTANTAN
JUNCTION
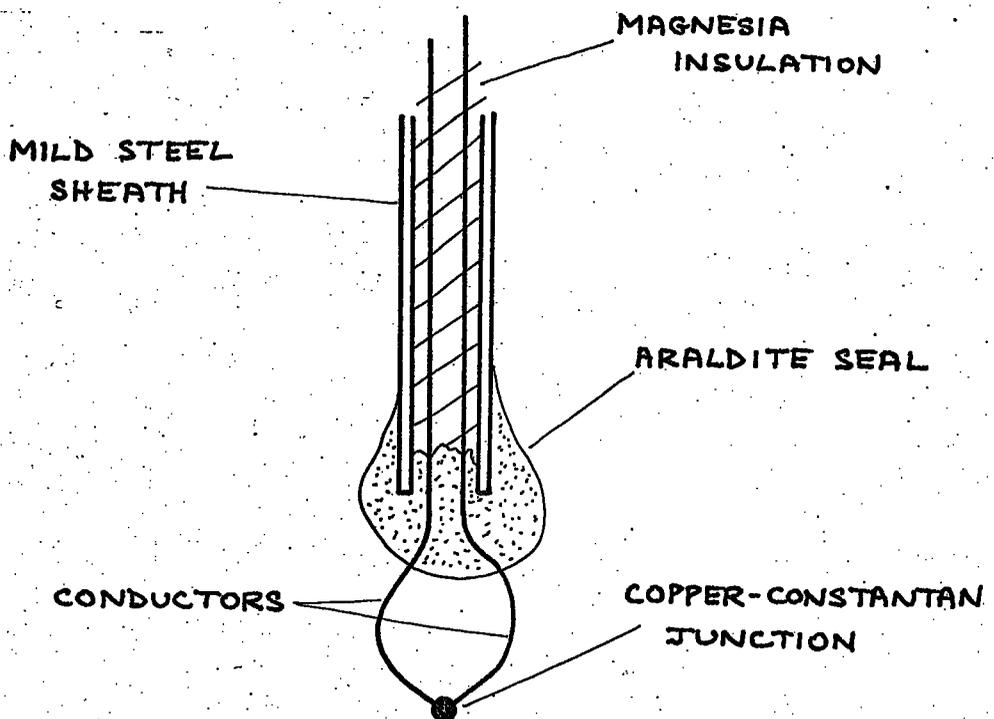
FIGURE 3.13 : DETAIL OF CONSTRUCTED
THERMOCOUPLES

bores, through which the thermocouple wires were passed, and was obtained from Thermal Syndicate.

The gas temperatures, T_{A21}, T_{A22} and T_{A23} were measured in a manner exactly similar to that described earlier in this section except that three thermocouples were used and fixed in place permanently.

3.4.2 Water Temperature

The seven Type T thermocouples in Heat Exchanger A, used to measure the water temperature, were constructed from a continuous coil of thermocouple cable. This consisted of a mild steel sheath, 1.6 mm. outside diameter, containing the copper and constantan conductors packed in magnesia insulation. It was obtained from Pyrotenax. The construction of the junctions was a delicate operation, and the advice contained in their manual (47), was followed. Due to the hygroscopic nature of the refractory insulant, the two ends of the thermocouple were dried and sealed with Araldite. The finished thermocouples (see Figure 3.13) were checked to ensure that the insulation resistance between conductors and sheath exceeded 100 $k\Omega$ and that the electrical circuit was continuous.

The remaining water temperatures, T_{W1}, T_{W9}, T_{W21}, T_{W22}, T_{W23}, T_{WTR}, and T_{WIN} were all measured with mercury-in-glass thermometers, Type TJ-070, obtained from Gallenkamp. These were total immersion thermometers, graduated in 0.2 $^{\circ}C$ with a range -5 to 105 $^{\circ}C$. They were immersed in oil in thermometer pockets of the type illustrated in Figure 3.14 in the case of T_{W1}, T_{W9}, T_{W21}, T_{W22} and T_{W23}, and of the type shown in Figure 3.14 in the case of T_{WTR} and T_{WIN}. The corrections to the readings due to the incorrect immersion is considered in Appendix C.

DEPTH OF
IMMERSION

OIL-FILLED THERMOMETER POCKET

10·5mm.

WATER
OUT

WATER
IN

FIBRE-GLASS
LAGGING
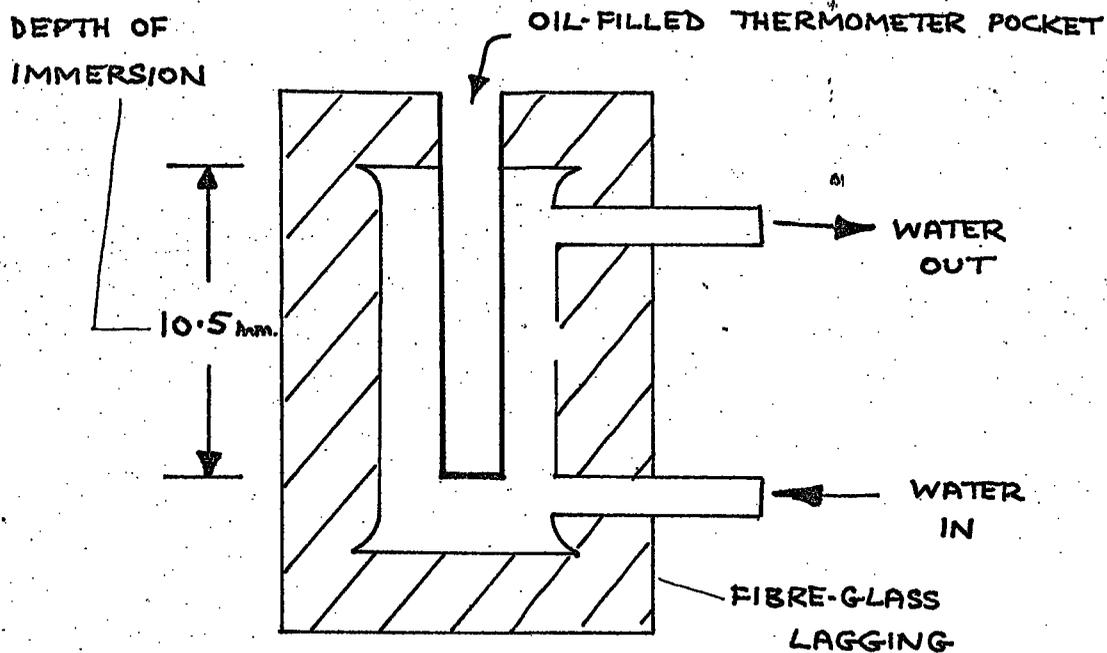
FIGURE 3.14 : THERMOMETER POCKET

SIGNAL CABLE
CONNECTION

BLEED HOLE
TO ATMOSPHERE

DIAPHRAGM

50 mm.

COVER (SEALED
BY O-RING)

TO PRESSURE

35mm.
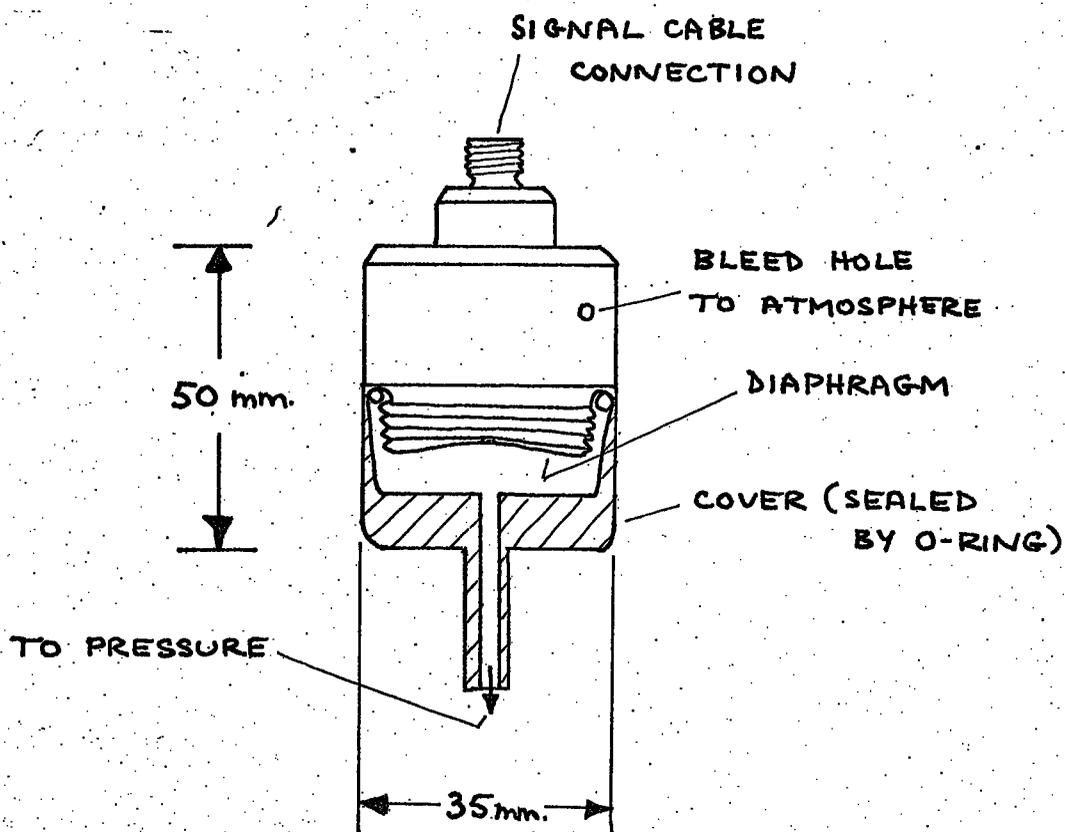
FIGURE 3.15 : KISTLER TYPE 412 PRESSURE
TRANSDUCER

3.5 Measurement of Pressure

A very important measurement in the experiments was that of pressure.   It was found in the preliminary experiments that:

a) the pressure waveform of the oscillations was approximately sinusoidal;

b) the mean static pressure throughout the combustor was approximately atmospheric.

Therefore it was decided not to take any further measurements of the static mean pressure, and to assume that the pressure oscillated about the mean atmospheric value.

There were ten sites on the resonating section where measurements of pressure amplitude could be taken.   They are listed in Table 3.2. It was decided to use one transducer, and this was inserted into each of the sites in turn.

Table 3.2 Axial Position of Measuring Sites

	x
P_{AC}	0.032
P_{A1}	0.190
P_{A2}	0.476
P_{A3}	0.654
P_{A4}	1.010
P_{A5}	1.365
P_{A6}	1.721
P_{A7}	2.076
P_{A8}	2.451
P_{A9}	2.821
P_{A10}	3.047
	$m.$

3.5.1   Time-dependent static gas pressure

The preliminary investigation showed that the instrument used

for measuring the pressure variations in the hot gases had to be

sensitive to oscillations between 30 and 300 Hz, to pressure

amplitudes in the range 1 to 20 Hz and to be independent of temperature.

It was decided to use a transducer available in the laboratory and

manufactured by the Kistler Instrument Ag.   Details are given in

Table 3.3 and Figure 3.15.

Table 3.3   Transducer data

Kistler Type 412 static pressure transducer Serial No. 8N33502		
Max. measuring range	0 - 10	Atm.
Calibrated partial ranges	0 - +1 -1 - 0	" "
Resolution	1.5×10^{-5}	"
Sensitivity	2230	pc/Atm
Resonant frequency	7500	Hz
" with cover	350	Hz
Max. error for each range	1	%
Working temperature range	-150 - +240	^{o}C

The mounting for the pressure transducer is shown in Figure 3.16, where

it is illustrated connected to a site on the heat exchanger.   The two

longer lengths of tube were found to be necessary due, firstly, to the

high wall temperature of the combustion chamber and, secondly, to the

augmenter sliding over the exhaust pipe, thus limiting access to it, as

shown by Figure 3.6.
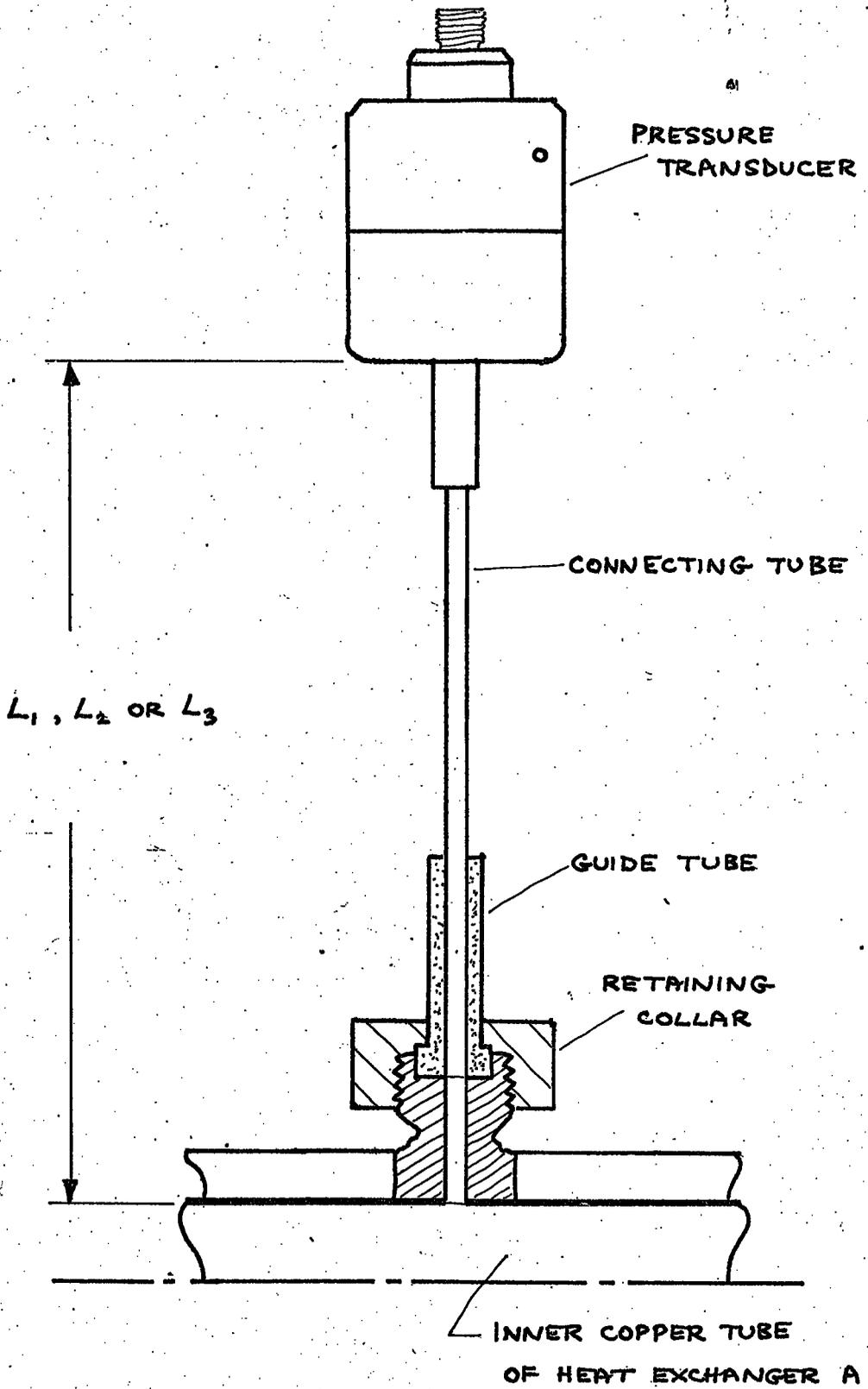
FIGURE 3.16 : PRESSURE TRANSDUCER MOUNTING

Considering the system shown in Figure 3.17, the attenuation of P_0 , the pressure signal, is given by Holman (48) to be:

$$\left| \frac{P}{P_0} \right| = 1 \Big/ \left\{ \left[1 - \left(\frac{\omega}{\omega_n} \right)^2 \right]^2 + 4h^2 \left(\frac{\omega}{\omega_n} \right)^2 \right\}^{1/2} \qquad 3.5.1$$

where the natural frequency, ω_n , of the transmitting volume is:

$$\omega_n = \left\{ \frac{3 \pi r^2 c^2}{4 L V} \right\}^{1/2} \qquad 3.5.2$$

The damping ratio, h , which is expressed as a laminar frictional resistance, is given by:

$$h = \frac{2 \mu}{\rho c r^3} \left\{ \frac{3 L V}{\pi} \right\}^{1/2} \qquad 3.5.3$$

and the phase angle for the pressure signal is:

$$\phi_{ph} = \tan^{-1} \left\{ \frac{-2h\left(\frac{\omega}{\omega_n} \right)}{1 - \left(\frac{\omega}{\omega_n} \right)^2} \right\} \qquad 3.5.4$$

It was assumed that the fluid in the connecting tube and dead volume was air at 20 $^\circ$C and the following data was put into equations 3.5.2 and 3.3.3;

$$V = 1.5 \times 10^{-6} m^3$$
$$r = 0.8 \ mm.$$
$$\mu = 1.85 \times 10^{-5} \ kg/m \ s$$
$$\rho = 1.18 \ kg/m^3$$
$$c = 345 \ m/s$$

Evaluation of the equations gives:

$$\omega_n = \frac{345}{\sqrt{L}} \qquad 3.5.5$$

$$h = 0.0213 \sqrt{L} \qquad 3.5.6$$

VOLUME, V

$2r$

P_0

PRESSURE
TRANSDUCER

L
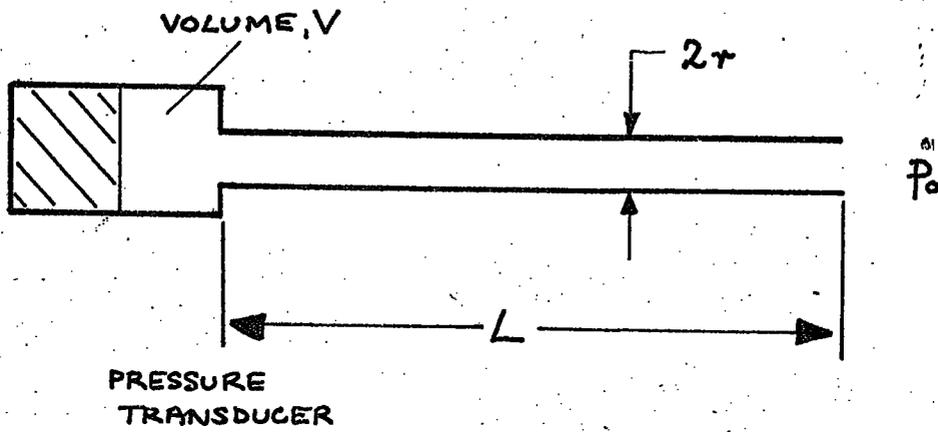
FIGURE 3.17 : IDEALISED PRESSURE MEASURING
SYSTEM

CONNECTION LEADS MAINTAINED
AT 14 MΩ INSULATION

VIBROMETER
TA-3/C
AMPLIFIER

DAWES TYPE 1461A
WAVE ANALYSER

ADVANCE OS 1000
OSCILLOSCOPE

KISTLER TYPE 412
PRESSURE TRANSDUCER
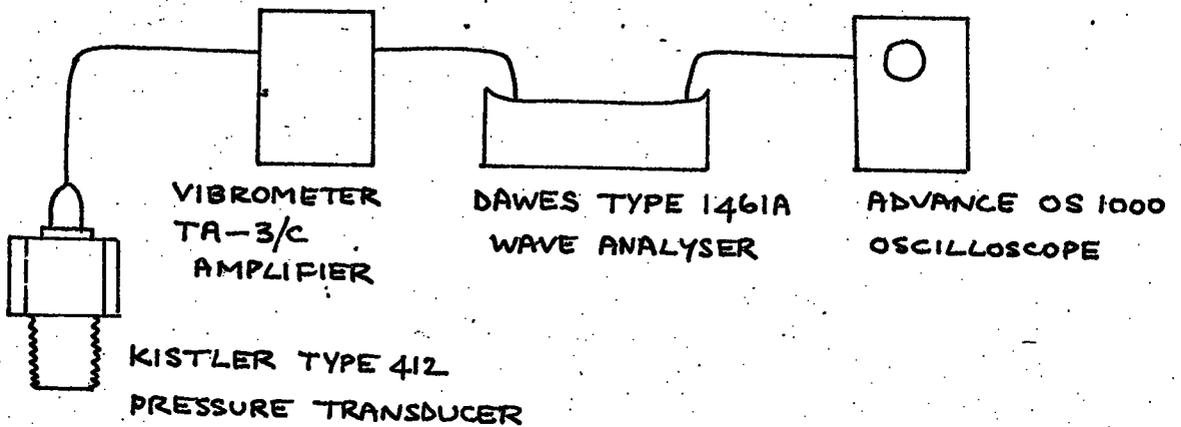
FIGURE 3.19 : APPARATUS FOR AMPLIFICATION
AND ANALYSIS OF PRESSURE SIGNALS

FIGURE 3.18: VARIATION OF PRESSURE SIGNAL ATTENUATION WITH FREQUENCY FOR THREE LENGTHS OF CONNECTING TUBE

82
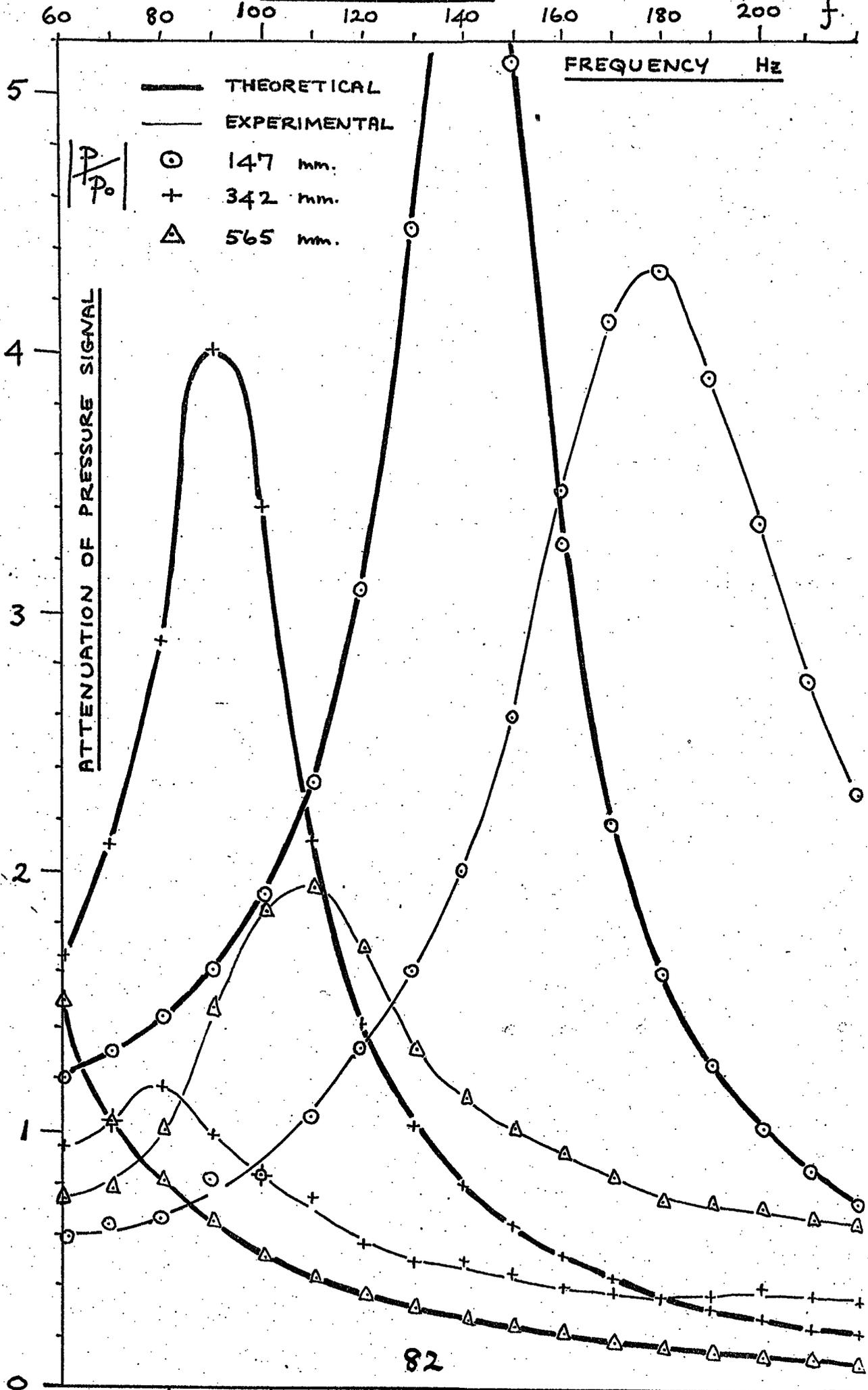
The resonant frequencies and damping factors are therefore:

$$\omega_{n_1} = 143 \ Hz \qquad\qquad h_1 = 0.0815$$
$$\omega_{n_2} = 94 \ Hz \qquad\qquad h_2 = 0.1246$$
$$\omega_{n_3} = 73 \ Hz \qquad\qquad h_3 = 0.1600$$

for
$$L_1 = 147 \ mm.$$
$$L_2 = 342 \ mm.$$
$$L_3 = 565 \ mm.$$

respectively.

It was decided to calibrate the transducer mountings experimentally, using a loudspeaker, driven by an audio wave generator, and a microphone of known response. The details of the experiment are given in Appendix D. The results of the experiment and of equation 3.5.1 are shown in Figure 3.18, where attenuation $\left|\dfrac{P}{P_o}\right|$ is plotted against frequency for the range 60 to 220 Hz. The main observations from the graph are summarised in Table 3.4, where the three different transducer mountings are identified by connecting tube length.

Table 3.4   Maxima from Figure 3.18

	Theoretical		Experimental	
Length	Attenuation	Frequency	Attenuation	Frequency
147	6.16	143	4.30	180
342	4.0	90	1.16	80
565	–	–	1.94	108
mm.		Hz		Hz

Numerically there is little agreement between the two sets of values. With respect to shape, the curves are substantially similar, the

resonances being displaced by from 10 Hz in the case of L_2 = 342 mm.
up to approximately 90 Hz in the case of L_3 = 565 mm. The reason
for this is not clear. The lower peak value of the experimental
resonances is in all probability due to underestimation of the
frictional losses in the connecting tube fluid.

The response of the Kistler transducer without cover and
connecting tubes was compared, using the same method and apparatus,
with that of the microphone. The two agreed to within ± 0.5% over
the whole range. The disparity between the experimental calibration
and the theoretical one was probably caused by distortion in the sound
field so close to the loud speaker cone. This would have been
accentuated by the difference in cross-sectional area between the
microphone diaphragm and the connecting tube end, which were 1960 and
2.01 mm^2 respectively. As it was impossible to estimate accurately
the errors in the experiment it was decided that the analysis of Holman
should be used to determine the attenuation of the pressure waves
within the transducer connections.

Figure 3.19 shows a diagram of the apparatus used to amplify the
signal from the Kistler transducer. The charge amplifier was Type
TA-3/C, manufactured by Vibro-Meter Ag. The amplified signal from it
was filtered by a Dawe Type 1461 A Wave Analyser, and the filtered
signal was displayed on an Advance OS 1000 oscilloscope. The
magnitude of the pressure amplitude was measured by means of the
graticule on the screen, graduated in millimetres. The signal
connections were made with coaxial leads, and it was vital, when
settling up the equipment, to maintain the insulation resistance to
14 MΩ. This was achieved with a Freon aerosol sprayed onto the

plugs and sockets before connection. The oscilloscope had a facility for rapid calibration of the y amplification and this was also done before experiments. This was always adjusted, when taking readings, so that the waveform filled the graticule. This procedure minimised reading errors. The oscilloscope was equipped with a single-shot facility and a mounting for a Polaroid camera. This permitted recordings of any pressure waveform to be obtained with difficulty. It was necessary only to set the brightness of the trace low, open the camera shutter, press the single-shot button and release the shutter. The film used was Kodak 107 and was developed in the recommended way.

The transducer sensitivity was 2230 ± 5 pc/Atm (Kistler calibration) and the charge amplifier potentiometer was set such that the system sensitivity was 0.199 ± 0.006 kN/m^2 per mm. on the oscilloscope graticule.

3.6.1 The Independent Variables

The independent variables for the experiments are listed in Table 3.5.   Of the five, the preliminary investigation (Appendix B) showed that the effects of changes in B, C and E were small compared to changes in A and D.

Table 3.5 Independent Variables

A	Fuel flowrate	$0.13 < \dot{m}_p < 0.8$ kg/h
B	Water flowrate	$120 < \dot{m}_w < 588$ kg/h
C	Coolant flowrate	$1 < \dot{m}_{gc} < 10$ kg/h
D	Aero' valve diameter	$D_I = 13, 16, 19$ mm.
E	Augmenter position	$2.08 < x_{AUG} < 3.05$ m.

The following experiments were therefore carried out:

1) the combustor was operated to establish an energy balance for values of D = 13,16,19 mm. and $\dot{m}_p$ in the range 0.13 to 0.6 kg/h. Application of the First Law to a control volume around the apparatus permitted a table of energy exchanges to be drawn up;

2) the combustor was operated at gradually increasing fuel flowrates, and measurements of frequency and gas and chamber temperatures were taken.   By this means, the resonant frequencies of the combustor were found for varying gas temperature distributions;

3) the combustor was finally operated to obtain data from which the local and overall heat transfer coefficients could be calculated. Pressure amplitudes were measured also, and the velocity amplitude of the gas was deduced by assuming a sinusoidal variation with time.   From these results correlations of $\dfrac{\overline{Nu}_p}{Nu}$ against x were plotted.

3.6.2 Experimental Technique

The combustor was started by supplying a combustible mixture of fuel and air to the chamber and igniting it with a high tension spark. A flow of propane in the range $0.19 < \dot{m}_p < 0.49$ kg/h was required for this purpose, and a suitable flow of air, directed into the aerodynamic valve, was found by experiment. Once the combustor had started, the forced air supply could be shut off, although the combustion would sometimes quench if this was done when the chamber walls were below approximately 260 ^{o}C. Great care was taken when using the trembler coil to ensure that all the electronic apparatus was grounded. Failure to follow this precaution could have led to an instrument malfunction due to the inductance of the connecting signal leads.

It was found that the combustor required nearly an hour to reach thermal equilibrium. This condition was taken to be when the chamber temperature varied by less than 2 ^{o}C per minute. Clearly the process was accelerated by setting a high fuel flowrate. Before readings could be recorded, it was necessary to check that the fuel gauge pressure, P_p, and temperature, T_p, were set correctly, and that the water flowrate was steady. For all experiments the local atmospheric pressure and temperature were recorded before and after the readings were taken.

The operation of the apparatus for experiment 1 presented no particular difficulties. Readings were taken every 5 minutes for a period of 30 minutes. For experiment 2, the combustor had to be operated at first at a very low fuel flowrate to obtain its lowest resonant frequency, and the pressure amplitude was found to be very

unsteady. The combustor also did not remain in thermal equilibrium as its lowest frequency. For these reasons, it was necessary to collect the data briskly and thus the accuracy of the experiment suffered. For higher fuel flowrates and thus higher frequencies, the combustor did reach equilibrium, and the accuracy improved.

During experiment 3, it was found that the combustion became slightly unstable when the caps on the instrument sites were removed. Thus several minutes were allowed to elapse while the apparatus, and the inserted instrument, reached equilibrium once more.

4.1. The Energy Balance

The results of Experiment 1 are presented in Appendix E. The double-orifice pulsating combustor is a flow process and, therefore, by drawing a Control Volume around the apparatus, as in Figure 4.1., the First Law of Thermodynamics may be applied in the form of the Steady Flow Energy Equation. The discrepancy between the two sides of the equation lay within the range -5.7 to +10.0%. This was regarded to be acceptable. The calculations also yielded the variation of the thermal efficiency with the fuel flowrate, and this has been plotted in Figure 4.2. The graph shows that the thermal efficiency decreases with increasing fuel flowrate. This trend was found with earlier combustors, as shown in Figure 3.5. and was observed by Hanby (39) and Reay (20). The thermal efficiency varies from 0.74 to a maximum of 0.94. It is difficult to choose an aerodynamic valve which performs best. D_I = 13mm. gave the best efficiency over the range of fuel flowrate but D_I = 16mm. attained the maximum efficiency.
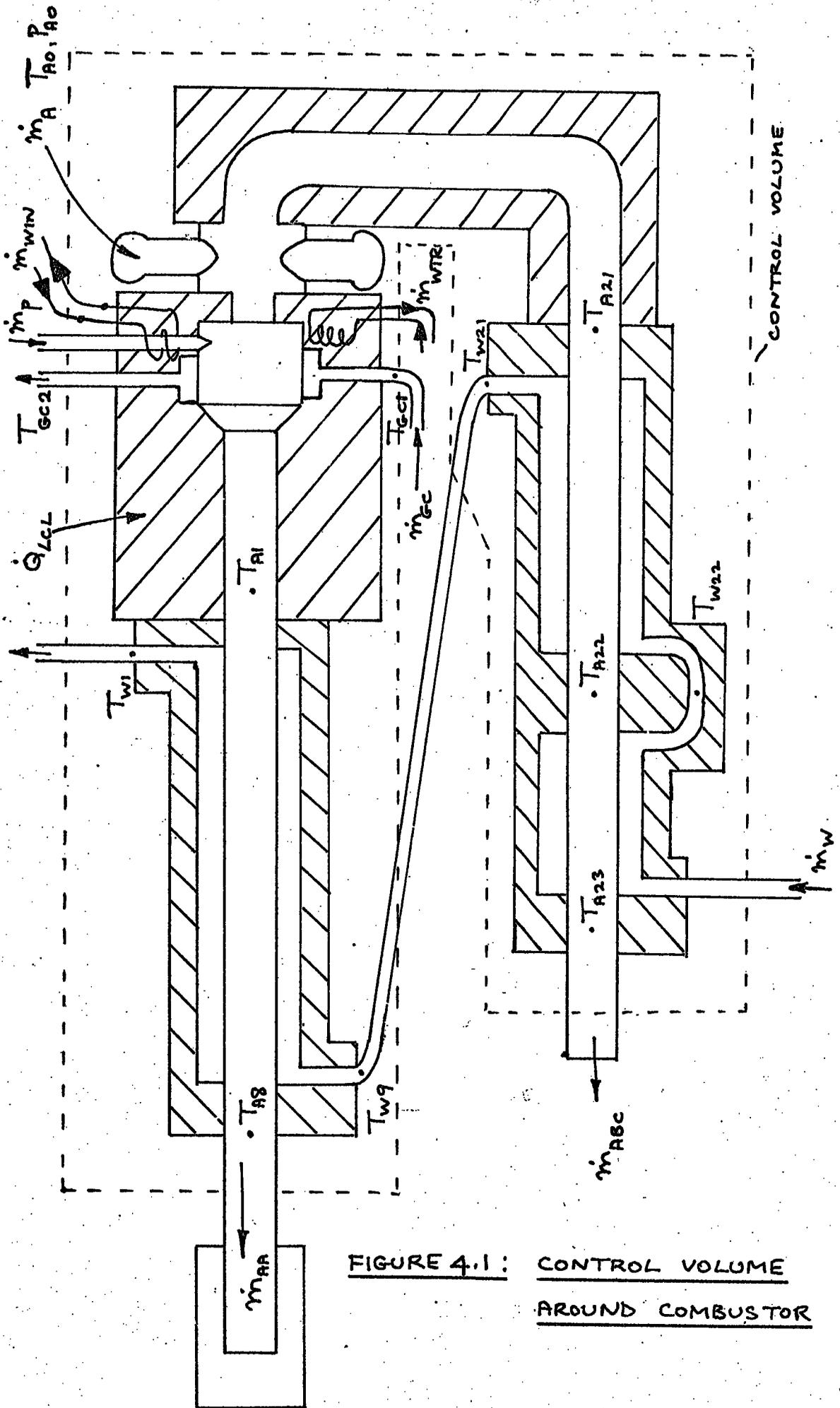
FIGURE 4.1: CONTROL VOLUME AROUND COMBUSTOR
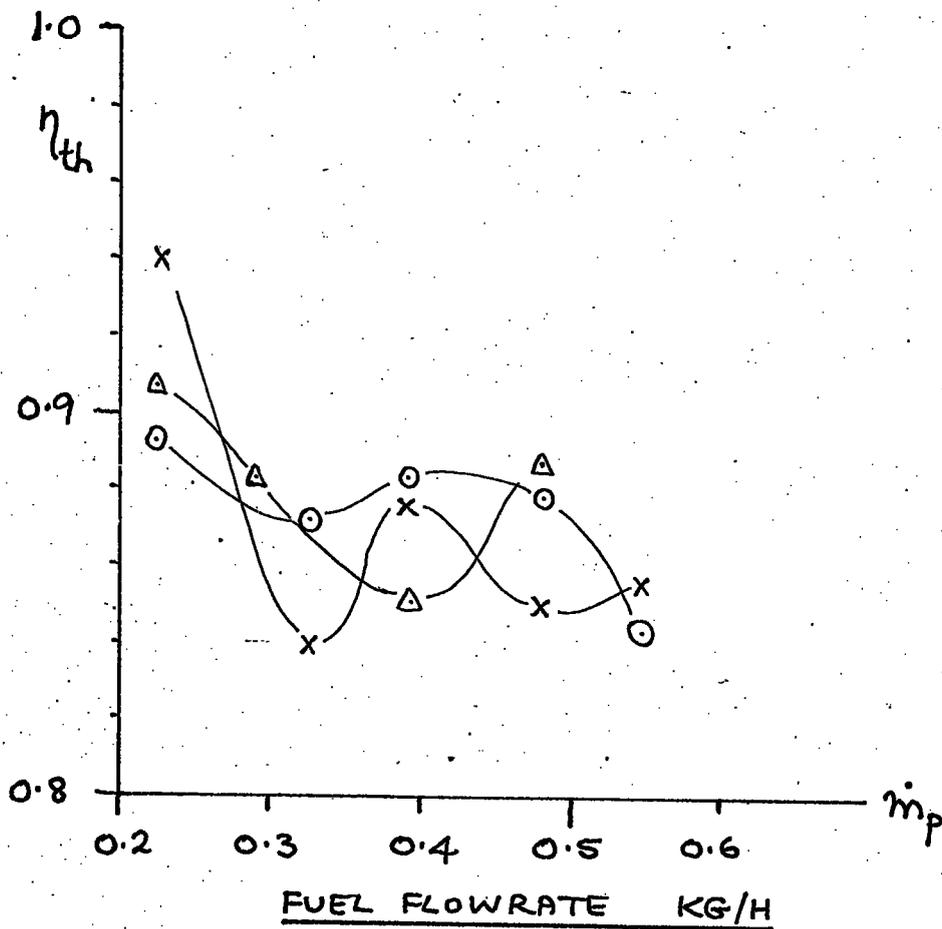
FIGURE 4.2: VARIATION OF THERMAL EFFICIENCY OF COMBUSTOR WITH FUEL FLOWRATE

4.2. The Aerodynamic Valve

The net flow of air, $\dot{m}_{AA}$, through the aerodynamic valve was deduced from the results using equation E.1.17. Knowing the corresponding pressure amplitude in the combustion chamber, it was possible to compare the experimental results with the values obtained by the quasi-steady state approach of Section 2.5. The comparison may be made in Figure 4.3.

It is evident that the experimental curves follow the theoretical ones approximately in shape, but, except the theoretical ones for D_I = 13mm., do not agree in magnitude. It is interesting to note that the pressure amplitude reaches its maximum value for D_I = 19mm. The curves verify the experimentally observed fact that the combustor pumps its own combustion air through itself. The difference between the curves is due to the assumptions made in the quasi-steady state approach. These were that the flow was a) isentropic and b) frictionless, and that c) the kinetic energy of the fluid entering the valve during the cycle was negligible compared to that leaving it, and that d) the equation held at all instants of time. Of these assumptions, b) and d) are the most suspect. In addition, the fluid during the exhaust part of the cycle was hot combustion gas. It was assumed that the inlet air was at 520 ^{o}C by taking a mean of the profile shown in Figure 4.4. A Type K thermocouple was mounted on a probe, and the probe onto a rack mechanism, and fed into the valve and chamber. It shows that the mean temperature of the gases in the aerodynamic valve to rose from 215 ^{o}C at entry to 850 ^{o}C for = 0.409 kg/h. Figure 4.5. shows a temperature traverse of the combustion chamber itself for the same fuel flowrate. The maximum temperature of the gases occurs at the axis of the chamber, and the minimum at the walls. There appears to be an annulus of relatively cooler gas extending from the valve lip into the chamber along the axis. Also from Figure 4.5. this low temperature gas extends across the cross-section in Plane 7. This gas is cooler due to the heat exchange between it and the valve walls. The core is clearly highly turbulent from its rapid rise in temperature - 830 ^{o}C just past Plane Y

93
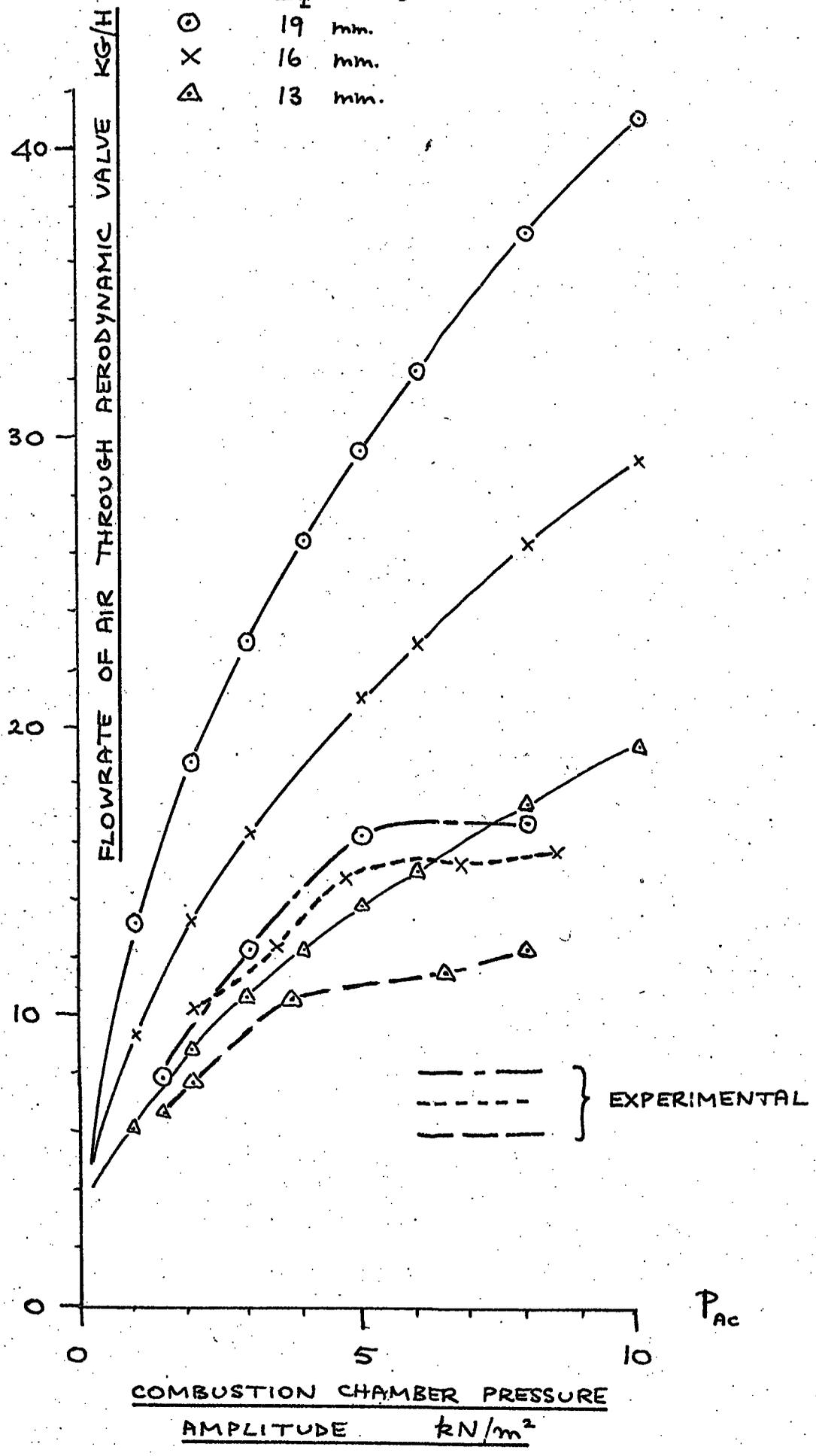
FIGURE 4.3 : NET FLOW THROUGH AERODYNAMIC
VALUE — COMPARISON OF EXPERIMENTAL
VALUES WITH THEORETICAL

FIGURE 4.4: AXIAL (TIME-AVERAGED) TEMPERATURE PROFILE OF GASES WITHIN COMBUSTION CHAMBER — $\dot{m}_p = 0.41$ kg/h
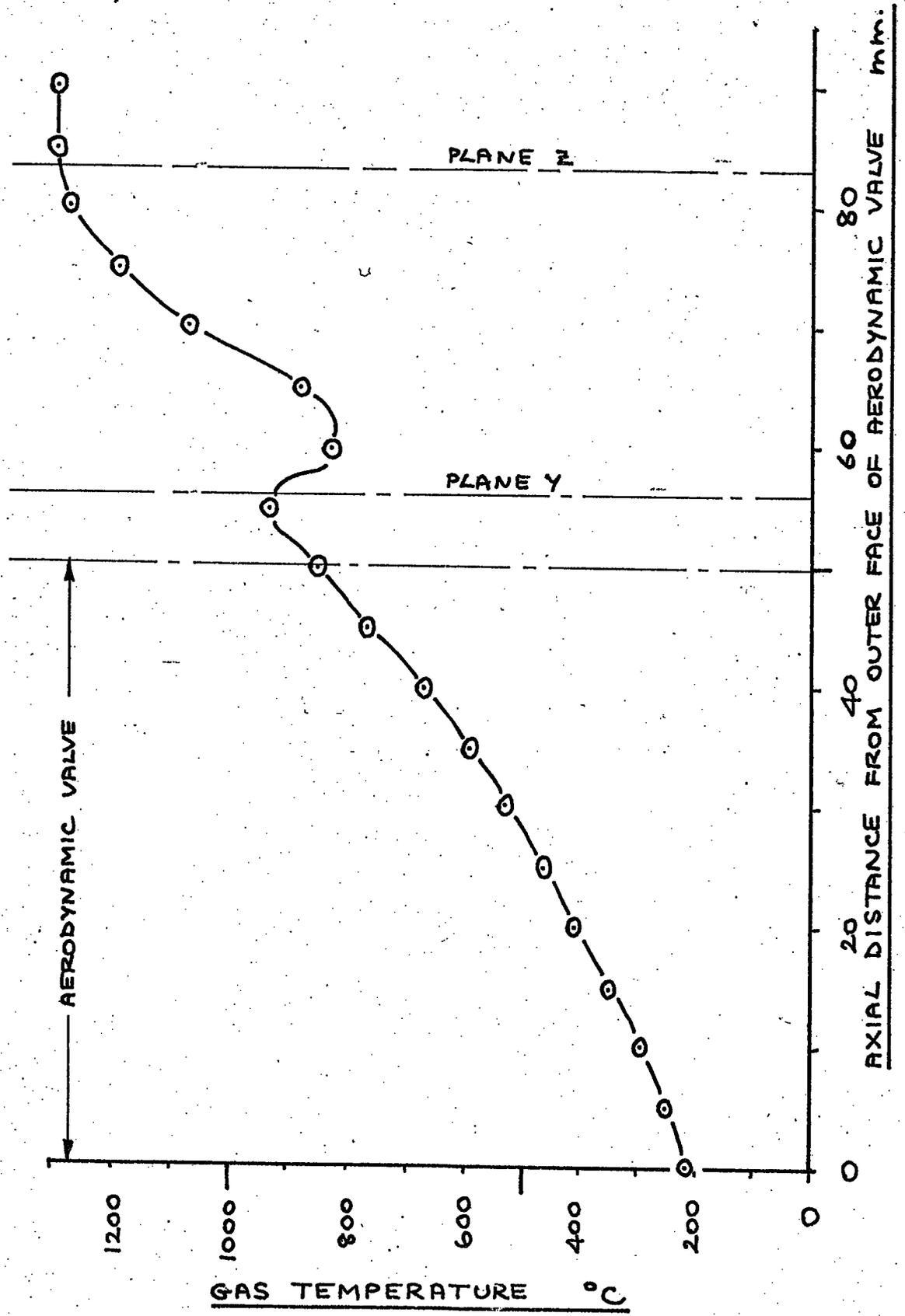
FIGURE 4.5 : TEMPERATURE TRAVERSES ACROSS COMBUSTION CHAMBER FOR TWO FUEL FLOWRATES

⊙ $\dot{m}_p$ = 0·50   KG/H

△ $\dot{m}_p$ = 0·41   KG/H
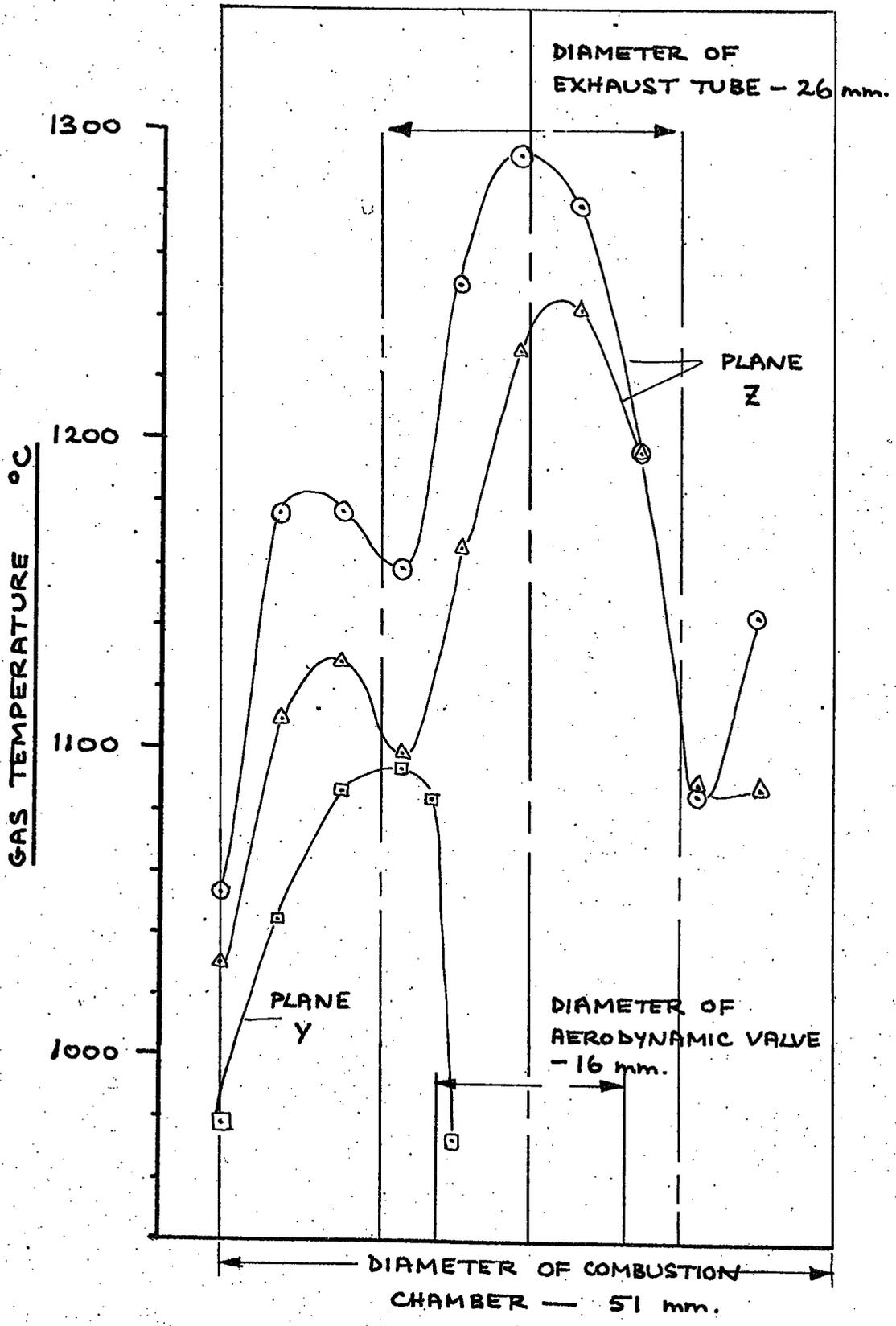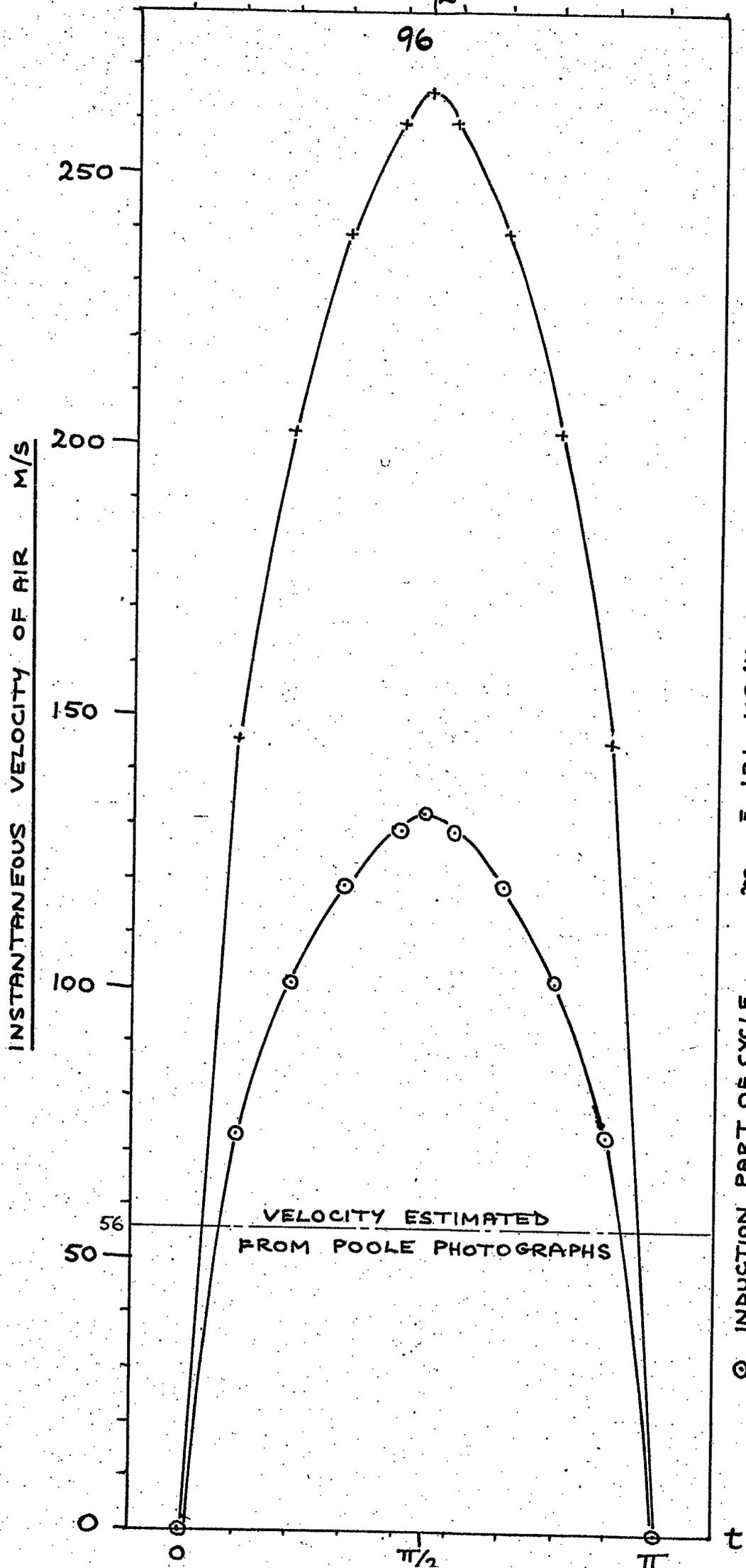
FIGURE 4.6: INSTANTANEOUS VELOCITY OF GASES WITHIN AERODYNAMIC VALVE

to 1300 $^{\circ}$C at Plane Z, 27 mm. into the chamber. It is important to remember these are time-mean temperatures, and that events are occurring in reality at the rate of one cycle in 4 mS. The abrupt cooling of the gases in Plane Y may be due to a nozzle expansion effect. At high fuel flowrates, the combustion process emerged from the aerodynamic valve. It was the energy dissipation represented by this flame that led to the addition of heat exchangers B and C.

Using equations 2.5.9. and 2.5.11., the velocity of the gases passing through the aerodynamic valve were calculated for regular intervals during the cycle. These have been plotted in Figure 4.6., and show that the exit velocity of the gases is higher than the induction velocity. Given the discrepancy in Figure 4.3., it is probable that these velocities are generally too high. Tentative confirmation of this view was provided in a photographic study by Poole (49). Poole studied a pulsating combustor whose combustion chamber was fitted with quartz windows. Using a schieren technique, the combustion was filmed with a rotating prism high-speed camera at a rate of 8000 pictures per second. A typical sequence of 5 frames is shown in Figure 4.7. The pictures show a column of gas progressing along the axis of the combustion chamber, whose dimensions were similar to those employed in this study, the main difference being that the cross-section of the Poole chamber was square. The scale of the pictures is 1:1.695 and the time interval between them is 50 μS. The mean velocity of the line, marked A, over the five pictures is 56 m/s. This compares favourably with the values of Figure 4.6. The difficulty in making a strict comparison is to place the sequence of pictures correctly during the cycle. Examination of several whole cycles of pictures, and further work of Poole synchronising the pressure amplitude onto the film, suggests that the sequence of events in Figure 4.7. occurs approx-imately $\frac{\omega}{12\pi}$ before the maximum pressure in the chamber.

FUEL INJECTOR

QUARTZ WINDOW
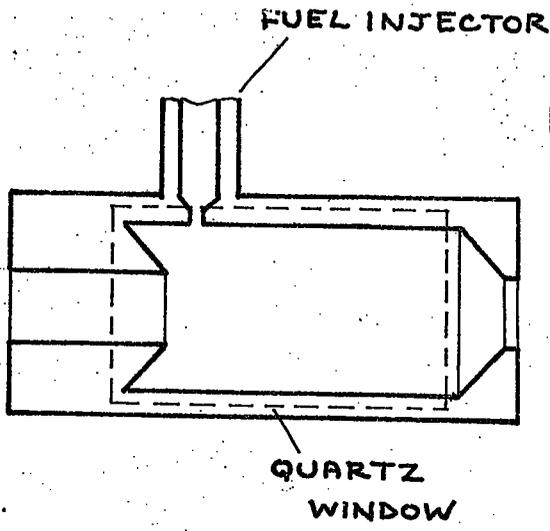
APPARATUS OF POOLE

The original of this photograph is held in the Science Library in the top copy.

A

TIME INCREASING
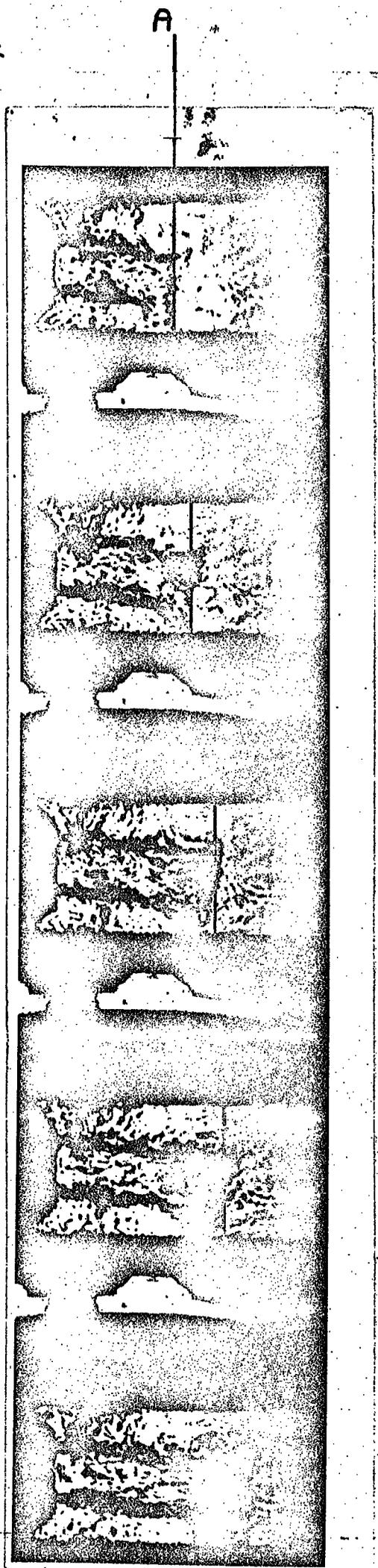
FIGURE 4.7: SCHLIEREN PHOTOGRAPHS FROM WORK BY K. POOLE

4.3. Characteristics of Resonating Section

The first result of experiment 2 is shown in Figure 4.8., where the operating frequency of the combustor is plotted against fuel flowrate. The graph has been divided into four parts by lines A, B, C and D. Up to A, the pressure oscillations in the combustion chamber were too small and irregular to be measured with any certainty. In the region AB the frequency varied from 59 to 70 Hz for D_I = 13 and 16 mm., and from 74 - 93 Hz for D_I = 19 mm. Then by increasing the fuel flowrate to and beyond B, the frequency would begin to jump and settle on a higher note. For D_I = 13 and 16 mm. this was approximately 117 Hz, and, for D_I = 19 mm., it was approximately 154 Hz. With increasing fuel flowrate a similar transition occurred around C where the frequency jumped to 193 Hz for D_I = 13 and 16 mm. and to 240 Hz for D_I = 19 mm. At D, the frequency jumped again for D_I = 16 mm. to 280 Hz. For clarity, the transition frequencies are shown in Table 4.A.

Table 4.A. Transition frequencies

D_I	13,16 mm.	19 mm.
Transition frequency, f	59	80
	117	154
	193	240
	280 (16 mm. only)	
	Hz	Hz

Figure 4.8. also shows that, for a given mode of operation, the frequency increases with fuel flowrate. The slope of the lines is approximately 100 Hz per kg/h fuel flowrate. The only exception is for D_I = 19 mm. at 154 Hz where the slope is approximately 2 Hz per kg/h. The explanation for the rise in frequency lies in the increasing mean temperature of the gases within the resonating section.
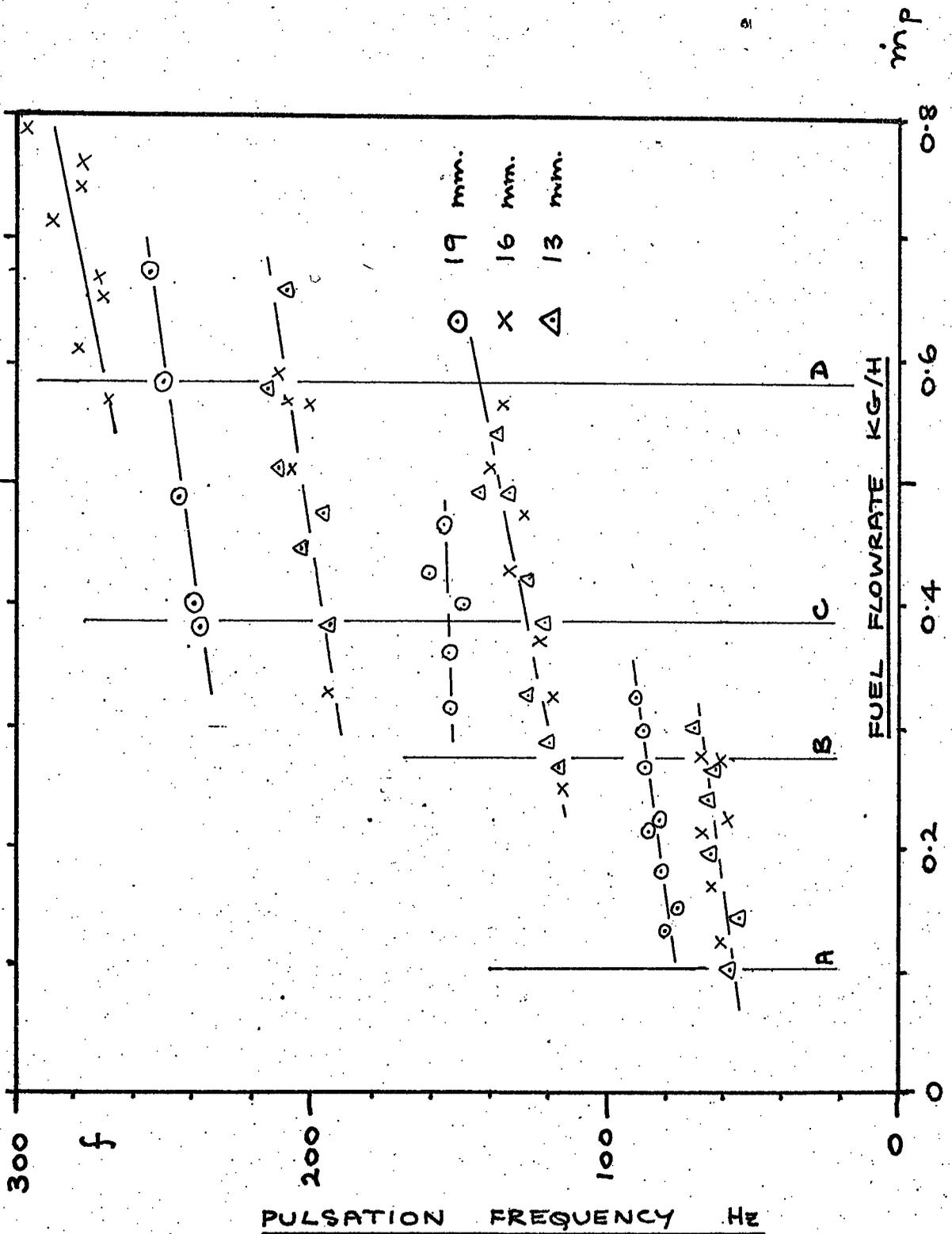
FIGURE 4.8 : VARIATION OF COMBUSTOR
PULSATION FREQUENCY WITH
FUEL FLOWRATE

4.3.1. Waveform

Due to the assumption of a sinusoidal pressure variation in Section 2, it was necessary to investigate the nature of the waveform. It was found that, at low fuel flowrates, the oscillations were irregular. This is demonstrated by Figures 4.9. and 4.10 which show the pressure variation in the combustion chamber for $D_r = 19$ mm. and for two low fuel flowrates. From Figure 4.8. it will be seen that, for $\dot{m}_p \approx 0.27$ kg/h, the frequency is in an unstable region and can jump to approximately 154 Hz, whereas, for $\dot{m}_p \approx 0.18$ kg/h the frequency is stable at approximately 80 Hz. Figure 4.10. shows that the fundamental frequency of 80 Hz is extremely irregular. In Figure 4.9. the waveform is more regular and its amplitude has increased from 2.5 to 5 divisions.

Figure 4.11. shows the pressure variation for the same aerodynamic values and for $\dot{m}_p = 0.42$ kg/h. The smoother nature of the oscillations is evident, and the amplitude has increased to 14 divisions. Figure 4.12. shows the pressure variation at 160 Hz which is fundamentally sinusoidal. It was found that the smoothness and stability of the oscillations at a particular fuel flowrate always improved when the combustor attained thermal equilibrium.

4.3.2. Pressure Amplitude Variation

The readings for the axial distribution of pressure amplitude in the resonating section were obtained by screwing the pressure transducer into each of the measuring sites in turn. During the experiments, the combustor was maintained in operation in order not to disturb its thermal equilibrium. The results of three such tests for $\dot{m}_p = 0.45$ kg/h are shown in Figures 4.16., 4.17. and 4.18. The distributions each show slight irregularities in the region of the combustion chamber. This was felt to be acceptable due to the combustion process and the flux of the inlet and exhaust gases. At the cold end of the resonating section in Figures 4.16. and 4.18, the reading has not fallen to zero as expected. This was felt to be due to the 'end effect' found in organ pipes.

The originals of these photographs are held in the Science Library in the top copy.

P06
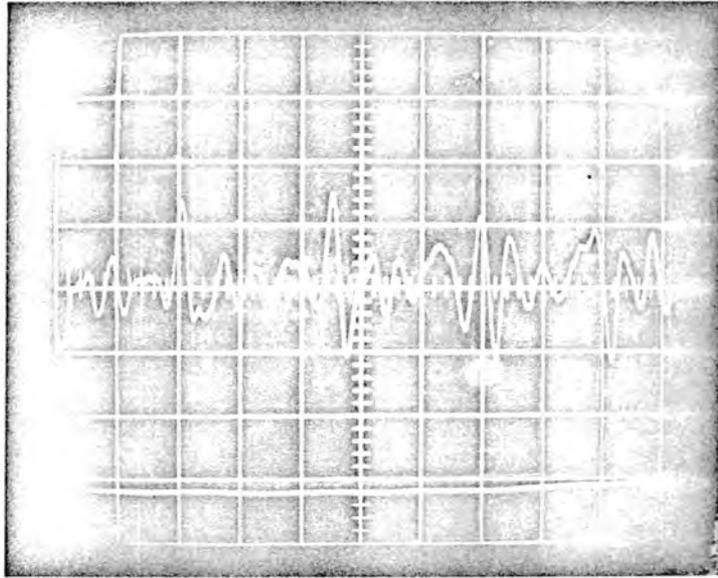
91 Hz

FIGURE 4.9 :   PRESSURE VARIATION FOR

$D_I = 19$ mm AND $\dot{m}_p = 0.27$ KG/H

P13
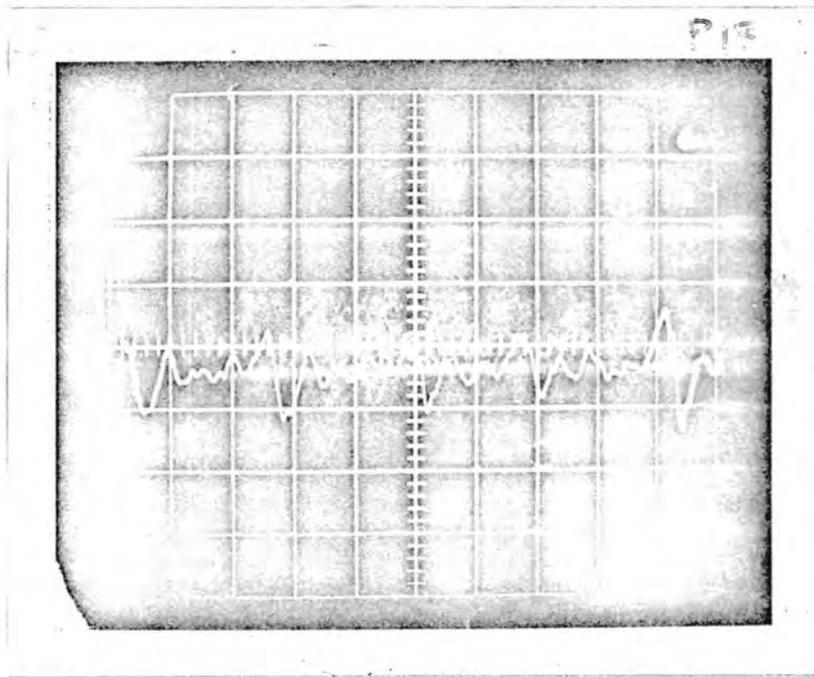
80 Hz

FIGURE 4.10 : PRESSURE VARIATION FOR

$D_I = 19$ mm. AND $\dot{m}_p = 0.18$ KG/H

The originals of these photographs are held in the Science Library in the top copy.
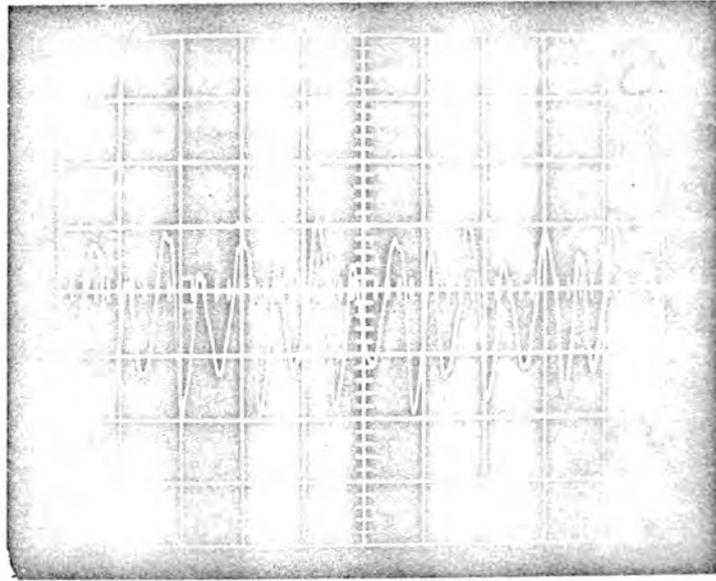
160 Hz

FIGURE 4.11 : PRESSURE VARIATION FOR
$D_I = 19$ mm. AND $\dot{m}_p = 0.42$ KG/H
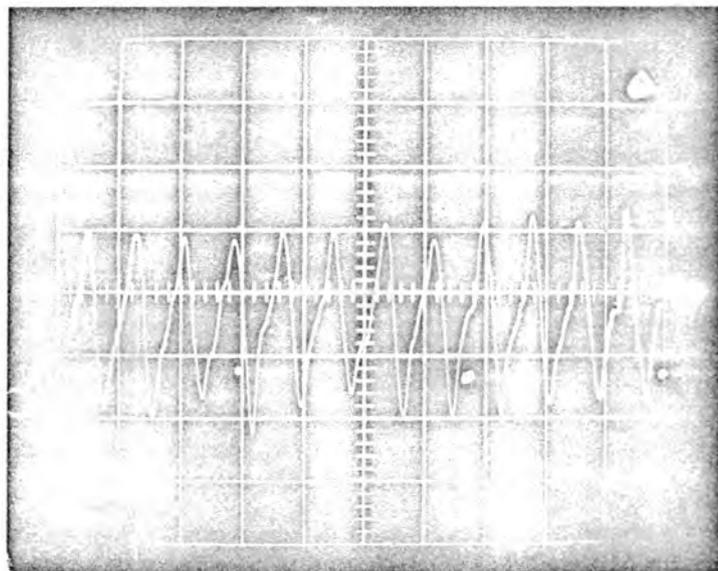
240 Hz

FIGURE 4.12 : PRESSURE VARIATION FOR
$D_I = 19$ mm. AND $\dot{m}_p = 0.47$ KG/H

The distributions are generally smoother than those of Reay (20), as shown in Figure 4.13. Reay reported in the work that the pressure measurements were complicated by the presence of harmonics.

The phase of the readings was found by comparing on the oscilloscope two traces; one from the combustion chamber as a reference, and the one being measured. The nodes of the distribution are at $x = 1.53$ m, $x = 1.0$ and 2.21 m., and $x = 1.68$ m. for $D_T = 13$, 16 and 19 mm. respectively. An attempt was made to measure the exact position of these nodes by passing a long, tubular probe into the combustor from the cold end. The tube was connected to the pressure transducer. Although the method was found to work in principle, the probe interfered with the combustor operation and thus altered the frequency.

It may be concluded from the magnitude of the distributions at $x = 0$ and $x = 3.05$ m. that the resonating section behaved as an 'open-closed' organ pipe for $D_T = 13$ and 16 mm. and as an 'open-open' organ pipe for $D_T = 19$ mm. Table 4.A. may now be written;

4.B. Transition frequencies showing wavenumber, n

$D_T = 13$, 16 mm.	$D_T = 19$ mm.
59 n = 1 (40)	80 n = 1 (80)
117 n = 2 (120)	154 n = 2 (160)
193 n = 3 (200)	240 n = 3 (240)
280 n = 4 (280)	
Hz Hz	Hz Hz

In Table 4.E. the transition frequencies are shown together with wavenumber, n. For $D_T = 13$ and 16 mm., the behaviour of the combustor during warm-up follows the sequence given by the simple acoustic relation;

$$f = \frac{(2n-1)c}{4L} \quad \text{Hz} \qquad\qquad 4.3.1.$$

and for $D_T = 19$ mm.

$$f = \frac{nc}{2L} \quad \text{Hz} \qquad\qquad 4.3.2.$$
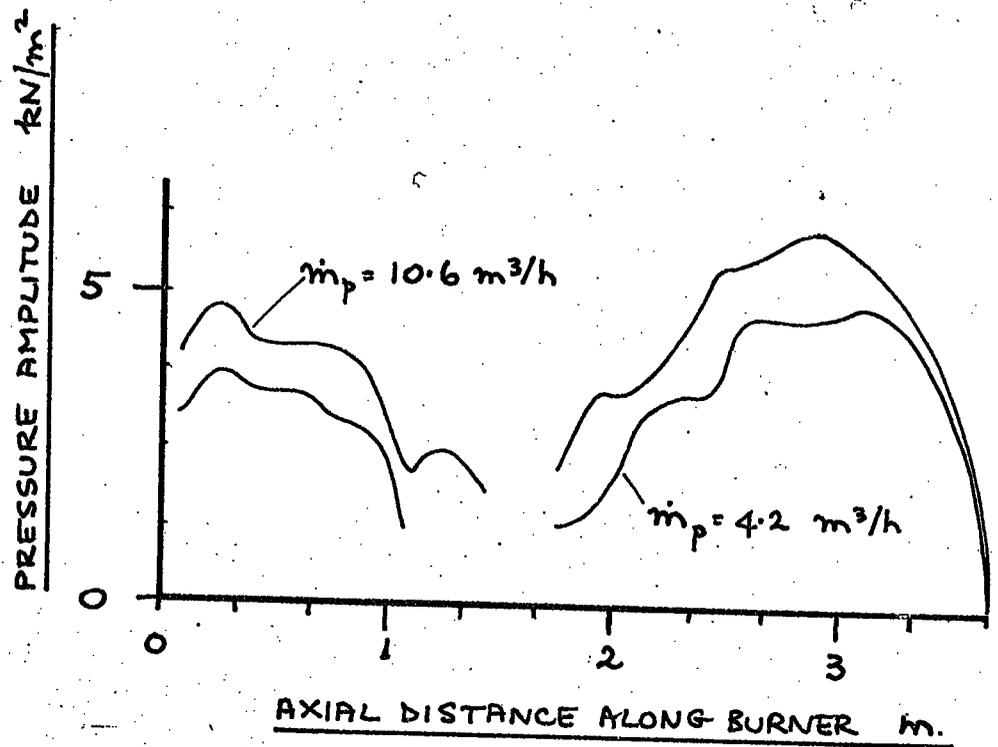
FIGURE 4.13: PRESSURE AMPLITUDE DISTRIBUTION IN A COMBUSTOR BY REAY (20) FOR TWO FUEL FLOWRATES

The exception occurs for $D_I = 13$ and 16 mm. with the initial frequency of 60 Hz. It is felt that, in this particular case, the resonating section behaves as an 'open-open' organ pipe. The objection to this is that the initial frequency is 21 Hz below that for $D_I = 19$ mm. It is possible that the mean temperature pf the gases was lower for $D_I = 13$ and 16 mm. but no measurements are available to support this view.

A Dawe Wave Analyser was used to examine the warm-up waveforms, illustrated by Figures 4.9. and 4.10. It was found that the waveform contained a frequency double that of the main one, but of lesser magnitude, in all cases. This observation could explain the first jumps of frequency at line B in Figure 4.8. With increasing fuel flowrate, the magnitude of the 80 Hz frequency, for example, decreased while that of the 160 Hz frequency increased. At a critical fuel flowrate, approximately 0.27 kg/h, both frequencies became unstable. With a further increase in fuel flowrate, the oscillations settled at 160 Hz.

4.3.3. Axial temperature distribution

Figure 4.14. shows the axial gas temperature distribution in Heat Exchanger A for $D_I = 16$ mm. and for four fuel flowrates. The temperature falls between 950 and 1450 K over the length of the heat exchanger. It was found that the exit temperature of the gases was generally below the condensing temperature, 100 $^\circ$C.

Figure 4.15. shows the fitting of curves to the experimental gas temperature distributions. The isothermal line, T = 715 K, is clearly very poor. The exponential curves were fitted to the temperatures T_{A1} and T_{A8} It was found that the resultant curve was very flat and tended to a straight line. In Figure 4.15 , the exponential curve fits the experimental points to within 26%. For the case of the general solution, Equation 2.3.24., it was decided that a sinusoidal curve was the best fit, as shown in Figure 4.15. The sine curve fits the points to within 8%, and it was found to fit all the temperature distributions to within 12%. As for the exponential curve, the

FIGURE 4.14: AXIAL GAS TEMPERATURE DISTRIBUTION IN HEAT EXCHANGER A FOR $D_I = 16$ mm. AND FOUR FUEL FLOWRATES
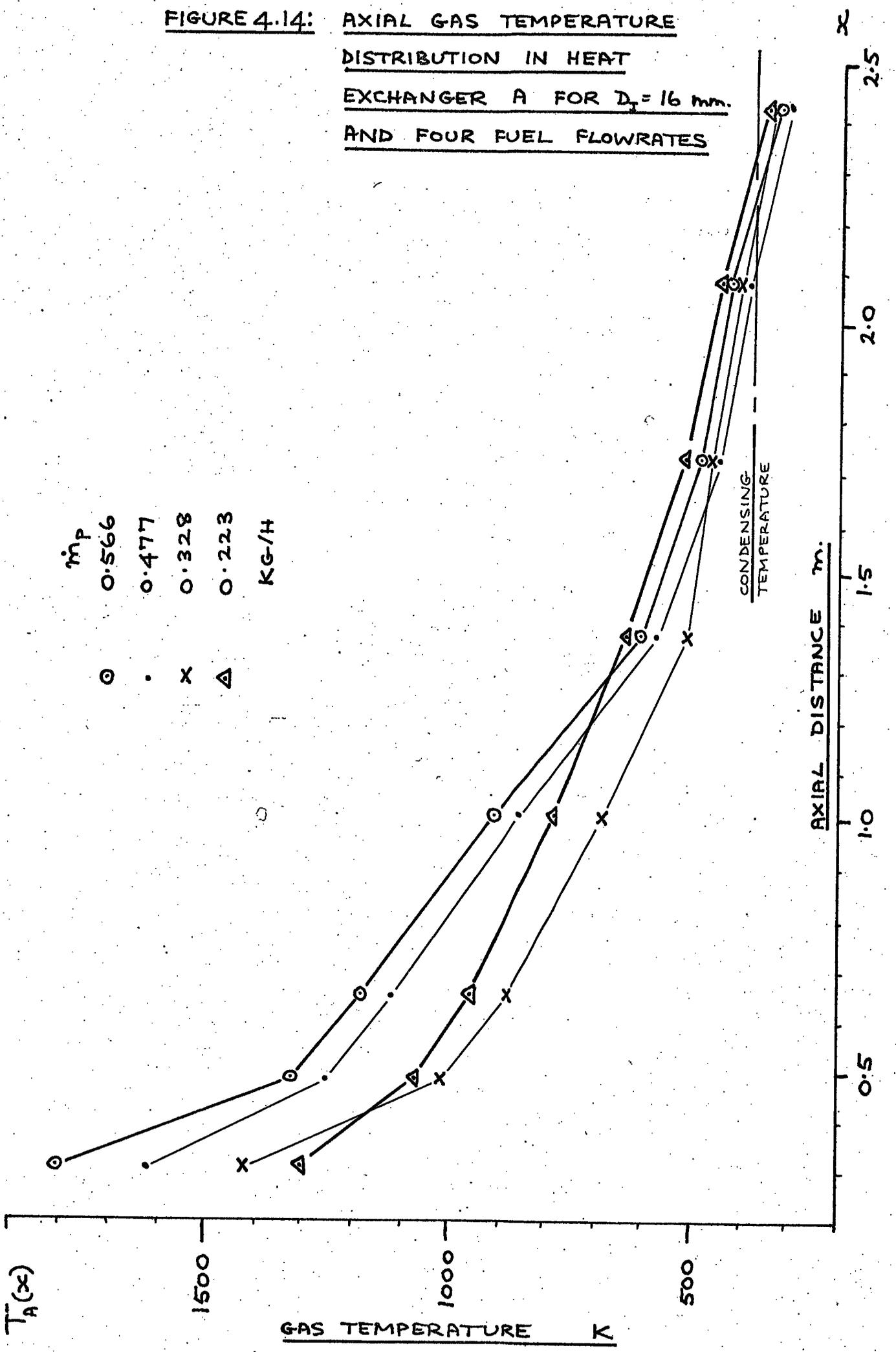
FIGURE 4.15: FITTING OF CURVES TO AXIAL GAS TEMPERATURE DISTRIBUTION IN RESONATING SECTION FOR $D_T = 16$ mm. AND $\dot{m}_p = 0.24$ KG/H

⊙ EXPERIMENTAL

——·—— $T = 715$ K

——— $T(x) = 1550\, e^{-0.5021\,x}$

——— $T(x) = 1550 - 1200 \sin\left(\dfrac{\pi x}{6}\right)$

X

HEAT EXCHANGER A

AXIAL DISTANCE m.

$T_A(x)$

1500

1000

500
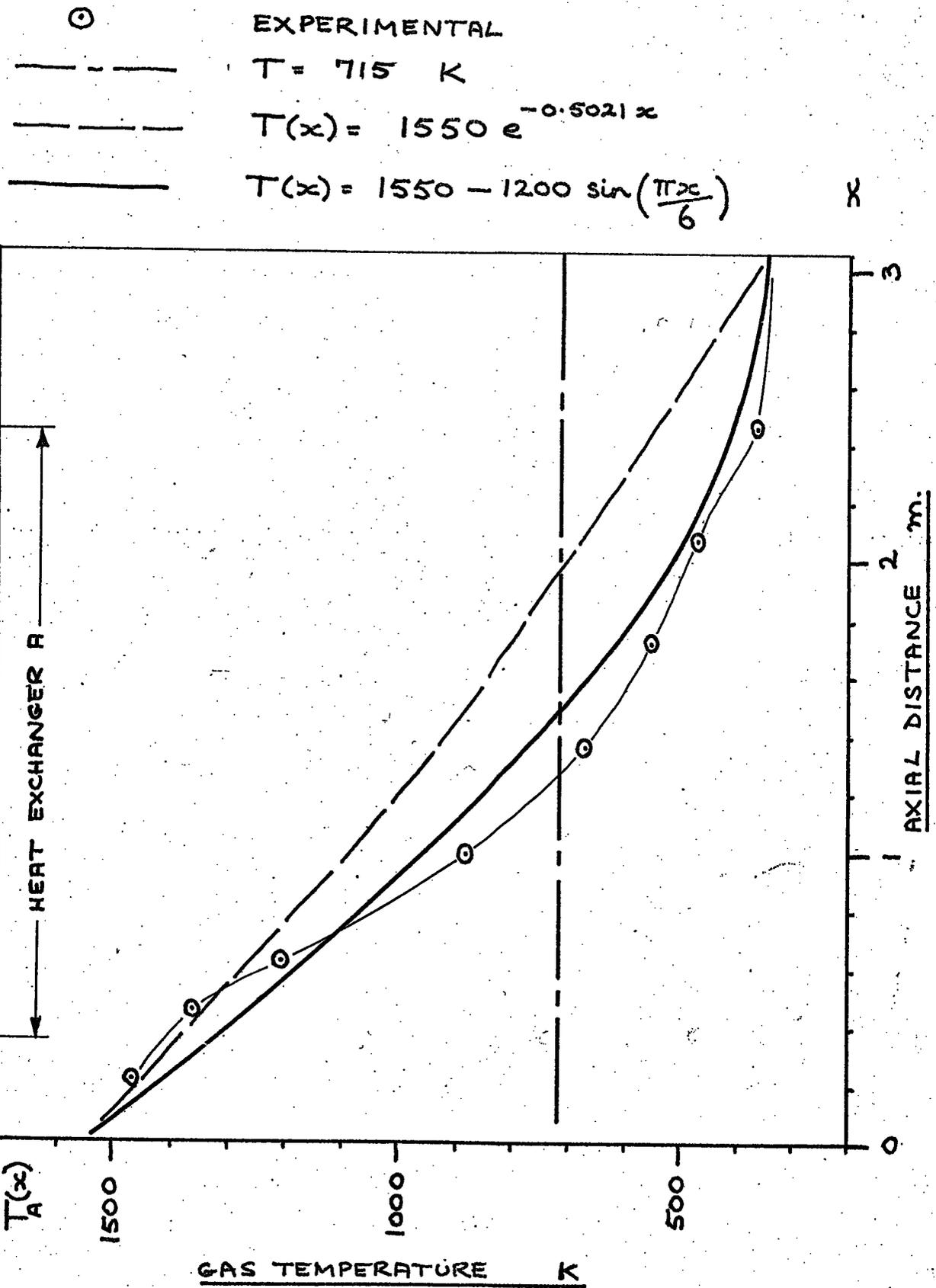
GAS TEMPERATURE K

fitted points were T_{A1} and T_{A8}.

4.3.4. Frequency & Pressure Amplitude Predictions

Table 4.C. shows the comparison between the experimental values and the analytical predictions, based on the temperature measurements.

TABLE 4.C.

Frequencies

Experimental	Isothermal	Exponential	General
116	126 (+ 8%)	111 (- 4.5%)	115 (- 0.8%)
195	223 (+ 12.6%)	188 (- 3.8%)	193 (- 1.0%)
132.5	121 (- 9.5%)	111 (- 19.5%)	132 (- 0.5%)
201	217 (+ 7.2%)	188 (- 7.0%)	198 (- 1.9%)
75.5	87 (+ 13.2%)	-	77 (+ 2.0%)
145	178 (- 19.5%)	-	146 (+ 0.7%)
Hz			

The agreement between the isothermal frequency and the experimental ones is not better than 7.2%, and is on average 11%. The agreement between the exponential frequencies and the experimental ones lies in the range 3.8 to 8.5%. The prediction by the general solution, using the sinusoidal fit, is clearly the best, being on average 1.1%.

The predictions of the general solution for the axial distributions of pressure amplitude have been plotted in Figures 4.16., 4.17 and 4.18. For D_I = 13 mm. and 116 Hz, the general solution fits the experimental points to within 8%. For D_I = 16 and 19 mm., the fit improved to within 6%. The curves demonstrate the increase in pressure amplitude at the cobler end of the resonating section, predicted in Section 2.3. In Figure 4.16., this is 15%, in Figure 4.17., 8%, and in Figure 4.18., 17%. The results also demonstrate the nodal shift towards the cold end. These are 0.51, 0.19 and 0.15 m. respectively for the three figures.

D_I = 13 mm.

f = 111 Hz

AXIAL DISTANCE m.

$\dfrac{P_a(x)}{\langle P_a \rangle}$

DIMENSIONLESS PRESSURE
AMPLITUDE
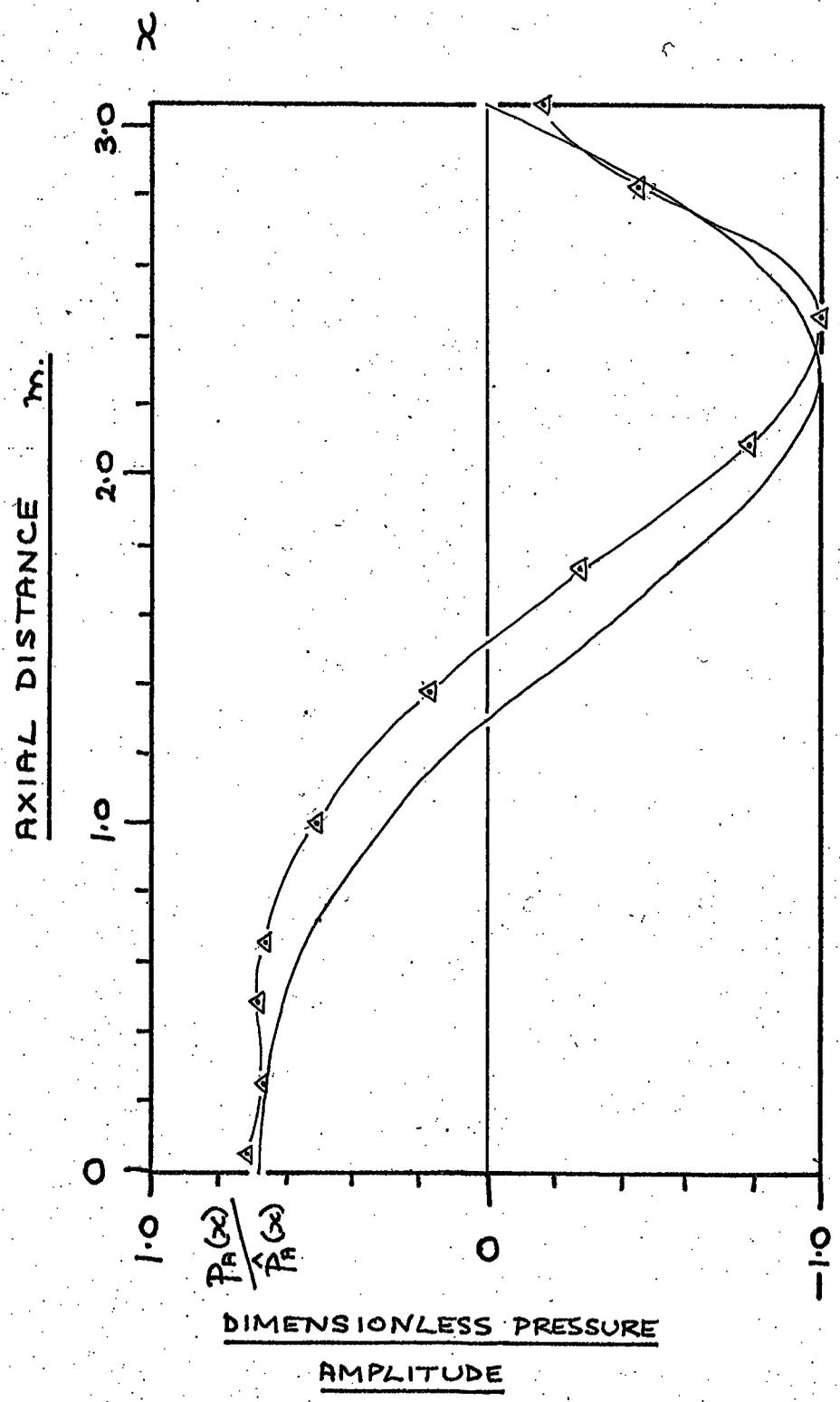
FIGURE 4.17: AXIAL DISTRIBUTION OF PRESSURE AMPLITUDE IN THE RESONATING SECTION

$D_T = 16$ mm.

$f = 202$ Hz
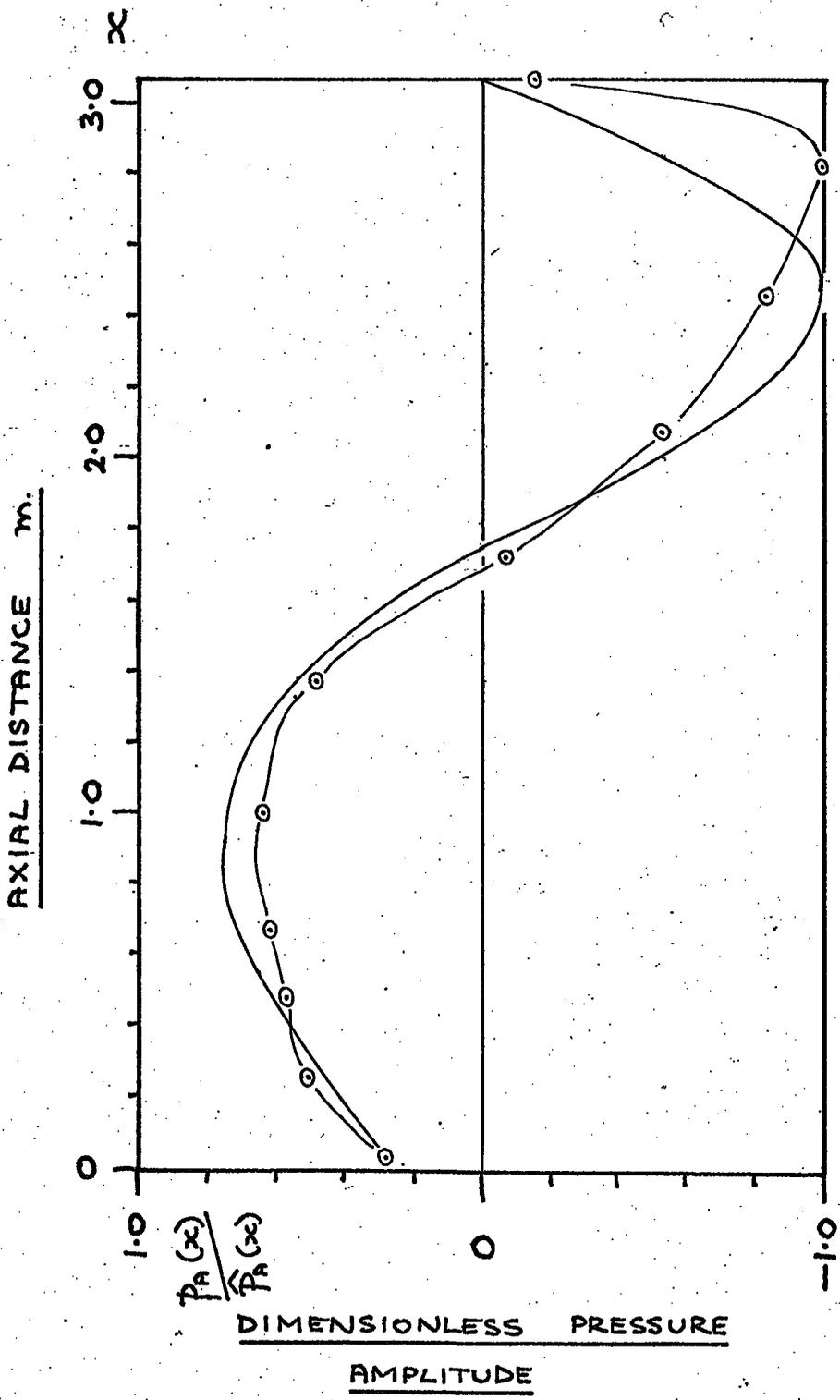
4.4. Heat Transfer

The results of Experiment 3 are tabulated in Appendix E. Both the readings, from which the heat transfer coefficients were calculated, and the derived parameters, are presented in Table E.4. et..seq. The overall heat transfer coefficient, U_A , lay in the range 32.8 to 61.0 W/m^2 K. The value of Reynolds Number, Re_W, for the water flow in Heat Exchanger A lay in the range 655 to 1256. The flow was therefore predominantly laminar. The value of Reynolds Number, $\overline{Re}_A$, for the gas flow through the Heat Exchanger was based on the mean gas velocity, $\overline{u}_A$. Thus;

$$\overline{Re}_A = \frac{\overline{u}_A D_o \rho_A}{\mu_A}$$

4.4.1.

$\overline{Re}_A$ lay in the range 1846 to 6689, and the gas flow was therefore predominantly turbulent. For a tube of 26 mm. diameter, a length of 0.5 m. would normally be required to allow a steady flow to become hydrodynamically developed. Thus it was assumed that the pulsating gas flow became fully developed in the lagged settling length of 0.22 m.

4.4.1. Experimental heat transfer coefficients

The experimental heat transfer coefficients were calculated by dividing the heat exchanger into the seven sections, lying between the gas temperature thermocouples. A typical section is shown in Figure 4.19. Application of the First Law to the control volume leads to the heat transfer coefficients:

$$h_{AS} = \frac{\Delta H_A}{S_S (\overline{\overline{T}}_A - \overline{\overline{T}}_S)}$$

4.4.2.

where S_S is the surface area based on the outside diameter of the inner tube,

$\overline{\overline{T}}_A$ is the mean gas temperature,

$\overline{\overline{T}}_S$ is the mean surface temperature,

ΔH_A is the change of enthalpy of the gas (equal to that of the water, assuming negligible losses through the lagging).

The water and surface temperatures corresponding to the points were found by linearly interpolating between the nearest adjacent readings. These calc-
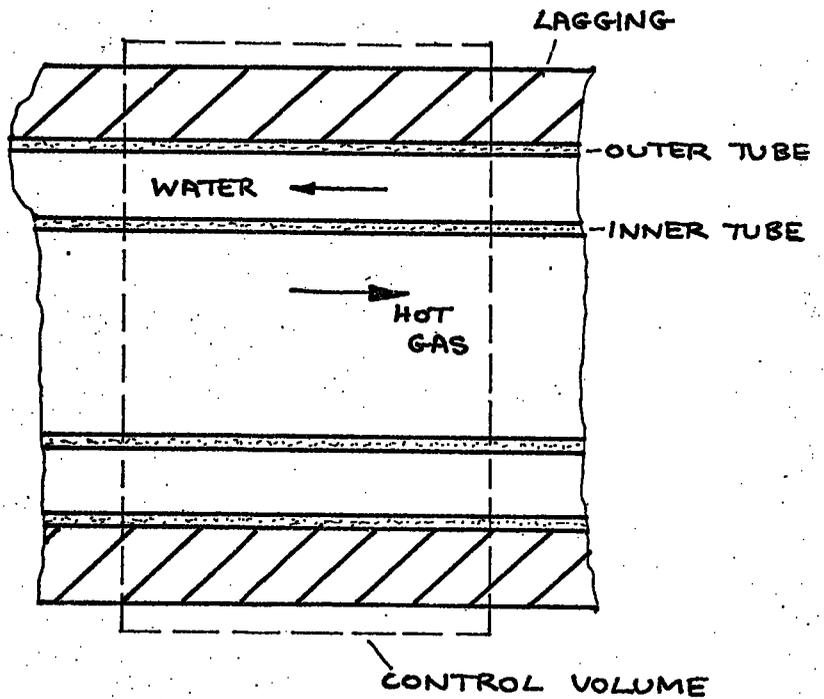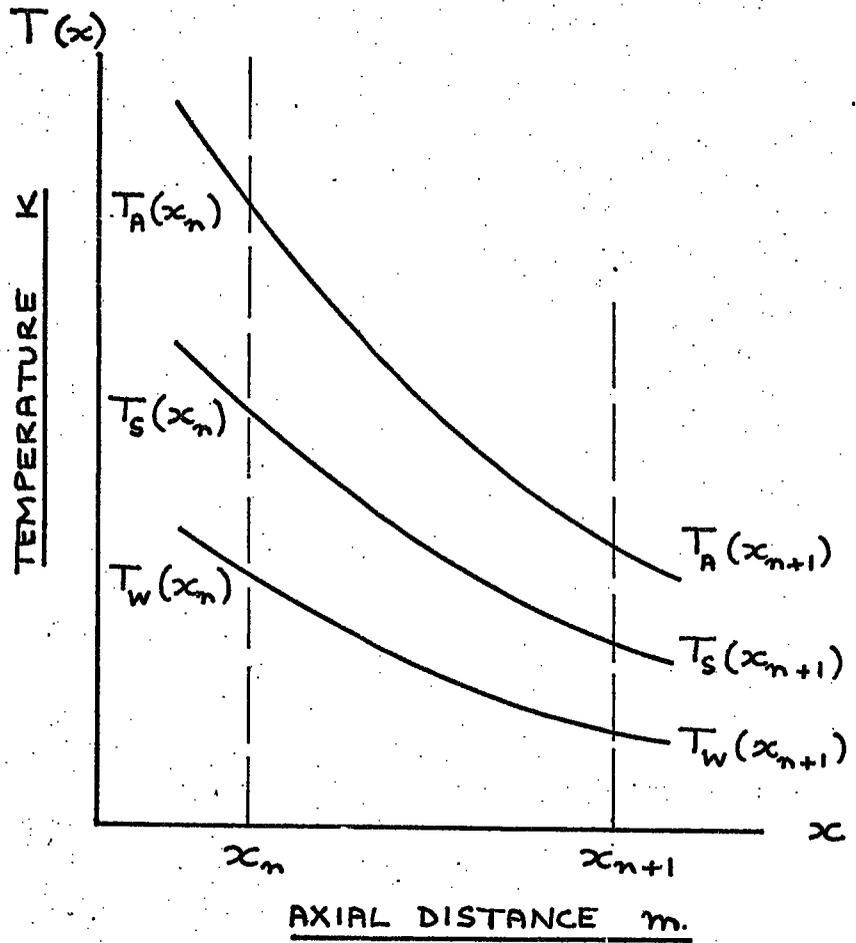
FIGURE 4.19 : TYPICAL SECTION OF
HEAT EXCHANGER A

ulations were performed with the computer programme shown in Appendix F. The properties of the gas and water were evaluated at the corresponding mean temperatures. The Nusselt numbers were also calculated, using:

$$\overline{Nu}_p = \frac{h_{AS} D_o}{k_A} \qquad\qquad 4.4.3.$$

$$Nu_w = \frac{h_{sw} D_{eq}}{k_w} \qquad\qquad 4.4.4.$$

It will be seen from Table 4.F. that the heat transfer coefficients between the water and the tube surface, h_{sw} , lie in the range 1391

$$< h_{sw} < 2327 \quad W/m^2 \, K.$$

4.4.2. Steady state heat transfer

In order to be able to correlate the experimental results, an estimate of the equivalent steady flow heat transfer was required. It was not possible to run the apparatus under identical conditions without oscillations. Therefore the empirical equation of Seider and Tate was used (see equation 2.4.5.). The procedure was to calculate the heat transfer in fully developed steady turbulent flow, using the same values of $\dot{m}_w, \dot{m}_{AA}, T_{AI}$, and T_{Wq} as in the experiments. The calculations were performed by the programme CKBA in Appendix F. This had to be started with an estimate of the outlet water temperature, T_{WI} . It was found that a step length of $\frac{4H}{50}$ converged satisfactorily, and by successively changing the original estimate, the inlet water temperature was obtained. The water side heat transfer coefficients lay within an average of 14% of the experimental ones, and the Reynolds numbers corresponded to within 5%. With this agreement established, the steady state gas to surface Nusselt numbers could be used as a basis of comparison for the experimentally measured ones.

4.4.3. Heat Transfer Correlations

The local heat transfer coefficients, h_{AS} , in the heat exchanger were correlated with local velocity amplitude, $\hat{u}$ by plotting $\frac{\overline{Nu}_p}{Nu}$, the ratio

of pulsating to steady state Nusselt number, against $\hat{u}/\bar{u}_A$, the ratio of the velocity amplitude to the mean flow velocity. The latter was deduced from the continuity equation, thus;

$$\bar{u}_A = \frac{\dot{m}_{AA}}{\bar{\rho}_{Ax} S_0} \qquad\qquad 4.4.5.$$

where $\bar{\rho}_{Ax}$ is the density of the gases at point x. The velocity amplitude at any point were derived from equation 2.4.13;

$$\hat{u} = \frac{1}{\omega \bar{\rho}_{Ax}} \frac{\partial p_x}{\partial x}$$

The correlations for D_I = 13, 16 and 19 mm. are shown in Figures 4.20, 4.21. and 4.22 respectively. Also shown on each graph is the quasi-steady-state relation, equation 2.4.8. In Figure 4.20., the experimental points follow equation 2.4.8. to within 21% up to $\hat{u}/\bar{u}_A \simeq 1.5$, and then diverge along a steeper slope. For D_I = 16 mm. the agreement is approximately 16%, and again, a steeper slope is suggested after $\hat{u}/\bar{u}_A \simeq 1.0$. For D_I = 19 mm. the agreement is approximately 13%, and the same trend is apparent. These results substantially agree with those of Hanby (39) and do not exhibit as much scatter. They tend to conflict with those of Hirst (57) in that his results follow a slope below equation 2.4.8. as shown in Figure 4.23. Hirst examined the heat transfer from a heated tube to a flow of air passing through it while excited by a siren. The axial temperature gradient in the tube was less than 15% of that in this study, and there was no combustion process.

In Figure 4.24., the Nusselt Number ratio, $\frac{\overline{Nu}_p}{Nu}$, has been plotted against distance in Heat Exchanger A, x , for D_I = 13, 16 and 19 mm. On these graphs, the position of the velocity antinodes has been marked V.A. In Figure 4.24 (a) the variation of $\frac{\overline{Nu}_p}{Nu}$ with x is approximately sinu-soidal and reaches a local maximum of 2.23 at x = 1.18 m. The nearest velocity antinode is at 0.92 m. The next velocity antinode is at x = 2.16 m. but here the value of $\frac{\overline{Nu}_p}{Nu}$ is large due to the end effect. In Figure 4.24 (b), the velocity antinodes do not coincide with local maxima. In

FIGURE 4.20: GRAPH OF NUSSELT NUMBER RATIO
AGAINST DIMENSIONLESS VELOCITY
AMPLITUDE FOR $D_I = 13$ mm.
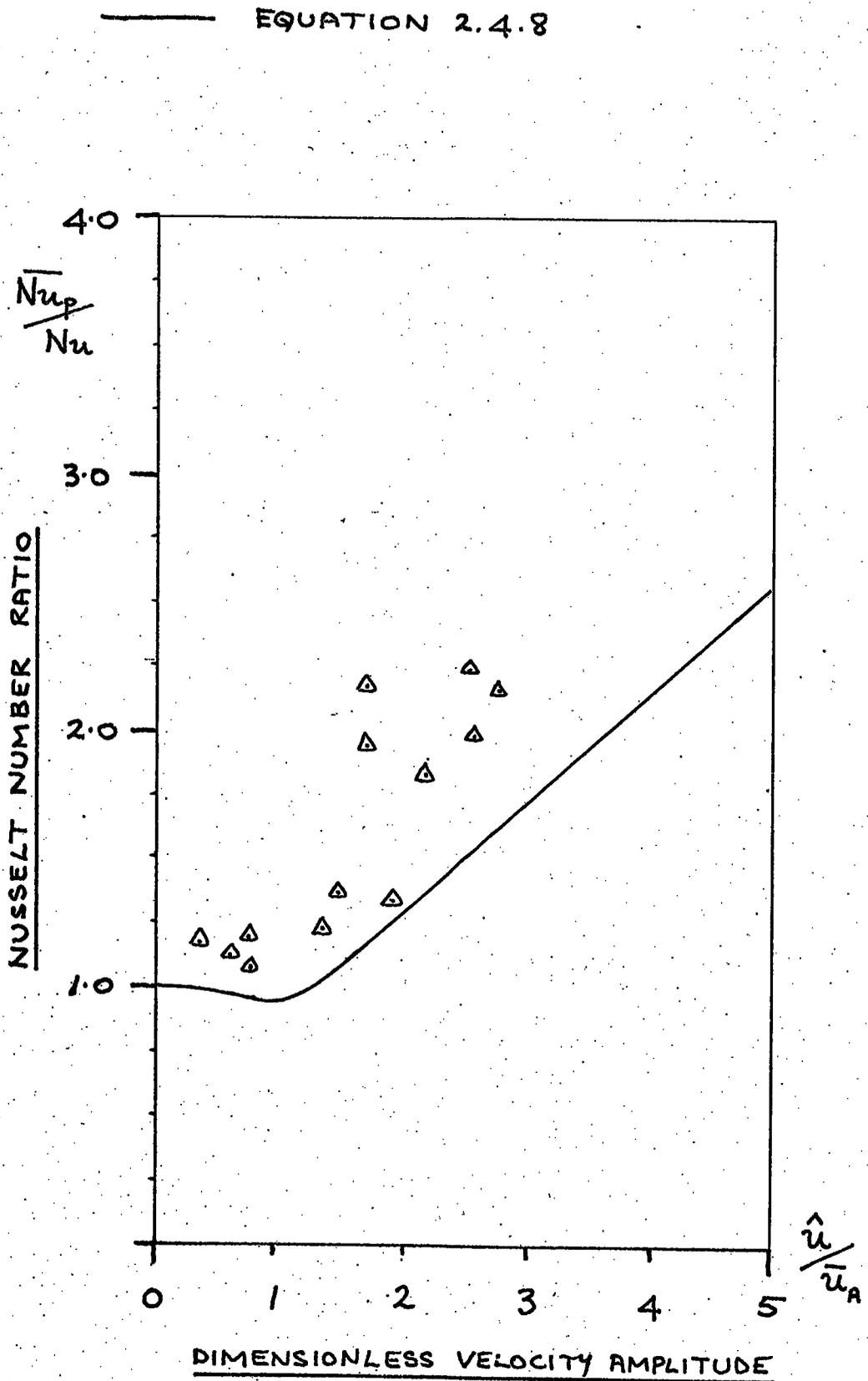
——— EQUATION 2.4.8

FIGURE 4.21: GRAPH OF NUSSELT NUMBER RATIO
AGAINST DIMENSIONLESS VELOCITY
AMPLITUDE FOR $D_I = 16$ mm.
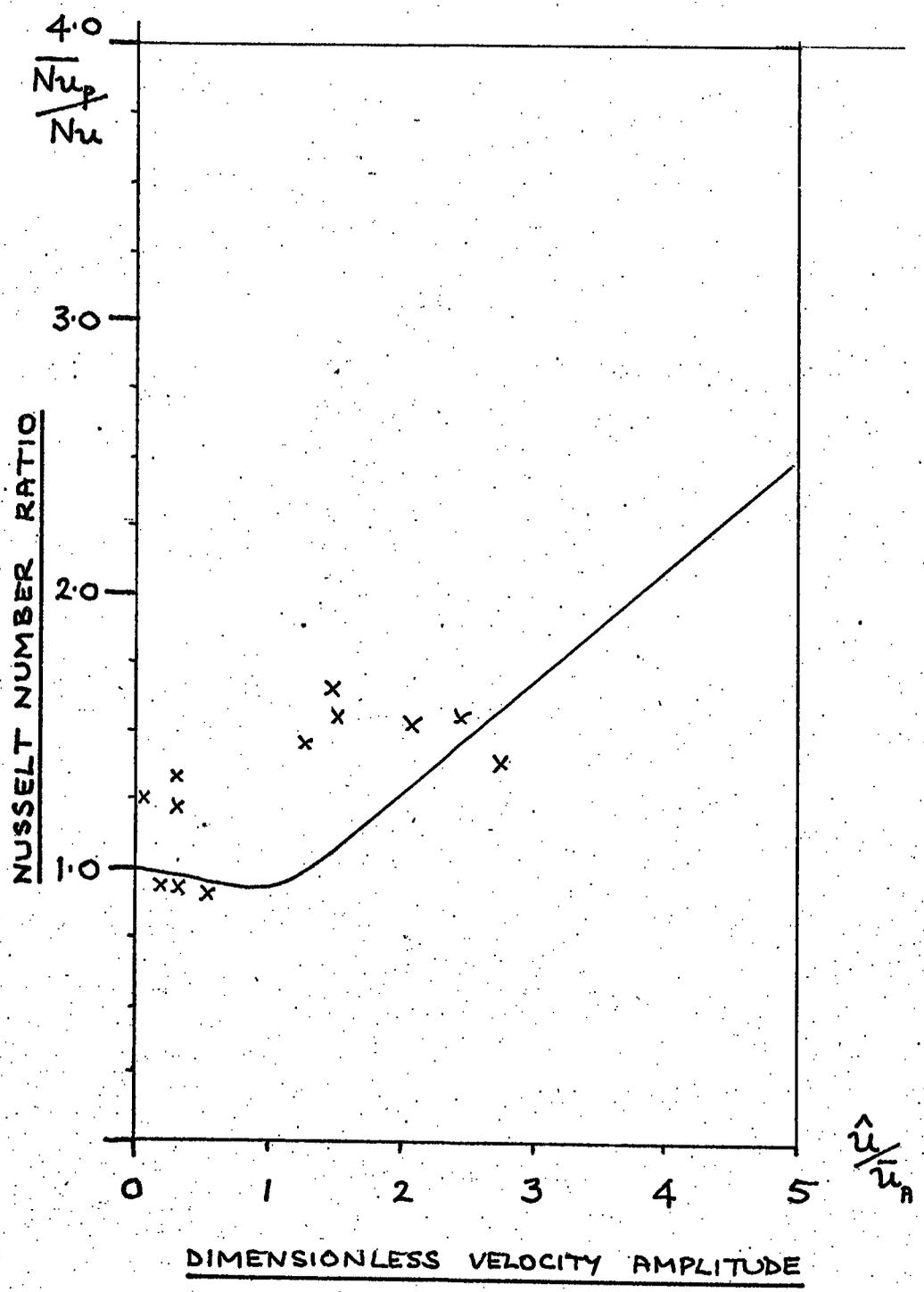
——————— EQUATION 2.4.8

FIGURE 4.22: GRAPH OF NUSSELT NUMBER RATIO AGAINST DIMENSIONLESS VELOCITY AMPLITUDE FOR $D_I = 19$ mm.

——— EQUATION 2.4.8
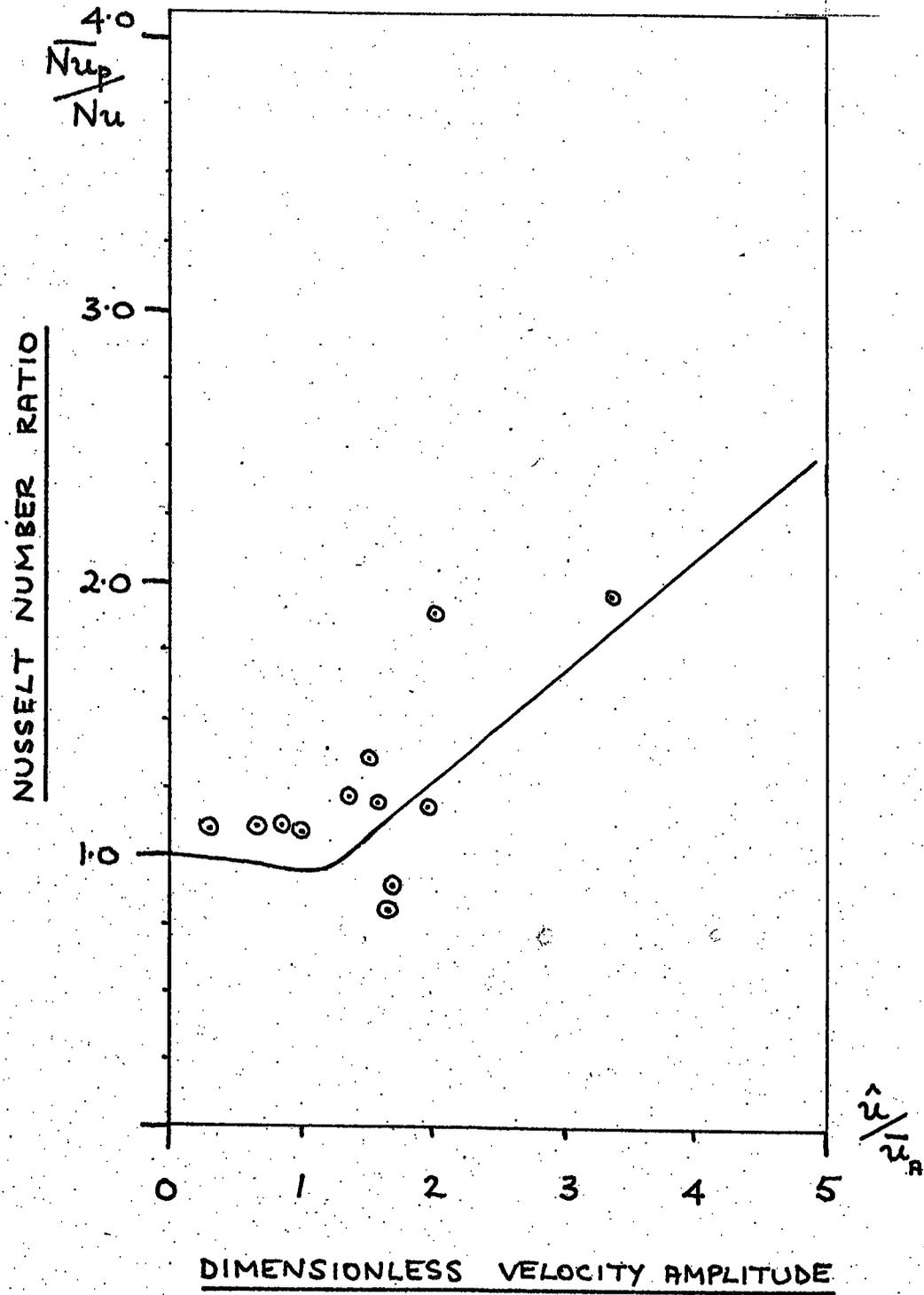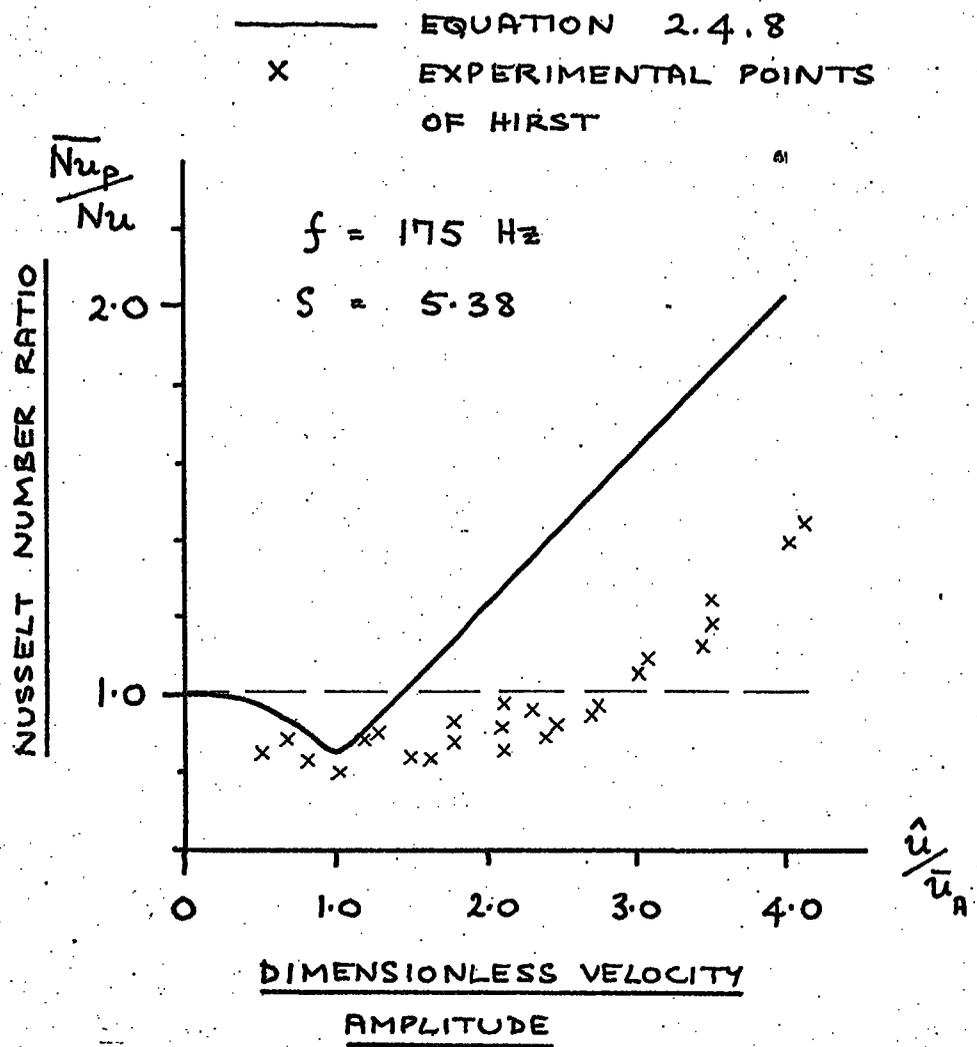
FIGURE 4.23 : GRAPH OF NUSSELT NUMBER RATIO AGAINST DIMENSIONLESS VELOCITY AMPLITUDE FROM HIRST (57)
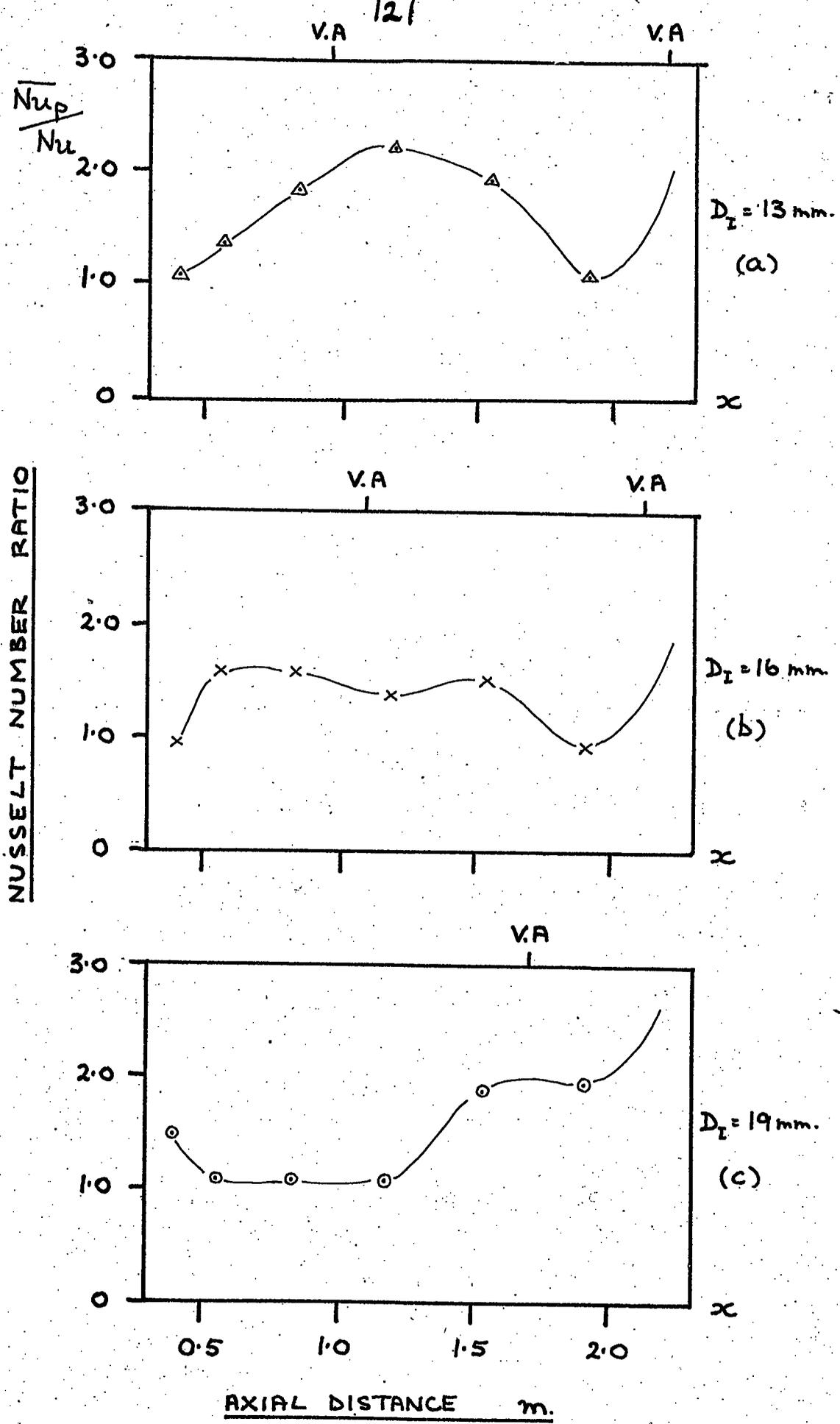
FIGURE 4.24: GRAPHS OF NUSSELT NUMBER RATIO AGAINST DISTANCE IN HEAT EXCHANGER A FOR D_I = 13,16 & 19 mm.

$$\overline{} \qquad \frac{\overline{Nu}_p}{Nu} = 1.0 + 0.20\,S$$
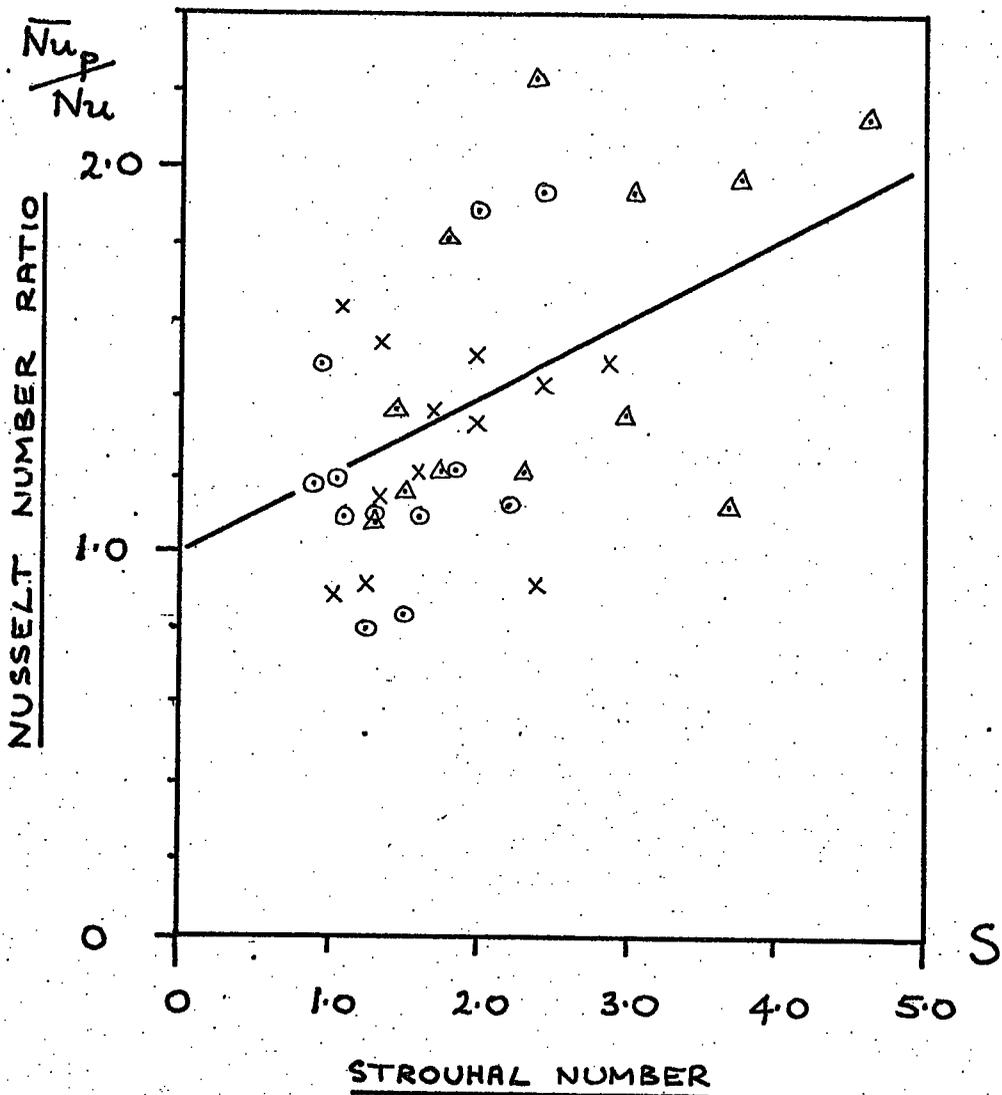
FIGURE 4.25 : GRAPH OF NUSSELT NUMBER
RATIO AGAINST STROUHAL
NUMBER

Figure 4.24 (c), the velocity antinode occurs at $x = 1.70$ m. and coincides with a local plateau in the curve where $\dfrac{\overline{Nu}_p}{Nu} \simeq 1.91$. These results are not as clear as those of Jackson and Purdy (34), discussed in Section 1.3.

In Section 2.4.1., dimensional analysis pointed to a relationship between $\overline{Nu}_p$, $\dfrac{\hat{u}}{\overline{u}_A}$, $\overline{Re}_A$ and S. In order to be able to derive an empirical relationship it is necessary to keep two factors constant while examining the other two. This was not possible with this apparatus due to its feature of pumping its own combustion air, which meant that $\overline{Re}_A$ could not be fixed while altering $\hat{u}$, for example. In Figure 4.25., $\dfrac{\overline{Nu}_p}{Nu}$ has been plotted against Strouhal number, S. The points are scattered, and the straight line shown is a least squares fit. The line is;

$$\frac{\overline{Nu}_p}{Nu} = 1.0 + 0.20\, S \qquad\qquad 4.4.6.$$

Hirst (57) produced a similar empirical relationship which related his experimental results to the quasi-steady state predictions.

5. Conclusions

A naturally-aspirating propane-fired pulsating combustor was constructed with aerodynamic valves of diameters 13, 16 and 19 mm. Provision was made to measure the fluid flowrates, and fluid temperatures and pressure amplitude of the oscillations at regular intervals along the resonating section. A linearised wave equation, governing the propagation of sound waves through a gas exhibiting an axial temperature gradient, was obtained, together with exact solutions of an exponential temperature gradient.

The results of an energy balance of the apparatus lay within - 5.7% to + 10.0%. It was found that the overall thermal efficiency of the combustor decreased with increasing fuel flowrate. It was found that the airflow through the resonating section lay in the range 6 to 17 kg/h. A quasi-steady-state analysis of the aerodynamic valve overestimated this airflow by two to three magnitudes. This was felt to be caused by the assumptions of isentropic, frictionless flow in the analysis.

It was found that, at low fuel flowrates and low mean temperatures, the combustor ran at a fundamental frequency of approximately 60 Hz for $D_I = 13$ and 16 mm. and approximately 80 Hz for $D_I = 19$ mm. With increasing fuel flowrates, the combustor 'jumped' to harmonics based on the mode of operation. This were 'closed-open' organ pipe and 'open-open' organ pipe for $D_I = 13$, 16 mm. and $D_I = 19$ mm. respectively. The waveform of the oscillations was found to be sinusoidal only at high fuel flowrates and high frequencies.

The prediction of the operating frequency by the exponential analysis lay within 3.8 to 19.5%, of the experimental readings, and that by the general wave equation lay within 0.5 to 2.0%. The predictions by the general wave equation for the axial distributions of pressure amplitude lay within 6 to 8%.

The heat transfer results sought relationships between a) $\dfrac{\overline{Nu_p}}{\overline{Nu}}$ and $\dfrac{\hat{u}}{u_A}$, and b) $\dfrac{\overline{Nu_p}}{\overline{Nu}}$ and S. The results of a) suggested a steeper relationship than predicted by the quasi-steady-state theory (based on an empirical steady state heat transfer equation). The results of b) produced

a scatter of points which were correlated by a least-squares line;

$$\frac{\overline{Nu_p}}{Nu} = 1.0 + 0.20 \, S$$

The range of the major parameters was;

$$\overline{Re}_A \qquad 1800 \ - \ 6690$$
$$\hat{u}/\overline{u}_A \qquad 0.04 \ - \ 3.54$$
$$S \qquad 0.8 \ - \ 4.7$$

$$\frac{\overline{Nu_p}}{Nu} = 1.0 + 0.20 \, S$$

REFERENCES

1. Higgins, B. On the sound produced by a current of hydrogen gas passing through a tube. By editor, Mr. Nicholson, with a letter from Dr. Higgins respecting the time of its discovery. J. Nat. Philos. Chem. and the Arts vl p. 129 1802.

2. Rijke, Pl L. Nature of a new method of causing a vibration of the air contained in a tube open at both ends. Phil. Mag. v17 p.419 1859.

3. Mallard, E. and Le Chatelier, H. Recherches experimentelles et theoriques sur la combustion des melanges gazeux explosifs. Annales des Mines, Partie Scientifique et Technique Series 8 n4 p.274 1883.

4. Reynst, F.H. Pulsating Combustion (collected works of F.H. Reynst. M.W. Thring, ed.) Pergamon Press, London, 1961.

5. Reynst, F.H. Pulsating Combustion (collected works of F.H. Reynst. M.W. Thring, ed.) Pergamon Press, London, 1961.

6. French Patent No. 373141.

7. French Patent No. 374124.

8. French Patent No. 376176.

9. French Patent No. 412478.

10. Dutch Patent No. 768 part 18 folio 38.

11. Reynst, F.H. Pulsating Combustion (collected works of F.H. Reynst. M.W. Thring ed.) Pergamon Press, London, 1961.

12. Swiss Patent No. 196312, Cl. 13b.

13. Reynst, F.H. Pulsating Combustion (see 11)

14. Huber, L. Central Heating, Air and Water-Heating with Pulsating Combustors. Paper presented at First Int. Symp. Pulsating Combustion, Univ. of Sheffield, 1971.

15. Alebon, J., Lee, G.K. & Geller, L.B. A Pulsating Combustion system for space heating. Proc. Boyar Conference pp. 61-89 May 1963 Univ. of Montreal.

16. Bottoms, C.H. Discussion of Paper.

17. Francis, W.E., Hoggarth, M.L. and Reay, D. A Study of gas-fired pulsating combustors for industrial applications. J. Inst. Gas Engrs. v3 p.301 1963.

18. Lord Rayleigh, Theory of Sound Vol. I & II.

19. Muller, J.L. The development of a resonant combustion heater for frying applications. The S.A. Mech. Engineer v137 February 1967 pp.137-146.

20. Reay, D. The thermal efficiency, silencing and practicability of gas-fired industrial pulsating combustors. J. Inst. Fuel v42 n339 p.135 1969.

21. Biffra, F.E.J., Staddon, P.W., Phillips, R.N. et Romaine, D.R. A study of unvalved pulse combustors. Inst. Gas Engineers Communication 860 37th Autumn Research Meeting, London 1971.

22. Reynst F.H. Pulsating Combustion (see 11)

23. Reynst, F.H. Pulsating Combustion (see 11).

24. Babkin, Yu. L. Pulsating Combustion Chambers as furnaces for steam boilers. Teploenergetika v12 n9 p.23 1959.

25. Hanby, V.I. and Brown, D.J. A 50 lb/h pulsating combustor for pulverised coal. J. Inst. Fuel v41 p.423 1968.

26. Martinelli, R.C. & Boelter, L.M.K. The Effect of Vibration on Heat Transfer by Free Convection from a Horizontal Cylinder. Proc. 5th Int. Congress Applied Mechanics 1938.

27. Martinelli, R.C., Boelter, L.M.K. Weinberg, E.B. and Yakati, S. Heat Transfer to a fluid flowing periodically at low frequencies in a vertical tube. A.S.M.E. v65 p.789 1943.

28. Schultz-Grunow, F. Pulsierender Durchfluss durch Rohre. Forschung auf dem Gebiere des Ingenieurewesens v11 pp.170-187 1940.

29. Estel see Bibliography No. 16.

30. Jackson, T.W., Harrison, W.B. & Boteler, W.C. Free convection, Forced convection and Acoustic Vibrations in a Constant Temperature Vertical Tube. J. Heat Transfer pp.68-74 February 1959 A.S.M.E. Paper No. 58-HT-6.

31. Zartmann, W.N. & Churchill, S.W. Heat transfer from acoustically resonating gas flames in a cylindrical burner A.I.Che.E. v7 n4 p.589 1961.

32. Sundstrom, D.W. & Churchill, S.W. Heat transfer from Premixed Gas Flames in a Cooled Tube. Che E Progress Symp. Series v56 n30 pp.65-73 1960.

33. Harrje, D.T. & Crocco, L. Heat Transfer in Oscillating Flow. Aeronautical Engineering Reports No. 483 - a,b,c 1959,60,61 Princeton University, New Jersy Contract USN-NONR 1858(29)

34. Jackson, T.W. & Purdy, K.R. Resonant Pulsating Flow and Convective Heat Transfer. J. Heat Transfer pp.507-512 Nov. 1965 A.S.M.E. Paper No. 65-HT-30

35. Miller, J. & Fejer, A. Transition phenomena in oscillating boundary layer flows. Jnl. Fluid Mech. v18 p.438 1974.

36. Purdy, K.R., Jackson, T.W. & Gorton, C.W. Viscous Fluid Flow under the Influence of a Resonant Acoustic Field. J. Heat Transfer pp.97-106 February 1964 A.S.M.E. Paper No. 62-WA-116.

37. Koshkin, V.K., Danilov, Y.I., Kalinin, E.K. Dreitser, D.A., Galitseysky, B.M. & Izosimov, V.G. Unsteady Heat Transfer in Tubes resulting from changes in Heat Flow, Gas Mass Flow Rate and Acoustic Resonance. 3rd Int. Heat Transfer Conf., Chicago 7-12 August 1966.

38. Galitseyskiy, B.M., Danilov, Yu. I., Dreytser, G.A., Kalinin, E.K. & Koshkin, V.N. Convective Heat Transfer for a flow in a pipe fluctuating about the first resonant harmonic. Heat Transfer - Soviet Research v1 n2 pp.164-176 1969.

39. Hanby, V.I. Convective Heat Transfer in a Gas-Fired Pulsating Combustor. Trans. A.S.M.E. v91 series a n1 p.48 1969.

40. Bogdanoff, D.W. A study of the mechanisms of heat transfer in oscillating flow. Technical Report No. 483-f Dep. Aerospace and Mech. Sci. Princeton, Oct. 1967.

41. Kapur, A., Cummings, A. et Mungur, P. Sound propagation in a combustion car with axial temperature and density gradients. J. Sound and Vibration v25 n1 pp.129-138 1972.

42. Morrell, G. An empirical method for calculating heat transfer rates in resonating gaseous pipe flow. Jet propulsion pp.829-831 Dec. 1958.

43. Holland, F. et al. Heat Transfer. Heinemann 1970.

44. Lewitt. Handbook of Mathematics.

45. Shapiro, A.H. Dynamics and Thermodynamics of compressible fluid flow. Vols I & II, Ronald Press Co. 1954.

46. Brudenberg Gauge Co. Handbook.

47. Thermal Syndicate Ltd. Handbook on use of Thermocoax

48. Holman, J.P. Experimental Methods for Engineers. McGraw-Hill, 1971.

49. Poole, K. Private Communication. Univ. of Durham 1973.

50. Numac Handbook - IBM Systems Reference Library 1972.

51. B.S. 726.

52. Beale, C.K., Clarke, P.H. & Everson, G. A Comparison of the dependence of the Pulsations in a single-orifice and a double-orifice Combustor on heat transfer or acoustic processes.

53. Simonson, J.R. An Introduction to Engineering Heat Transfer. McGraw Hill 1967

54. Holman, J.P. Experimental methods for Engineers. McGraw-Hill 1966.

55. Chapman, A.J. Heat Transfer. Macmillan 1967.

56. Bayley, F et al, Heat Transfer. Nelson 1972.

57. Hirst, S.L. Heat Transfer to a Resonant Pulsating Air Stream in a Pipe. Ph.D Thesis. Univ. of Durham 1974.

BIBLIOGRAPHY

1. A.A. Putnam — General survey of pulse combustion.
   1st Int. Symposium on Pulsating Combustion, University of Sheffield. Sept. 1971.

2. G.H. Markstein ed. — Non-steady flame propatation
   Pergamon Press 1964.

3. A.A. Putnam — Combustion-driven oscillations in industry
   American Elsevier 1971.

4. D.D. McCracken — A guide to Fortran IV Programming
   Wiley 1966.

5. F. West,
   A. Taylor — Effect of pulsations on heat transfer.
   Chemical Engineering Progress. Vol. 48, No. 1, 1952 Pg. 39-43.

6. P.G. Morgan — The effect of vibration and pulsation on heat transfer.
   Engineering and Boiler House Review. April 1963, Pg. 128-129.

7. H. Havemann — Heat transfer in pulsating flow.
   Nature No. 4418, July 3, 1954, Pg. 41.

8. F. Romie — Heat transfer to fluids flowing with velocity pulsations in pipes.
   Thesis, University of California, 1956.

9. D.T. Harrje — Heat transfer in oscillating flow.
   Aero. Eng. Rep. No. 483c, Princeton University, Sept. 1961.

10. D. Bogdanoff,
    D.T. Harrje — A study of the mechanisms of heat transfer in oscillating flow.
    Aero. Eng. Rep. No. 483f, Princeton University, Sept.1967.

11. C. Feiler,
    E. Yeager — Effect of large amplitude oscillations on heat transfer.
    N.A.S.A. Tech. Report R-142, 1962.

12. A.H. Shapiro — Dynamics and thermodynamics of compressible fluid flow.
    Vol. I and II, Ronald Press Co. 1954.

13. R. Beyer — Physical Acoustics Vol. II, Part B.
    Academic Press 1965.

14. A.B. Wood — Textbook of Sound
    G. Bell and Sons Ltd., 1932.

15. C.E. Froberg — Introduction to numerical analysis.
    Addson-Wesley Pub. Co. Ltd., 1964.

16. W.M. Kays — Convective heat and mass transfer.
    McGraw-Hill Co. Ltd. 1966.

17. H. Schlichting — Boundary layer theory.
    Pergamon 1955.

18. J.K. Kilham et al   Oscillatory combustion in tunnel burners.
10th International Symp. on Combustion, 1965.

19. Arranged by   Thermodynamic and transport properties of fluids.
T.R. Mayhew,   Oxford 1967.
G.F.C. Rogers

20. P.J. Westervelt   Effect of sound waves on heat transfer.
Journal of Acoustical Society of America, Vol. 32,
No. 3 March 1960, Pg. 337-338.

21. M.H.I. Baird   Vibrations and Pulsations
British Chemical Engineering, Vol. 11, No. 1, Jan. 1966
Pg. 20-25.

22. R. Wick   Unsteady boundary layer and heat transfer phenomena -
a literature survey.
California Institute Technology, Technical Report
20-279, 1955.

23. G. Morell   An Empirical method for calculating heat transfer rates
in resonating gaseous pipe flow.
Jet Propulsion, Dec. 1958, Pg. 829-831.

24. R. Lemlich   A musical heat exchanger.
Trans. A.S.M.E. - Journal of Heat Transfer, Aug. 1961
Pg. 385-386.

25. J. Dent   Effect of vibration on condensation heat transfer to a
horizontal tube.
Institute of Mechanical Eng. Proc. 1969/70, Vol 184,
Part 1, No. 5.

26. M.J. Lighthill   The response of laminar skin friction and heat transfer
to fluctuations of the stream velocity.
Proceedings of Royal Society, Series A, Vol. 224,
No. 1156 June 1954.

27. T. Sarpkaya   Experimental determination of critical Reynolds number
for pulsating flow.
Journal of Basic Engineering, Vol. 88, No. 3, Sept.
1966, Pg. 5-9.

28. P.M. Morse   Vibration and Sound
McGraw-Hill 1948.

29. P.M. Morse,   Theoretical Acoustics.
K.U. Ingard   McGraw Hill 1968.

30. A. Cambel,   Gas Dynamics.
B.H. Jennings   McGraw Hill 1958.

31. F. Cheers   Elements of Compressible Flow
Wiley 1963.

32. A.J. Ede   An Introduction to Heat Transfer
Pergamon Press 1967.

33. F. Holland et al — Heat Transfer
Heinemann 1970.

34. R.P. Benedict — Fundamentals of Temperature, Pressure and Flow
Measurements.
Wiley 1969.

35. E. Owen,
R.C. Pankhurst — Measurement of Air Flow.
Pergamon 1966.

36. C. Rektorys — Survey of Applicable Mathematics.
Iliffe 1969.

37. Owen, E,
Pankhurst, R.C. — The Measurement of Airflow.
Pergamon 1966.

38. Lewis, B,
von Elbe, G. — Combustion Flames and Explosions of Gases.
Academic Press 1961.

39. D.D. McCracken,
W.S. Dorn — Numerical Methods and Fortran Programming.
Wiley 1964.

40. J.M. Beer,
N.A. Chigier — Combustion Aerodynamics.
Applied Science Publ. 1972.

41. F. Cheers — Elements of Compressible flow.
Wiley 1963.

42. NPL — Noise Measurement Techniques - Notes of Applied Sci.
No. 10.
HMSO 1958.

43. A. Schack — Industrial Heat Transfer.
Chapman and Hall 1965.

44. W.M. Kays — Convective Heat & Mass Trans.
McGraw Hill 1966.

45. C.C. Lin, ed. — Vol. 5 high speed Aero & Jet Propulsion
Turbulent flows and heat transfer.
Oxford 1959.

46. R.P. Benedict — Fundamentals of T, P and flow measurements.
Wiley 1969.

47. J. Heading — Mathematical Methods.
Univ. Press Belfast 1963.

48. D.C. Baird — Exptn. - An Introduction to Measurement Theory and
Expt. design.
Prentice-Hall 1962.

49. Bruel & Kjoer — Instructions, Applications & Calibration.

50. B.V. Ranshenbakh — Vibrational Combustion.
FTD-TT-62-942/1 & 2
AD 402909   1963.

51. The Rayleigh
Criterion — Stability of Systems Containing a Heat Source - Boa-Teh
Chn
NACA RM 56D27 1956.

6.A Solution of the general wave equation

Equation 2.3.24 is:

$$\frac{d^2 p}{dx^2} - \frac{1}{\bar{\rho}} \frac{\partial \bar{\rho}}{\partial x} \frac{dp}{dx} + \frac{\omega^2}{\bar{c}^2} p = 0$$

where

$$\bar{\rho} = \bar{\rho}(x)$$

$$\bar{c} = \bar{c}(x)$$

It may be written in the form:

$$p'' + f(x) p' + g(x) p = 0$$

where

$$f(x) = - \frac{1}{\bar{\rho}} \frac{\partial \bar{\rho}}{\partial x}$$

$$g(x) = \frac{\omega^2}{\bar{c}^2}$$

This may be split up into two simultaneous first order differential equations by writing:

$$y = p'$$
$$y' = p''$$

thus giving:

$$y' = - f(x) y - g(x) p$$

The boundary conditions for the tube are:

$$p(0) = P_0$$
$$p(L) = 0$$

This is an initial value problem and was solved using the subroutine DRKGS in the Numac Library (50). This uses a fourth-order Runga-Kutta method, and requires only the values of $p(0)$ and $p'(0)$ to start it. In order to meet the boundary condition $p(L) = 0$, a Newton-Raphson iteration loop was written into the procedure. The output of the programme was the pressure amplitude at any required point in the tube.

```
C   CKBGPX -- GENERAL SOLN.
      IMPLICIT REAL*8(A-Z)
      DIMENSION Y(2),DERY(2),AUX(16,2),PRMT(5)
      INTEGER NDIM,J,N,NUM,JM
      COMMON OMEGA
      EXTERNAL FCT,OUTP
      N=0
      READ(5,1000)OMEGA,PAC,GRAD
1000 FORMAT(4(F10.3))
C   COMPUTE STARTING VALUE OF P(L)
      Y(1)=PAC
      Y(2)=GRAD
      DERY(1)=0.5
      DERY(2)=0.5
      PRMT(1)=0.0
      PRMT(2)=3.3
      PRMT(3)=0.3
      PRMT(4)=0.0001
      NDIM=2
      CALL DRKGS(PRMT,Y,DERY,NDIM,IHLF,FCT,OUTP,AUX)
      FA=Y(1)
      WA=OMEGA
C   START ZERO SEEKING LOOP
      OMEGA=OMEGA+25.0
   10 CONTINUE
C   RESET INPUT PARAMETERS FOR DRKGS
      Y(1)=PAC
      Y(2)=GRAD
      DERY(1)=0.5
      DERY(2)=0.5
      PRMT(1)=0.0
      PRMT(2)=3.3
      PRMT(3)=0.3
      PRMT(4)=0.0001
      NDIM=2
      CALL DRKGS(PRMT,Y,DERY,NDIM,IHLF,FCT,OUTP,AUX)
      FB=Y(1)
      WB=OMEGA
      K=(FB-FA)/(WB-WA)
      OMEGA=WB-(FB/K)
      IF(DABS(OMEGA-WB).LE.0.01.OR.N.GE.20)GO TO 9
      N=N+1
      WRITE(6,3311)N,OMEGA
3311 FORMAT(4X,I2,3(F15.2))
      FA=FB
      WA=WB
      GO TO 10
    9 CONTINUE
C
      X=0.0
      DO 12 J=1,12
      Y(1)=PAC
      Y(2)=GRAD
      DERY(1)=0.5
      DERY(2)=0.5
      PRMT(1)=0.0
      PRMT(2)=X
      PRMT(3)=X/10
```

```
      PRMT(4)=0.0001
      NDIM=2
      CALL DRKGS(PRMT,Y,CERY,NDIM,IHLF,FCT,CUTP,AUX)
      WRITE(6,9091)J,X,Y(1),DERY(1)
 9091 FORMAT(6X,I2,3(4X,F10.3))
      X=X+0.3
   12 CONTINUE
      WRITE(6,9092)OMEGA
 9092 FORMAT(4X,'OMEGA =   ',F10.2)
      STOP
      END
      SUBROUTINE FCT(X,Y,DERY)
      IMPLICIT REAL*8(A-Z)
      DIMENSION Y(2),DERY(2)
      COMMCN CMEGA
C
      DATA A,B,RR,GAMMA/-373.4,1400.0,287.1,1.4/
      TX=1500.0-1200.0*DSIN((X-0.3)*2.14159/6)
      DTX=-200.0*3.14159*DCOS((X-0.3)*3.14159/6)
      FX=DTX/TX
      GX=(OMEGA**2)/(GAMMA*RR*TX)
      DERY(1)=Y(2)
      DERY(2)=-FX*Y(2)-GX*Y(1)
      RETURN
      END
      SUBROUTINE OUTP(X,Y,CERY,IHLF,NDIM,PRMT)
      IMPLICIT REAL*8(A-Z)
      DIMENSION Y(2),DERY(2),AUX(16,2),PRMT(5)
      INTEGER NDIM,IHLF
      RETURN
      END
```

6.B. The Preliminary Investigation

The first combustor to be constructed was based on a design of the Gas Council (17) and is shown in Figure B.1.   It was found that stable combustion oscillations could be sustained only by directing a blast of air continuously towards the aerodynamic valve.   The mean static pressure in the chamber was 0.3 kN/m^2g for an energy release of 18 kW on propane fuel, and the exhaust temperature was approximately 1350°C.   It was observed that flames emerged from both ends of the chamber.

A number of modifications were made to the design in order to measure the overall rate of heat transfer, and the result of these is shown in Figure B.2.   The fuel injection was changed to a radial configuration, a system used by Francis et al. (17) and Muller (19), and a heat exchanger was fitted to the exhaust end of the chamber.   The combustion chamber was fitted with a cooling jacket.   It was found that the maximum volumetric combustion rate was 78 MW/m^3, that the operating frequency was 175 Hz and that the overall rate of heat transfer was 64 kW/m^2.   These figures were compared with those of Reynst (13), Muller (19) and Alebon et al. (15), which were 17.5 MW/m^3, 71 and 150 MW/m^3, and 44.5 MW/m^3 and 59 kW/m^2 respectively.   A sample of exhaust gas from the centre of the heat exchanger was analysed with an Orsat apparatus, which yielded 6.5 per cent carbon dioxide, 3.6 per cent oxygen and 0.1 per cent carbon monoxide.   It was concluded from this analysis that the combustor was inducting excess air and that, therefore, the dimensions of the aerodynamic valve could be reduced without detriment to the combustion process.

As the original combustion chamber had become distorted, a new one of 51 mm. internal diameter was constructed, and a tail-pipe added to the heat exchanger to prevent end-effects due to reverse flow.   The revised apparatus is shown in Figure B.3.   It was found that, over the range of fuel flowrate, 0.68 to 0.92 kg/h, the gas temperature at the exit of the heat exchanger fell from 260 to 175°C while that of a thermocouple placed just outside the aero-
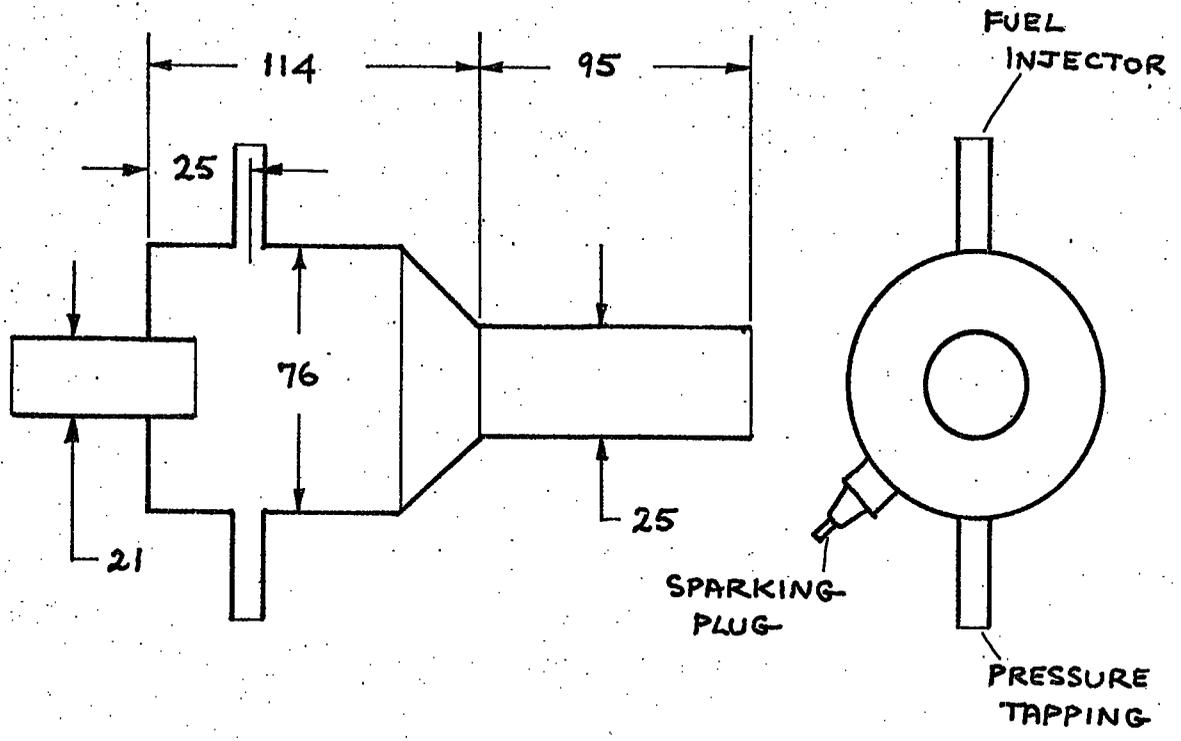
FIGURE B.1 : FIRST COMBUSTION CHAMBER
(DIMENSIONS IN MM)
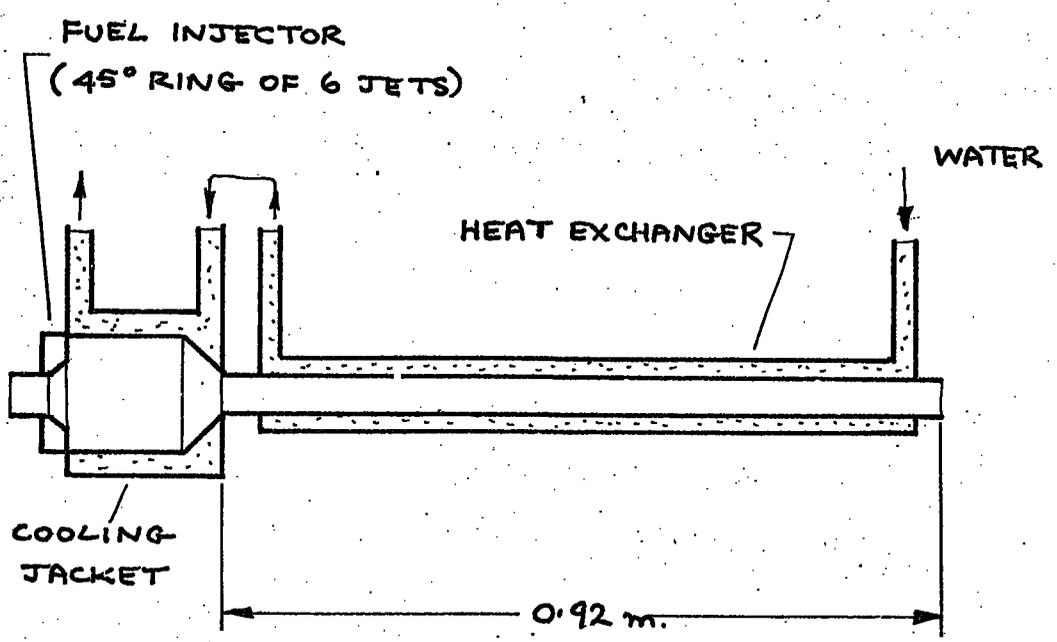
FIGURE B.2 : FIRST COMBUSTION CHAMBER WITH
HEAT EXCHANGER, COOLING JACKET
AND MODIFIED FUEL INJECTION
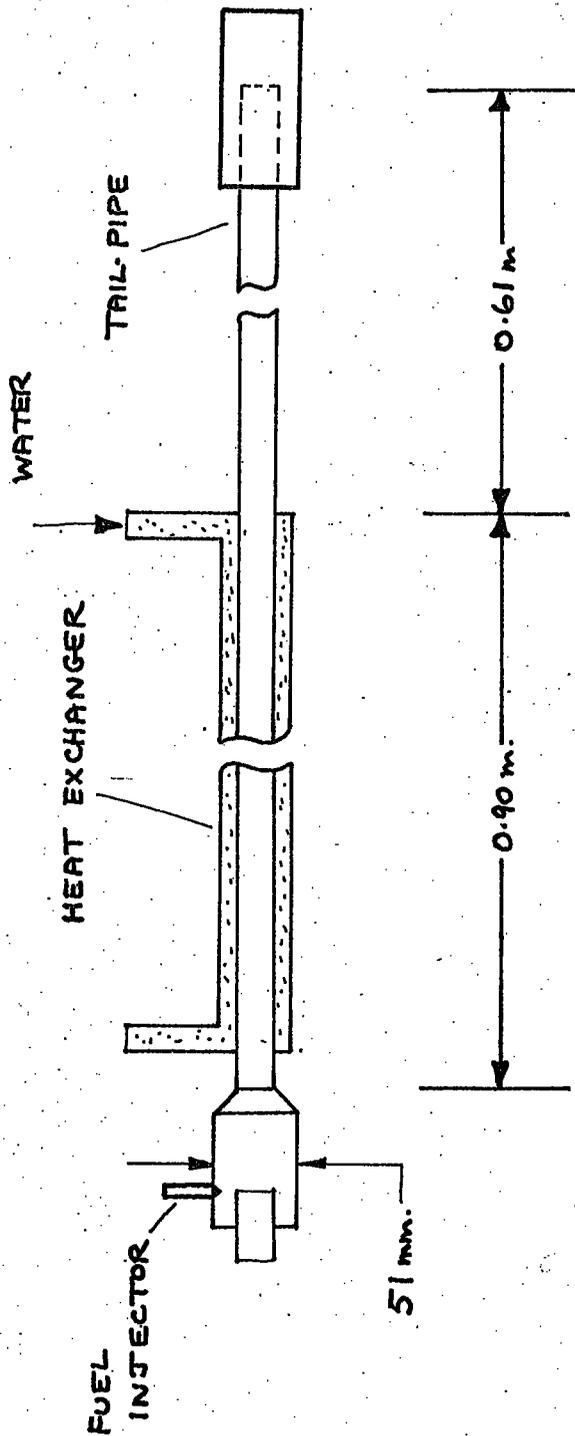
FIGURE B.3 : SECOND COMBUSTOR WITH HEAT EXCHANGER AND AUGMENTER
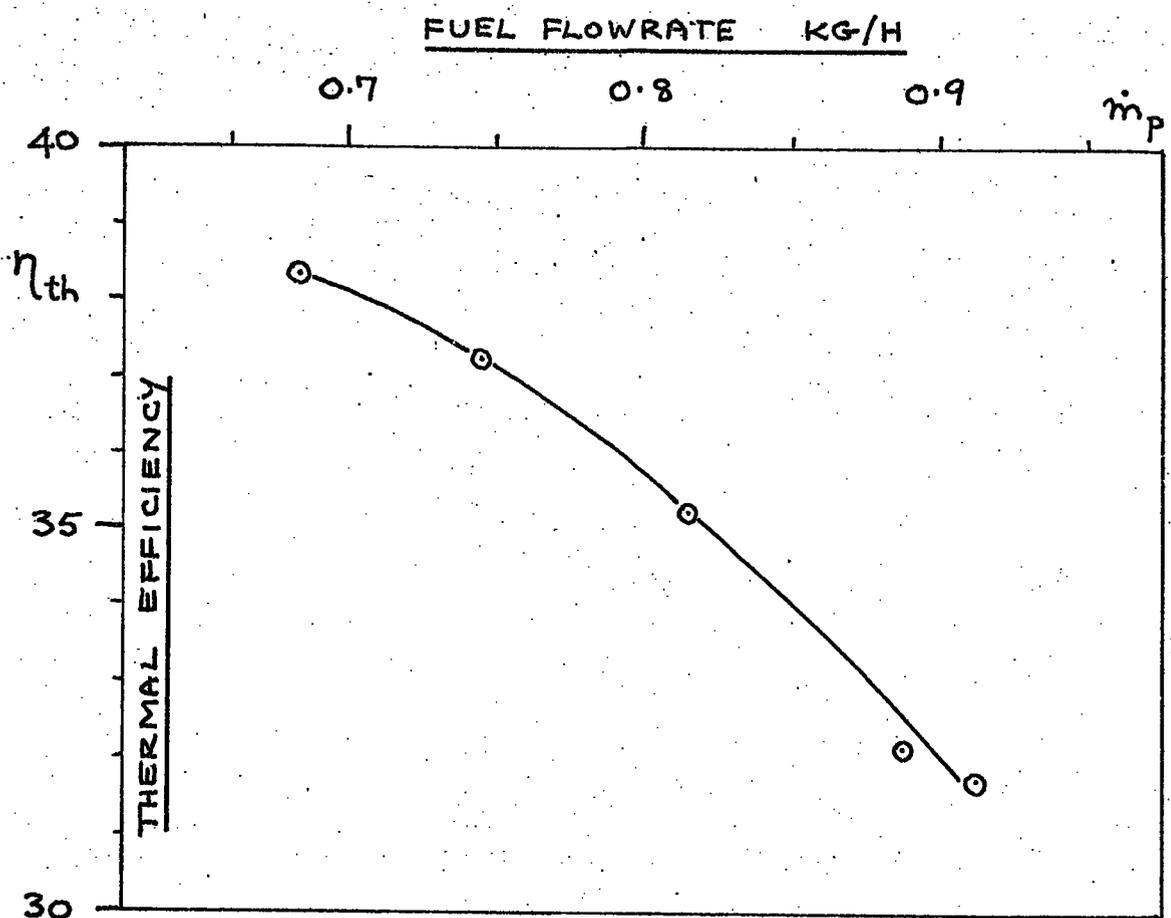
FIGURE B.5 : VARIATION OF THERMAL EFFICIENCY WITH FUEL FLOWRATE
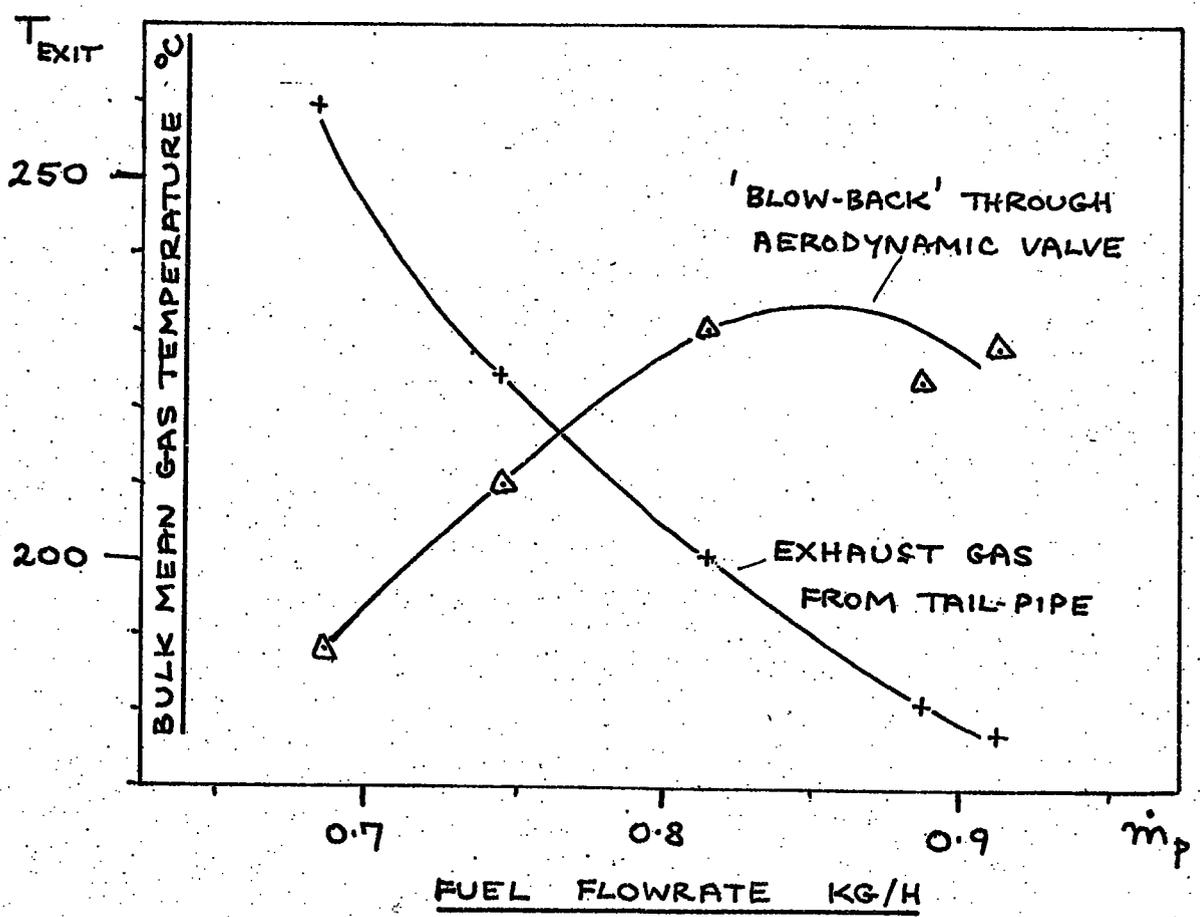
FIGURE B.4 : VARIATION OF GAS OUTLET TEMPERATURES WITH FUEL FLOWRATE

dynamic valve rose from 185 to 225°C, as may be seen from Figure B.4. It was also found that, over the same range of fuel flowrate, the thermal efficiency (Figure B.5.) of the combustor fell from 38.5 to 32 per cent. It was concluded from these observations that the reverse flow of hot gases through the aerodynamic valve ('blowback') represented a significant energy loss which would be difficult to measure without placing heat exchangers suitably. It was realised that, if this was done, cool air would be entrained into such a heat exchanger, thus reducing the temperature difference between the hot gases and the cooled walls. A further experiment was made to determine the effect of aerodynamic valve length upon the volumetric combustion rate. The results are shown in Figure B.6. where maximum fuel flowrate is plotted against valve length for an internal diameter of 16 mm. It was concluded from this graph that, in order to obtain a wide turn-down ratio, a short valve was desirable.

It was decided then to construct an apparatus in which local heat transfer coefficients could be measured, (see Figure B.7.). Two identical combustors were aligned horizontally opposite each other. It was intended that, by operating the combustor under counterphase conditions, the blowback from one valve would be inducted by the other, and thus virtually eliminate energy losses. The combustion chambers were mounted on a slide within a large wooden box so that the gap between the two valves could be varied from 5 to 260 mm. The box was lined with tin foil to reduce radiation losses from the unlagged chambers. Its purpose was to act as a smoothing reservoir so that a measurement of the airflow could be made. The volume of the box was 0.45 m³, calculated from the formula in B.S.726 (51).

The design of the combustors is shown in more detail in Figures B.8. & 9. The aerodynamic valves were 50 mm. long and 16 mm. internal diameter. Each combustor had nine sampling sites; those of Combustor A were used to measure gas and water temperatures, while those of Combustor B were for pressure measurements and exhaust sampling. The gas temperatures were measured by
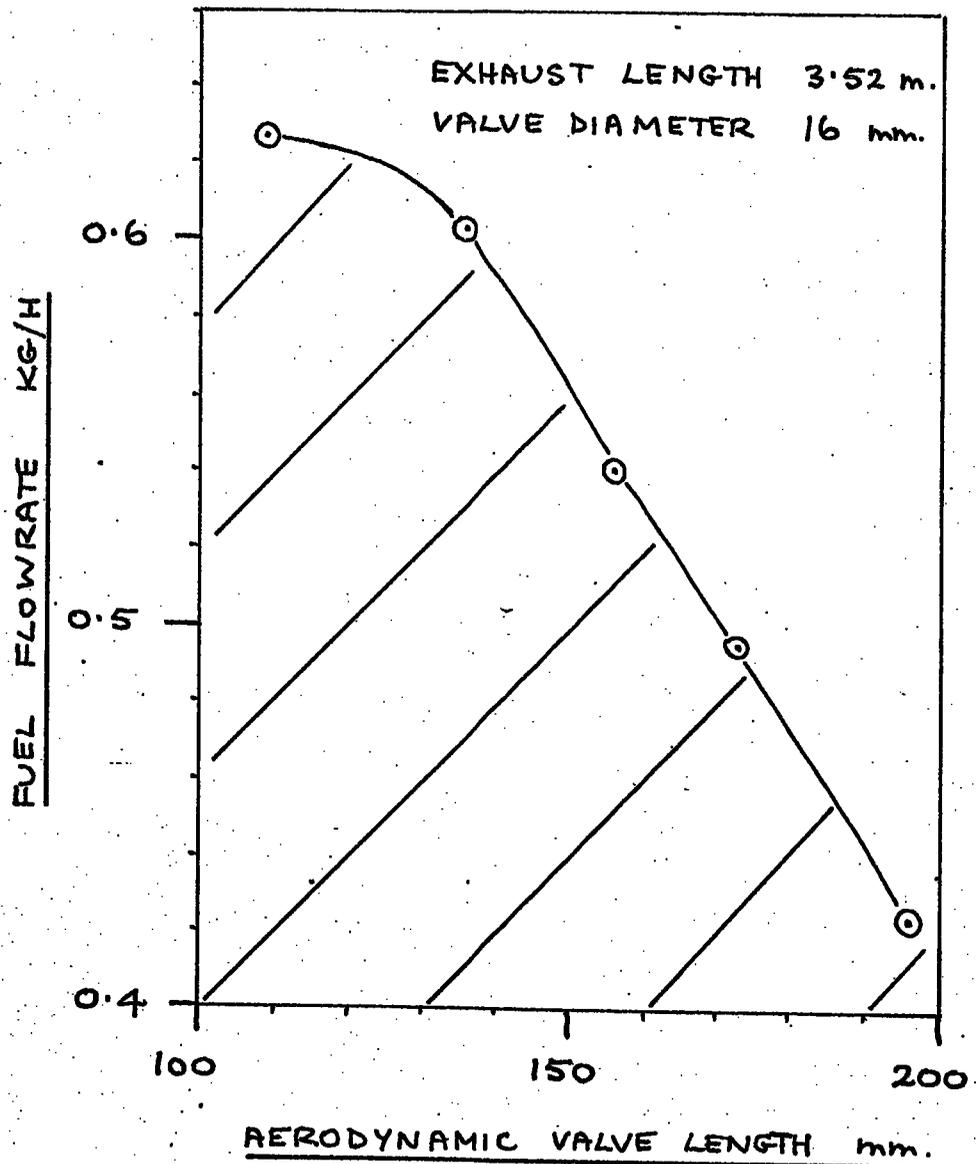
FIGURE B.6 : VARIATION OF 'BLOW-OFF' LIMIT WITH AERODYNAMIC VALVE LENGTH
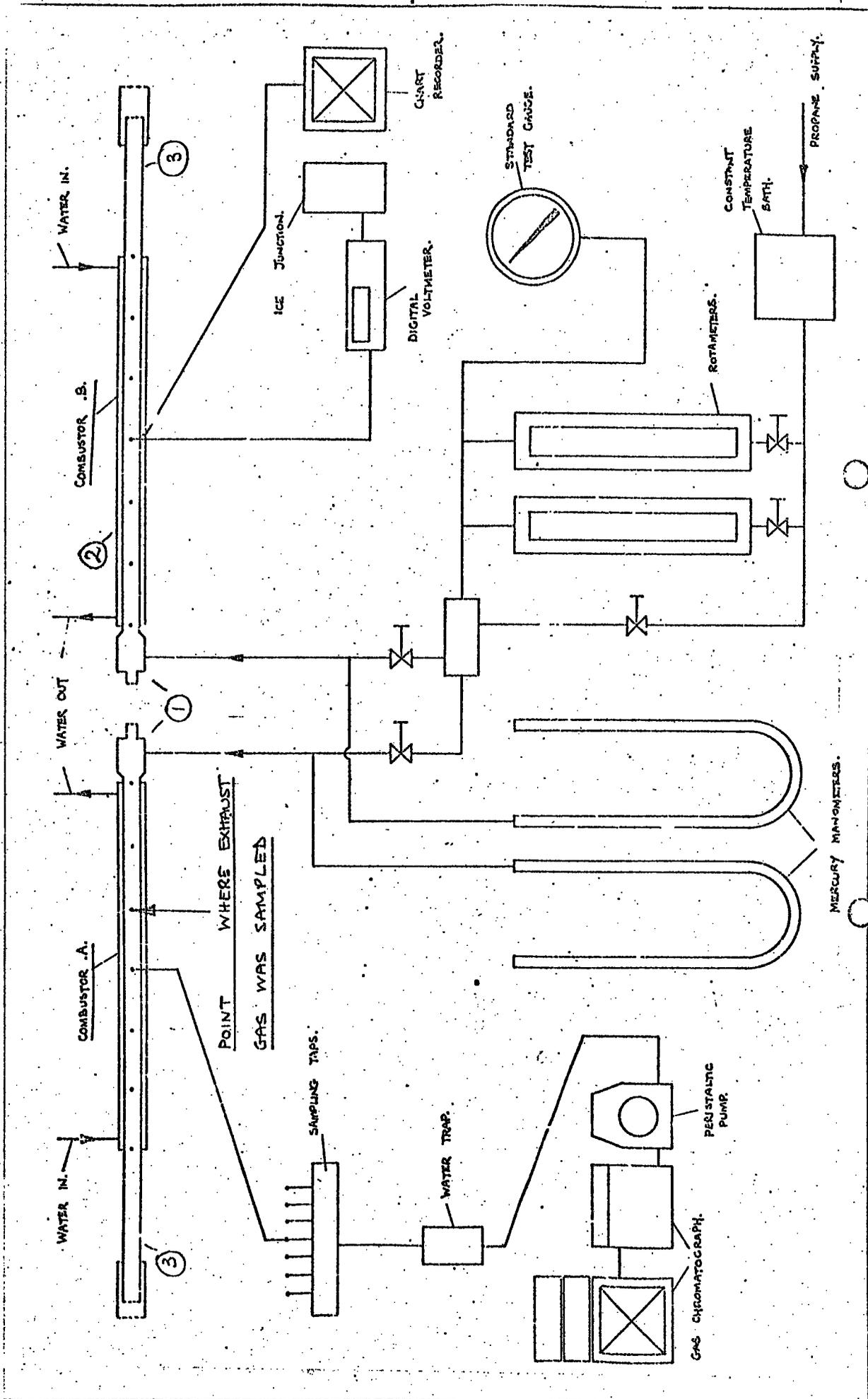
FIGURE B.7 : OPPOSED COMBUSTOR APPARATUS
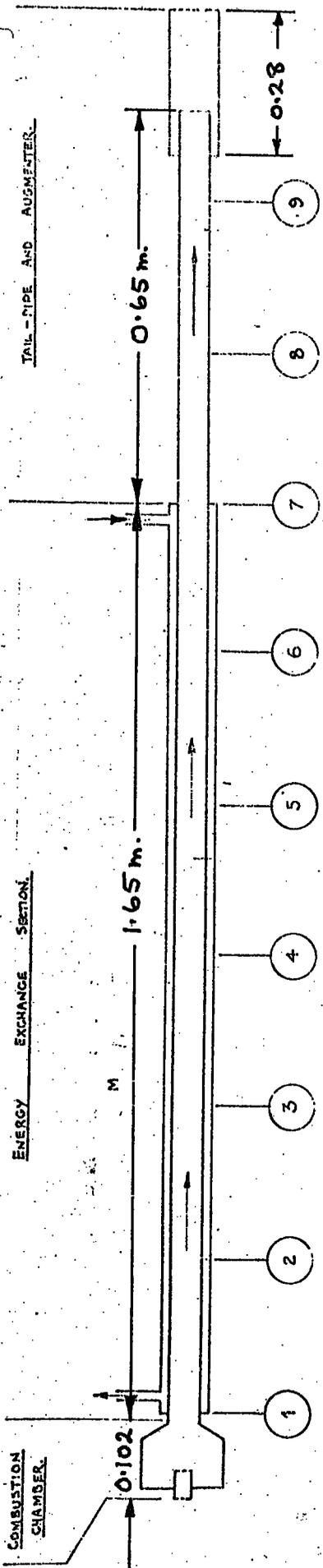
FIGURE B.8: LAY-OUT OF INSTRUMENTED COMBUSTOR
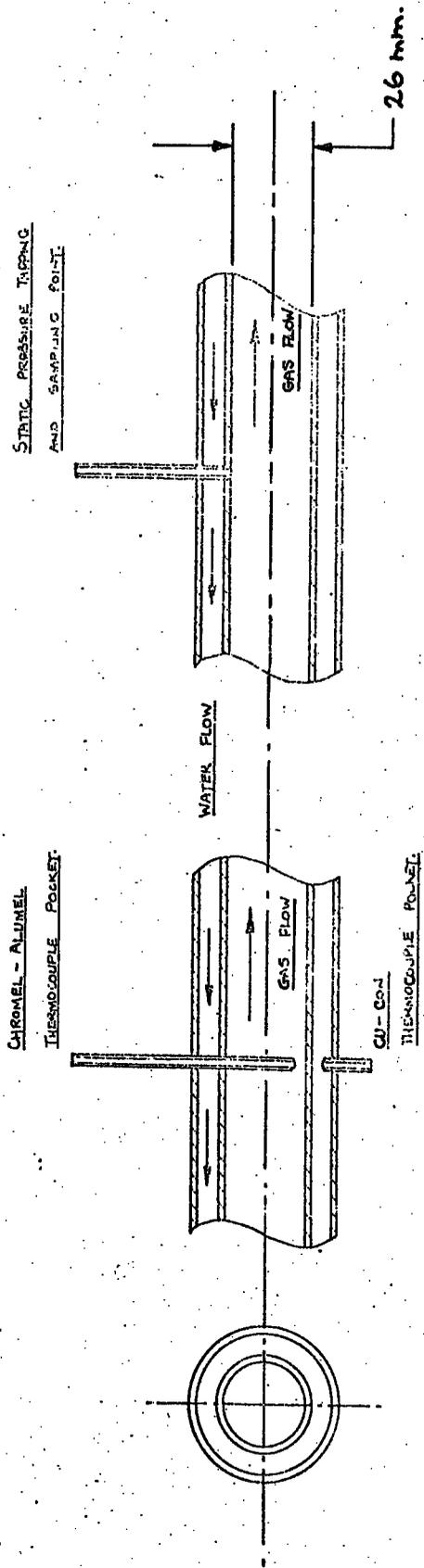
FIGURE B.9: SAMPLING SITES IN THE HEAT EXCHANGERS

inserting a chromel-alumel thermocouple into the chosen pocket, which was sealed when not in use. The water temperature sites were all provided with copper-constantan thermocouples which indicated directly on a chart recorder. The static pressure measurements were measured by an inclined water multi-manometer.

During early experiments on this apparatus it was observed that a short length of 37 mm. diameter tube, when held over the end of the tail-pipe, caused the combustion-driven oscillations to jump to a higher frequency. In addition the pressure variation became very regular, and the maximum volumetric combustion rate was increased. This tube is similar to the augmenters of Muller (19), and, although he intended them to perform as ejectors and used slightly divergent tubes, this term is used henceforward. The diameter of the augmenter was found not to be critical, but its length was important, and one of 0.45 m. gave the best results. The reason for the improving effect of the augmenter was not clear.

Results

The results of tests on Combustor 4 are presented here. Figure B.10. illustrates a typical sequence of frequency jumps during the warm-up period of the combustor. The frequency was measured by a piezo-electric transducer, and the chamber wall temperature by a chromel-alumel thermocouple. The frequency jumped from 93 to 160 to 245 Hz. If the mean gas temperature is taken to be $500^{\circ}C$, and the length of the resonator being 2.4 m., the natural frequencies are given by simple acoustic theory to be:

open-open tube;   104, 208, 312   Hz

closed-open tube;   52, 156, 260   Hz

The bands have been marked to show a region of instability in which the operating frequency of the combustor alternated randomly. From the comparison of the experimental and calculated operating frequencies shown, it was evident that simple acoustic theory was inadequate.

FIGURE B.10: VARIATION OF COMBUSTOR FREQUENCY WITH COMBUSTION CHAMBER WALL TEMPERATURE DURING WARM-UP

CHAMBER WALL TEMPERATURE °C
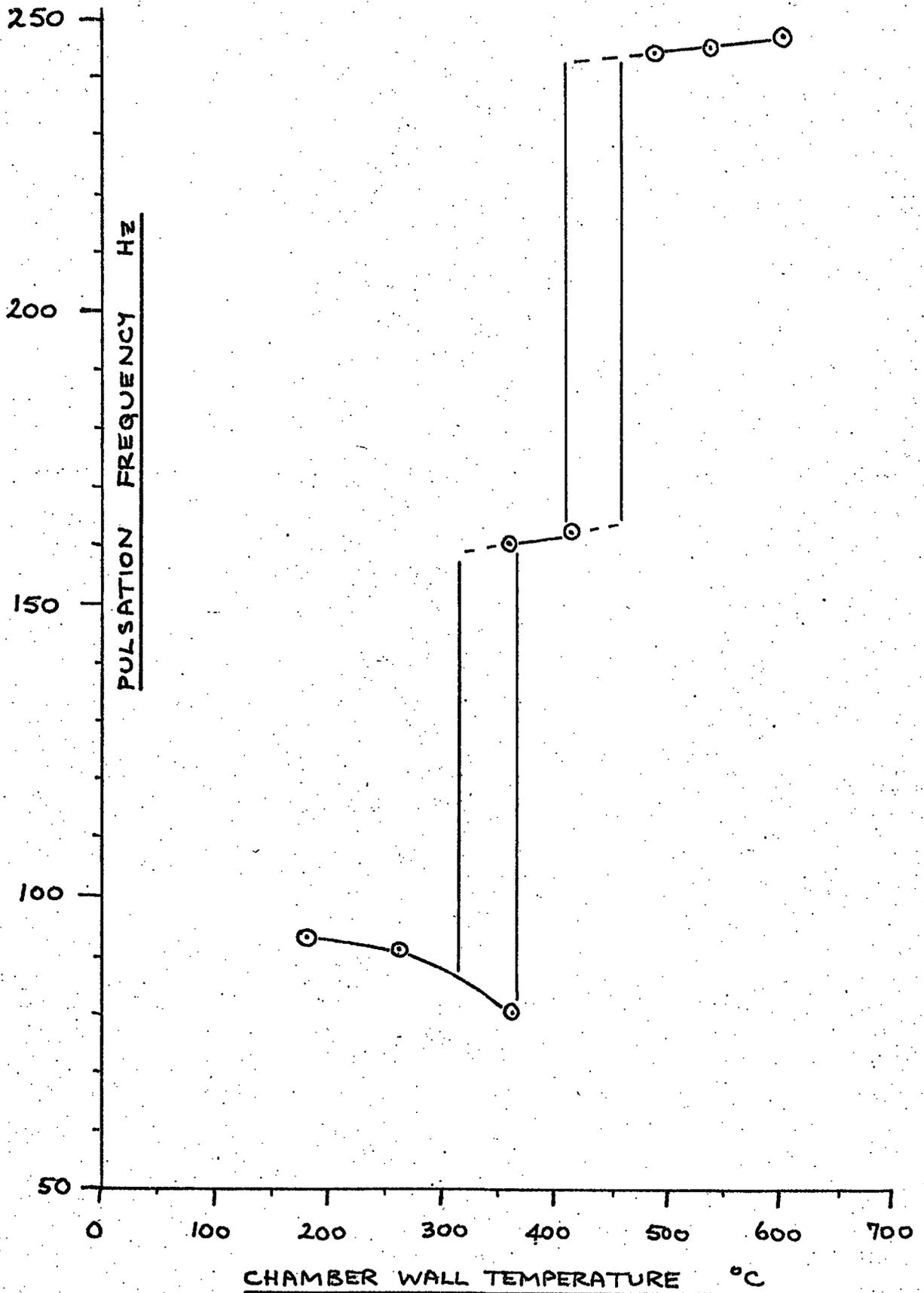
FIGURE B.11 : VARIATION OF COMBUSTOR FREQUENCY
WITH COMBUSTION CHAMBER WALL
TEMPERATURE
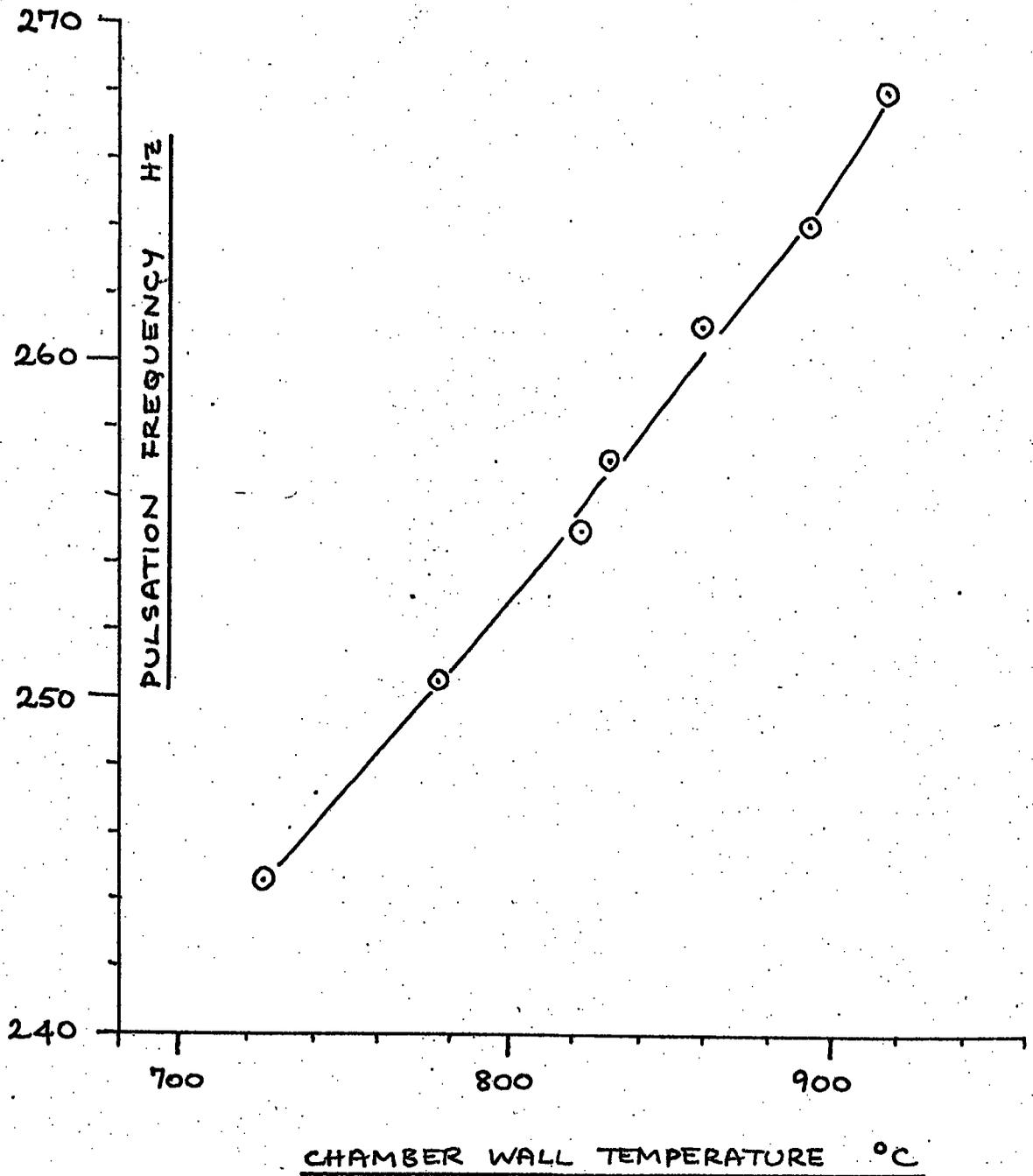
Figure B.11. shows that, having reached the 245 Hz mode, the combustor frequency rose at the rate of 0.25 Hz/°C but did not jump higher as the chamber reached its maximum temperature of approximately 920°C. The rise was attributed to the increasing velocity of sound in the gases.

Figures B.12. and B.13. illustrate the gas and water temperature distributions found within the heat exchanger of Combustor A. The gas temperature fell approximately 380°C in the final 1.375 m. of the heat exchanger. No measurement at the entrance was taken, but from Figure B.11, it was approximately 900°C. Thus the gas temperature fell 600°C in the first 0.275 m. of the heat exchanger. The water temperature showed the greatest rise, of 60°C, in the first 0.54 m. of the heat exchanger, the rise up to that point, of 18°C, being approximately linear. The greatest energy transfer therefore occurred at the entrance to the heat exchanger. This was expected because the difference in temperature between the gases and the water was greatest in this region. During the tests the Reynolds number of the water flow in the annulus was 650, and that of the gas flow ranged from 2700 at the hot end to 6750 at the cold end. It was concluded from this that the water flow was essentially laminar, and that the gas flow could be regarded as turbulent.

The data permitted heat transfer coefficients to be calculated. By drawing a control volume around each of the six sections of the heat exchanger and applying the First Law, the mean heat transfer coefficient, based on the area separating the two fluids, was:

$$h = \frac{\dot{m}_w \, c_{p_w} \, \Delta T_w}{\pi \, d_o \, \Delta x \, (T_{Am} - T_{wm})} \qquad \text{6-B.1}$$

The heat transfer coefficients thus calculated are plotted against distance along the combustor in Figure B.14. The coefficients fall steeply from a value of 240 W/m^2 °K at the hot end to a minimum of 22 W/m^2 °K and then rise again to 137 W/m^2 °K at the cold end. Shown on the same graph is the variation in the pressure amplitude along the combustor. This was assumed to be sinusoidal, and the combustor was assumed to be operating as a closed-

147
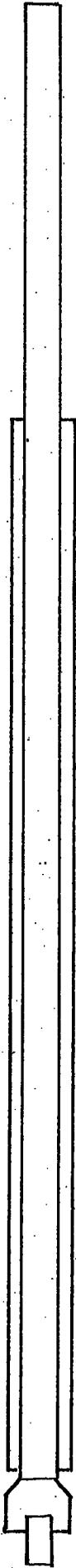
FIGURE B.14 : VARIATION OF HEAT TRANSFER COEFFICIENT AND PRESSURE AMPLITUDE ALONG COMBUSTOR

$\hat{P}(x)$ — SINUSOIDAL VARIATION ASSUMED

V.A

V.A

AXIAL DISTANCE ALONG COMBUSTOR m.

LOCAL HEAT TRANSFER COEFFICIENT W/m²K

h

200

100

0

0.5   1.0   1.5   2.0

x
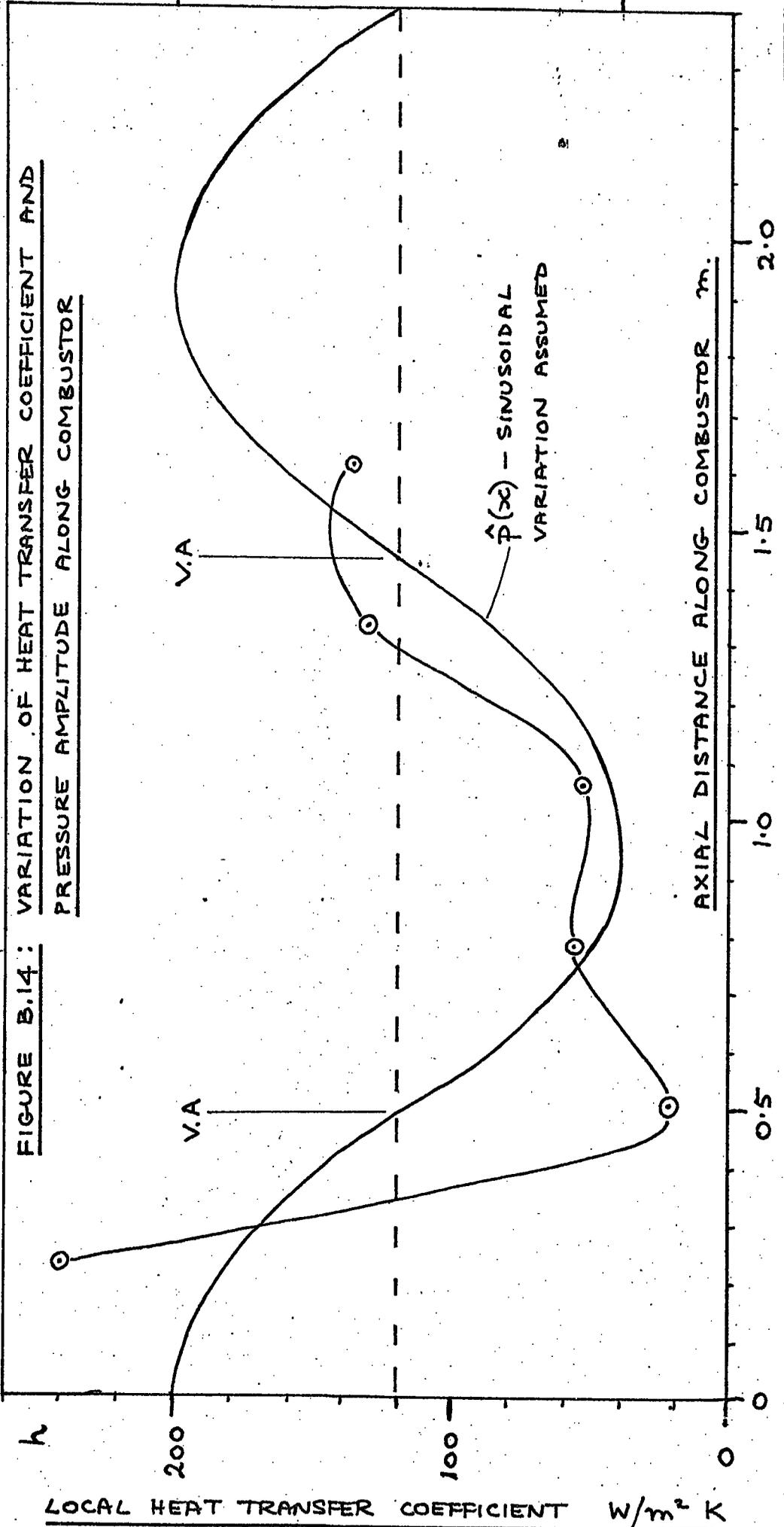
FIGURE B.15: CORRELATION BETWEEN OVERALL HEAT TRANSFER COEFFICIENT IN HEAT EXCHANGER A AND COMBUSTION CHAMBER PRESSURE AMPLITUDE

148
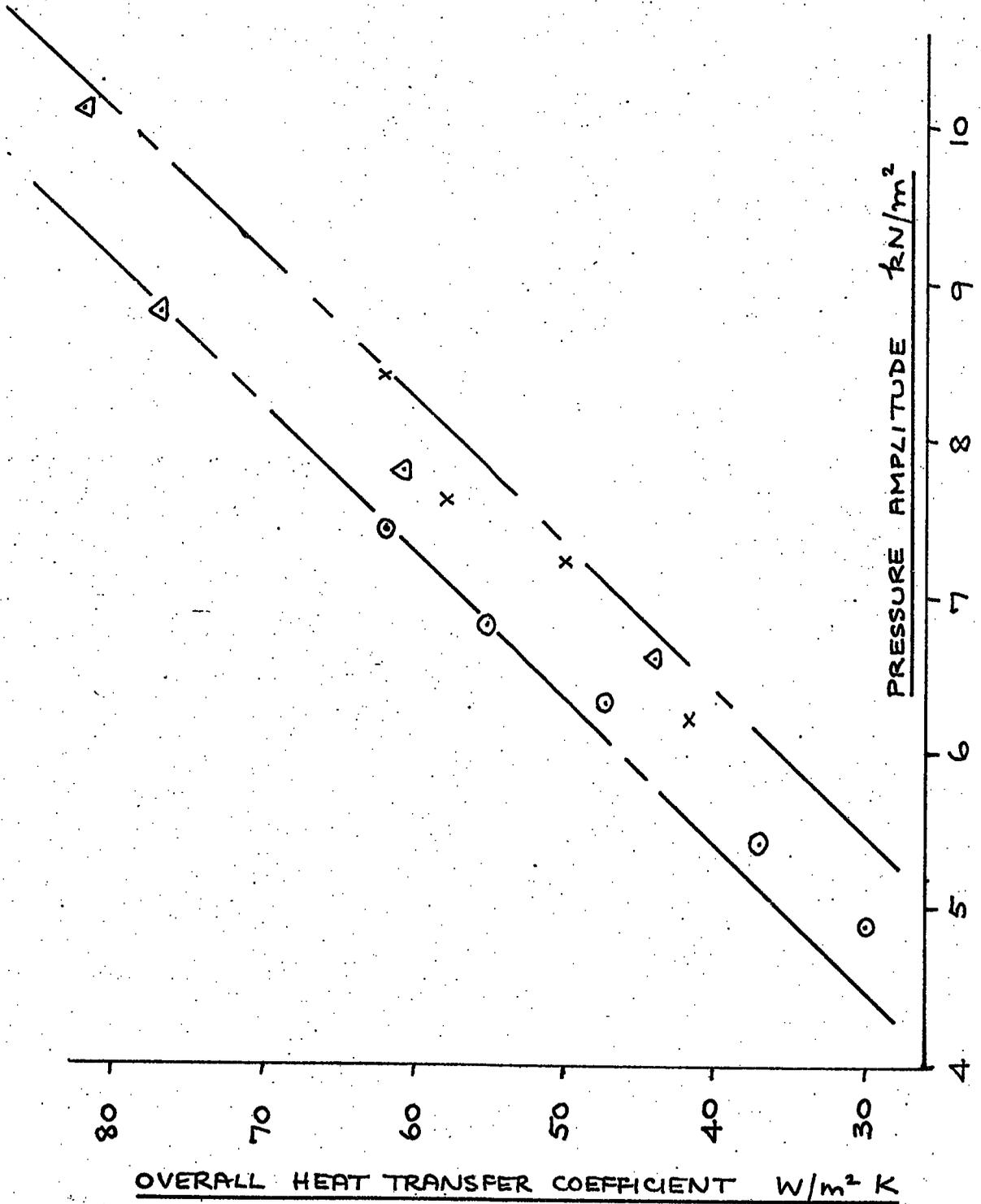
open tube. The only measurement of pressure amplitude was taken at the combustion chamber with a piezo-electric transducer. Assuming that oscillations in particle velocity within the tube were phased 90° ahead of the pressure oscillations, the velocity antinodes may be taken to lie on the graph at the pressure nodes. At the first velocity antinode at $x = 0.48$ m, the heat transfer coefficient reaches a minimum. At $x = 0.96$ m, a velocity node, the heat transfer coefficient is approximately constant. At $x = 1.44$ m, the heat transfer coefficient attains a local maximum. According to this evidence, therefore, it appears that the local velocity variations in the gas flow affect the heat transfer coefficient in opposite ways. This anomaly was caused by:

a) the pressure amplitude variation shown took no account of the severe axial temperature gradient existing in the gas flow;

b) the uncertainty in the deduction of the heat transfer coefficient.

The effect of a) is that, in reality, the waveform would be compressed towards the cold exhaust end because, for a given frequency, the decrease of the sound velocity in the cooling gases would be accompanied by a shorter wavelength. This means that the pressure nodes, as shown, are shifted towards the combustion chamber. Regarding b), an analysis of equation 6-B.1 showed that the temperature rise in the water, ΔT_W, was calculated by subtracting two values taken from the chart recorder. It was estimated that the maximum possible error arising from this source was 25%, with an expected highest error of 15%.

Figure B.15 shows a graph of overall heat transfer coefficient against combustion chamber pressure amplitude. The overall heat transfer coefficient was based on the logarithmic mean temperature difference. The linear character of the graph is evident.

As the apparatus had given a great deal of trouble in operation, it was decided to construct a single new combustor, incorporating a longer heat exchange section and improved measurement techniques.

Exhaust Gas Analysis

A Pye Series 104 Gas Chromatograph was used to analyse the products of combustion passing through the heat exchangers of the combustor. The carrier gas was argon, which was passed through a drying agent before entering the instrument. A coiled tube, 1 m. long and filled with Molecular sieve was used to elute hydrogen, oxygen, nitrogen and carbon monoxide from the sample, and a similar one filled with Silica Gel to elute carbon dioxide. A peristaltic pump drew samples from the combustor, in which the mean pressure was approximately atmospheric, through a water trap.

It was found by experiment that the best settings for the chromatograph were:

Detector oven temperature	$50^\circ C$
Analyser oven temperature	$50^\circ C$
Argon flowrate	22 ml/min
Sample flowrate	33 ml/min
Katherometer current	60 mA
Chart speed	12 in/h

A typical chromatogram is shown in Figure B.16 and Figure B.17 shows the result of the tests. It is evident that the combustor operated on the lean side of stoichiometric. With increasing fuel flowrate the air/fuel ration approached stoichiometric. The graph suggests a connection between the maximum volumetric combustion intensity and the attainment of stoichiometric conditions. If this were so, it could be concluded that pulsating combustors extinguish under fuel rich conditions. It was also observed that no carbon monoxide was present in measurable quantities, although up to 0.5 per cent hydrogen was found occasionally.

Summary

The preliminary work showed that the Helmholtz-type combustor would be satisfactory for the investigation. It was felt that it could be improved
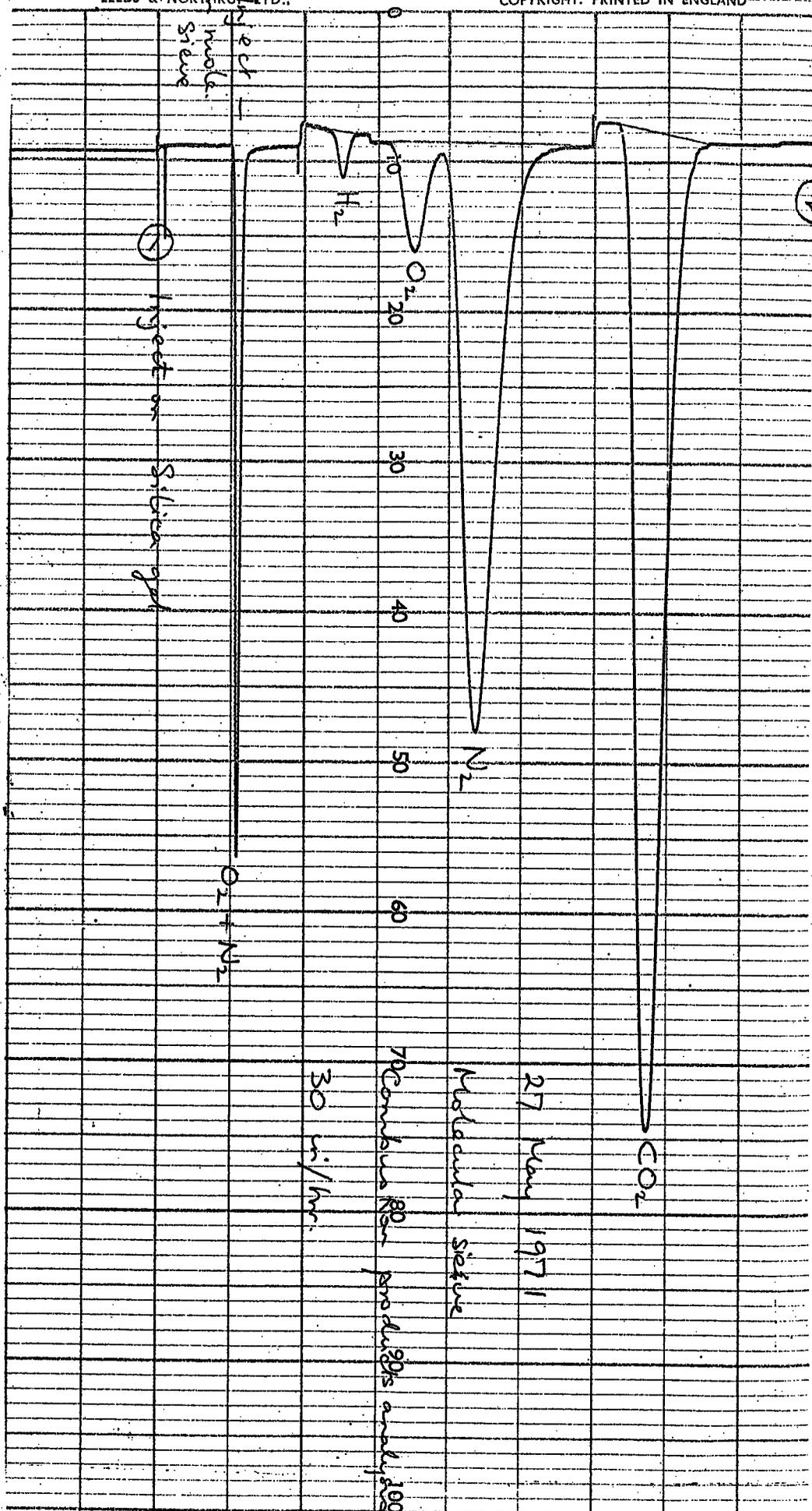
FIGURE B.16 : CHROMATOGRAM OF EXHAUST GASES

FIGURE B.17: RESULT OF DRY VOLUMETRIC ANALYSIS OF EXHAUST PRODUCTS
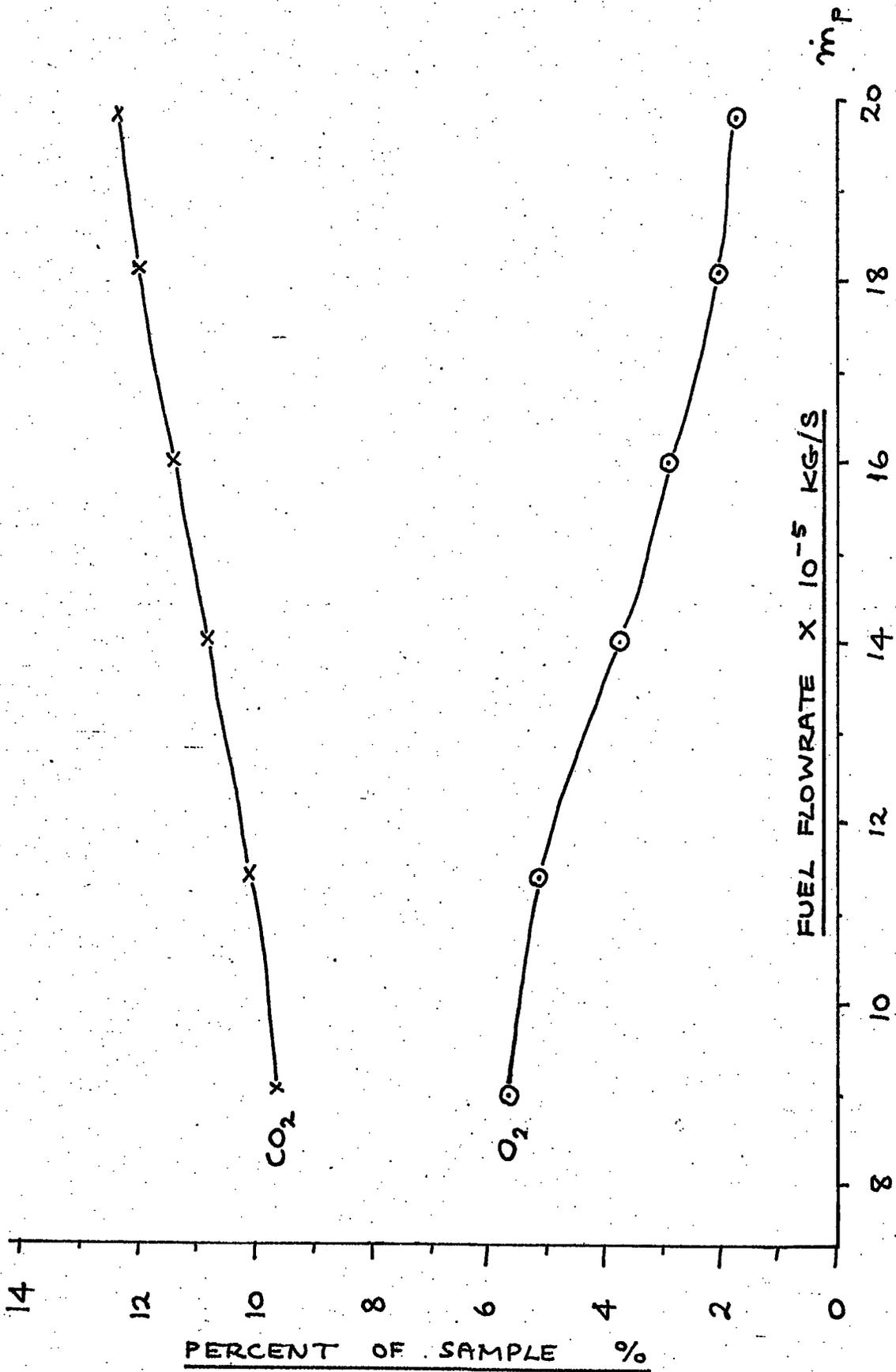
by lengthening the heat exchanger to spread out the effects under observation, and by adding heat exchangers to the inlet side to recover the energy loss caused by blowback through the valve. It was felt that the dimensions of the valve should lie in the range 12 - 26 mm. diameter and be 50 mm. long. It was found that the waveform of the pressure oscillation was approximately sinusoidal, and that, compared to it, the mean static pressure within the combustor was approximately atmospheric. It was decided that the accuracy of the fuel flowrate measurement should be improved.

6.C. Gas Temperature Corrections

As stated in Section 3.4.1., two types of thermocouple were used to measure the gas temperature. These were a bare Type S junction mounted on a silica rod and a Type K sheathed thermocouple. The temperature of the junction in both cases required corrections for three reasons:

a) convective and radiant heat exchange occurred between the gas, tube walls and the thermocouple, as well as conduction from the junction;

b) the thermocouple was heated due to stagnation of the gas velocity;

c) as the junctions were at fixed radii in the tube, the reading had to be corrected to the bulk fluid temperature.

a) Thermocouple A

This thermocouple junction, a bead of 0.8 mm. diameter, projected 9.0 mm. into the gas flow. It was supported by its two constituent wires, which were threaded through a silica rod of low thermal conductivity. It was decided that, even though the thermocouple wires did not run parallel to the flow for a few millimetres, the predominant influences on the bead were radiation and convection. To simplify calculation, it was assumed that the surroundings were large and that the effective radiation temperature of the surroundings was $T_{S\phi}$. The following energy balance may then be made, as in Figure C.1;

$$h_c S_B (T_{A1} - T_{A1}') = S_B \sigma \varepsilon_B (T_{A1}'^4 - T_{S\phi}^4)$$

6-C.1

where T_{A1}' is the temperature recorded by the thermocouple. The normal total emissivity of a platinum filament lies in the range 0.036 to 0.192 over the temperature range 27 to 1230°C, according to Simonson (53). Thus was taken to be 0.19. The correlation used for forced convection over spheres was taken from Holman (54):

$$Nu_d = 0.37 (Re_d)^{0.6}$$

6-C.2

Thus:

$$h_c = 462 \, k_A \left\{ \frac{0.8}{10^3} \, \frac{\bar{u}_A \varrho_A}{\mu_A} \right\}^{0.6}$$

6-C.3
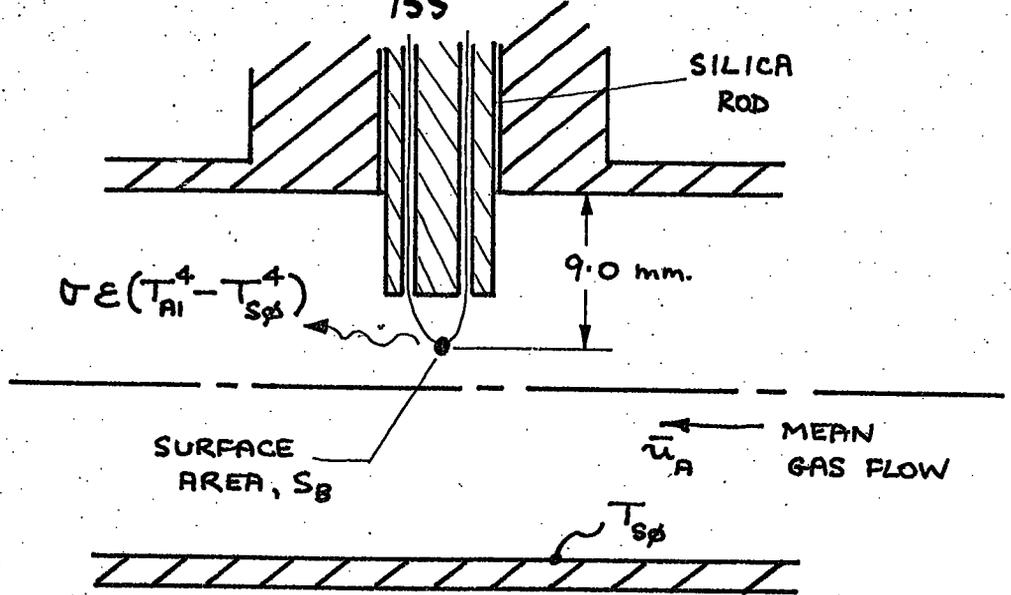
FIGURE C.1: EXAGGERATED T_{A1} INSTALLATION
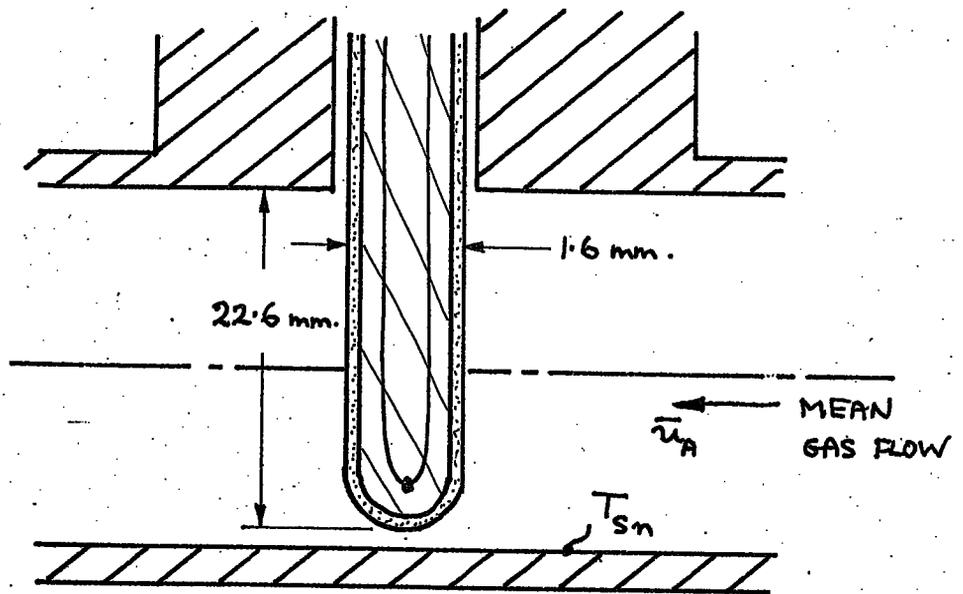
FIGURE C.2: EXAGGERATED T_{An} INSTALLATION
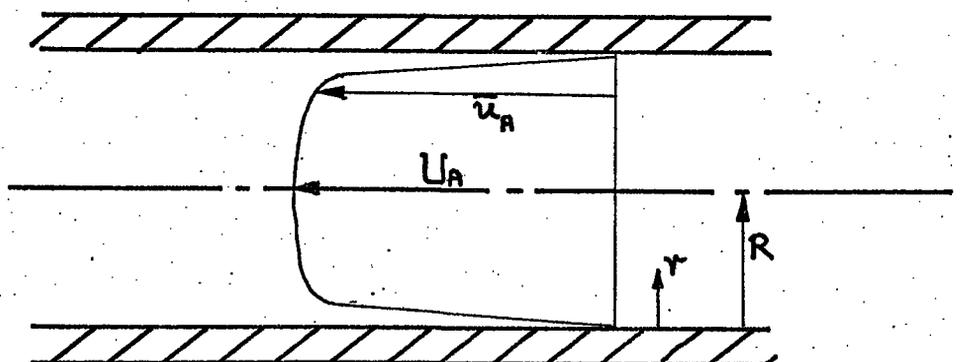
FIGURE C.3: TIME-AVERAGED VELOCITY PROFILE

The properties of air in equation 6-C.3 were evaluated at T_{A1}', and u_A was deduced from $\dot{m}_{AA}$ by the continuity equation:

$$\bar{u}_A = \frac{\dot{m}_{AA}}{3600 \, \rho_A \, S_\phi}$$

6-C.4

The total correction is, from equations 6-C.1:

$$T_{A1} = T_{A1}' + \frac{1.08 \left(T_{A1}'^4 - T_{S\phi}^4 \right)}{10^8 \, h_c}$$

6-C.5

where h_c is calculated from equations 6-C.3 and 6-C.4.

Thermocouple B

This thermocouple junction was embedded in magnesium silicate powder and sheathed in 25/20 Chromium/Nickel steel. It projected 22.6 mm. into the flow and was mounted in a brass collar so that it could be screwed into the measuring sites on the resonating section. (See Figure C.2). Due to this requirement, the thermocouple was straight, and again not bent along an isothermal to reduce conduction. It was decided that the temperature of the junction was affected by radiation, convection and conduction, and the analysis of Chapman (55) was used:

$$\frac{T_{An}' - T_{Sn}}{T_{An} - T_{Sn}} = \frac{h_c}{h_c + h_r} \, \frac{\cosh(m_1 L) - 1}{\cosh(m_1 L)}$$

6-C.6

where T_{An}' was the reading of the thermocouple at the Site number n, L was the immersion of the thermocouple and m_1 was given by:

$$m_1 = \left\{ \frac{h_c + h_r}{k_{sh} \, t_{sh}} \right\}^{1/2}$$

6-C.7

t_{sh}, the thickness of the sheath wall, was 0.15 mm. The radiation and convection coefficients were taken from Chapman and Holman respectively:

$$h_r = \sigma \, \varepsilon_{sh} \, \frac{\left(T_{An}'^4 - T_{Sn}^4 \right)}{\left(T_{An}' - T_{Sn} \right)}$$

6-C.8

$$h_c = 0.5 \, \frac{k_{sh}}{d_{sh}} \, R_d^{0.5}$$

6-C.9

Again, the properties of air were evaluated at T_{An}' . The normal total emissivity of the sheath was taken from Simonson to be 0.82, as the surface became blackened with use. The thermal conductivity of 18/8 Chromium Nickel steel is 22.5 W/m°K at 600°C, and this value was used for k_{sh} .

b)   Assuming that the two installations completely stagnate the moving gas adiabatically, the thermocouples recorded the total temperature of the gas.   Therefore:

$$T_{An}' = T_{An} + \frac{u_A^2}{2\,c_{p_A}}$$ 6-C.10

Now, the velocity of the gas at any instant, u_A, is given by equation 2.3.6:

$$u_A = \bar{u}_A + u_A'$$ 2.3.6.

The stagnation temperature of the gas at any instant thus depends on the velocity amplitude of the oscillations as well as the mean velocity, $\bar{u}_A$, of the gas.

c)   The bulk fluid temperature at a cross-section may be defined, for an incompressible fluid of constant properties, as:

$$T_B = \frac{\int_0^R c_p\, T\, \rho\, u\, r\, dr}{c_p \int_0^R \rho\, u\, r\, dr}$$ 6-C.11

T_B is dependent on the velocity distribution across the tube.   In the absence of a direct measurement, which would have required a special hot-wire anemometer, it was assumed that the time-averaged velocity distribution in the tube was given by an equation of the type:

(see Figure C.3)

$$\frac{u}{U} = \left(\frac{r}{R}\right)^{1/n}$$ 6-C.12

For Re = 4000, Bayley et al (56) give n = 6 and the ratio:

$$\frac{\bar{u}_A}{U_A} = 0.791 \qquad \text{6-C.13}$$

Now equation 6-C.11 may be written:

$$T_B = \frac{3600}{\dot{m}_{AA}} \, \rho_A \int_0^R T_A \, u_A \, r \, dr \qquad \text{6-C.14}$$

Substitution of 6-C.4, 6-C.12 and 6-C.13 into 6-C.14 yields:

$$T_B = \frac{1}{0.791 \, S_\phi} \int_0^R T_A(r) \left(\frac{r}{R}\right)^{1/6} r \, dr \qquad \text{6-C.15}$$

It was therefore necessary to measure the temperature profile, $T_A(r)$ at a cross-section. This was done at Site 7 for two fuel flowrates, and the results are shown in Figure C.4. A Type K thermocouple, of 0.5 mm. diameter, was mounted on a slide with a micrometer and traversed across the tube. Immediately after the traverse, the Pyrotenax Type K thermocouple was inserted, and a reading obtained under the same conditions. It was assumed that the corrections to the readings from these thermocouples were identical, although this is an approximation since the immersion of the traversing thermocouple necessarily changed.

The data from the traverses was used to integrate equation 6-C.15 by Simpson's Rule, and the results are shown in Table C.1.

<div align="center">

Table C.1.

Comparison of experimental reading with corrected temperature

</div>

$\bar{Re}_A$	Experimental Reading	T_B
3840	152	141
4800	144	128
	°C	°C

FIGURE C.4: GAS TEMPERATURE PROFILE
AT SITE 7 FOR TWO FUEL
FLOWRATES.

D_I = 13 mm.

⊙ $\dot{m}_p$ = 0.29 kg/h

△ $\dot{m}_p$ = 0.48 kg/h
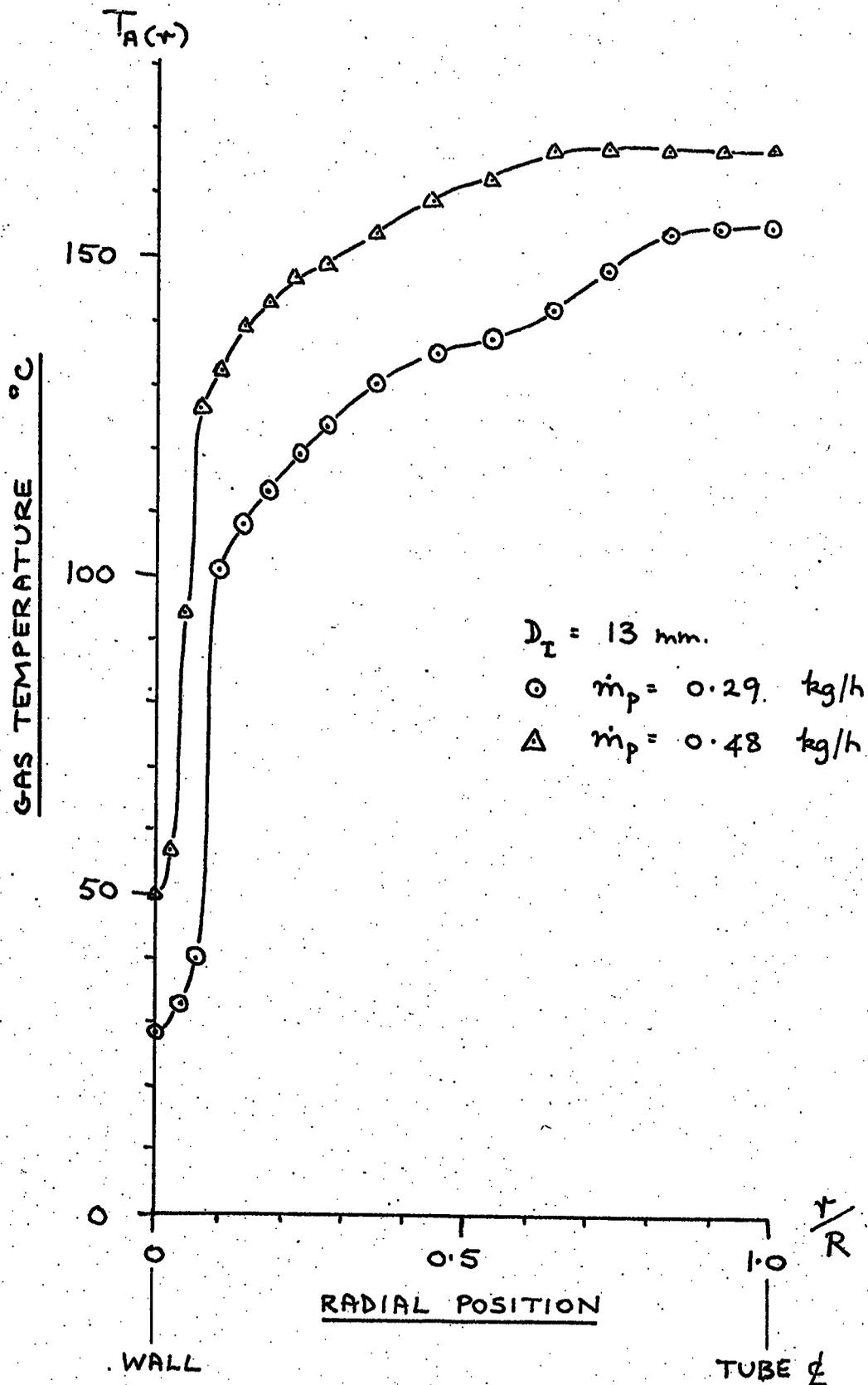
It transpired that the product $m_1 L$ always exceeded 5, and thus equation 6-C.6 became:

$$T_{An} = T_{Sn} + \left(\frac{h_c + h_r}{h_c} \right) \left(T_{An}' - T_{Sn} \right)$$

6-C.17

The correction to the Pyrotenax installation therefore depended only on the relative magnitudes of the convection and radiation coefficients. The ratio $(h_c + h_r / h_c)$ lay in the range 1.01 to 1.2, corresponding to corrections of approximately $0.5°C$ and $130°C$ at the cold and hot ends respectively.

The gas temperature corrections were applied using the programmes overleaf.

```
C   TA1 TEMP. CORRECTION PROG
       IMPLICIT REAL*8(A-Z)
    3 CONTINUE
      READ(5,1000)TA,TS,MAA
      IF(TA)6,6,4
    4 CONTINUE
      RED=MAA/(2497*MUA(TA))
      HC=462*KA(TA)*(RED**0.6)
      TA=TA+1.08*(TA**4-TS**4)/(100000000*HC)
      WRITE(6,1001)TA
 1001 FORMAT(6X,F10.2)
 1000 FORMAT(5(F10.3))
      GO TO 3
    6 CONTINUE
      STOP
      END
```

```
C   TAN TEMP. CORRECTION PROG
       IMPLICIT REAL*8(A-Z)
    3 CONTINUE
      READ(5,1000)TA,TS,MAA
 1000 FORMAT(5(F10.3))
      IF(TA)6,6,4
    4 CONTINUE
      RED=0.0016*MAA/MUA(TA)
      HC=384*KA(TA)*(RED**0.47)
      HR=(TA**4-TS**4)*4.69/((TA-TS)*100000000)
      R=(HC+HR)/HC
      TA=TS+(R*(TA-TS))
      WRITE(6,1001)TA
 1001 FORMAT(6X,F10.2)
      GO TO 3
    6 CONTINUE
      STOP
      END
```

Type T thermocouple Calibrations

This was achieved by lagging the resonating section thoroughly with Cosywrap and running a constant flow of water through the heat exchangers without firing up the combustor. The system was allowed to reach equilibrium and then readings of all the surface and water thermocouples were taken, together with the mercury-in-glass thermometer readings T_{W1} and T_{W9}. The mean of these last two was taken, and all other readings compared. In the case of the surface thermocouples, the corrections lay in the range -1.7 to +1.3 K, and in the case of the water thermocouples, the corrections lay in the range -0.3 to +1.3 K. These corrections were applied to the experimental readings by the programme CKBC.

6.D. Calibration of Pressure transducer mountings

The Kistler pressure transducer mountings were calibrated by comparing their response to a range of frequencies with that of a calibrated Bruel and Kjer microphone.   The apparatus is shown in Figure D.1 and was set up in the middle of high, open laboratory to minimise reflections.   The loud-speaker was excited by an audio wave generator at the highest level that could be sustained over the range 60 to 220 Hz without overloading the cone.   The transducer mountings and calibrated microphone were held by a clamp so that the open end of the tubes and the diaphragm, respectively, were in the same position relative to the loudspeaker.   The procedure followed was to set the sound level, run through the frequency range at 10 Hz intervals taking the transducer readings, and then, having exchanged the microphone for the transducer, repeat the experiment.   The transducer signal was amplified using the same amplifier and oscilloscope as was used in the main experiments, and was transmitted by the same connecting cables.   The results of the calibration are shown in Figure 3.19.

The charge sensitivity of the Bruel and Kjer Type 4117 Microphone was calculated as follows, from (57) ;

Charge sensitivity, $$S_{charge} = S_v \times C_m$$

and the voltage sensitivity was given as:

$$S_v = 0.37 \ mV/\mu Bar$$

The sensitivity correction was:

$$S_{v(c)} = \frac{S_v \, (C_m + 0.1)}{C_m + C_c + C_i}$$

where

$$C_m = 4.2 \ nF$$
$$C_c = 3.04 \ m \times 90 \ pF/m$$
$$C_i = 0.0001 \ pF$$

Thus
$$S_{v(c)} = 0.3556 \ mV/\mu Bar$$

and
$$S_{charge} = 14.9 \ pC/ \ N/m^2$$

FIGURE D.1: APPARATUS FOR CALIBRATION OF PRESSURE MEASURING SYSTEM
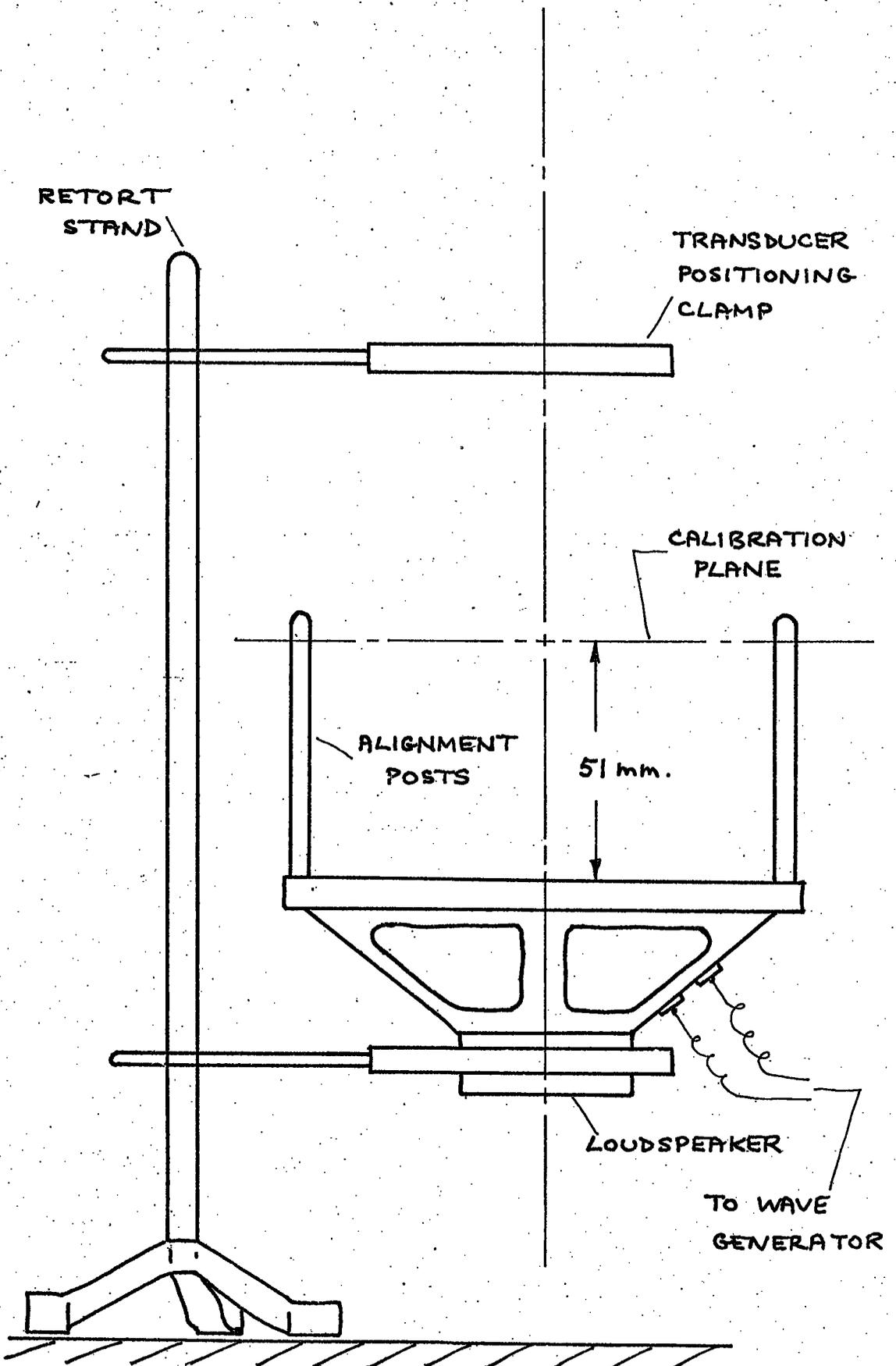
The amplifier was set to an amplification of 1.49 x 1000 and the time-constant to 0.1 mS . From the Vibro-Meter Ag Handbook ($Biblio.49$), and the setting of the oscilloscope, the final amplification was, on the oscilloscope screen: $1 \ V \ \equiv \ 10 \ \pm \ 0.05 \ N/m^2$

6.E.1. The Energy Balance

The readings for Experiment 1 were converted to S.I. units and corrected to a standard temperature and pressure, 293.16 K and 101.325 kN/m^2 respectively. The following correction factors were used:

Temperature, T $\qquad$ $T \times T_0/T_{A_0}$ $\qquad$ E.1.1

Pressure, P $\qquad$ $P \times P_0/P_{A_0}$ $\qquad$ E.1.2

Mass flowrate, $\dot{m}$ $\qquad$ $\dot{m} \times \dfrac{P_0}{P_{A_0}} \times P_{A_0} \left\{ \dfrac{T_{A_0}}{T_A} \right\}^{1/2}$ $\qquad$ E.1.3

where T_{A_0}, P_{A_0} were the ambient conditions. The mass flowrate, of fuel, water and coolant air were obtained with the following factors to give kg/h:

$\dot{m}_p$ $\qquad$ 1.905 x reading $\qquad$ E.1.4

$\dot{m}_w$ $\qquad$ 105.64 + (37.512 x reading) $\qquad$ E.1.5

$\dot{m}_{gc}$ $\qquad$ 0.1168 x reading $\qquad$ E.1.6

The thermocouple readings were converted by subroutines of the main computation which interpolated quadratically the reference tables. All these operations were performed by a computer programme, CKBC, listed in Appendix F.

E.1.1 Application of the First Law

The Steady Flow Energy Equation is;

$$\dot{Q} - \dot{W}_x = \sum_{OUT} \dot{m} \left(h + \frac{u^2}{2g_0} + \frac{a_g z}{g_0} \right) - \sum_{IN} \dot{m} \left(h + \frac{u^2}{2g_0} + \frac{a_g z}{g_0} \right) + \left[\Delta H' \right]_{t_0}$$

E.1.7

where the terms accounting for the effects of capillarity, electricity and magnetism have been ignored. The streams of material entering the control volume are cold water, cold air, propane and cold coolant water, and those leaving were hot water, two streams of combustion products, and hot coolant water. There are no work interactions at the control boundary, if the radiation of sound waves from the open ends of the combustor is regarded as negligible. There are heat interactions in the form of heat transfer through the lagging.

Assuming that the heat transfers through the heat exchanger lagging were negligible, and that the conduction through the combustion chamber lagging is given by;

$$\dot{Q}_{LCL} = - \frac{2\pi k_{LAG} (T_{LAG} - T_{SC}) L_{CL}}{\log_e (D_{L2}/D_{L1})}$$

E.1.8

Ignoring changes in kinetic and potential energy, equation E.1.7 may be written:

$$\dot{Q}_{LCL} = \dot{m}_W \Delta h_W + \dot{m}_A \Delta h_A + \dot{m}_{WTR} \Delta h_{WTR}$$
$$+ \dot{m}_{WIN} \Delta h_{WIN} + \dot{m}_{gc} \Delta h_{gc} + \dot{m}_P [\Delta h']_{t_o}$$

E.1.9

The connecting pipe carrying the water flow from Heat Exchangers B and C to A lies outside the control volume in Figure 4.1, so:

$$\Delta h_W = \Delta h_{WA} + \Delta h_{WBC}$$

E.1.10

and by continuity:

$$\dot{m}_A = \dot{m}_{AA} + \dot{m}_{ABC}$$

E.1.11

The assumption is now made that the combustion products flowing through the apparatus are predominantly air, and the properties used hereafter for the combustion products are those of pure air. Assuming that air and water behave as pure substance, the changes in enthalpy through the control volume are:

$$\Delta h_{AA_o} = \bar{c}_{P_{AA_o}} (T_{A8} - T_{A_o})$$

E.1.12

$$\Delta h_{AC_o} = \bar{c}_{P_{AC_o}} (T_{A23} - T_{A_o})$$

E.1.13

$$\Delta h_{WTR} = \bar{c}_{P_{WTR}} (T_{WTR} - T_{W23})$$

E.1.14

$$\Delta h_{WIN} = \bar{c}_{P_{WIN}} (T_{WIN} - T_{W23})$$

E.1.15

$$\Delta h_{gc} = \bar{c}_{P_{gc}} (T_{gc2} - T_{gc1})$$

E.1.16

where the specific heats of the substances are evaluated at the arithmetic mean of the inlet and outlet temperatures.

The mass flowrates of the two streams of air flowing through the apparatus

may be deduced by applying equation E.1.7 to control volumes around Heat Exchanger A and around Heat Exchangers B and C. Using the assumptions already made, the mass flowrates are given by:

$$\dot{m}_{AA} = - \frac{\dot{m}_W \, \bar{c}_{P_{WA}} (T_{W1} - T_{W9})}{\bar{c}_{P_{AA}} (T_{A8} - T_{A1})} \qquad \text{E.1.17}$$

and

$$\dot{m}_{ABC} = - \frac{\dot{m}_W \, \bar{c}_{P_{ABC}} (T_{W21} - T_{W23})}{\bar{c}_{P_{ABC}} (T_{A23} - T_{A21})} \qquad \text{E.1.18}$$

In equation E.1.17, and specific heat, $\bar{c}_{P_{AA}}$, is evaluated at a mean temperature, $\bar{T}_A$, defined by:

$$\bar{T}_A = \frac{1}{(x_c - x_H)} \int_{x_H}^{x_c} T_A(x) \, dx \qquad \text{E.1.19}$$

which may conveniently be integrated by Simpson's Rule;

$$\bar{T}_A = \frac{\Delta L_A}{3} \left[T_{A1} + 4T_{A3} + 2T_{A4} + 4T_{A5} \right. \\ \left. + 2T_{A6} + 4T_{A7} + T_{A8} \right] \qquad \text{E.1.20}$$

where $\Delta L_A = 0.345 \, m.$

In equation E.1.18, the specific heats are evaluated as for equations E.1.12 to E.1.16.

These calculations were performed also by computer programme CKBC.

E.1.2 Results of the Energy Balance

The results of the energy balance are shown in Tables E.1, E.2 and E.3 where the discrepancy between the two sides of equation 4.1.9 is expressed as a percentage of the energy released, $[\Delta \dot{H}']_{t_o}$ The discrepancy lies within the limits -5.7 to +10.0%. This was regarded as satisfactory. In the next column, the overall thermal efficiency of the combustor has been calculated, using:

$$\eta_{th} = - \frac{(\Delta \dot{H}_{WA} + \Delta \dot{H}_{WBC} + \Delta \dot{H}_{WTR} + \Delta \dot{H}_{WIN} + \Delta \dot{H}_{gc})}{[\Delta \dot{H}']_{t_o}} \qquad 1.21$$

		TABLE E.1				
$\dot{m}_P$		0.479	0.391	0.292	0.223	kg/h
$\dot{Q}_{LCL}$		-319	-244	-197	-203	W
$\Delta\dot{H}_{WA}$		4186	3348	2511	2104	W
$\Delta\dot{H}_{WBC}$		886	635	577	518	W
$\Delta\dot{H}_{AA\phi}$		47	62	38	37	W
$\Delta\dot{H}_{AC\phi}$		250	250	199	134	W
$\Delta\dot{H}_{WTR}$		54	56	30	37	W
$\Delta\dot{H}_{WIN}$		220	222	216	149	W
$\Delta\dot{H}_{GC}$		200	102	58	0	W
$[\Delta\dot{H}']_{t\phi}$		-6662	-5432	-4061	-3098	W
ENERGY BALANCE		+8.2	+10.0	+6.0	-2.7	%
η_{th}		0.886	0.85	0.882	0.906	-
		TABLE E.2				
$\dot{m}_P$	0.562	0.477	0.383	0.328	0.223	kg/h
$\dot{Q}_{LCL}$	-294	-237	-217	-204	-182	W
$\Delta\dot{H}_{WA}$	4278	3660	3266	2848	2307	W
$\Delta\dot{H}_{WBC}$	1827	1432	1104	723	381	W
$\Delta\dot{H}_{AA\phi}$	68	62	48	95	111	W
$\Delta\dot{H}_{AC\phi}$	422	372	298	164	92	W
$\Delta\dot{H}_{WTR}$	52	66	67	52	53	W
$\Delta\dot{H}_{WIN}$	230	225	226	198	168	W
$\Delta\dot{H}_{GC}$	-	-	-	-	-	W
$[\Delta\dot{H}']_{t\phi}$	-7818	-6627	-5332	-4558	-3107	W
ENERGY BALANCE	+8.2	+8.8	+2.0	+6.0	-5.7	%
η_{th}	0.853	0.849	0.874	0.838	0.936	-

$D_I = 13$ mm (Table E.1)

$D_I = 16$ mm (Table E.2)

$A_I = 19 \text{ mm}$

		TABLE E.3				
$\dot{m}_P$	0.563	0.477	0.381	0.330	0.224	kg/h
$\dot{Q}_{LCL}$	−331	−245	−227	−211	−190	W
$\Delta\dot{H}_{WA}$	4185	3784	3107	2828	2185	W
$\Delta\dot{H}_{WBC}$	1765	1491	1132	780	297	W
$\Delta\dot{H}_{AA\phi}$	112	100	89	79	86	W
$\Delta\dot{H}_{AC\phi}$	362	298	157	126	110	W
$\Delta\dot{H}_{WTR}$	64	65	51	42	31	W
$\Delta\dot{H}_{WIN}$	250	219	217	204	173	W
$\Delta\dot{H}_{GC}$	−	−	−	−	−	W
$[\Delta\dot{H}']_{t\phi}$	−7820	−6627	−5352	−4564	−3112	W
ENERGY BALANCE	+9.5	+6.5	+7.1	+6.2	+4.5	%
η_{th}	0.842	0.879	0.882	0.872	0.893	−

TABLE E.4

D_I	13	13	16	16	19	19
$\dot{m}_P$	0.292	0.572	0.291	0.569	0.293	0.573
$\dot{m}_W$	145	141	151	144	149	159
$\dot{m}_{AA}$	7.16	11.8	9.57	14.2	7.30	11.7
T_{S1}	311.7	320.2	314.6	327.2	312.9	321.2
T_{S2}	310.8	325.7	318.4	333.1	309.3	322.8
T_{S3}	300.7	308.8	306.9	317.1	303.4	309.0
T_{S4}	293.9	297.7	301.0	305.7	295.7	300.3
T_{S5}	293.9	299.4	300.0	306.9	298.1	300.5
T_{W1}	301.4	310.0	307.1	319.2	302.4	310.1
T_{W2}	297.8	301.3	303.0	307.2	297.9	303.8
T_{W3}	294.9	298.9	300.0	304.0	295.0	299.8
T_{W4}	292.9	294.1	297.3	299.7	293.3	295.7
T_{W5}	292.4	292.9	296.8	297.5	292.8	294.5
T_{W6}	291.4	290.7	295.4	295.5	291.5	292.9
T_{W7}	290.2	288.0	293.1	291.1	289.6	289.2
T_{W8}	290.0	287.5	292.6	290.4	289.3	288.5
T_{W9}	289.3	287.1	291.7	289.9	289.4	288.6
$\Delta \dot{H}_{WA}$	2028	3770	2705	4907	2246	3966
U_A	37.5	53.3	41.2	61.0	32.8	49.8
$\bar{c}_{P_{AA}}$	1061	1087	1081	1110	1082	1096
f	115	193	132	198	77	146

TABLE E.5

D_I	13	13	16	16	19	19
T_{A1}	1289	1420	1308	1509	1385	1497
T_{A2}	997	1176	1091	1298	1088	1195
T_{A3}	891	1076	989	1177	973	1090
T_{A4}	705	837	817	968	824	911
T_{A5}	573	650	681	823	701	764
T_{A6}	454	544	574	697	582	621
T_{A7}	385	464	495	598	498	522
T_{A8}	328	362	367	388	361	384
T_{A1}	1336	1479	1351	1580	1454	1573
T_{A2}	1131	1368	1252	1549	1270	1399
T_{A3}	980	1215	1102	1353	1094	1236
T_{A4}	743	893	874	1055	891	988
T_{A5}	590	672	710	871	738	804
T_{A6}	461	555	589	723	600	640
T_{A7}	388	470	503	612	508	531
T_{A8}	329	363	368	390	363	386

GAS TEMPERATURE

CORRECTED GAS TEMPERATURE

TABLE E.6

D_I	13	13	16	16	19	19
$\overline{Re}_A$ (1)	1846	2771	2382	3136	1764	2671
(2)	2046	2953	2545	3293	1936	2890
(3)	2339	3375	2856	3720	2172	3230
(4)	2775	4109	3306	4310	2475	3724
(5)	3262	4836	3774	4885	2822	4298
(6)	3800	5471	4246	5498	3207	4950
(7)	4321	6352	4984	6689	3802	5870
$\overline{Re}_w$ (1)	903	1041	1057	1256	947	1177
(2)	885	1004	1031	1205	927	1138
(3)	855	944	987	1123	894	1074
(4)	814	870	935	1018	849	995
(5)	774	796	882	916	804	916
(6)	792	724	828	820	835	836
(7)	698	655	875	784	720	766
$\overline{u}_A$ (1)	12.5	23.8	17.6	31.5	14.1	24.6
(2)	10.7	21.6	16.0	29.2	12.2	21.8
(3)	8.75	17.6	13.4	24.2	10.3	18.4
(4)	6.78	13.1	10.7	19.4	8.43	14.9
(5)	5.34	10.3	8.83	16.0	6.93	12.0
(6)	4.32	8.58	7.43	13.5	5.75	9.73
(7)	3.70	6.98	5.94	10.1	4.53	7.65

TABLE E.7

D_I	13	13	16	16	19	19
$\hat{u}$ (1)	4.2	17.8	5.14	8.7	41.4	33.8
(2)	7.95	31.7	0.59	21.2	37.8	21.4
(3)	11.8	37.7	4.12	29.2	34.1	5.4
(4)	13.0	33.0	8.0	26.8	26.9	9.7
(5)	13.5	17.3	11.0	16.5	19.8	24.0
(6)	11.9	5.1	11.5	1.2	10.6	32.4
(7)	8.45	24.6	10.0	18.6	0.8	32.8
Nu (1)	9.1	9.4	9.3	9.9	9.5	9.8
(2)	9.9	10.1	9.6	10.7	10.3	10.1
(3)	11.5	11.7	11.4	11.9	11.4	10.6
(4)	12.0	12.3	11.9	12.9	12.4	11.7
(5)	13.2	13.4	13.0	14.1	13.5	12.8
(6)	14.4	14.5	14.1	15.3	14.5	13.9
(7)	15.3	15.5	15.1	16.2	15.3	15.1
$\overline{Nu}_p$ (1)	10.7	10.2	8.7	8.9	11.2	14.7
(2)	12.1	14.0	12.1	17.6	11.6	11.2
(3)	14.2	21.4	13.9	18.6	9.3	11.7
(4)	16.5	27.6	16.0	17.9	10.6	12.9
(5)	26.2	26.2	18.8	21.4	15.0	24.1
(6)	30.8	16.4	21.2	14.3	16.4	27.1
(7)	62.3	91.3	77.5	119	62.5	84.1

TABLE E.8

D_I	13	13	16	16	19	19
h_{sw}(1)	1275	1391	1394	2021	1246	1810
(2)	1328	1415	1424	1987	1262	1820
(3)	1426	1456	1476	1932	1292	1834
(4)	1580	1516	1552	1865	1333	1855
(5)	1773	1581	1636	1801	1377	1876
(6)	1638	1326	1730	1743	1146	1898
(7)	2327	1727	1456	1374	1472	1920
h_{As}(1)	42.6	32.8	26.1	10.0	35.0	48.6
(2)	31.4	41.9	36.8	57.0	32.6	43.1
(3)	31.7	55.5	34.4	53.0	23.0	39.6
(4)	30.2	57.2	33.5	43.3	22.7	38.8
(5)	39.7	44.8	33.6	45.0	27.5	47.0
(6)	39.4	46.9	33.2	44.5	25.9	44.8
(7)	69.5	115	101.1	174	81.5	114
S (1)	1.5	1.32	1.23	1.03	0.89	0.97
(2)	1.75	1.46	1.35	1.11	1.03	1.09
(3)	2.3	1.79	1.61	1.34	1.22	1.29
(4)	2.97	2.4	2.02	1.67	1.49	1.6
(5)	3.78	3.06	2.44	2.02	1.81	1.98
(6)	4.67	3.67	2.9	2.4	2.19	2.45
(7)	5.45	4.52	3.64	3.2	2.77	3.11

6.F. Computer Programmes

The following programmes are listed in this Appendix:

CKBA — This programme calculated the steady state heat transfer coefficients and flow parameters according to Section 4.4.2 for given air and water mass flow-rates and inlet and outlet temperatures.

CKBB — This programme calculated the experimental heat transfer coefficients according to Section 4.4.1. from data provided by CKBC.

CKBC — This programme read in the experimental data, corrected it according to Section 4.1 and calculated the energy balance. All water and air properties were obtained by quadratic interpolation.

PCVPP01 — This programme solved the Bessel boundary conditions for an exponential gas temperature gradient according to Section 2.2 for given T_{A1} and T_{A8} .

VALVE — This programme calculated the air mass flow through the aerodynamic valve according to Section 2.5 for a given pressure amplitude and valve diameter.

The programmes are written in Fortran IV and were run on N.U.M.A.C.

```
C  CKBA   --   THEORETICAL STEADY STATE HEAT TRANSFER IN HEAT EXCHANGER
      REAL*8 XH,XC,DO,SO,SANN,DEQ,DEP,SS,DL,TA1,TW1,TA2,TW2,TAX1,TWX1,
     >X,DH,DHA,TWL,REA,REW,NUA,NUW,MUA,MUW,PRA,PRW,CPA,CPW,KA,KW,TA,TW
     >MUAS,MUWS,U,H1,H2,TAXM,TSXM,TWXM,XX
     >,MAA,MW,DHR
      DATA XH,XC,DO,SO,SANN,DEQ,DEP
     >/0.33,2.40,0.026594,0.00055546,0.00061322,0.027616,0.011478/
      J=50
    3 CONTINUE
      READ(5,1070)MAA,MW,TAX1,TWX1,TWL
 1070 FORMAT(5(F10.5))
      IF(MAA.LE.0.0)GO TO 33
      WRITE(6,2073)
 2073 FORMAT(6X,'XX',5X,'TAXM',6X,'TSXM',6X,'TWXM',6X,'NUA',7X,'NUW',
     >7X,'REA',7X,'REW',7X,'H1',8X,'H2'//)
C
      DL=(XC-XH)/J
      SS=3.14159265358*DO*DL
      MAA=MAA/3600.0
      MW=MW/3600.0
      TW1=TWX1
  200 CONTINUE
      DH=0.0
      TA1=TAX1
      DHA=0.0
      X=XH
      DO 80 IJ=1,J
      X=X+DL
      TA=TA1
      TW=TW1-273.16
      PRA=CPA(TA)*MUA(TA)/KA(TA)
      PRW=CPW(TW)*MUW(TW)/KW(TW)
      REA=4.0*MAA/(3.14159265358*DO*MUA(TA))
C  EQU, 8.15 P.336 CHAPMAN
      NUA=0.023*(REA**0.8)*(PRA**0.3)
      H1=(NUA*KA(TA))/DO
      REW=MW*DEP/(SANN*MUW(TW))
C  EQU, 8.11 P.333 CHAPMAN      (LESS VISCOSITY TERM)
      NUW=0.023*(REW**0.8)*(PRW**0.4)
      H2=(NUW*KW(TW))/DEQ
      U=H1*H2/(H1+H2)
C  ENTHALPY CHANGES
      DH=U*SS*(TA1-TW1)
C  CALC. FIRST ESTIMATE OF OUTLET TEMPS. FROM SECTION
      TA2=TA1-(DH/(MAA*CPA(TA)))
      TW2=TW1-(DH/(MW*CPW(TW)))
      TAXM=0.5*(TA1+TA2)
      TWXM=0.5*(TW1+TW2)
      TSXM=((H1*TAXM)+(H2*TWXM))/(H1+H2)
C  CALC. AGAIN USING DYNAMIC VISCOSITY RATIO & MEAN TEMPS.
      TA=TSXM
      TW=TSXM-273.16
      MUAS=MUA(TA)
      MUWS=0.0001798
```

```
      TA=TAXM
      TW=TWXM-273.16
      PRA=CPA(TA)*MUA(TA)/KA(TA)
      PRW=CPW(TW)*MUW(TW)/KW(TW)
      REA=4.0*MAA/(3.14159265358*DO*MUA(TA))
C  EQU, 8.16 P.336 CHAPMAN
C
      IF(TAXM.LE.373.16)GO TO 73
      NUA=0.023*(REA**0.8)*(PRA**0.3)
      GO TO 76
   73 CONTINUE
      NUA=5.03*(REA**0.33333333)*(PRA**0.33333333)
      GO TO 76
   76 CONTINUE
C
      H1=(NUA*KA(TA))/DO
      REW=MW*DEP/(SANN*MUW(TW))
C  EQU, 8.11 P.333 CHAPMAN
      NUW=0.023*(REW**0.8)*(PRW**0.4)
C
      H2=(NUW*KW(TW))/DEQ
      U=H1*H2/(H1+H2)
C  ENTHALPY CHANGES
      DH=U*SS*(TAXM-TWXM)
C  CALC. FIRST ESTIMATE OF OUTLET TEMPS. FROM SECTION
      TA2=TA1-(DH/(MAA*CPA(TA)))
      TW2=TW1-(DH/(MW*CPW(TW)))
      TAXM=0.5*(TA1+TA2)
      TWXM=0.5*(TW1+TW2)
      TSXM=((H1*TAXM)+(H2*TWXM))/(H1+H2)
      DH=U*SS*(TAXM-TWXM)
      DHR=0.17*SS*(((TAXM/100)**4)-((TSXM/100)**4))
      DH=DH+DHR
      DHA=DHA+DH
      XX=X-DL/2
      WRITE(6,2010)IJ,XX,TAXM,TSXM,TWXM,NUA,NUW,REA,REW,H1,H2
 2010 FORMAT(1H ,I3,F7.3,10(1PD10.3))
      TA1=TA2
      TW1=TW2
   80 CONTINUE
C  TEST FOR TW2 = TWL
      IF(DABS(TW2-TWL).LE.0.8)GO TO 100
      TW1=TWX1-(TW1-TWL)
      GO TO 200
  100 CONTINUE
      WRITE(6,2020)MAA,MW,TAX1,TWX1,TWL,J
 2020 FORMAT(7X,'MA =',1PD12.5/7X,'MW =',1PD12.5/5X,'TAX1 =',
     +1PD12.5/5X,'TWX1 =',1PD12.5/6X,'TWL =',1PD12.5/8X,'J =',I3)
      WRITE(6,2017)DHA
 2017 FORMAT(10X,'DHA =',5X,1PD10.3)
      GO TO 3
   33 CONTINUE
      STOP
      END
```

```fortran
C  EXPERIMENTAL RESULTS PROG
      IMPLICIT REAL*8(A-Z)
      DIMENSION XA(20),XS(20),XW(20),TG(20),TS(20),TF(20),
     >UA(20),CVEL(20),HAS(20),HSW(20),NUA(20),NUW(20),REA(20),REW(20)
      INTEGER I,J,K
      DATA XA/0.33,0.477,0.654,1.011,1.366,1.722,2.077,2.4/
      DATA XS/0.33,0.84,1.375,1.93,2.4/
      DATA XW/0.33,0.450,0.628,0.805,1.162,1.518,1.874,2.23,2.4/
      DATA DO,SO,SAN,CEQ,DEP
     >/0.026594,0.00055546,0.00061322,0.027616,0.011478/
      READ(5,1000)(TG(I),I=1,8)
      READ(5,1000)(TS(I),I=1,5)
      READ(5,1000)(TF(I),I=1,9)
      READ(5,1000)MAA,MW
 1000 FORMAT(10(F10.4))
      GRADS=(TS(1)-TS(5))/(XS(1)-XS(5))
      GRADW=(TF(1)-TF(9))/(XW(1)-XW(9))
      CONSTS=(XS(1)*TS(5)-XS(5)*TS(1))/(XS(1)-XS(5))
      CONSTW=(XW(1)*TF(9)-XW(9)*TF(1))/(XW(1)-XW(9))
      DA=0.0
      DW=0.0
      X1=0.33
      TS1=CONSTS+GRADS*X1
      TW1=CONSTW+GRADW*X1
      DO 10 I=1,7
      X2=XA(I+1)
      TS2=CONSTS+GRADS*X2
      TW2=CONSTW+GRADW*X2
      SS=3.14159265358*DO*(X2-X1)
      TAXM=0.5*(TG(I)+TG(I+1))
      TSXM=0.5*(TS1+TS2)
      TWXM=0.5*(TW1+TW2)
      TA=TAXM
      TW=TWXM-273.16
      UA(I)=MAA/(SO*3600*RHOA(TA))
      CVEL(I)=CA(TA)
      DHA=MAA*CPA(TA)*(TG(I)-TG(I+1))/3600
      DHW=MW*CPW(TW)*(TW1-TW2)/3600
      HAS(I)=DHA/(SS*(TAXM-TSXM))
      HSW(I)=DHW/(SS*(TSXM-TWXM))
      NUA(I)=HAS(I)*DO/KA(TA)
      NUW(I)=HSW(I)*DEQ/KW(TW)
      REA(I)=4*MAA/(3.14159265358*DO*3600*MUA(TA))
      REW(I)=MW*DEP/(SAN*3600*MUW(TW))
      DW=DW+DHW
      DA=DA+DHA
      TS1=TS2
      TW1=TW2
      X1=X2
   10 CONTINUE
      DO 20 I=1,7
      WRITE(6,3030)I,REA(I),REW(I),NUA(I),NUW(I),HAS(I),
     >HSW(I),UA(I),CVEL(I)
 3030 FORMAT(I10,10(F10.2))
   20 CONTINUE
      WRITE(6,3040)DA,DW




 3040 FORMAT(F10.2/F10.2)
      STOP
      END
```

```
C    GKBC  A PROGRAM TO PROCESS EXPERIMENTAL READINGS FRCM THE DOUBLE
C  ORIFICE COMBUSTOR .
      REAL*8 PAO,TAO,PO,TO,TFAC,PFAC,MFAC,MP,MW,MWTR,MWIN,CM,ROTAMW,
     >PAMP,F,PSCALE,TSO,TS1,TS2,TS3,TS4,TS5,TYPEK,TYPES,TYPET,E,
     >TW1,TW2,TW3,TW4,TW5,TW6,TW7,TW8,TW9,TW21,TW22,TW23,TWTR,TWIN,
     >TA1,TA2,TA3,TA4,TA5,TA6,TA7,TA8,TA21,TA22,TA23,LAUG,XAUG,DI,
     >TGC1,TGC2,MGC,TREF,TLAG,ROTAMA,HCVP,KLAG,AA,AB,AC,TW,CPWC,CPWB,
     >CPWA,CPWTR,CPWIN,CPWBC,TA,CPAC,CPAB,CPABC,CPAA,CPAAO,CPACO,
     >CPGC,CPA,CPW,MAC,MAB,MABC,MAA,QLCL,DHW,DHA,DHWTR,DHWIN,DHGC,
     >DHTO,EQ1,TAM,TBM,TCM,UA,UB,UC,NUTH,NUVOL,TYPEK,TYPES,TYPET,
     >TREFK,TREFS,TREFT,TAMB,VOLC,DHWA,PERC,
     >XA1,XA2,XA3,XA4,XA5,XA6,XA7,XA8,XS1,XS2,XS3,XS4,XS5,
     >XW1,XW2,XW3,XW4,XW5,XW6,XW7,XW8,XW9
     >,DX,VAL(10),TEMP1(10)
C  PART 1 - READ IN DATA AND CORRECT TO S.I. UNITS & TO CHOSEN DATUM .
      READ(5,1000)PAO,TAO
 1000 FORMAT(2(F10.4))
      READ(5,1001)MP,MW,MWTR,MWIN.
 1001 FORMAT(4(F10.4))
      READ(5,1002)PAMP,F
 1002 FORMAT(2(F10.4))
      READ(5,1003)TSO,TS1,TS2,TS3,TS4,TS5
 1003 FORMAT(6(F10.4))
      READ(5,1004)TW1,TW2,TW3,TW4,TW5,TW6,TW7,TW8,TW9,TW21,TW22,TW23,
     >TWTR,TWIN
 1004 FORMAT(8(F10.4)/6(F10.4))
      READ(5,1005)TA1,TA2,TA3,TA4,TA5,TA6,TA7,TA8,TA21,TA22,TA23
 1005 FORMAT(8(F10.4)/3(F10.4))
      READ(5,1006)LAUG,XAUG,DI,NJET
 1006 FORMAT(3(F10.4),I3)
      READ(5,1007)TGC1,TGC2,MGC,TREF,TLAG
 1007 FORMAT(5(F10.4))
      PAO=PAO*133.333333
      TAO=TAO+273.16
C  CALCULATE CORRECTION FACTORS
      PO=101325.0
      TO=293.16
      TFAC=TO/TAO
      PFAC=PO/PAO
      MFAC=PFAC/(CSQRT(TFAC))
      MP=MP*1.905*MFAC
      MWTR=MWTR*3.6*MFAC
      MWIN=MWIN*3.6*MFAC
      CM=MW
      MW=ROTAMW(CM)*MFAC
      PAMP=PAMP*1723.69*PFAC
      TAMB=0.5*(TREF+TAO-273.16)
      E=TSO
      E=E+TREFK(TAMB)
      TSO=TYPEK(E)*TFAC
      E=TS1
      E=E+TREFT(TAMB)
      TS1=TYPET(E)*TFAC
      E=TS2
      E=E+TREFT(TAMB)
      TS2=TYPET(E)*TFAC
      E=TS3
      E=E+TREFT(TAMB)
```

```
      TS3=TYPET(E)*TFAC                          E=E+TREFK(TAMB)
      E=TS4                                      TA21=TYPEK(E)*TFAC
      E=E+TREFT(TAMB)                            E=TA22
      TS4=TYPET(E)*TFAC                          E=E+TREFK(TAMB)
      E=TS5                                      TA22=TYPEK(E)*TFAC
      E=E+TREFT(TAMB)                            E=TA23
      TS5=TYPET(E)*TFAC                          E=E+TREFK(TAMB)
      E=TW2                                      TA23=TYPEK(E)*TFAC
      E=E+TREFT(TAMB)                            E=TGC1
      TW2=TYPET(E)*TFAC                          E=E+TREFK(TAMB)
      E=TW3                                      TGC1=TYPEK(E)*TFAC
      E=E+TREFT(TAMB)                            E=TGC2
      TW3=TYPET(E)*TFAC                          E=E+TREFK(TAMB)
      E=TW4                                      TGC2=TYPEK(E)*TFAC
      E=E+TREFT(TAMB)                            TREF=(TREF+273.16)*TFAC
      TW4=TYPET(E)*TFAC                          TLAG=(TLAG+273.16)*TFAC
      E=TW5                                      CM=MGC
      E=E+TREFT(TAMB)                            MGC=ROTAMA(CM)*TFAC
      TW5=TYPET(E)*TFAC                 C    SET CONSTANTS
      E=TW6                                      HCVP=50060000.0
      E=E+TREFT(TAMB)                            KLAG=0.0845
      TW6=TYPET(E)*TFAC                          AA=0.183862
      E=TW7                                      AB=0.108856
      E=E+TREFT(TAMB)                            AC=0.072759
      TW7=TYPET(E)*TFAC                 C    CALCULATE MEAN SPECIFIC HEATS FO5
      E=TW8                                      TW=0.5*(TW23+TW22)-273.16
      E=E+TREFT(TAMB)                            CPWC =CPW(TW)
      TW8=TYPET(E)*TFAC                          TW=0.5*(TW22+TW21)-273.16
      TW1=(TW1+273.16)*TFAC                      CPWB =CPW(TW)
      TW9=(TW9+273.16)*TFAC                      TW=0.5*(TW9 +TW1 )-273.16
      TW21=(TW21+273.16)*TFAC                    CPWA =CPW(TW)
      TW22=(TW22+273.16)*TFAC                    TW=0.5*(TW23+TWTR)-273.16
      TW23=(TW23+273.16)*TFAC                    CPWTR=CPW(TW)
      TWTR=(TWTR+273.16)*TFAC                    TW=0.5*(TW23+TWIN)-273.16
      TWIN=(TWIN+273.16)*TFAC                    CPWIN=CPW(TW)
      E=TA1                                      TW=0.5*(TW23+TW21)-273.16
      E=E+TREFS(TAMB)                            CPWBC=CPW(TW)
      TA1=TYPES(E)*TFAC                          TA=0.5*(TA23+TA22)
      E=TA2                                      CPAC =CPA(TA)
      E=E+TREFK(TAMB)                            TA=0.5*(TA22+TA21)
      TA2=TYPEK(E)*TFAC                          CPAB =CPA(TA)
      E=TA3                                      TA=0.5*(TA23+TA21)
      E=E+TREFK(TAMB)                            CPABC=CPA(TA)
      TA3=TYPEK(E)*TFAC                          TA=TA1
      E=TA4                                      VAL(1)=CPA(TA)
      E=E+TREFK(TAMB)                            TA=TA3
      TA4=TYPEK(E)*TFAC                          VAL(2)=CPA(TA)
      E=TA5                                      TA=TA4
      E=E+TREFK(TAMB)                            VAL(3)=CPA(TA)
      TA5=TYPEK(E)*TFAC                          TA=TA5
      E=TA6                                      VAL(4)=CPA(TA)
      E=E+TREFK(TAMB)                            TA=TA6
      TA6=TYPEK(E)*TFAC                          VAL(5)=CPA(TA)
      E=TA7                                      TA=TA7
      E=E+TREFK(TAMB)                            VAL(6)=CPA(TA)
      TA7=TYPEK(E)*TFAC                          TA=TA8
      E=TA8                                      VAL(7)=CPA(TA)
      E=E+TREFK(TAMB)                            DX=2.132/6.0
      TA8=TYPEK(E)*TFAC                          NORD=7
      E=TA21                                     CALL DQSF(DX,VAL,TEMP1,NORD)
```

```
      CPAA=TEMP1(NORD)/2.132
      TA=0.5*(TAO +TA8 )
      CPAAO=CPA(TA)
      TA=0.5*(TAO +TA23)
      CPACO=CPA(TA)
      TA=0.5*(TGC2+TGC1)
      CPGC =CPA(TA)
C     PART 2(A) - APPLY S.F.E.E. TO CONTROL VOLUME AROUND HEAT EXCHANGER
      MAC=-MW*(CPWC/CPAC)*(TW22-TW23)/(TA23-TA22)
C     PART 2(B) - APPLY S.F.E.E. TO CONTROL VOLUME AROUND HEAT EXCHANGER
      MAB=-MW*(CPWB/CPAB)*(TW21-TW22)/(TA22-TA21)
C     PART 2(C) - APPLY S.F.E.E. TO CONTROL VOLUME AROUND HEAT EXCHANGERS
      MABC=-MW*(CPWBC/CPABC)*(TW21-TW23)/(TA23-TA21)
C     PART 2(D) - APPLY S.F.E.E. TO CONTROL VOLUME AROUND HEAT EXCHANGER
      MAA=-MW*(CPWA/CPAA)*(TW1-TW9)/(TA8-TA1)
C     PART 2(E) - APPLY S.F.E.E. TO CONTROL VOLUME AROUND WHOLE DOUBLE OR
C     COMBUSTOR
      CALCULATE QLCL & SEPARATE ENTHALPY CHANGES FIRST .
      QLCL=-2.0*3.14159265358*0.43*KLAG*(TSO-TLAG)*0.99969873436
      DHW=MW*(CPWA*(TW1-TW9)+CPWBC*(TW21-TW23))
      DHW=DHW/3600.0
      DHA=MAA*CPAAO*(TA8-TAO)+MABC*CPACO*(TA23-TAO)
      DHA=DHA/3600.0
      DHWTR=MWTR*CPWTR*(TWTR-TW23)
      DHWTR=DHWTR/3600.0
      DHWIN=MWIN*CPWIN*(TWIN-TW23)
      DHWIN=DHWIN/3600.0
      DHGC=MGC*CPGC*(TGC2-TGC1)
      DHGC=DHGC/3600.0
      DHTO=MP*HCVP
      DHTO=DHTO/3600.0
      EQ1=DHW+DHA+DHWTR+DHWIN+DHGC+(-DHTO)-QLCL
C     PART 3     - OVERALL HEAT TRANSFER COEFFICIENTS .
C     CALCULATE LOG. MEAN TEMPERATURES DIFFERENCES FIRST .
      TAM=(TA1-TW1-TA8+TW9)/DLOG((TA1-TW1)/(TA8-TW9))
      TBM=(TA21-TW21-TA22+TW22)/DLOG((TA21-TW21)/(TA22-TW22))
      TCM=(TA22-TW22-TA23+TW23)/DLOG((TA22-TW22)/(TA23-TW23))
      UA=MW*CPWA*(TW1-TW9)/(AA*TAM)
      UA=UA/3600.0
      UB=MW*CPWB*(TW21-TW22)/(AB*TBM)
      UB=UB/3600.0
      UC=MW*CPWC*(TW22-TW23)/(AC*TCM)
      UC=UC/3600.0
C     PART 4     - THERMAL EFFICIENCY OF DOUBLE ORIFICE COMBUSTOR .
      NUTH=(DHW+DHWTR+DHWIN)/DHTO
C     PART 5     - VOLUMETRIC COMBUSTION EFFICIENCY .
      VOLC=0.00018
      NUVOL=DHTO/VOLC
      DHWA=MW*CPWA*(TW1-TW9)/3600.0
      PERC=100.0*EQ1/DHTO
C     PRINT OUT CORRECTED EXPERIMENTAL DATA & CALCULATED PARAMETERS .
      WRITE(6,8000)MP,MW,MWTR,MWIN,MAC,MAB,MABC,MAA,MGC,PAMP,F
 8000 FORMAT(
     >11H  MP        =,1PD16.5,8H     KG/H/
     >11H  MW        =,1PD16.5,8H     KG/H/
     >11H  MWTR      =,1PD16.5,8H     KG/H/
     >11H  MWIN      =,1PD16.5,8H     KG/H/
     >11H  MAC       =,1PD16.5,8H     KG/H/
     >11H  MAB       =,1PD16.5,8H     KG/H/
     >11H  MABC      =,1PD16.5,8H     KG/H/
```

```
     >11H  MAA       =,1PD16.5,8H      KG/H/
     >11H  MGC       =,1PD16.5,8H      KG/H/
     >11H  PAMP      =,1PD16.5,8H     N/M**2/
     >11H  F         =,1PD16.5,8H        HZ/
     >//)
      WRITE(6,8001)
     >TSO,TS1,TS2,TS3,TS4,TS5,TW1,TW2,TW3,TW4,TW5,TW6,TW7,TW8,TW9
 8001 FORMAT(
     >11H  TSO       =,1PD16.5,8H        K/
     >11H  TS1       =,1PD16.5,8H        K/
     >11H  TS2       =,1PD16.5,8H        K/
     >11H  TS3       =,1PD16.5,8H        K/
     >11H  TS4       =,1PD16.5,8H        K/
     >11H  TS5       =,1PD16.5,8H        K/
     >11H  TW1       =,1PD16.5,8H        K/
     >11H  TW2       =,1PD16.5,8H        K/
     >11H  TW3       =,1PD16.5,8H        K/
     >11H  TW4       =,1PD16.5,8H        K/
     >11H  TW5       =,1PD16.5,8H        K/
     >11H  TW6       =,1PD16.5,8H        K/
     >11H  TW7       =,1PD16.5,8H        K/
     >11H  TW8       =,1PD16.5,8H        K/
     >11H  TW9       =,1PD16.5,8H        K/
     >//)
      WRITE(6,8002)
     >TW21,TW22,TW23,TWTR,TWIN,TA1,TA2,TA3,TA4,TA5,TA6,TA7,TA8
 8002 FORMAT(
     >11H  TW21      =,1PD16.5,8H        K/
     >11H  TW22      =,1PD16.5,8H        K/
     >11H  TW23      =,1PD16.5,8H        K/
     >11H  TWTR      =,1PD16.5,8H        K/
     >11H  TWIN      =,1PD16.5,8H        K/
     >11H  TA1       =,1PD16.5,8H        K/
     >11H  TA2       =,1PD16.5,8H        K/
     >11H  TA3       =,1PD16.5,8H        K/
     >11H  TA4       =,1PD16.5,8H        K/
     >11H  TA5       =,1PD16.5,8H        K/
     >11H  TA6       =,1PD16.5,8H        K/
     >11H  TA7       =,1PD16.5,8H        K/
     >11H  TA8       =,1PD16.5,8H        K/
     >//)
      WRITE(6,8003)
     >TA21,TA22,TA23,LAUG,XAUG,TGC1,TGC2,TREF,TLAG,DHW,DHA,DHWTR
 8003 FORMAT(
     >11H  TA21      =,1PD16.5,8H        K/
     >11H  TA22      =,1PD16.5,8H        K/
     >11H  TA23      =,1PD16.5,8H        K/
     >11H  LAUG      =,1PD16.5,8H        M/
     >11H  XAUG      =,1PD16.5,8H        M/
     >11H  TGC1      =,1PD16.5,8H        K/
     >11H  TGC2      =,1PD16.5,8H        K/
     >11H  TREF      =,1PD16.5,8H        K/
     >11H  TLAG      =,1PD16.5,8H        K/
     >11H  DHW       =,1PD16.5,8H        W/
     >11H  DHA       =,1PD16.5,8H        W/
     >11H  DHWTR     =,1PD16.5,8H        W/
     >//)
      WRITE(6,8004)
     >DHWIN,DHGC,DHTO,QLCL,EQ1,PERC,DHWA,UA,UB,UC,NUTH,NUVOL,DI
 8004 FORMAT(
```

```
      >11H   DHWIN    =,1PD16.5,8H        W/
      >11H   DHGC     =,1PD16.5,8H        W/
      >11H   DHTO     =,1PD16.5,8H        W/
      >11H   QLCL     =,1PD16.5,8H        W/
      >11H   EQ1      =,1PD16.5,8H        W/
      >11H   PERC     =,1PD16.5,8H        %/
      >11H   DHWA     =,1PD16.5,8H        W/
      >11H   UA       =,1PD16.5,10H    W/M**2 K/
      >11H   UB       =,1PD16.5,10H    W/M**2 K/
      >11H   UC       =,1PD16.5,10H    W/M**2 K/
      >11H   NUTH     =,1PD16.5,8H        %/
      >11H   NUVOL    =,1PD16.5,8H    W/M**3/
      >11H   DI       =,1PD16.5,8H        M/
      >//)
       WRITE(6,8010)NJET
 8010 FORMAT(19H  AMAL JET NUMBER =,I6/)
       DATA XA1,XA2,XA3,XA4,XA5,XA6,XA7,XA8/
      >0.33,0.477,0.654,1.011,1.366,1.722,2.077,2.4/
       DATA XS1,XS2,XS3,XS4,XS5/0.33,0.84,1.375,1.93,2.4/
       DATA XW1,XW2,XW3,XW4,XW5,XW6,XW7,XW8,XW9/
      >0.33,0.45,0.628,0.805,1.162,1.518,1.874,2.23,2.4/
       DATA M1,XA9/8,3.05/
       WRITE(2,5050)M1
       WRITE(2,5000)XA1,XA3,XA4,XA5,XA6,XA7,XA8,XA9
       WRITE(2,5000)TA1,TA3,TA4,TA5,TA6,TA7,TA8,TA8
       WRITE(2,5000)XS1,XS5
       WRITE(2,5000)TS1,TS5
       WRITE(2,5000)XW1,XW9
       WRITE(2,5000)TW1,TW9
 5000 FORMAT(9(1PC10.3))
 5050 FORMAT(I1)
       WRITE(2,9898)MP,MW,MAA,PAMP,F,LAUG,XAUG,DHWA,UA
 9898 FORMAT(5(1PD16.5)/4(1PD16.5))
       STOP
       END
       FUNCTICN TYPEK(E)
C  SUBROUTINE TO PERFORM QUADRATIC INTERPOLATICN ON THERMOCOUPLE REFER
C  TABLES . E - E.M.F. IN MILLIVOLTS TO DEGREES CELSIUS .
C      TYPEK - NICKEL-CHROMIUM / NICKEL-ALUMINIUM
C  REFERENCE :  B.S.4937:PART 4:1973
       REAL A
       REAL*8 TEMP(60),EMF(60),E,H01,H02,H03,D1,D2,D3,D12,D23,D123
      >,TYPEK,TYPES,TYPET,TREFK,TREFS,TREFT
       DATA EMF/
      >   0.0,      1.0,      2.0,      3.0,      4.0,      5.0,
      >   6.0,      7.0,      8.0,      9.0,      10.0,     11.0,
      >   12.0,     13.0,     14.0,     15.0,     16.0,     17.0,
      >   18.0,     19.0,     20.0,     21.0,     22.0,     23.0,
      >   24.0,     25.0,     26.0,     27.0,     28.0,     29.0,
      >   30.0,     31.0,     32.0,     33.0,     34.0,     35.0,
      >   36.0,     37.0,     38.0,     39.0,     40.0,     41.0,
      >   42.0,     43.0,     44.0,     45.0,     46.0,     47.0,
      >   48.0,     49.0,     50.0,     51.0,     52.0,     53.0,
      >   54.0/
       DATA TEMP/
      >    0.0,     25.0,     49.5,     73.6,     97.7,    122.0,    146.6,
      >  171.5,    196.6,    221.5,    246.3,    270.7,    295.0,    319.1,
      >  343.0,    366.9,    390.6,    414.3,    437.9,    461.5,    485.0,
      >  508.4,    531.9,    555.3,    578.8,    602.3,    625.9,    649.5,
      >  673.2,    696.9,    720.8,    744.8,    769.0,    793.3,    817.7,
```

```
     >     842.3,     867.0,     891.9,     916.9,     942.2,     967.5,     993.1,
     >    1018.8,    1044.7,    1070.8,    1097.1,    1123.7,    1150.4,    1177.4,
     >    1204.7,    1232.3,    1260.3,    1288.6,    1317.3,    1346.3/
       DATA HO1,HO2,HO3/1.0,1.0,0.5/
       IF(E.LE.0.9)GO TO 21
       IF(E.LT.53.2)GO TO 22
       IF(E.GT.54.0)GO TO 23
       N=53
       GO TO 24
   21 CONTINUE
       IF(E.LT.0.0)GO TO 23
       N=1
       GO TO 24
   22 CONTINUE
       A=SNGL(E/HO1)
       N=IFIX(A)
   24 CONTINUE
       D1=E-EMF(N)
       D2=E-EMF(N+1)
       D3=E-EMF(N+2)
       D12=(D1*TEMP(N+1)-D2*TEMP(N))*HO2
       D23=(D2*TEMP(N+2)-D3*TEMP(N+1))*HO2
       D123=((D1*D23)-(D3*D12))*HO3
       TYPEK=D123+273.16
       GO TO 25
   23 CONTINUE
       TYPEK=0.0
   25 CONTINUE
       RETURN
       END
       FUNCTION TYPES(E)
C SUBROUTINE TO PERFORM QUADRATIC INTERPOLATION ON THERMOCOUPLE REFER
C TABLES . E - E.M.F. IN MILLIVOLTS TO DEGREES CELSIUS .
C     TYPES - PLATINUM-10%RHODIUM/PLATINUM
C REFERENCE :  B.S.4937:PART 1:1973
       REAL A
       REAL*8 TEMP(60),EMF(60),E,HO1,HO2,HO3,D1,D2,D3,D12,D23,D123
     >,TYPEK,TYPES,TYPET,TREFK,TREFS,TREFT
       DATA EMF/
     >  0.0,       0.5,       1.0,       1.5,       2.0,       2.5,       3.0,       3.5,
     >  4.0,       4.5,       5.0,       5.5,       6.0,       6.5,       7.0,       7.5,
     >  8.0,       8.5,       9.0,       9.5,      10.0,      10.5,      11.0,      11.5,
     > 12.0,      12.5,      13.0,      13.5,      14.0,      14.5,      15.0,      15.5,
     > 16.0,      16.5,      17.0,      17.5,      18.0,      18.5/
       DATA TEMP/
     >    0.0,      79.8,     146.4,     207.1,     264.3,     319.3,     372.7,
     >  425.0,     476.3,     526.8,     576.6,     625.7,     673.9,     721.3,
     >  768.1,     814.2,     859.7,     904.6,     948.9,     992.6,    1035.8,
     > 1078.5,    1120.8,    1162.7,    1204.4,    1245.9,    1287.2,    1328.5,
     > 1369.7,    1410.9,    1452.2,    1493.6,    1535.3,    1577.2,    1619.4,
     > 1661.9,    1705.1,    1749.7/
       DATA HO1,HO2,HO3/0.5,2.0,1.0/
       IF(E.LE.0.4)GO TO 21
       IF(E.LT.18.1)GO TO 22
       IF(E.GT.18.5)GO TO 23
       N=36
       GO TO 24
   21 CONTINUE
       IF(E.LT.0.0)GO TO 23
       N=1
```

```
      GO TO 24
   22 CONTINUE
      A=SNGL(E/HO1)
      N=IFIX(A)
   24 CONTINUE
      D1=E-EMF(N)
      D2=E-EMF(N+1)
      D3=E-EMF(N+2)
      D12=(D1*TEMP(N+1)-D2*TEMP(N))*HO2
      D23=(D2*TEMP(N+2)-D3*TEMP(N+1))*HO2
      D123=((D1*D23)-(D3*D12))*HO3
      TYPES=D123+273.16
      GO TO 25
   23 CONTINUE
      TYPES=0.0
   25 CONTINUE
      RETURN
      END
      FUNCTION TYPET(E)
C SUBROUTINE TO PERFORM QUADRATIC INTERPOLATION ON THERMOCOUPLE REFER
C TABLES . E - E.M.F. IN MILLIVOLTS TO DEGREES CELSIUS .
C      TYPET - COPPER-CONSTANTAN .
C REFERENCE :   B.S.1828:1961
      REAL A
      REAL*8 TEMP(60),EMF(60),E,HO1,HO2,HO3,D1,D2,D3,D12,D23,D123
     >,TYPEK,TYPES,TYPET,TREFK,TREFS,TREFT
      DATA EMF/
     >  0.0,     0.5,     1.0,     1.5,     2.0,     2.5,     3.0,     3.5,
     >  4.0,     4.5,     5.0,     5.5,     6.0,     6.5,     7.0,     7.5,
     >  8.0,     8.5,     9.0,     9.5,    10.0,    10.5,    11.0,    11.5,
     >12.0,    12.5,    13.0,    13.5,    14.0,    14.5,    15.0,    15.5,
     > 16.0,    16.5,    17.0,    17.5,    18.0,    18.5,    19.0,    19.5,
     > 20.0,    20.50/
      DATA TEMP/
     >    0.0,    12.9,    25.4,    37.6,    49.5,    61.2,    72.6,    83.8,
     >   94.8,   105.6,   116.3,   126.8,   137.1,   147.3,   157.4,   167.4,
     >  177.2,   187.0,   196.6,   206.1,   215.6,   224.9,   234.2,   243.4,
     >  252.5,   261.6,   270.5,   279.5,   288.3,   297.1,   305.8,   314.5,
     >  323.1,   331.7,   340.2,   348.6,   357.1,   365.4,   373.8,   382.0,
     >  390.3,   398.5/
      DATA HO1,HO2,HO3/0.5,2.0,1.0/
      IF(E.LE.0.49)GO TO 21
      IF(E.LT.20.1)GO TO 22
      IF(E.GT.20.5)GO TO 23
      N=40
      GO TO 24
   21 CONTINUE
      IF(E.LT.0.0)GO TO 23
      N=1
      GO TO 24
   22 CONTINUE
      A=SNGL(E/HO1)
      N=IFIX(A)
   24 CONTINUE
      D1=E-EMF(N)
      D2=E-EMF(N+1)
      D3=E-EMF(N+2)
      D12=(D1*TEMP(N+1)-D2*TEMP(N))*HO2
      D23=(D2*TEMP(N+2)-D3*TEMP(N+1))*HO2
      D123=((D1*D23)-(D3*D12))*HO3
```

```
      TYPET=D123+273.16
      GO TO 25
   23 CONTINUE
      TYPET=0.0
   25 CONTINUE
      RETURN
      END
      FUNCTICN TREFK(TAMB)
C SUBROUTINE TO PERFORM QUADRATIC INTERPOLATICN ON THERMOCOUPLE TABLE
C FOR A GIVEN RANGE OF ATMOSPHERIC TEMPERATURE          0 < TAMB < 30.0
C     TYPEK - NICKEL-CHROMIUM / NICKEL-ALUMINIUM
C DEGREES CELSIUS TO MILLIVCLTS .
C REFERENCE :  B.S.4937:PART 4:1973
      REAL A
      REAL*8 TEMP(60),EMF(60),E,H01,H02,H03,D1,D2,D3,D12,D23,D123
     >,TYPEK,TYPES,TYPET,TREFK,TREFS,TREFT,TAMB
      DATA TEMP/ 0.0,    2.0,    4.0,    6.0,    8.0,   10.0,   12.0,   14.0,
     >   16.0,   18.0,   20.0,   22.0,   24.0,   26.0,   28.0,   30.0/
      DATA EMF/ 0.000,  0.079,  0.158,  0.238,  0.317,  0.397,  0.477
     >   0.557,  0.637,  0.718,  0.798,  0.879,  0.960,  1.041,  1.122
     >   1.203/
      DATA H01,H02,H03/2.0,0.5,0.25/
      IF(TAMB.LE.1.8)GO TO 21
      IF(TAMB.LT.28.4)GO TO 22
      IF(TAMB.GT.30.0)GO TO 23
      N=14
      GO TO 24
   21 CONTINUE
      IF(TAMB.LT.0.0)GO TO 23
      N=1
      GO TO 24
   22 CONTINUE
      A=SNGL(TAMB/H01)
      N=IFIX(A)
   24 CONTINUE
      D1=TAMB-TEMP(N)
      D2=TAMB-TEMP(N+1)
      D3=TAMB-TEMP(N+2)
      D12=(D1*EMF(N+1)-D2*EMF(N))*H02
      D23=(D2*EMF(N+2)-D3*EMF(N+1))*H02
      D123=((D1*D23)-(D3*D12))*H03
      TREFK=D123
      GO TO 25
   23 CONTINUE
      TREFK=0.0
   25 CONTINUE
      RETURN
      END
      FUNCTICN TREFS(TAMB)
C SUBROUTINE TO PERFORM QUADRATIC INTERPOLATION ON THERMOCOUPLE TABLE
C FOR A GIVEN RANGE OF ATMCSPHERIC TEMPERATURE          0 < TAMB < 30.0
C     TYPES - PLATINUM-10%RHODIUM/PLATINUM
C DEGREES CELSIUS TO MILLIVCLTS .
C REFERENCE :  B.S.4937:PART 1:1973
      REAL A
      REAL*8 TEMP(60),EMF(60),E,H01,H02,H03,D1,D2,D3,D12,D23,D123
     >,TYPEK,TYPES,TYPET,TREFK,TREFS,TREFT,TAMB
      DATA TEMP/ 0.0,    2.0,    4.0,    6.0,    8.0,   10.0,   12.0,   14.0,
     >   16.0,   18.0,   20.0,   22.0,   24.0,   26.0,   28.0,   30.0/
      DATA EMF/ 0.000,  0.011,  0.022,  0.033,  0.044,  0.055,  0.067
```

```
    >   0.078,   0.090,   0.101,   0.113,   0.125,   0.137,   0.148,   0.161
    >   0.173/
      DATA HO1,HO2,HO3/2.0,0.5,0.25/
      IF(TAMB.LE.1.8)GO TO 21
      IF(TAMB.LT.28.4)GO TO 22
      IF(TAMB.GT.30.0)GO TO 23
      N=14
      GO TO 24
   21 CONTINUE
      IF(TAMB.LT.0.0)GO TO 23
      N=1
      GO TO 24
   22 CONTINUE
      A=SNGL(TAMB/HO1)
      N=IFIX(A)
   24 CONTINUE
      D1=TAMB-TEMP(N)
      D2=TAMB-TEMP(N+1)
      D3=TAMB-TEMP(N+2)
      D12=(D1*EMF(N+1)-D2*EMF(N))*HO2
      D23=(D2*EMF(N+2)-D3*EMF(N+1))*HO2
      D123=((D1*D23)-(D3*D12))*HO3
      TREFS=D123
      GO TO 25
   23 CONTINUE
      TREFS=0.0
   25 CONTINUE
      RETURN
      END
      FUNCTION TREFT(TAMB)
C SUBROUTINE TO PERFORM QUADRATIC INTERPOLATION ON THERMOCOUPLE TABLE
C FOR A GIVEN RANGE OF ATMOSPHERIC TEMPERATURE          0 < TAMB < 30.0
C    TYPET - COPPER-CONSTANTAN .
C DEGREES CELSIUS TO MILLIVOLTS .
C REFERENCE :  B.S.1828:1961
      REAL A
      REAL*8 TEMP(60),EMF(60),E,HO1,HO2,HO3,D1,D2,D3,D12,D23,D123
    >,TYPEK,TYPES,TYPET,TREFK,TREFS,TREFT,TAMB
      DATA TEMP/ 0.0,    2.0,    4.0,    6.0,    8.0,   10.0,   12.0,   14.0,
    >   16.0,   18.0,   20.0,   22.0,   24.0,   26.0,   28.0,   30.0/
      DATA EMF/  0.000,  0.077,  0.154,  0.232,  0.309,  0.388,  0.466
    >   0.545,  0.624,  0.703,  0.783,  0.863,  0.944,  1.025,  1.106
    >   1.188/
      DATA HO1,HO2,HO3/2.0,0.5,0.25/
      IF(TAMB.LE.1.8)GO TO 21
      IF(TAMB.LT.28.4)GO TO 22
      IF(TAMB.GT.30.0)GO TO 23
      N=14
      GO TO 24
   21 CONTINUE
      IF(TAMB.LT.0.0)GO TO 23
      N=1
      GO TO 24
   22 CONTINUE
      A=SNGL(TAMB/HO1)
      N=IFIX(A)
   24 CONTINUE
      D1=TAMB-TEMP(N)
      D2=TAMB-TEMP(N+1)
      D3=TAMB-TEMP(N+2)
```

```
      D12=(D1*EMF(N+1)-D2*EMF(N))*HO2
      D23=(D2*EMF(N+2)-D3*EMF(N+1))*HO2
      D123=((D1*D23)-(D3*D12))*HO3
      TREFT=D123
      GO TO 25
   23 CONTINUE
      TREFT=0.0
   25 CONTINUE
      RETURN
      END
      FUNCTION ROTAMW(CM)
C REFERENCE ; CALIBRATION OF METRIC 24E ROTAMETER FOR WATER . 21 SEPT
      REAL*8 ROTAMW,CM
      ROTAMW=105.64+(37.512*CM)
C UNITS   ---   KG/H
      RETURN
      END
      FUNCTICN ROTAMA(CM)
      REAL*8 ROTAMA,CM
      ROTAMA=CM*0.1168
      RETURN
      END
      FUNCTICN CPA(TA)
C     SUBROUTINE TO PERFORM QUADRATIC INTERPOLATION ON DATA FOR
C SPECIFIC HEAT AT CONSTANT PRESSURE OF
C DRY AIR AT ONE ATMOSPHERE
C REFERENCE :   TABLES CF THERMODYNAMIC & TRANSPORT PROPERTIES OF
C AIR,AR,CO2,CO,H2,N2,O2 & H2O .
C HILSENRATH,J. ET AL .      PERGAMON  1960
      REAL A
      REAL*8 TAB(30),TT(30),TA,HO1,HO2,HO3,D1,D2,D3,D12,D23,D123,
     +CPA
      DATA TT/200.0,300.0,400.0,500.0,600.0,700.0,800.0,900.0,1000.0,
     +1100.0,1200.0,1300.0,1400.0,1500.0,1600.0,1700.0,1800.0,1900.0,
     +2000.0,2100.0,2200.0,2300.0,2400.0,2500.0,2600.0,
     +2700.0,2800.0,2900.0,3000.0/
      DATA TAB/
     +     3.5062,     3.5059,     3.5333,     3.5882,     3.6626,     3.7455,
     +     3.828,      3.906,      3.979,      4.046,      4.109,      4.171,
     +     4.230,      4.289,      4.352,      4.418,      4.487,      4.566,
     +     4.662,      4.781,      4.947,      5.179,      5.484,      5.882,
     +     6.40,       7.06,       7.87,       8.86,       9.96
     +/
      DATA HO1,HO2,HO3/100.0,0.01,0.005/
      IF(TA.LE.299.0)GO TO 21
      IF(TA.LT.2940.0)GO TO 22
      IF(TA.GT.3000.0)GO TO 23
      N=16
      GO TO 24
   21 CONTINUE
      IF(TA.LT.200.0)GO TO 23
      N=1
      GO TO 24
   22 CONTINUE
      A=SNGL(TA/HO1)
      N=IFIX(A)-2
   24 CONTINUE
      D1=TA-TT(N)
      D2=TA-TT(N+1)
      D3=TA-TT(N+2)
```

```
      D12=(D1*TAB(N+1)-D2*TAB(N))*H02
      D23=(D2*TAB(N+2)-D3*TAB(N+1))*H02
      D123=((D1*D23)-(D3*D12))*H03
      CPA=D123*287.041
C  UNITS OF CPA : J/KG  K
      GO TO 25
   23 CONTINUE
      WRITE(6,700)TA
  700 FORMAT('CPA    ARGUMENT CF ',F12.5,' IS CUTSIDE TEMPERATURE RANGE
     +OF 200.0 --  3000.0  DEG. K')
   25 RETURN
      END
      FUNCTICN CPW(TW)
C     SUBROUTINE TO PERFCRM QUADRATIC INTERPOLATION ON DATAFOR
C     SPECIFIC HEAT AT CCNSTANT PRESSURE FOR WATER
C     FROM TABLE 5 ,PAGE 119 ,UK STEAM TABLES IN SI UNITS 1970 .
      REAL A
      REAL*8 TAB(11),TT(11),TW,H01,H02,H03,D1,D2,D3,D12,023,D123,
     +CPW
      DATA TT/10.0,20.0,30.0,40.0,50.0,60.0,70.0,80.0,90.0,100.0,
     +110.0/
      DATA TAB/4.194,4.182,4.179,4.179,4.181,4.185,4.191,4.198,
     +4.207,4.218,4.230/
      DATA H01,H02,H03/10.0,0.1,0.05/
      IF(TW.LE.19.0)GC TO 21
      IF(TW.LT.104.0)GO TO 22
      IF(TW.GT.110.0)GO TO 23
      N=9
      GO TO 24
   21 CONTINUE
      IF(TW.LT.10.0)GO TC 23
      N=1
      GO TO 24
   22 CONTINUE       --
      A=SNGL(TW/H01)
      N=IFIX(A)-1
   24 CONTINUE
      D1=TW-TT(N)
      D2=TW-TT(N+1)
      D3=TW-TT(N+2)
      D12=(D1*TAB(N+1)-D2*TAB(N))*H02
      D23=(D2*TAB(N+2)-D3*TAB(N+1))*H02
      D123=((D1*D23)-(D3*D12))*H03
      CPW=D123*1000.0
      GO TO 25
   23 CONTINUE
      WRITE(6,700)TW
  700 FORMAT(' CPW   ARGUMENT OF ',F12.5,' IS CUTSIDE TEMP RANGE OF
     + 10.0 ---  110.0  DEG. C')
   25 RETURN
      END
```

```
C       PCFPP01
C PULSATING COMBUSTOR FREQUENCY PREDICTION PROGRAM  --  ONE
C THE PURPOSE OF THIS PROGRAM IS TO SOLVE THE BESSEL BOUNDARY
C CONDITIONS FOR AN EXPONENTIAL GAS TEMPERATURE GRADIENT IN THE
C HEAT EXCHANGER SECTIONS OF THE MARK 5 COMBUSTOR .
C           6 JUNE 1972
C  NUMBER CODE : M = 1        OPEN-OPEN        MODEL
C                M = 2        OPEN-CLOSED      MODEL
      IMPLICIT REAL*8(A-H,O-Z)
      DIMENSION BJ(6),BY(6),IER(12)
      REAL*8 LANDA
   18 CONTINUE
      READ(5,7799)T1,T2
 7799 FORMAT(2(F10.3))
      IF(T1)53,53,12
   12 CONTINUE
      DATA X1,X2/0.33,2.4/
      ALPHA=(-DLOG(T1/T2))/(2*(X1-X2))
      TO=T1/(DEXP(-2*ALPHA*X1))
      CO=DSQRT(401.94*TO)
      EL=3.3
      M=2
C
      WRITE(6,2000)M,ALPHA,CO,EL
 2000 FORMAT(3X,'M =',I3,4X,'OPEN-CLOSED MODEL'//8X,'ALPHA = ',1PE12.6
     1//11X,'CO = ',1PE12.6,3X,'METRE/SECOND'//11X,'EL = ',1PE12.6,
     23X,'METRE'/)
C234567
C CALCULATE A & B
      A=(DEXP(ALPHA*EL))/ALPHA
      B=1.0/ALPHA
C
      WRITE(6,9111)T1,T2
 9111 FORMAT(11X,'T1 = ',1PD12.6,7X,'K'/11X,'T2 = ',1PD12.6,7X,'K'/)
C
      D=0.001
C READ STARTING VALUE OF LANDA
   11 READ(5,1001)LANDA
 1001 FORMAT(F10.5)
C
C
      IF(LANDA)18,18,10
   10 CONTINUE
C SET N EQUAL TO ZERO
      N=0
C
C
C
    4 CONTINUE
      ALANDA=A*LANDA
      BLANDA=B*LANDA
C CALCULATE BESSEL ARRAYS FOR GIVEN ORDER AND ARGUEMENT
      CALL DBESJ(ALANDA,0,BJ(1),D,IER(1))
      CALL DBESJ(BLANDA,0,BJ(2),D,IER(2))
      CALL DBESJ(ALANDA,1,BJ(3),D,IER(3))
      CALL DBESJ(BLANDA,1,BJ(4),D,IER(4))
      CALL DBESJ(ALANDA,2,BJ(5),D,IER(5))
      CALL DBESJ(BLANDA,2,BJ(6),D,IER(6))
```

```
C234567
      CALL DBESY(ALANCA,0,BY(1),IER(7))
      CALL DBESY(BLANDA,0,BY(2),IER(8))
      CALL DBESY(ALANDA,1,BY(3),IER(9))
      CALL DBESY(BLANCA,1,BY(4),IER(10))
      CALL DBESY(ALANDA,2,BY(5),IER(11))
      CALL DBESY(BLANCA,2,BY(6),IER(12))
      FLANDA=BJ(2)*BY(3)-BJ(3)*BY(2)
      GLANDA=B*BJ(3)*BY(4)-B*BY(3)*BJ(4)+0.5*A*BJ(2)*(BY(1)-BY(5))
     >-0.5*A*BY(2)*(BJ(1)-BJ(5))
      IF(DABS(GLANDA) .LT. 1.0D-06)GO TO 90
      Y=LANDA-(FLANDA/GLANDA)
      IF(DABS(LANDA-Y) .LT. 1.0D-06 .OR. N .GT. 50)GO TO 9
      N=N+1
      LANDA=Y
C
C
C
      GO TO 4
    9 WRITE(6,2004)Y,N
 2004 FORMAT(4X,'FINAL VALUE CF LANDA =',2X,1PE12.6,4X,'AT N =',I3//)
      FREQ=CC*Y/6.2831853072
      WRITE(6,2005)FREQ
 2005 FORMAT(10X,'COMPUTED FREQUENCY =',2X,1PE12.6,6X,' HERTZ'/)
      GO TO 11
   90 WRITE(6,2150)
 2150 FORMAT(3X,' GLANDA DEFAULT '//)
      GO TO 11
   53 STOP
      END
C     PCFPP01
C PULSATING COMBUSTOR FREQUENCY PREDICTION PROGRAM  --  CNE
C THE PURPOSE OF THIS PROGRAM IS TO SOLVE THE BESSEL BOUNDARY
C CONDITIONS FOR AN EXPONENTIAL GAS TEMPERATURE GRADIENT IN THE
C HEAT EXCHANGER SECTIONS OF THE MARK 5 COMBUSTOR .
C           6 JUNE 1972
C NUMBER CODE : M = 1         OPEN-OPEN       MODEL
C               M = 2         OPEN-CLOSED     MODEL
      IMPLICIT REAL*8(A-H,O-Z)
      DIMENSION BJ(6),BY(6),IER(12)
      REAL*8 LANDA
   18 CONTINUE
      READ(5,7799)T1,T2
 7799 FORMAT(2(F10.3))
      IF(T1)53,53,12
   12 CONTINUE
      DATA X1,X2/0.33,2.4/
      ALPHA=(-DLOG(T1/T2))/(2*(X1-X2))
      TO=T1/(DEXP(-2*ALPHA*X1))
      CO=DSQRT(401.94*TO)
      EL=3.3
      M=1
      WRITE(6,2000)M,ALPHA,CO,EL
 2000 FORMAT(3X,'M = ',I2,4X,'OPEN-OPEN MODEL'//8X,'ALPHA = ',1PE12.6
     1//11X,'CO = ',1PE12.6,3X,'METRE/SECOND'//11X,'EL = ',1PE12.6,
     23X,'METRE'/)
C234567
C CALCULATE A & B
      A=(DEXP(ALPHA*EL))/ALPHA
      B=1.0/ALPHA
      WRITE(6,9111)T1,T2
```

```
 9111 FORMAT(11X,'T1 = ',1PD12.6,7X,'K'/11X,'T2 = ',1PD12.6,7X,'K'/)
      WRITE(6,2001)A,B
 2001 FORMAT(7X,'A = ',1PE12.6/7X,'B = ',1PE12.6/)
      D=C.001
C READ STARTING VALUE OF LANDA
   11 READ(5,1001)LANDA
 1001 FORMAT(F10.5)
      WRITE(6,2002)LANDA
 2002 FORMAT(3X,'LANDA STARTING VALUE = ',1PE12.6/)
      IF(LANDA)18,18,10
   10 CONTINUE
C SET N EQUAL TO ZERO
      N=0
      WRITE(6,6000)
 6000 FORMAT(3X,'N',6X,'ALANDA',6X,'BLANDA',6X,'FLANDA',6X,'GLANDA',
     46X,'LANDA'//)
    4 CONTINUE
      ALANDA=A*LANDA
      BLANDA=B*LANDA
C CALCULATE BESSEL ARRAYS FOR GIVEN ORDER AND ARGUEMENT
      CALL DBESJ(ALANDA,0,BJ(1),D,IER(1))
      CALL DBESJ(BLANDA,0,BJ(2),D,IER(2))
      CALL DBESJ(ALANDA,1,BJ(3),D,IER(3))
      CALL DBESJ(BLANDA,1,BJ(4),D,IER(4))
      CALL DBESJ(ALANDA,2,BJ(5),D,IER(5))
      CALL DBESJ(BLANDA,2,BJ(6),D,IER(6))
C234567
      CALL DBESY(ALANDA,0,BY(1),IER(7))
      CALL DBESY(BLANDA,0,BY(2),IER(8))
      CALL DBESY(ALANDA,1,BY(3),IER(9))
      CALL DBESY(BLANDA,1,BY(4),IER(10))
      CALL DBESY(ALANDA,2,BY(5),IER(11))
      CALL DBESY(BLANDA,2,BY(6),IER(12))
      FLANDA=BJ(4)*BY(3)-BJ(3)*BY(4)
      GLANDA=0.5*B*BY(3)*(BJ(2)-BJ(6))+0.5*A*BJ(4)*(BY(1)-BY(5))
     >-0.5*A*BY(4)*(BJ(1)-BJ(5))-0.5*B*BJ(3)*(BY(2)-BY(6))
      IF(DABS(GLANDA) .LT. 1.0D-06)GO TO 90
      Y=LANDA-(FLANDA/GLANDA)
      IF(DABS(LANDA-Y) .LT. 1.0D-06 .OR. N .GT. 50)GO TO 9
      N=N+1
      LANDA=Y
      WRITE(6,7000)N,ALANDA,BLANDA,FLANDA,GLANDA,LANDA
 7000 FORMAT(2X,I2,4X,5(1PE12.5))
      GO TO 4
    9 WRITE(6,2004)Y,N
 2004 FORMAT(4X,'FINAL VALUE OF LANDA =',2X,1PE12.6,4X,'AT N =',I3//)
      FREQ=CO*Y/6.2831853072
      WRITE(6,2005)FREQ
 2005 FORMAT(10X,'COMPUTED FREQUENCY =',2X,1PE12.6,6X,' HERTZ'/)
      GO TO 11
   90 WRITE(6,2150)
 2150 FORMAT(3X,' GLANDA DEFAULT '//)
      GO TO 11
   53 STOP
      END
C     TEST PROGRAM               10 SEPT 1972
C     EVALUATION OF P(X,T) FOR C(X) = CO*EXP(ALPHA*X)
      IMPLICIT REAL*8(A-H,O-Z)
      REAL*8 LANDA
      DIMENSION BJ(9),BY(9),IER(9)
```

```
      DATA BA,EL,D/135000.0,3.3,0.00001/
    4 READ(5,1050)ALPHA,CO,PMAX
      IF(ALPHA)24,24,73
   73 CONTINUE
 1050 FORMAT(5(F10.7))
      WRITE(6,5000)CO,ALPHA,EL,PMAX,BA
 5000 FORMAT(2X,'   CO = ',1PD12.5,' METRES/SEC'/2X,'ALPHA = '
     1,1PD12.5/2X,'   EL = ',1PD12.5,' METRES'/2X,' PMAX = '
     2,1PD12.5,' N/M**2'/2X,'   BA = ',1PD12.5,' N/M**2'//)
      READ(5,1000)LANDA
 1000 FORMAT(F15.6)
      WRITE(6,4000)LANDA
 4000 FORMAT(2X,'LANDA = ',1PD12.5/)
      IF(LANDA)24,24,25
   25 CONTINUE
      ZL=(DEXP(ALPHA*EL))*LANDA/ALPHA
      Z0=LANDA/ALPHA
      CALL DBESJ(Z0,0,BJ(1),D,IER(1))
      CALL DBESY(Z0,0,BY(1),IER(2))
      RMN=-BY(1)/BJ(1)
      CALL DBESJ(Z0,1,BJ(2),D,IER(3))
      CALL DBESY(Z0,1,BY(2),IER(4))
      CONST=(RMN*BJ(2))+BY(2)
      WRITE(6,2001)
 2001 FORMAT(4X,'J',9X,'X',15X,'P',13X,'V'//)
      X=0.0
      DO 90 J=1,12
      Z=(DEXP(ALPHA*X))*LANDA/ALPHA
      CALL DBESJ(Z,1,BJ(3),D,IER(5))
      CALL DBESY(Z,1,BY(3),IER(6))
      P=PMAX*DEXP(ALPHA*X)*((RMN*BJ(3))+BY(3))/CONST
      CALL DBESJ(Z,0,BJ(4),D,IER(7))
      CALL DBESY(Z,0,BY(4),IER(8))
      V=PMAX*CO*((RMN*BJ(4))+BY(4))/(BA*CONST)
      WRITE(6,2000)J,X,P,V
 2000 FORMAT(I5,3(5X,1PD10.3))
      X=X+0.3
   90 CONTINUE
      WRITE(6,2002)
 2002 FORMAT(//4X,'-',7X,'METRES',10X,'N/M**2',9X,'M/SEC'//)
      GO TO 4
   24 STOP
      END
```

```
C   PROGRAMME TO CALCULATE AIR MASS FLOW THROUGH AERODYNAMIC VALVE ;
C   CALCULATION BASED ON QUASI-STEADY-STATE THEORY . THUS MASS FLOW
C   IS INDEPENDENT OF FREQUENCY .        5  MARCH  1973
        REAL*8 MAIN(200),MAEX(200),RHO1,RHO2,P1,P2,GAM1,GAM2,GAMMA,TA,
      +M1,M2,A,AE,CD,C1,C2,PXO,PAT,D,KG,KP,T,DT,RR,U1(200),U2(200)
C   READ  D           INTERNAL DIAMETER OF VALVE
C         PXO  .   PRESSURE AMPLITUDE IN COMBUSTION CHAMBER
C         TA        MEAN TEMPERATURE IN COMBUSTION CHAMBER
   98 CONTINUE
      READ(5,1000)D,PXO,TA
      IF(D)94,94,95
   95 CONTINUE
 1000 FORMAT(3(F10.0))
C   SET CONSTANTS FOR INDUCTION PART OF CYCLE ;   2PI >  T  >  PI
      PAT=101350.0
      RHO1=1.177
      NORD=20
      T=3.14159265358
      DT=3.14159265358/NORD
      P1=PAT
      NORD=NORD+1
      GAM1=1.4
      KG=(GAM1-1.0)/GAM1
      RR=287.1
      C1=DSQRT(GAM1*RR*300.0)
      WRITE(6,3003)
 3003 FORMAT(10X,'T',13X,'U1(I)'//)
      DO 10 I=1,NORD
      P2=PAT+PXO*DSIN(T)
      KP=P2/P1
      RHO2=RHO1*(KP**(1.0/GAM1))
C   CALCULATE INSTANTANEOUS VELOCITY & MACH NO.
      U1(I)=DABS((2.0*P1/(KG*RHO1))*(1.0-KP**KG))
      U1(I)=DSQRT(U1(I))
      M1=U1(I)/C1
C   CALCULATE COEFFICIENT OF DISCHARGE & EFFECTIVE AREA
      CD=0.5+(M1**2)*0.125+(M1**4)*0.04166666667
      AE=3.14159265358*(D**2)*CD*0.25
C   CALCULATE INSTANTANEOUS AIR MASS FLOWRATE
      MAIN(I)=RHO2*AE*U1(I)
C   WRITE ANGLE & VELOCITY
      WRITE(6,3000)T,U1(I)
 3000 FORMAT(2(4X,1PD13.5))
      T=T+DT
   10 CONTINUE
C   INTEGRATE BY SIMPSONS RULE
      CALL DCSF(DT,MAIN,MAIN,NORD)
      WRITE(6,3010)MAIN(NORD)
 3010 FORMAT(4X,'INDUCTION AIR MASS =',1PD13.5//)
C   RESET CONSTANTS FOR EXHAUST PART OF CYCLE ;  0  <  T  <  PI
      NORD=20
      T=0.0
      DT=3.14159265358/NORD
      GAM2=1.3
      KG=(GAM2-1.0)/GAM2
      C2=DSQRT(GAM2*RR*TA)
      NORD=NORD+1
      RHO2=P1/(RR*TA)
```

```
      WRITE(6,3004)
 3004 FORMAT(10X,'T',13X,'U2(J)'//)
      DO 11 J=1,NORD
      P2=PAT+PXO*DSIN(T)
      KP=P1/P2
      RHO1=RHO2*(KP**(1.0/GAM2))
C  CALCULATE INSTANTANEOUS VELOCITY & MACH NO.
      U2(J)=CQ
      U2(J)=DSQRT((2.0*P2/(KG*RHO2))*(1.0-KP**KG))
      M2=U2(J)/C2
C  CALCULATE COEFFICIENT OF DISCHARGE & EFFECTIVE AREA
      CD=0.5+(M2**2)*0.125+(M2**4)*0.04166666667
      AE=3.141592€5358*(D**2)*CD*0.25
C  CALCULATE INSTANTANEOUS AIR MASS FLOWRATE
      MAEX(J)=RHO1*AE*U2(J)
C  WRITE ANGLE & VELOCITY
      WRITE(6,3006)T,U2(J)
 3006 FORMAT(2(4X,1PD13.5))
      T=T+DT
   11 CONTINUE
C  INTEGRATE BY SIMPSONS RULE
      CALL DQSF(DT,MAEX,MAEX,NORD)
      WRITE(6,3007)MAEX(NORD)
 3007 FORMAT(4X,'EXHAUST AIR MASS =',1PD13.5//)
      MAIN(NORD)=MAIN(NORD)-MAEX(NORD)
      WRITE(2,1235)MAIN(NORD)
 1235 FORMAT(4X,' MAA = ',1PD13.5)
      WRITE(2,2222)D,PXO,TA
 2222 FORMAT(4X,'D =',F10.5/4X,'PXO =',F10.2/4X,'TA =',F10.2//)
      GO TO 98
   94 CONTINUE
      STOP
      END
```